# 量子ドットの緩和とコヒーレント制御

(研究課題番号　13852003)

平成13年度～平成17年度科学研究費補助金（基盤研究（S））

研 究 成 果 報 告 書

平 成 18 年 3 月

研究代表者　舛 本 泰 章

(筑波大学大学院数理物質科学研究科教授)

# 量子ドットの緩和とコヒーレント制御

（研究課題番号　13852003）

平成13年度～平成17年度科学研究費補助金（基盤研究（S））

研 究 成 果 報 告 書

平 成 18 年 3 月

研究代表者　舛 本 泰 章

（筑波大学大学院数理物質科学研究科教授）

# 目次

# Ⅰ．研究組織および研究経費

## １．研究組織

研究代表者：舛本泰章（筑波大学大学院数理物質科学研究科教授）
研究分担者：奥野剛史（筑波大学大学院数理物質科学研究科講師、平成１３～１５年度；
現在電気通信大学量子・物質工学科助教授）
池沢道男（筑波大学大学院数理物質科学研究科助手）

## ２．研究経費

（金額単位：千円）

| | 直接経費 | 間接経費 | 合　計 |
|---|---|---|---|
| 平成13年度 | 25,000 | 7,500 | 32,500 |
| 平成14年度 | 32,300 | 9,690 | 41,990 |
| 平成15年度 | 11,700 | 3,510 | 15,210 |
| 平成16年度 | 11,600 | 3,480 | 15,080 |
| 平成17年度 | 11,600 | 3,480 | 15,080 |
| 総計 | 92,200 | 27,660 | 119,860 |

# Ⅱ．研究発表

## 1．学会誌等

量子ドットの緩和とコヒーレント制御に関する論文
（*印は「IV. 発表論文集」に別刷りを再録したもの）

1)* Y. Masumoto, M. Ikezawa, B.-R. Hyun, K. Takemoto and M. Furuya:
"Homogeneous Width of Confined Excitons in Quantum Dots at Very Low Temperatures"
physica status solidi (b) 224, 613 (2001); Int. Conf. Semiconductor Quantum Dots (Munich, 2000). //INVITED PAPER//

2) S.V. Nair and Y. Masumoto:
"Muli-Exciton States and Many-Body Correlations in Quantum Dots"
physica status solidi (b) 224, 739 (2001); Int. Conf. Semiconductor Quantum Dots (Munich, 2000).

3) M. Sugisaki, H.-W. Ren, I.S. Osadko, K. Nishi and Y. Masumoto:
"Fluorescence Intermittency in InP Self-Assembled Quantum Dots"
physica status solidi (b) 224, 67 (2001); Int. Conf. Semiconductor Quantum Dots (Munich, 2000).

4)* A.V. Baranov, V. Davydov, A.V. Fedorov, H.-W. Ren, S. Sugou and Y. Masumoto:
"Coherent Control of Stress-Induced InGaAs Quantum Dots by Means of Phonon-Assisted Resonant Photoluminescence"
physica status solidi (b) 224, 461 (2001); Int. Conf. Semiconductor Quantum Dots (Munich, 2000).

5) V.G. Davydov, A.V. Fedorov, I.V. Ignatiev, I.E. Kozin, H.-W. Ren, M. Sugisaki, S. Sugou and Y. Masumoto:
"Quantum Beats in Photoluminescence of InP Quantum Dots in Electric Field"
physica status solidi (b) 224, 425 (2001) ; Int. Conf. Semiconductor Quantum Dots (Munich, 2000).

6) V. Davydov, I.V. Ignatiev, I.E. Kozin, S.V. Nair, J.-S. Lee, H.-W. Ren, S. Sugou and Y. Masumoto:
"Carrier Relaxation Dynamics in Self-Assembled Quantum Dots Studied by Artificial Control of Nonradiative Losses"
physica status solidi (b) 224, 493 (2001); Int. Conf. Semiconductor Quantum Dots (Munich, 2000).

7)* Y. Masumoto, I.V. Ignatiev, I.E. Kozin, V.G. Davydov, S.V. Nair, H.-W. Ren, J.-S. Lee and S. Sugou:
"Breakdown of the Phonon Bottleneck Effect in Self-Assembled Quantum Dots"
Jap. J. Appl. Phys. 40, 1947 (2001); Proc. Third Int. Symp on Formation, Physics and Device Application of Quantum Dot Structures (Sapporo, 2000).

8)* K. Nishibayashi, T. Okuno, T. Mishina, S. Sugou, H.-W. Ren and Y. Masumoto:
"Optical Study of Strain-Induced GaAs Quantum Dots"
Jap. J. Appl. Phys. 40, 2084 (2001); Proc. Third Int. Symp on Formation, Physics and Device Application of Quantum Dot Structures (Sapporo, 2000).

9)* M. Sugisaki, H.-W. Ren, K. Nishi and Y. Masumoto:
"Fluorescence Intermittency in Self-Assembled InP Quantum Dots"
Phys. Rev. Lett. 86, 4883 (2001).

10)* J. Zhao, S.V. Nair and Y. Masumoto:
"Exciton-phonon coupled states in CuCl quantum cubes"
Phys. Rev. B 63, 033307 (2001).

11)* I.V. Ignatiev, I.E. Kozin, V.G. Davydov, S.V. Nair, J.-S. Lee, H.-W. Ren, S. Sugou and Y. Masumoto:
"Phonon resonances in photoluminescence spectra of self-assembled quantum dots in an electric field"
Phys. Rev. B 63, 075316 (2001).

12) M. Sugisaki, H.-W. Ren, K. Nishi and Y. Masumoto:
"Photoluminescence and micro-imaging study of optically anisotropic InP self-assembled quantum dots"
Solid State Commun. 117, 679 (2001).

13) M. Sugisaki, H.-W. Ren, S.V. Nair, K. Nishi and Y. Masumoto:
"Many carrier effects in self-assembled InP quantum dots"
Solid State Commun. 117, 435 (2001).

14) A.V. Fedorov, A.V. Baranov, A. Itoh and Y. Masumoto:
"Renormalization of Energy Spectrum of Quantum Dots under Vibrational Resonance Conditions"
Semiconductors 35, 1390 (2001). Translated from *Fizika i Technika Poluprovodnikov* 35, 1452 (2001).

15) Y. Masumoto:
"Energy and phase relaxation in quantum dots"
Abstracts of 8th Int. Workshop on Femtosecond Technology, p. 31 (Tsukuba, 2001). //INVITED PAPER//

16) T. Okuno, G.R. Hayes, B. Deveaud, A.A. Lipovskii and Y. Masumoto:
"Intraband transition in PbSe quantum dots"
Abstracts of 8th Int. Workshop on Femtosecond Technology, p. 82 (Tsukuba, 2001).

17) T. Okuno, M. Nomura, Y. Masumoto, Y. Terai, S. Kuroda and K. Takita:
"Eighteenth order optical phonons in CdTe quantum dots in ZnTe"
Abstracts of 1st Int. Workshop on Quantum Nonplanar Nanostructures & Nanoelectronics '01, p. 103 (Tsukuba, 2001).

18)* M. Ikezawa, T. Okuno, Y. Masumoto and A.A. Lipovskii:
"Complementary detection of confined acoustic phonons in quantum dots by coherent phonon measurement and Raman scattering"
Phys. Rev. B 64, 201315(R) (2001).

19) A.V. Fedorov, A.V. Baranov and Y. Masumoto:
"Acoustic phonon problem in nanocrystal-dielectric matrix systems"
Solid State Commun. 122, 139 (2002).

20) A.V. Fedorov, A.V. Baranov and Y. Masumoto:
"Coherent Control of the Quasi-Elastic Resonant Secondary Emission: Semiconductor Quantum Dots"
Optics and Spectroscopy 92, 732 (2002). Translated from *Optika i Spektroskopiya* 92, 797 (2002).

21) M. Sugisaki, H.-W. Ren, K. Nishi and Y. Masumoto:
"Optical Properties of InP Self-Assembled Quantum Dots Studied by Imaging and Single Dot Spectroscopy"
Jpn. J. Appl. Phys. 41, 958 (2002); 13th Int. Conf. Indium Phosphide and Related Materials (Nara, 2001). // INVITED PAPER//

22)* I.E. Kozin, V.G. Davydov, I.V. Ignatiev, A.V. Kavokin, K.V. Kavokin, G. Malpuech, H.-W. Ren, M. Sugisaki, S. Sugou and Y. Masumoto:
"Zero-field spin quantum beats in charged quantum dots"
Phys. Rev. B 65, 241312(R) (2002).

23)* I.A. Yugova, V.G. Davydov, I.Ya. Gerlovin, I.V. Ignatiev, I.E. Kozin, M. Sugisaki and Y. Masumoto:
"Spin Quantum Beats in the Stokes Shifted Photoluminescence of InP Quantum Dots"
physica status solidi (a) 190, 547 (2002).

24) 舛本泰章：
"量子ドットの分光学"
分光研究 51, 118 (2002).

25) T. Okuno, Y. Masumoto, S. Kadono, S. Kitade, H. Bando and H. Okamoto:
"Ultrafast and Wideband Response in Optical Nonlinearity of Molecular-Beam-Epitaxy-Grown GaAs"
Jpn. J. Appl. Phys. 41, L745 (2002).

26)* A.V. Baranov, V. Davydov, A.V. Fedorov, M. Ikezawa, H.-W. Ren, S. Sugou and Y. Masumoto:

"Interferometric coherence measurement of stress-induced $In_xGa_{1-x}As$/GaAs quantum dots at the resonant-luminescence phonon sideband"
Phys. Rev. B 66, 075326 (2002).

27) M. Ikezawa, K. Takemoto, J. Zhao and Y. Masumoto:
"Coherent acoustic phonons in quantum dots"
Proc. 26th Int. Conf. Physics of Semiconductors, H140.pdf. (Edinburgh, 2002).

28) K. Takemoto, M. Ikezawa and Y. Masumoto:
"Residual Dephasing mechanism at low temperature in semiconductor quantum dots"
Proc. 26th Int. Conf. Physics of Semiconductors, H145.pdf. (Edinburgh, 2002).

29) I.V. Ignatiev, I.Ya. Gerlovin, S.Yu. Verbin, I.A. Yugova and Y. Masumoto:
"Spin dynamics in the charged InP quantum dots"
Proc. 26th Int. Conf. Physics of Semiconductors, H158.pdf. (Edinburgh, 2002).

30) K. Nishibayashi, T. Okuno, I.V. Ignatiev, S. Verbin and Y. Masumoto:
"Quantum beat of strain-induced GaAs quantum dots"
Proc. 26th Int. Conf. Physics of Semiconductors, M3.4.pdf. (Edinburgh, 2002).

31) Y. Masumoto, J.L. Zhao and A. Kanno:
"Excited state LO phonons in quantum dots"
Proc. 26th Int. Conf. Physics of Semiconductors, R2.5.pdf. (Edinburgh, 2002).

32)* Y. Masumoto, M. Nomura, T. Okuno, Y. Terai, S. Kuroda and K. Takita:
"Highest-order optical phonon-mediated relaxation in CdTe/ZnTe quantum dots"
J. Lumin. 102-103, 623 (2003); Int. Conf. on Luminescence and Optical Spectroscopy of Condensed Matter (ICL '02) (Budapest, 2002).

33) Y. Masumoto, F. Naruse and A. Kanno:
"Photoinduced electric dipole in CuCl Quantum dots"
J. Lumin. 102-103, 629 (2003); Int. Conf. on Luminescence and Optical Spectroscopy of Condensed Matter (ICL '02) (Budapest, 2002).

34) Y. Masumoto, I.V. Ignatiev, I.E. Kozin, K. Nishibayashi, T. Okuno and S.Yu. Verbin:
"Luminescence quantum beats of semiconductor quantum dots"
Abstracts of 2nd Int. Workshop on Quantum Nonplanar Nanostructures & Nanoelectronics '02, p. 81 (Tsukuba, 2002). // INVITED PAPER//

35)* Y. Masumoto:
"Coherent spectroscopy of semiconductor quantum dots"
J. Lumin. 100, 191 (2002).

36) Y. Masumoto, I. Gerlovin, M. Ikezawa, I. Ignatiev, T. Okuno, S. Verbin and I. Yugova:
"Spin relaxation in InP quantum dots"
physica status solidi (c) 0, 1368 (2003); Proc. 2nd Int. Conf. on Semiconductor Quantum Dots (Tokyo, 2002).

37) A.V. Fedorov, A.V. Baranov and Y. Masumoto:
"Coherent control of resonant secondary emission of semiconductor quantum dots"
physica status solidi (c) 0, 1372 (2003); Proc. 2nd Int. Conf. on Semiconductor Quantum Dots (Tokyo, 2002).

38) K. Takemoto, M. Ikezawa and Y. Masumoto:
"Low-temperature dephasing mechanism of very small quantum dots: the role of confined phonons and surrounding matrices"
physica status solidi (c) 0, 1279 (2003); Proc. 2nd Int. Conf. on Semiconductor Quantum Dots (Tokyo, 2002).

39) A.V. Baranov, A.V. Fedorov, I.D. Rukhlenko and Y. Masumoto:
"New mechanism of intraband carrier relaxation in quantum dots"
physica status solidi (c) 0, 1217 (2003); Proc. 2nd Int. Conf. on Semiconductor Quantum Dots (Tokyo, 2002).

40) V.K. Kalevich, M. Ikezawa, T. Okuno, A.Yu. Shiryaev, A.E. Zhukov, V.M. Ustinov, P.N. Brunkov and Y. Masumoto:
"Optical spin polarization in negatively charged InAs self-assembled quantum dots under applied electric field"
physica status solidi (b) 238, 250 (2003); Proc. 2nd Int. Conf. on Semiconductor Quantum Dots (Tokyo, 2002).

41) A.V. Fedorov, A.V. Baranov and Y. Masumoto:

"Coherent Control of Thermalized Luminescence in Semiconductor Quantum Dots"
Optics and Spectroscopy 93, 555 (2002). Translated from *Optika i Spektroskopiya* 93, 604 (2002).

42)* A.V. Fedorov, A.V. Baranov and Y. Masumoto:
"Coherent Control of the fundamental transition in a single quantum dot"
Solid State Commun. 124, 311 (2002).

43) V.S. Dneprovskii, E.A. Zhukov, O.A. Shalygina, V.L. Lyaskovskii, E.A. Muljarov, S.A. Gavrilov and Y. Masumoto:
"Excitons in CdS and CdSe Semiconducting Quantum Wires with Dielectric Barriers"
J. Experimental and Theoretical Physics 94, 1169 (2002). Translated from *Zhurnal Eksperimental 'noi i Teoreticheskoi Fiziki* 121, 1362 (2002).

44)* M. Sugisaki, H.-W. Ren, S.V. Nair, K. Nishi and Y. Masumoto:
"External-field effects on the optical spectra of self-assembled InP quantum dots"
Phys. Rev. B 66, 235309 (2002).

45)* I.A. Yugova, I. Ya. Gerlovin, V.G. Davydov, I.V. Ignatiev, I.E. Kozin, H.W. Ren, M. Sugisaki, S. Sugou and Y. Masumoto:
"Fine structure and spin quantum beats in InP quantum dots in a magnetic field"
Phys. Rev. B 66, 235312 (2002).

46)* T. Okuno, M. Nomura, Y. Masumoto, Y. Terai, S. Kuroda and K. Takita:
"Optical Study of Phonon-Mediated Carrier Relaxation in CdTe/ZnTe Self-Assembled Quantum Dots"
J. Phys. Soc. Jpn. 71, 3052 (2002).

47) A.V. Fedorov, A.V. Baranov and Y. Masumoto:
"Coherent Control of Optical-Phonon-Assisted Resonance Secondary Emission in Semiconductor Quantum Dots"
Optics and Spectroscopy 93, 52 (2002).

48) Y. Masumoto:
"Optical Coherence in Semiconductor Quantum Dots"
Digest of 8th Int. Symp. on Advanced Physical Fields, p.17 (Tsukuba, 2003). // INVITED PAPER//

49)* K. Takemoto, B.-R. Hyun, M. Furuya, M. Ikezawa, J. Zhao and Y. Masumoto:
"Universal Dephasing Mechanism in Semiconductor Quantum Dots Embedded in a Matrix"
J. Phys. Soc. Jpn. 72, 249 (2003).

50) T. Okuno, M. Ikezawa, Y. Masumoto, G.R. Hayes, B. Deveaud and A.A. Lipovskii:
"1.5- μm Intraband Transitions in PbSe Quantum Dots"
Jpn. J. Appl. Phys. 42, L123 (2003).

51)* I.V. Ignatiev, I.Ya. Gerlovin, M. Ikezawa, V.K. Kalevich, S.Yu. Verbin and Y. Masumoto:
"Long-lived spin polarisation in the charged InP quantum dots"
Physica E 17, 361 (2003).

52)* I.V. Ignatiev, T. Okuno, S.Yu. Verbin, I.A. Yugova and Y. Masumoto:
"Spin quantum beats in charged and neutral InP quantum dots"
Physica E 17, 365 (2003).

53)* K. Nishibayashi, T. Okuno, Y. Masumoto and H.-W. Ren:
"Luminescence quantum beats of strain-induced GaAs quantum dots"
Phys. Rev. B 68, 035333 (2003).

54) Y. Masumoto, K. Nishibayashi and T. Okuno:
"Quantum beat of strain-induced GaAs quantum dots"
Physica E 21, 1012 (2004); 11th Int. Conf. on Modulated Semiconductor Structures (Nara, 2003).

55)* J. Zhao, A. Kanno, M. Ikezawa and Y. Masumoto:
"Longitudinal optical phonons in the excited state of CuBr quantum dots"
Phys. Rev. B 68, 113305 (2003).

56)* Y. Masumoto, I.V. Ignatiev, K. Nishibayashi, T. Okuno, S.Yu. Verbin and I.A. Yugova:
"Quantum beats in semiconductor quantum dots"
J. Lumin. 108, 177 (2004); 14th Int. Conf. on Dynamical Processes in Excited States of Solids (Christchurch, 2003).

57) K. Bando, T. Sawabe and Y. Masumoto:
"Room-temperature excitonic lasing from ZnO single nanobelts"
J. Lumin. 108, 385 (2004); 14th Int. Conf. on Dynamical Processes in Excited States of Solids (Christchurch, 2003).

58) A.V. Baranov, Yu.P. Rakovich, J.F. Donegan, T.S. Perova, R.A. Moore, D.V. Talapin, A.L. Rogach, Y. Masumoto and I. Nabiev:
"Effect of ZnS shell thickness on the phonon spectra in CdSe quantum dots"
Phys. Rev. B 68, 165306 (2003).

59) 池沢道男、奥野剛史、舛本泰章、A.A. Lipovskii：
"PbSe量子ドットの光物性"
ナノ学会会報 1, 27 (2003).

60)* A.V. Baranov, A.V. Fedorov, I.D. Rukhlenko and Y. Masumoto:
"Intraband carrier relaxation in quantum dots embedded in doped heterostructures"
Phys. Rev. B 68, 205318 (2003).

61) A.V. Fedorov, A.V. Baranov, I.D. Rukhlenko and Y. Masumoto:
"New many-body mechanism of intraband carrier relaxation in quantum dots embedded in doped heterostructures"
Solid State Commun. 128, 219 (2003).

62) Y. Masumoto:
"Four Kinds of Quantum Beats in Semiconductor Quantum Dots: A Tool to Study the Spin Structure of Quantum Dots"
Extended Abstracts of Int. Symp. on Photonics and Spintronics in Semiconductor Nanostructures, p.22 (Kyoto, 2003). //INVITED PAPER//

63) V.K. Kalevich, M. Ikezawa, T. Okuno, K.V. Kavokin, A.Yu. Shiryaev, P.N. Brunkov, A.E. Zhukkov, V.M. Ustinov and Y. Masumoto:
"Optical spin polarization of holes in negatively charged InAs/GaAs self-assembled quantum dots"
Physica E 21, 1018 (2004).

64)* Y. Masumoto, F. Suto, M. Ikezawa, C. Uchiyama and M. Aihara:
"Tunneling-induced dephasing in InP quantum dots"
Physica E 26, 413 (2005); Quantum Dots 2004 (Banff, 2004).

65)* M. Ikezawa, Y. Masumoto and H.-W. Ren:
"Observation of biexcitonic quantum beat in strain-inaduced GaAs quantum dots"
Physica E 26, 149 (2005); Quantum Dots 2004 (Banff, 2004).

66) Y. Chen, T. Okuno, Y. Masumoto, Y. Terai, S. Kuroda and K. Takita:
"Spin relaxation in CdTe/ZnTe quantum dots"
Proc. 27th Int. Conf. Physics of Semiconductors, p. 1351 (Flagstaff, 2004).

67) M. Ikezawa, Y. Masumoto and H.-W. Ren:
"Direct comparison of biexciton binding energy in a quantum well and quantum dots"
Proc. 27th Int. Conf. Physics of Semiconductors, p. 721 (Flagstaff, 2004).

68) W. Maruyama, Y. Masumoto and H.-W. Ren:
"Observation of the light-hole quantum dots in a strained GaAs quantum well"
Proc. 27th Int. Conf. Physics of Semiconductors, p. 723 (Flagstaff, 2004).

69) Y. Masumoto, F. Suto and M. Ikezawa:
"Tunneling induced dephasing and Pauli blocking in InP quantum dots"
Proc. 27th Int. Conf. Physics of Semiconductors, p. 729 (Flagstaff, 2004).

70)* S.Yu. Verbin, I.V. Ignatiev, I.Ya. Gerlovin and Y. Masumoto:
"Optical orientation of electron and nuclear spins in negatively charged InP QDs"
Proc. 27th Int. Conf. Physics of Semiconductors, p. 1417 (Flagstaff, 2004).

71) K. Bando, T. Sawabe, K. Asaka and Y. Masumoto:
"Direct observation of excitonic lasing from single ZnO nanobelts at room temperature"
Proc. 27th Int. Conf. Physics of Semiconductors, p. 894 (Flagstaff, 2004).

72)* V.K. Kalevich, I.A. Merkulov, A.Yu. Shiryaev, K.V. Kavokin, M. Ikezawa, T. Okuno, P.N. Brunkov, A.E. Zhukov, V.M. Ustinov and Y. Masumoto:
"Optical spin polarization in double charged InAs self-assembled quantum dots"
physica status solidi (a) 202, 387 (2005); 4th Int. Conf. Physics of Light-Matter Coupling in Nanostructures (St. Petersburg, 2004).

73) S. Kuroda, N. Itoh, Y. Terai, K. Takita, T. Okuno, M. Nomura and Y. Masumoto:
"MBE growth and optical properties of self-organized dots of CdTe and (Cd,Mn) Te"
J. Alloys and Compounds 371, 31 (2004).

74)* Y. Chen, T. Okuno, Y. Masumoto, Y. Terai, S. Kuroda and K. Takita:
"Spin relaxation in CdTe quantum dots"
Phys. Rev. B 71, 033314 (2005).

75)* P.-F. Braun, X. Marie, L. Lombez, B. Urbaszek, T. Amand, P. Renucci, V.K. Kalevich, K.V. Kavokin, O. Krebs, P. Voisin and Y. Masumoto:
"Direct Observation of the Electron Spin Relaxation Induced by Nuclei in Quantum Dots"
Phys. Rev. Lett. 94, 116601 (2005).

76)* V.K. Kalevich, I.A. Merkulov, A.Yu. Shiryaev, L.V. Kavokin, M. Ikezawa, T. Okuno, P.N. Brunkov, A.E. Zhukov, V.M. Ustinov and Y. Masumoto:
"Optical spin polarization and exchange interaction in doubly charged InAs self-assembled quantum dots"
Phys. Rev. B 72, 045325 (2005).

77) A.V. Maleev, U.V. Ignatiev, I.Y. Gerlovin, I.E. Kozin and Y. Masumoto:
"Temperature behavior of hot carrier dynamics in InP quantum dots"
Phys. Rev. B 71, 195323 (2005).

78) Y. Masumoto, K. Mizuochi, K. Bando and Y. Karasuyama:
"Optical anisotropy of excitons and biexcitons in InP quantum dots"
To be published in J. Lumin.; Int. Conf. on Luminescence and Optical Spectroscopy of Condensed Matter (ICL'05) (Beijing, 2005).

79) M. Ikezawa, , S.V. Nair, F. Suto, Y. Masumoto, C. Uchiyama, M. Aihara and H. Ruda:
"Photon echo study of excitons and excitonic complexes in self-assembled quantum dots"
To be published in J. Lumin.; Int. Conf. on Luminescence and Optical Spectroscopy of Condensed Matter (ICL'05) (Beijing, 2005).//INVITED PAPER//

80) A. Kanno and Y. Masumoto:
"Highly sensitive time-resolved Kerr rotation measurements on single-layer quantum dots"
To be published in J. Lumin; 15th Int. Conf. on Dynamical Processes in Excited States of Solids (DPC'05), (Shanghai, 2005).

81)* Y. Masumoto, F. Suto, M. Ikezawa, C. Uchiyama and M. Aihara:
"Non-Markovian tunneling induced dephasing in InP quantum dots"
J. Phys. Soc. Jpn. 74(11), 2933-2936 (2005).

82)* M. Ikezawa, J. Zhao, A. Kanno, and Y. Masumoto:
"Confined Acoustic Vibration Modes in CuBr Quantum Dots"
J. Phys. Soc. Jpn. 74(11), 3082-3087 (2005).

83) P.-F. Braun, X. Marie, L. Lombez, B. Urbaszek, T. Amand, P. Renucci, V.K. Kalevich, K.V. Kavokin, O. Krebs, P. Voisin and Y. Masumoto:
"Direct observation of the electron spin dephasing induced by nuclei in InAs/GaAs quantum dots"
Proc. Ioffe Institute 13th Int. Symp. "Nanostructures: Physics and Technology", p.45 (St. Petersburg, 2005).

84) I.V. Ignatiev, I.Ya. Gerlovin, S.Yu. Verbin, W. Maruyama and Y. Masumoto:
"Effect of nuclear spins on the electron spin dynamics in negatively charged InP quantum dots"
Proc. Ioffe Institute 13th Int. Symp. "Nanostructures: Physics and Technology", p.47 (St. Petersburg, 2005).

85) I.Ya. Gerlovin, I.V. Ignatiev, B. Pal, S.Yu. Verbin and Y. Masumoto:
"Spin relaxation in magnetic field for InP quantum dots"
Proc. Ioffe Institute 13th Int. Symp. "Nanostructures: Physics and Technology", p.63 (St. Petersburg, 2005).

86)* M. Ikezawa, B. Pal, Y. Masumoto, I.V. Ignatiev, S.Yu. Verbin and I.Ya. Gerlovin:
"Submillisecond electron spin relaxation in InP quantum dots"
Phys. Rev. B 72, 153302 (2005).

87) M. Ikezawa, F. Suto, Y. Masumoto and H.-W. Ren:

"Detection of four-wave mixcing signal from single layer quantum dots"
in "Ultrafast Phenomena XIV" ed. T. Kobayashi, T. Okada, T. Kobayashi, K.A. Nelson and S. De Silvestri (Springer 2005) p.301-p.303; Proc. 14th Int. Conf. on Ultrafast Phenomena, (Niigata, 2004).

88)* A. Kanno and Y. Masumoto:
"Spin relaxation mechanism of strain-induced GaAs quantum dots studied by time-resolved Kerr rotation"
To be published in Phys. Rev. B.

89)* M. Ikezawa, S.V. Nair, H.-W. Ren, Y. Masumoto and H. Ruda:
"Biexciton binding energy in parabolic GaAs quantum dots"
To be published in Phys. Rev. B.

90)* B. Pal, M. Ikezawa, Y. Masumoto and I.V. Ignatiev:
"Millisecond-range electron spin memory in singly-charged InP quantum dots"
Submitted to J. Phys. Soc. Jpn.

その他の論文

91) J. Qi, T. Matsumoto and Y. Masumoto:
"Characterization of Simultaneously Fabricated Silicon and Silicon Monoxide Nanowires"
Jpn. J. Appl. Phys. 40, L134 (2001).

92) J. Qi, X. Guo, K. Sakurai and Y. Masumoto:
"Atomic structure around Mn ions in $Zn_{1-x}Mn_xS$ (x = 0.01-0.02) nanocrystals prepared by colloidal chemistry procedure"
Scripta Materialia 44, 2315 (2001); Proc. 5th Int. Conf. Nanostructured Materials (Sendai, 2000).

93) J. Qi and Y. Masumoto:
"Copper silicide nanocrystals in silicon nanowires"
Materials Research Bulletin 36, 1407 (2001).

94) T. Matsumoto, J. Suzuki, M. Ohnuma, Y. Kanemitsu and Y. Masumoto:
"Evidence of Quantum Size Effect in Nanocrystalline Silicon by Optical Absorption"
Phys. Rev. B 63, 195322 (2001).

95) E. Tokunaga, A.L. Ivanov, S.V. Nair and Y. Masumoto:
"Hopfield coefficients measured by inverse polariton series"
Phys. Rev. B 63, 233203 (2001).

96) T. Okuno, Y. Masumoto, Y. Sakuma, Y. Hayasaki, S. Kadono and H. Okamoto:
"Fast Response Time in Optical Nonlinearity of MBE-grown GaAs/AlAs MQW at aroud n=2 Level"
Abstracts of 8th Int. Workshop on Femtosecond Technology, p. 145 (Tsukuba, 2001).

97) E. Tokunaga, K. Kurihara, M. Baba, Y. Masumoto and M. Matsuoka:
"Bipolariton coupling in biexciton optical decay: Degenerate and nondegenerate polariton emissions in CuCl"
Phys. Rev. B 64, 045209 (2001).

98) T. Okuno, Y. Masumoto, Y. Sakuma, Y. Hayasaki and H. Okamoto:
"Femtosecond response time in beryllium-doped low-temperature-grown GaAs/AlAs multiple quantum wells"
Appl. Phys. Lett. 79, 764 (2001).

99) M. Tanaka and Y. Masumoto:
"Energy transfer mechanism in $Mn^{2+}$ doped CdS nanocrystals"
Solid State Commun. 120, 7 (2001).

100) I.Ya. Gerlovin, Yu.K. Dolgikh, S.A. Eliseev, V.V. Ovsyankin, Yu.P. Efimov, V.V. Petrov, I.V. Ignatiev, I.E. Kozin and Y. Masumoto:
"Fine structure and spin dynamics of excitons in the $GaAs/Al_xGa_{1-x}As$ superlattices"
Phys. Rev. B 65, 035317 (2001).

101) T. Miyajima, T. Hino, S. Tomiya, K. Yanashima, H. Nakajima, T. Araki, Y. Nanishi, A. Satake, Y. Masumoto, K. Akimoto, T. Kobayashi and M. Ikeda:
"Threading Dislocations and Optical Properties of GaN and GaInN"

physica status solidi (b) 228, 395 (2001).

102) T. Matsumoto, Y. Masumoto, S. Nakashima and N. Koshida:
"Luminescence from deuterium-terminated porous silicon"
Thin Solid Films 297, 31 (1997).

103) T. Matsumoto, A.I. Belogorokhov, L.I. Belogorokhova, Y. Masumoto and E.A. Zhukov:
"The effect of deuterium on the optical properties of free-standing porous silicon layers"
Nanotechnology 11, 340 (2000).

104) J. Qi, J.M. White, A.M. Belcher and Y. Masumoto:
"Optical spectroscopy of silicon nanowires"
Chem. Phys. Lett. 372, 763 (2003).

105) I.Ya. Gerlovin, Yu.K. Dolgikh, S.A. Eliseev, V.V. Ovsyankin, Yu.P. Efimov, I.V. Ignatiev, V.V. Petrov, S.Yu. Verbin and Y. Masumoto:
"Spin dynamics of carriers in GaAs quantum wells in an external electric field"
Phys. Rev. B 69, 035329 (2004).

106) H. Udono, I Kikuma, T. Okuno, Y. Masumoto and H. Tajima:
"Indirect optical absorption of single crystalline β-$FeSi_2$"
Appl. Phys. Lett. 85, 1937 (2004).

107) H. Udono, I. Kikuma, T. Okuno, Y. Masumoto, H. Tajima and S. Komuro:
"Optical properties of β-$FeSi_2$ single crystals grown from solutions"
Thin Solid Films 461, 182 (2004).

108) T. Okuno, Y. Masumoto, A. Higuchi, H. Yoshino, H. Bando and H. Okamoto:
"Absorption Saturation Energy Density of InGaAs-InAlAs Multiple Quantum Well under Tensile and Compressive Strain"
Jpn. J. Appl. Phys. 44, L558 (2005).

109) H. Bando, M. Kosuge, K. Ban, H. Yoshino, R. Takahashi, H. Okamoto, T. Okuno and Y. Masumoto:
"Crosshatch observation in MBE-grown Be-doped InGaAs epilayer on InP"
J. Cryst. Growth 278, 610 (2005).

110) A.Yu. Egorov, V.K. Kalevich, M.M. Afanasiev, A.Yu.Shiryaev, V.M. Ustinov, M. Ikezawa and Y. Masumoto:
"Determination of strain-induced valence-band splitting in GaAsN thin films from circularly polarized photoluminescence"
J. Appl. Phys. 98, 013539 (2005).

111) V.K. Kalevich, E.L. Ivchenko, M.M. Afanasiev, A.Yu. Egorov, A.Yu. Shiryaev, V.M. Ustinov, B. Pal and Y. Masumoto:
"Spin-dependent recombination in GaAsN alloys"
JETP Letters, 82, 455 (2005).

112) K. Bando, T. Nakamura, Y. Masumoto, F. Sasaki, S. Kobayashi and S. Hotta:
"Origin of the amplified spontaneous emission from thiophene/phenylene co-oligomer single crystals: Towards co-oligomer lasers"
J. Appl. Phys. 99, 013518 (2006).

## 2．口頭発表

1) 池沢道男、奥野剛史、舛本泰章、A.A. Lipovskii：“PbSe量子点に閉じ込められた音響型フォノンのラマン散乱とコヒーレントフォノン”日本物理学会（2001年9月）
2) 奥野剛史、池沢道男、A.A. Lipovskii、舛本泰章：“PbSe量子点における近赤外バンド内遷移”日本物理学会（2001年9月）
3) 舛本泰章、成瀬文隆、菅野敦史：“CuCl量子点における光誘起電気双極子”日本物理学会（2001年9月）
4) 舛本泰章、I.E. Kozin, I.V. Ignatiev, V.G. Davydov, H.-W. Ren, 杉崎満、K.V. Kavokin, A.V. Kavokin, G. Malpuech：“イオン化量子点の発光が示す量子ビート”日本物理学会（2001年9月）
5) 門野真二郎、北出晋介、岡本紘、奥野剛史、舛本泰章：“GaAsの光吸収飽和過渡特性の波長依存性”応用物理学会（2001年9月）

6) 北出晋介、早崎裕一、岡本紘、奥野剛史、舛本泰章：“GaAs/AlAs量子井戸構造の光吸収飽和過渡特性の波長依存性”応用物理学会（2001年9月）
7) 竹本一矢、池沢道男、舛本泰章：“CuBr量子点の均一幅の温度依存性再考”日本物理学会（2002年3月）
8) 奥野剛史、野村光宏、舛本泰章、寺井慶和、黒田眞司、滝田宏樹：“CdTe自己形成量子ドットにおけるキャリア緩和と多フォノン観測”日本物理学会（2002年3月）
9) 舛本泰章：“量子ドットのコヒーレンスと量子ビート”（シンポジウム講演）日本物理学会（2002年3月）
10) 舛本泰章、I.A. Yugova, I.V. Ignatiev, I.E. Kozin, V.G. Davydov, I.Ya. Gerlovin, 杉崎満：“InP量子ドットの発光が示す量子ビート”日本物理学会（2002年3月）
11) 原田慎一朗、北出晋介、岡本紘、奥野剛史、舛本泰章：“低温MBE成長BeドープGaAsの二重パルス励起における光吸収飽和過渡特性” 応用物理学会 （2002年3月）
12) 北出晋介、門野真二郎、岡本紘、奥野剛史、舛本泰章：“低温MBE成長BeドープGaAsの光吸収飽和過渡特性の波長依存性” 応用物理学会（2002年3月）
13) 坂東弘之、守山佳、岡本紘、奥野剛史、舛本泰章：“GaAs-AlAs MQWの光非線形性とその高速応答化における井戸幅依存性” 応用物理学会（2002年3月）
14) M. Ikezawa, V.K. Kalevich, A.E. Zhukov, V.M. Ustinov, Y. Masumoto: “Optical spin polarization in n-i-n structure with InAs self-assembled quantum dots” 日本物理学会（2002年9月）
15) 舛本泰章、I.V. Ignatiev, I.A. Yugova, S.Yu. Verbin, 西林一彦、奥野剛史：“量子ドットの発光の示す4種類の量子ビート” 日本物理学会（2002年9月）
16) 阪東一毅、沢辺大樹、舛本泰章：“ZnO単一ナノワイヤーの光学的特性” 日本物理学会（2002年9月）
17) 三上紋、丸山理、舛本泰章：“自己形成InP量子ドットの非線形発光” 日本物理学会（2002年9月）
18) 丸山理、舛本泰章：“歪誘起InGaAs量子ドットの非線形発光” 日本物理学会（2002年9月）
19) 菅野敦史、舛本泰章：“銅ハライド量子点におけるLOフォノンのソフトニング” 日本物理学会（2002年9月）
20) 池沢道男、舛本泰章：“ガラス中の半導体量子点におけるLOフォノンのソフトニング” 日本物理学会（2002年9月）
21) 鵜殿治彦、菊間勲、奥野剛史、舛本泰章：“β-$FeSi_2$バルク単結晶の光吸収測定（Ⅱ）” 応用物理学会（2002年9月）
22) 坂東弘之、神園利成、岡本紘、奥野剛史、舛本泰章：“低温MBE成長BeドープGaAs薄膜におけるアンチサイトAs濃度” 応用物理学会（2002年9月）
23) 北出晋介、坂東弘之、岡本紘、奥野剛史、舛本泰章：“低温MBE成長BeドープGaAsの光吸収飽和過渡特性のパルス幅依存性” 応用物理学会（2002年9月）
24) 奥野剛史、池沢道男、舛本泰章：“半導体量子ドットにおける光非線形性の高速緩和” 第1回ナノテクノロジー総合シンポジウム（JAPAN NANO 2003） 東京都有明 2003年2月3, 4日 講演予稿集 pp.130-131.
25) 樋口彰、坂東弘之、岡本紘、奥野剛史、舛本泰章：“低温MBE成長BeドープGaAs薄膜における$Be^{-}$-$As_{Ga}^{+}$複合欠陥による発光再結合の調査” 応用物理学会（2003年3月）
26) 桜井あやの、樋口彰、坂東弘之、岡本紘、奥野剛史、舛本泰章：“$In_xGa_{1-x}As$/AlAs歪量子井戸構造における光吸収飽和特性” 応用物理学会（2003年3月）
27) 藤谷論、吉野英生、吉成伸夫、坂東弘之、岡本紘、奥野剛史、舛本泰章：“$In_xGa_{1-x}As/In_{0.52}Al_{0.48}As$歪量子井戸構造の吸収飽和過渡特性” 応用物理学会（2003年3月）
28) 阪東一毅、沢辺大樹、舛本泰章：“ZnO単一ナノベルトの室温レーザー発振” 日本物理学会（2003年3月）
29) 西林一彦、奥野剛史、I.V. Ignatiev、舛本泰章：“歪み誘起GaAs量子ドットにおける量子ビートの研究” 日本物理学会（2003年3月）
30) 菅野敦史、池沢道男、舛本泰章：“歪み誘起GaAs量子ドットの四光波混合” 日本物理学会（2003年3月）
31) 樋口彰、高橋了、吉野英生、坂東弘之、岡本紘、奥野剛史、舛本泰章：“$In_xGa_{1-x}As/In_{0.52}Al_{0.48}As$

歪量子井戸構造における光吸収飽和特性”　応用物理学会（2003年8月）
32) 高橋了、樋口彰、吉野英生、坂東弘之、岡本紘、奥野剛史、舛本泰章：“低温MBE成長Beドープ InGaAs薄膜及びInGaAs/InAlAs MQWにおける吸収飽和励起光密度の波長依存性” 応用物理学会（2003年8月）
33) 池沢道男、舛本泰章：“光ヘテロダイン法による半導体量子点におけるFWM信号検出”　日本物理学会（2003年9月）
34) 菅野敦史、舛本泰章：“銅ハライド量子点のスピン緩和”　日本物理学会（2003年9月）
35) 阪東一毅、沢辺大樹、舛本泰章：“ZnOナノベルトのレーザー発振特性”　日本物理学会（2003年9月）
36) V.K. Kalevich, M. Ikezawa, A.Yu. Shiryaev, A.Yu. Egorov, V.M. Ustinov and Y. Masumoto：“Influence of strain-induced valence band-splitting on optical orientation in dilute $GaAs_{1-x}N_x$ alloys”　日本物理学会（2003年9月）
37) Y. Chen, T. Okuno and Y. Masumoto：“Relaxation of carriers in CdTe self-assembled quantum dots in the magnetic field”　日本物理学会（2003年9月）
38) 丸山理、舛本泰章：“歪誘起GaAs量子ドットの円偏光励起スペクトル”　日本物理学会（2003年9月）
39) 舛本泰章、西林一彦、奥野剛史：“歪誘起GaAs量子ドットにおけるスピン量子ビート”　日本物理学会（2003年9月）
40) 舛本泰章、池沢道男、奥野剛史、I.V. Ignatiev, S. Yu. Verbin：“電子がドープされたInP量子ドットの示す長時間スピン偏極”　日本物理学会（2003年9月）
41) 舛本泰章、V.K. Kalevich、池沢道男、奥野剛史、A.Yu. Shiryaev、K.V. Kavokin、P.N. Brunkov、A.E. Zhukov、V.M. Ustinov：“電子ドープInAs量子ドットの円偏光メモリー”　日本物理学会（2004年3月）
42) 丸山理、池沢道男、舛本泰章：“結合GaAs量子井戸に形成される歪誘起量子ドットの円偏光励起スペクトル”　日本物理学会（2004年3月）
43) 池沢道男、舛本泰章：“歪誘起GaAs量子ドットのフォトンエコー”　日本物理学会（2004年3月）
44) 徳永英司、小林孝嘉、李定植、西研一、舛本泰章：“マルチチャンネルロックインによる単一量子点の非線形吸収分光”　日本物理学会（2004年3月）
45) 須藤史敬、池沢道男、舛本泰章：“単層InP量子ドットにおけるフォトンエコー”　日本物理学会（2004年3月）
46) 坂東弘之、野口あゆみ、岡本紘、奥野剛史、舛本泰章：“InGaAs/InAlAs MQWにおける外部応力による吸収飽和励起光密度の変化”，応用物理学会（2004年3月）
47) 吉田道弘、高橋了、坂東弘之、岡本紘、奥野剛史、舛本泰章：“MBE成長InGaAs/InAlAs MQWにおける電界効果による吸収飽和励起光密度の低減”，応用物理学会（2004年3月）
48) 高橋了、吉野英生、坂東弘之、岡本紘、奥野剛史、舛本泰章：“低温MBE成長BeドープInGaAs薄膜における吸収飽和励起光密度の波長特性”，応用物理学会（2004年3月）
49) 樋口彰、坂東弘之、岡本紘、奥野剛史、舛本泰章：“低温MBE成長BeドープGaAs薄膜における$Be^{-}$-$As_{Ga}^{+}$複合欠陥による発光再結合”，応用物理学会（2004年3月）
50) 中村俊輝、阪東一毅、舛本泰章、小林俊介、佐々木史雄、堀田収：“（チオフェン/フェニレン）コオリゴマー結晶の低温における光物性”　応用物理学会（2004年3月）
51) 阪東一毅、沢辺大樹、舛本泰章：“単一ZnOベルト状ウィスカー結晶の室温励起子レーザー発振”　応用物理学会（2004年3月）
52) 丸山理、舛本泰章：“歪誘起 GaAs 量子ドットの円偏光時間分解発光”　日本物理学会（2005年 9 月）
53) Ye Chen、奥野剛史、舛本泰章、寺井慶和、黒田眞司、瀧田宏樹：“CdTe 量子ドットにおけるスピン緩和”　日本物理学会（2005 年 9 月）
54) 池沢道男、舛本泰章：“磁場下における歪誘起 GaAs 量子ドットのフォトンエコー”　日本物理学会（2005 年 9 月）
55) 須藤史敬、池沢道男、舛本泰章、内山智香子、相原正樹：“InP 量子ドットにおけるトンネリングに起因した位相緩和”　日本物理学会（2005 年 9 月）
56) 坂東弘之、高橋了、伊藤靖浩、岡本紘、奥野剛史、舛本泰章：“InGaAs バルク薄膜の光吸収飽和特性の加圧効果”　応用物理学会（2004 年 9 月）

57) 菅野敦史、舛本泰章："半導体ナノ構造の光誘起カー回転Ⅱ"　日本物理学会（2005年3月）
58) 舛本泰章："半導体量子ドットのスピンダイナミクス"　日本物理学会（2005年3月）
59) 阪東一毅、中村俊輝、舛本泰章、小林俊介、佐々木史雄、堀田収："(チオフェン/フェニレン)コオリゴマー結晶の光励起レーザー発振"　応用物理学会（2005年3月）
60) 高橋了、坂東弘之、松本俊夫、奥野剛史、舛本泰章："Ⅲ-Ⅴ族化合物半導体における2光子吸収特性"　応用物理学会（2005年3月）
61) 阪東一毅、中村俊輝、舛本泰章、小林俊介、佐々木史雄、堀田収："(チオフェン/フェニレン)コオリゴマー結晶の吸収端近傍における光学遷移"　日本物理学会（2005年9月）
62) 菅野敦史、舛本泰章："半導体ナノ構造の光誘起カー回転Ⅲ"　日本物理学会（2005年9月）
63) 藤原聖士、阪東一毅、舛本泰章、佐々木史雄、小林俊介、堀田収："高密度励起下における（チオフェン/フェニレン）コオリゴマー結晶の時間分解分光"　日本物理学会（2005年9月）
64) 池沢道男、大島隆治、舛本泰章、岡田至崇："InGaAs量子ドットにおけるフォトンエコー"　日本物理学会（2005年9月）
65) B. Pal、池沢道男、舛本泰章、I.V. Ignatiev："Very long spin memory in InP quantum dots observed in pump-probe photoluminescence spectroscopy"　日本物理学会（2005年9月）
66) 烏山陽子、水落清、阪東一毅、舛本泰章："InP単一量子ドットの励起子・励起子分子の光学異方性"　日本物理学会（2005年9月）
67) 小口修平、池沢道男、舛本泰章："InP量子ドットにおけるスピン緩和2"　日本物理学会（2005年9月）
68) 舛本泰章："半導体量子ドット中のキャリア間相互作用の時間分解測定"　日本物理学会（2006年3月）
69) 舛本泰章、須藤史敬、池沢道男："チャージチューナブルInP量子ドットのフォトンエコー"（2006年3月）
70) 藤原聖士、阪東一毅、舛本泰章、佐々木史雄、小林俊介、堀田収："高密度励起下における(チオフェン/フェニレン)コオリゴマー結晶の時間分解分光Ⅱ"　日本物理学会（2006年3月）

3．出版物

B1) Y. Masumoto and T. Takagahara, eds., *Semiconductor Quantum Dots - Physics, Spectroscopy and Applications*, Springer-Verlag, 2002.
B2) Y. Masumoto: "Persistent Spectral Hole Burning in Semiconductor Quantum Dots" in "Semiconductor Quantum Dots - Physics, Spectroscopy and Applications" eds. Y. Masumoto and T. Takagahara p.209-p.244 (Springer-Verlag, 2002).
B3) Y. Masumoto: "Homogeneous Width of Confined Excitons in Quantum Dots - Experimental" in "Semiconductor Quantum Dots - Physics, Spectroscopy and Applications" eds. Y. Masumoto and T. Takagahara p.325-p.351 (Springer-Verlag, 2002).
B4) 舛本泰章：人工原子，量子ドットとは何か（pp.129-204）（「現代物理最前線6」大槻義彦編、共立出版、2002）
B5) 舛本泰章：28・5・1 超高速分光—1（pp.665-670）（「レーザーハンドブック（第2版）」レーザー学会編、オーム社、2005）
B6) 舛本泰章：フェムト秒分光の原理，技術と応用（「フェムト秒テクノロジー—基礎と応用」平尾一之、邱建栄編、化学同人、2006）(出版予定)

4．研究成果による工業所有権の出願・取得状況

[1] 舛本泰章：「輝尽性発光素子及びその製造方法」、出願番号：特願平 11-024578、出願日：1999.2.2、公開番号：特開 2002-219877、公開日：2000.8.8、特許番号：特許第 3529654 号、登録日：2004.3.5
[2] 舛本泰章：「アップ・コンバージョン素子」、出願番号：特願 2000-008029、2000.1.17 出願
[3] 戚継発、舛本泰章：「酸化珪素のナノワイヤの製造方法」、出願番号：特願 2000-342408、2000.11.9 出願　特許第 3571287 号、登録日：2004.7.2

[4] 岡本紘、舛本泰章、奥野剛史、佐久間康、早崎裕一、門野真二郎：「面型光－光スイッチおよびその製造方法」、出願番号：特願 2001-105633、2001.04.04 出願、公開番号：特許公開 2002-303893
[5] 岡本紘、舛本泰章、奥野剛史、佐久間康、早崎裕一、門野真二郎：「半導体光非線形装置」、出願番号：特願 2001-273313、2001.09.10 出願、公開番号：特許公開 2003-084321
[6] 岡本紘、坂東弘之、舛本泰章、奥野剛史：「超高速・広帯域の光可飽和吸収半導体装置」、出願番号：特願 2002-1577、2002.01.08 出願
[6'] [6]より手続き補正 岡本紘、坂東弘之、舛本泰章、奥野剛史：「超高速・広帯域の光可飽和吸収半導体装置、それを用いた半導体装置および導波路型光－光スイッチ」、出願番号：特願 2002-141011、2002.05.16 出願 公開番号：特開 2003-270696
[7] 岡本紘、坂東弘之、舛本泰章、奥野剛史、樋口彰、吉野英生、高橋了：「光非線形半導体装置およびその製造方法」、出願番号：特願 2003-297542、2003.08.22 出願
[8] 岡本紘、坂東弘之、高橋了、吉野英生、舛本泰章、奥野剛史：「半導体素子」、出願番号：特願 2004-249408、2004.8.30 出願

## Ⅲ．研究成果

# 量子ドットの緩和とコヒーレント制御

筑波大学大学院数理物質科学研究科　舛本泰章

### １．研究の背景と目的

人工原子と呼ばれる半導体量子ドットは、量子化されたエネルギースペクトルを持つ。この量子化されたエネルギースペクトルが、“線幅がどこまで狭くなるか？”言い換えれば、“どこまで長いコヒーレンス時間を持つか？”を明らかにすることは、“原子状”の、しかし原子とは異なる量子ドットの本質と関わる重要な課題である。

本研究ではこの問題意識のもとに、2001年度から開始された研究の当初、次に列挙する問題を研究する目的でスタートを切った。

1) レーザー分光法を用いスペクトル領域と時間領域の両面から、**低温の極限で量子ドット中に量子化された電子や励起子のコヒーレント緩和（均一幅）を明らかにする。**すなわち半導体量子ドットの量子化されたエネルギースペクトルの“線幅がどこまで狭くなるか？”言い換えれば、“どこまで長いコヒーレンス時間を持つか？”を明らかにする。この問題は、“原子状”の、しかし原子とは異なる量子ドットの本質と関わる基本問題である。
2) 次に、**量子ドットのコヒーレント制御を実現する。**長時間コヒーレンスを利用して量子ドットのコヒーレント制御とその応用が可能になる。量子ドットの双極子のコヒーレント振動を励起したり、止めたり、自由自在に制御することで、量子コンピューティングに繋がる基本的技術を開拓する。
3) また、**量子化された電子準位間のエネルギー緩和（フォノン緩和）機構を明らかにする。**フォノンボトルネック効果に関する実験と理論の対立を明確な形で決着させる。

一方、2003年までのInP自己形成量子ドットの量子ビートの研究の進展により、これが電気バイアスにより自由にドットの電荷状態を制御できる**チャージチューナブル量子ドットであることを見出し、電荷状態を制御しながら量子ドットの電子スピンの緩和やコヒーレンスの研究**を行うことを量子ドットの緩和とコヒーレント制御研究の次の重要な展開と位置づけることとした。また、単層量子ドットのコヒーレンス研究が可能となる超高感度ヘテロダイン検出フォトンエコー測定法を開発し、単層量子ドットのコヒーレンス研究を展開することとした。

### ２．研究実績の概要

量子ドット中の電子や励起子の高速エネルギー緩和およびコヒーレント緩和、量子ビート、フォノンと励起子－フォノン結合状態について系統的な研究を行った。

### ２．１　量子ドット中の高速エネルギー緩和

＜自己形成量子ドットにおけるフォノン緩和＞[論文 6,7*,11*,15,B1,B4]

InP や InGaAs 自己形成量子ドットに負のバイアスをかけ、量子ドットから光励起された正孔を抜き取る事で非輻射緩和速度を制御し、量子ドット中の離散的なエネルギー準位間の電子の光学型フォノン（LO）、音響型フォノンを伴うエネルギー緩和と競合させる事で、フォノン緩和を定常ルミネッセンススペクトルおよびその励起スペクトル上にフォノン構造として明瞭に観測できる。一方、バイアスを増加させながら発光スペクトル中の各部をストリークカメラにより時間変化を調べると、LO フォノン構造の部分では減衰時間が速くなり、非輻射減衰にむかう様子がよく観測される。発光の立ち上がりの部分では、LO フォノン構造が発光スペクトル中に観測されるエネルギーではストリークカメラシステムの時間分解能で制約される立ち上がりを示すが、音響型フォノン構造がスペクトル中に観測されるエネルギーでは約 50ps の立ち上がり時間を示し、フォノンボトルネック効果を示す理論計算で予想されるフォノン緩和に比べはるかに速い緩和速度にはなっている。こうした定常発光スペクトルおよび時間分解発光の両面からフォノン緩和の様子が明らかにされた。量子ドット中の LO フォノン緩和は十分速く、理想的量子ドットについて考えられたフォノンボトルネック効果は、自己形成量子ドットでは実験的に否定されたことにな

る。これにより、初期の研究目的の３）は達成された。

＜CdTe 自己形成量子ドットにおけるフォノン緩和＞［論文 17,32*,46*］

ZnTe 上に成長された自己形成 CdTe 量子ドットについて、ZnTe 層を励起したとき 19 次もの高次 LO フォノンカスケード緩和過程を発光の励起スペクトルに観測した（図１）。これは、ZnTe 層中で強い電子・LO フォノン相互作用が高速の高次 LO フォノンカスケード緩和過程を引き起こし、CdTe 量子ドットが ZnTe のバンドギャップより高いエネルギーで光励起されたキャリアーを高効率に集めていることを表す。また、共鳴励起の発光スペクトルに観測される LO フォノン構造のエネルギーから、CdTe 量子ドットのまわりは $Zn_xCd_{1-x}Te$ 混晶（x は約 0.8 で、0.5 から 1 の範囲に分布）になっていることが明らかにされた。

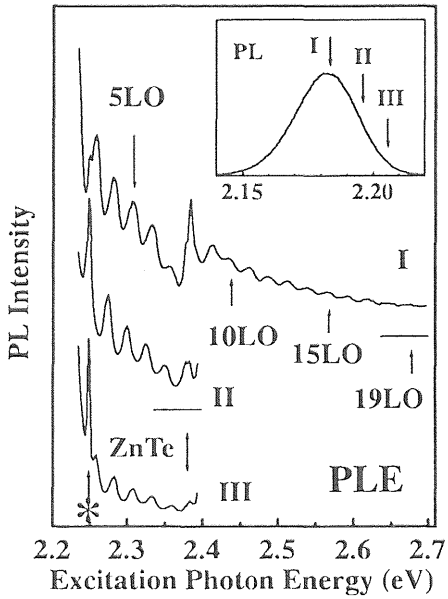


図１　自己形成 CdTe 量子ドットの発光の励起スペクトルに見られる 19 次 LO フォノンカスケード緩和過程

＜電子ドープされた半導体基板上の量子ドットにおける電子のエネルギー緩和＞[論文 60*,61]

n-GaAs 基板上に成長された自己形成 InAs 量子ドットにおいて、量子ドットの共鳴二次発光スペクトル中に量子ドットから 100nm 離れた n-GaAs 基板の LO-プラズモン結合モードの上枝、下枝の二つの分枝が見られ、量子ドットの電子準位に共鳴増大する現象が観測された。長距離クーロン相互作用がこのような離れた位置での LO-プラズモン結合モードが観測される原因であるが、LO-プラズモン結合モードは LO フォノンに比べてエネルギー的に広い広がりを持ち、電子の LO モードの放出によるエネルギー緩和においてフォノンボトルネック効果を示す理論計算で予想されるフォノン緩和に比べ LO-プラズモン結合モードによる緩和はるかに緩和速度を速めることが理論的に示された。

２．２　量子ドットの光スペクトルの均一幅とコヒーレンス緩和機構の解明

“原子状”の量子ドットの本質と関わる基本問題である量子ドット中のコヒーレント緩和（均一幅）を解明した。マイケルソン干渉計で作られたフェーズロック光パルス列で励起しながら、＜共鳴二次発光を用いた歪誘起 InGaAs/GaAs 量子ドットの位相緩和測定＞を実証し、励起子の均一幅を蓄積フォトンエコー法により時間領域から＜マトリックス中の CdSe および CuBr 量子ドットにおける励起子の位相緩和メカニズム＞を 0.7K の極低温まで測定し、量子ドットにおける低温均一幅の温度依存性は、温度に依存しない成分、励起子－二準位系間の相互作用、励起子－閉じ込め音響フォノン間の相互作用（２フォノンラマン過程）の３つの和で統一的・普遍的に記述できることを明らかにした。

＜共鳴二次発光を用いた歪誘起 InGaAs/GaAs 量子ドットの位相緩和測定＞[論文 4,20,24,26*,35*]

マイケルソン干渉計を用いて作られたフェーズロックされた光パルス列で励起しながら、共鳴光励起下の歪誘起 InGaAs/GaAs 量子ドットの光スペクトルの均一幅（あるいは位相緩和時間）を LO フォノンのエネルギーだけストークスシフトした共鳴二次発光をモニターすることで測定した。この新しい方法は弱励起下で低密度の量子ドットの位相緩和測定法として有効である。共鳴二次発光の時間相関は位相緩和時間に由来する幅や裾を示し、2 K で量子ドットの位相緩和時間は発光スペクトル中の低エネルギー部分で 16～18 ps と評価され、高エネルギー側で短くなっていく様子が観測された。

＜マトリックス中の CdSe および CuBr 量子ドットにおける励起子の位相緩和メカニズム＞[論文 1*,15,24,28,35*,38,49*,B1,B4]

ヘテロダイン蓄積フォトンエコー法を用いて、弱励起で量子ドットの位相緩和時間を評価する試みを行った。ヘテロダイン蓄積フォトンエコー法は、特徴として①高感度なため微弱光を用い

て強励起効果を避けることができる、②単一ドット発光のように分光器の分解能に制限されない、という点が挙げられる。

強い閉じ込め領域の典型である CdSe 量子ドットと、弱い閉じ込め領域の CuBr 量子ドットの2種類の試料を用いて、0.7K の極低温まで励起子の均一幅を蓄積フォトンエコー法により時間領域から測定し、その温度依存性の詳細な検討を行った（図2）。その結果量子ドットにおける低温均一幅の温度依存性は、温度に依存しない成分、励起子－二準位系間の相互作用、励起子－閉じ込め音響フォノン間の相互作用（2フォノンラマン過程）の3つの和で統一的に記述できることが明らかにされた。低温で均一幅として 1μeV にもなり、マトリクスの違いが低温において顕著になっていることが明らかにされた。CuCl 量子ドットについての以前の研究と CdSe, CuBr 量子ドットについての研究から、強い閉じ込め領域から弱い閉じ込め領域にわたる量子ドットで、量子ドットに閉じ込められ量子化された音響フォノンと、それを囲むマトリクス中の微小エネルギーの励起が、寿命に加えて低温における量子ドットの均一幅を決定づける普遍的メカニズムであると結論することができる。

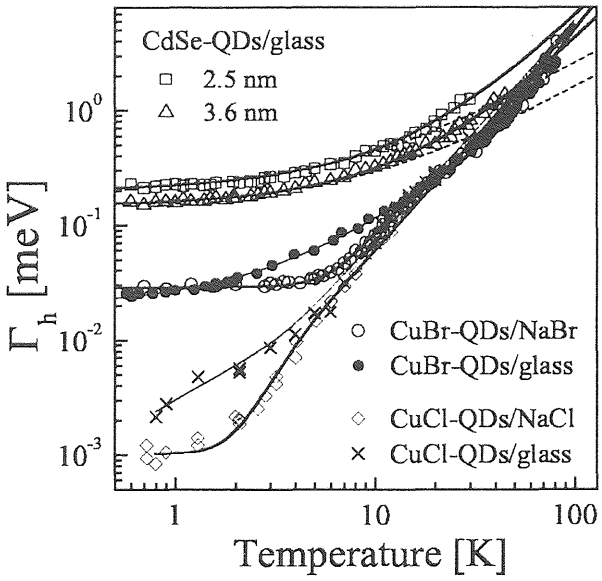


図2　CuCl、CuBr、CdSe 量子ドット中の励起子の均一幅の温度依存性

この研究により量子ドットにおける励起子のコヒーレント緩和機構について統一的な描像を得た。これにより、初期の研究目的1）は達成した。

## 2．3　量子ドットのフォノンと励起子－フォノン結合状態

量子ドットでは、音響フォノンのエネルギーが、閉じ込めによって離散的になる。離散化は励起子のドットのエネルギー緩和やコヒーレント緩和過程をバルクのものとは著しく変えるので、緩和過程の理解のためフォノンの理解が必要になる。量子ドット特有の閉じ込めを受けた音響型フォノンと電子励起状態における光学型フォノンのソフトニングについて集中的に研究した。

＜PbSe 量子ドットのコヒーレントフォノンとラマン散乱＞[論文 18*,24,59]

量子ドットに閉じ込めを受けた音響型フォノンは量子ドットの光スペクトルの均一幅や位相緩和時間を低温で支配しており極めて重要である。燐酸ガラス中に析出させた PbSe 量子ドットに閉じ込めを受けた音響型フォノンを、コヒーレントフォノンとラマン散乱による2つの観測を行い、それぞれ l=0 の全対称なブリージングモードとよりエネルギーの低い l=2 のスフェロイダルモードという異なる相補的な閉じ込めを受けた音響型フォノンが観測されることが示された。

図3で(a)は半径 2.9nm の PbSe 量子ドットの吸収スペクトル、(b)はコヒーレントな音響フォノンの振動の様子を示している。コヒーレントフォノンは、吸収スペクトルを僅かに（~$10^{-8}$）時間的に変調し、透過率の変化として観測される。得られた信号をフーリエ変換したものが、(b)の挿入図の破線である。同試料についてラマン散乱を測定した結果が挿入図に点で示してあるが、二つのピークは明らかに一致しない。連続的な弾性体のモデルで音響フォノンモードの計算を行って、実験結果と比較したところ、ラマン散乱では最低振動数の l=2 のスフェロイダルモード、コヒーレントフォノンでは1つ上の l=0 の全対称なブリージングモードに対応していることが明らかにされた。

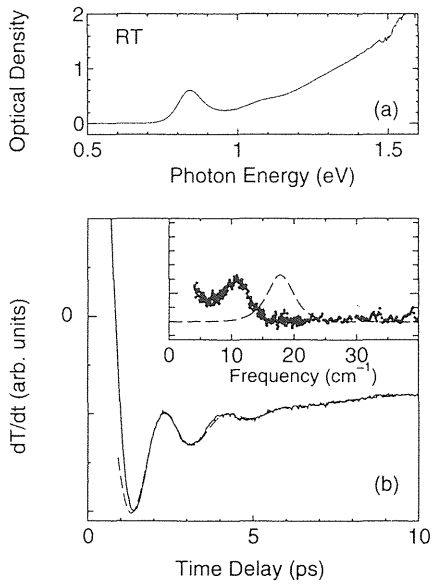


図3　PbSe 量子ドットに閉じ込めを受けた音響型フォノンを、コヒーレントフォノンとラマン散乱による2つの観測

＜CuBr 量子ドットのコヒーレントフォノンとラマン散乱＞[論文 27,82*]

ガラスおよび NaBr 結晶中に成長させた、粒径が数 nm の CuBr 量子ドットについて、X 線小角散乱および、透過電子顕微鏡観測により、ドットのサイズを精密に計測しながらドットに閉じ込められた音響フォノンのコヒーレントフォノンを観測し（図４）、またこの系で知られていた永続的ホールバーニング現象を利用したドットに閉じ込められた音響フォノンの観測を行い、それらの粒径依存性を明らかにした。最低振動数の l=2 のスフェロイダルモードがコヒーレントフォノン、永続的ホールバーニング両者で観測され、コヒーレントフォノンでは１つ上の l=0 の全対称なブリージングモードも観測された。

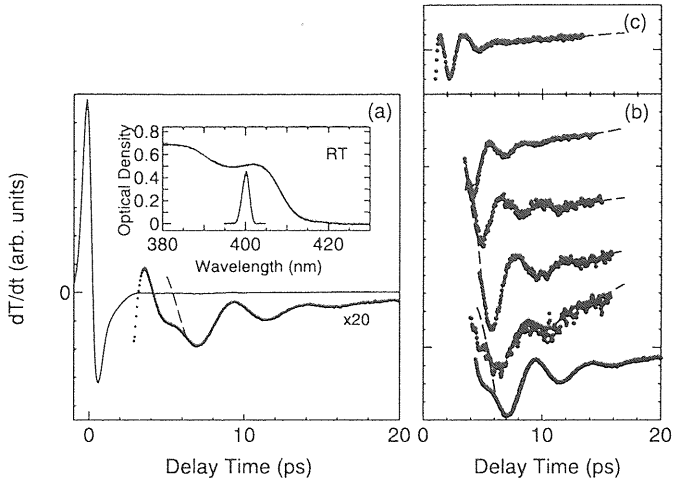


図４　CuBr 量子点のコヒーレントフォノンの観測

＜CuCl量子キューブ、CuBr量子ドットにおける励起子ーフォノン結合状態とLOフォノンのソフトニング＞[論文10*,31,55*]

NaCl結晶中のCuCl量子ドットは量子キューブに特徴的な量子状態が存在する。LOフォノンのエネルギーが量子キューブに閉じ込められた励起子の基底状態と励起状態とのエネルギー間隔に近づいたときの振る舞いを励起光子エネルギーを変えながら永続的ホールバーニング分光で研究し、励起子ーフォノン結合状態を示すストークスシフトの反交差を見出した。

ガラスおよびNaBr結晶中のCuBr量子ドットにおいても、 LOフォノンのエネルギーが量子ドットに閉じ込められた1S基底状態と2P励起状態とのエネルギー間隔に近づいたとき、励起子ーフォノン結合状態を示すストークスシフトの反交差を永続的ホールバーニング分光で見出した。また、ガラスおよびNaBr結晶中の小さなCuBr量子ドットにおいて励起状態におけるLOフォノンのエネルギーの減少（ソフトニング）を、CuClの量子ドットに続いて見出した。量子ドットにおける励起状態のLOフォノンのエネルギーソフトニングはCuI量子ドットでも観測され、フォノンの繰り込みモデルにより系統的に理解された。

## ２．４　量子ドットの量子ビート、量子ドット中の電子スピンの緩和とコヒーレンス

＜トリオン発光の量子ビートとスペクトル微細構造＞[論文 5,22*,23*]

１個の電子は基底状態にあり、もう１個の電子は励起状態にある電子２個と正孔１個からなる（励起状態にある）トリオン（イオン化励起子）が量子ドットに閉じ込められると、下式に記述される交換相互作用が働き、トリオンはエネルギー微細構造を持つ。電子２個と正孔１個が存在すると、同種の電子間に働く相互作用は電子･正孔間に働く相互作用に比べてはるかに強いので、まず同じ電子２個から $f=s_1(1/2)+s_2(1/2)$ を合成して一重項($f=0$)と三重項($f=1$)を作り、これらの合成電子スピンと正孔の角運動量($J=L+s$)の間の相互作用を考える。量子ドットに閉じ込められたトリオンに働く交換相互作用エネルギーは

$$\hat{H}_{hec}^{ex} = 2\tilde{\Delta}_0 f_z j_z + \tilde{\Delta}_1 (f_x j_x - f_y j_y) + \tilde{\Delta}_2 (f_x j_x + f_y j_y),$$

で与えられる。ここで $\tilde{\Delta}_{0,1,2} = (\Delta_{0,1,2}^{e1} + \Delta_{0,1,2}^{e2})/2$、$\Delta_{0,1,2}^{ei}$ は正孔と i 番目の電子に働くエネルギーである。こうして（励起状態にある）トリオンは図５に示すようにエネルギー分裂し、この状態を直線偏光で励起し、直線偏光発光を観測すると、電子を１個ドープされた InP 量子ドットからは電子スピンの異なる２つのトリオン状態の間の干渉が量子ビートとなって観測される（図６）。量子ビートの周期 T から、トリオンに働く交換相互作用エネルギーが h/T により測定でき、値はほぼ 100meV で量子ドットのサイズの減少とともにエネルギーが増大することが量子ビートの周期が短くなることから明らかになった。電気バイアスで量子ドット中の電子準位と電子ドープ層のフェルミ準位の相対的な関係を変えて電子数の制御できるチャージチューナブル量子ドットで

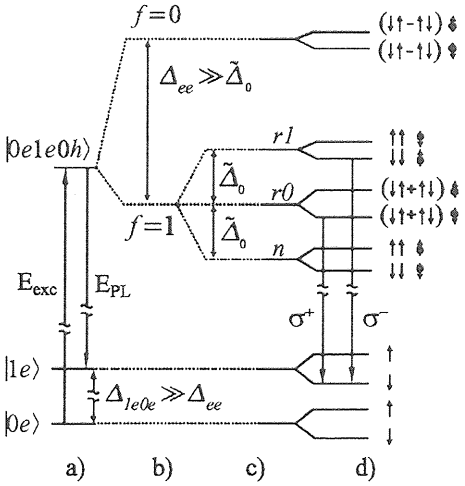


図5　電子をドープされた量子ドットのエネルギー準位

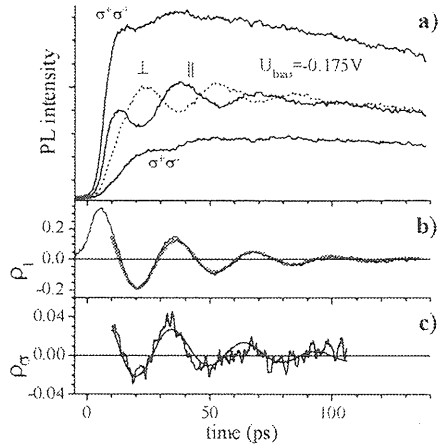


図6　電子をドープされたInP量子ドット発光の量子ビート

は、トリオン量子ビートは、ドットが電子を1個含んでいる良い指標になる。トリオン発光の量子ビートの発見はチャージチューナブル量子ドットの概念を生み出した。

＜量子ドットの発光の示す4種類の量子ビートと量子ビートによる量子ドットのスピン依存微細構造の研究＞[論文 5,22*,23*,29,30,34,36,51*,52*,53*,54,56*,62]

エネルギーの近い2つの光学遷移が時間の短い光パルスで励起されると、光励起された2つの分極はわずかに異なる振動数で振動し、うなり—量子ビート—を生ずる。量子ドットで、サブレベル間コヒーレンスが保たれた微細構造が量子干渉して生じた4種類の発光量子ビートを観測した。これらは自己形成InP量子ドットや歪誘起GaAs量子ドットにおいてファラディー配置で円偏光をもちいて観測されるbright励起子のゼーマン分裂による量子ビート、ファラディー配置で励起と観測に同じ円偏光、直線偏光で観測されるbright励起子と磁場により部分的に許容となったdark励起子の分裂による量子ビート、無磁場のとき直線偏光で観測されるトリオンの分裂による量子ビート、フォークト配置で円偏光をもちいて観測される電子のゼーマン分裂による量子ビートである。図7と表Iに量子ドットにおける4種類の発光量子ビートをまとめる。

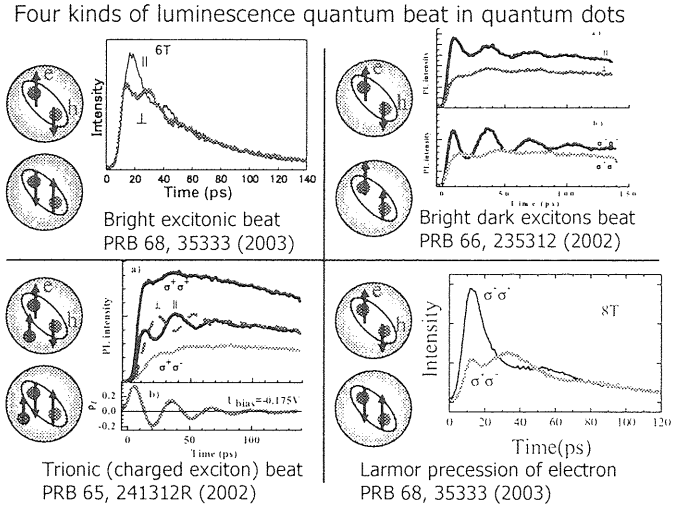


図7　量子ドットの発光が示す4種類の量子ビート

量子ビートの研究から量子ドットのスピンに依存したエネルギー微細構造の知見が得られる。エネルギー微細構造の磁場依存性から電子、正孔、励起子のg-因子を求めることができる。こうした研究から、歪み誘起GaAs量子ドット中の電子のg-因子は等方的で0.17、正孔のg-因子（[001]-成分）は0.34、励起子のg-因子（[001]-成分）は0.51と求まった。また、InP量子ドット中の電子のg-因子は等方的で1.5と求まった。

表I　量子ドットの4種類の量子ビート

| Quantum Beats (QB) | Magnetic field | Configuration | Polarization |
|---|---|---|---|
| Excitonic QB<br>Exciton Zeeman split | B ≠ 0 | Faraday<br>θ = 0° | Linear Polarization |

| | | | |
|---|---|---|---|
| Excitonic QB<br>Bright-dark exciton split | B ≠ 0 | Faraday<br>0° < θ ≤90° | Co-Linear and Co-Circular Polarization |
| Trionic QB<br>Trionic split | B = 0 | θ = 0° | Linear Polarization |
| Electron Spin QB<br>Electron Zeeman split | B ≠ 0 | Voigt<br>θ = 0° | Circular Polarization |

＜CdTe量子ドットにおけるスピン緩和＞[論文66,74*]

CdTe量子ドットの電子のスピン緩和を偏光フォトルミネッセンスとその時間分解を通じて調べ、磁場の強度とともにスピン緩和速度が遅くなる事を示した。電子スピンの緩和機構として、電子スピン・核スピン間の超微細相互作用と核スピンが形成する核磁場のゆらぎを考えると、磁場の増加と共に核磁場のゆらぎの寄与は小さくなるので、電子スピンの緩和時間は長くなる。局在電子のスピン緩和に用いられたこの考えを用いると、フォトルミネッセンスの円偏光度から求めたスピン緩和速度も偏光フォトルミネッセンスの時間依存性から求めたスピン緩和速度も同じ縦磁場依存性で説明されることが明らかになった。

＜電子スピンの緩和時間に対する弱磁場による核スピン揺らぎの凍結効果＞ [論文75*]

正孔をドープされた量子ドットでは、ドープされた正孔と光励起された正孔は基底状態ではスピンが反平行になるので、発光の偏光は電子のスピンの向きを直接反映することとなり、電子スピンの緩和を直接観測することができる。Amand(仏/Toulouse)のグループと共同研究により、時間分解偏光発光分光法により、p-InAs量子ドット中の電子スピン緩和を研究した。試料はBeをδドープされた10層の自己形成InAs/GaAs量子ドットで、面密度$4\times10^{10}$ $cm^{-2}$に生成された量子ドットは平均として正孔を1～2個がドープされている。CWまたはピコ秒Ti:サファイアレーザーでぬれ層の重い励起子の低エネルギー側の裾を準共鳴励起し、量子ドットからの発光の円偏光度と円偏光発光の時間変化から円偏光度の時間トレースを計測した。図8はInAs量子ドットの発光スペクトル(a)、磁場$B_z = 0$Tおよび$B_z = 100$mTのもとでの円偏光度スペクトル(b)、および最低量子準位に電子を1個、正孔を2個含むときのスピン配置(c)である。この図から判ることは、円偏光度は、電子スピンが担っており、円偏光度はp-InAs量子ドットでは10％を超え、わずか100 mTの磁場印加により円偏光度は10％程上昇することである。Merkulovによれば、ランダムに分布した核スピンによる超微細相互作用により電子におよぼす有効磁場により、電子スピンの時間特性は、時間の初期に、電子スピンの初期値の1/3に$T_\Delta = \hbar/(g_e\mu_B\Delta_B)$の時間で減衰し、その後は初期値の

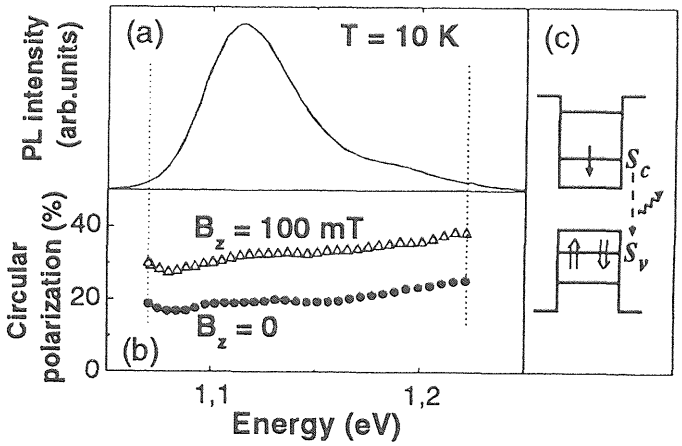


図 8　InAs 量子ドットの発光スペクトル(a)と磁場$B_z = 0$T、$B_z = 100$mTのもとでの円偏光度スペクトル

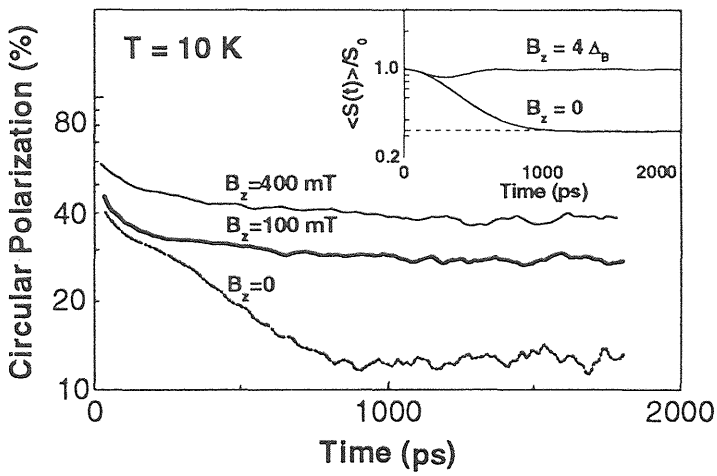


図 9　InAs 量子ドット発光の円偏光度の時間変化

1/3という一定値に保たれる。ここで、ランダムに向いた核スピンによる超微細相互作用により電子に働く磁場分布を$W(B_N) = \exp[-(B_N)^2/\Delta_B^2]$というガウス分布で記述すると、$\Delta_B$はランダムに分布した核スピンによる超微細相互作用により電子スピンに働く有効磁場の分布幅である。図9に見られるように、初期値40%であった円偏光度は800 psでその1/3、およそ12%に減少し、その後は一定値となっており、図9の円偏光度の時間変化はMerkulovの理論計算をほぼ完全に支持している。正孔をドープされたInAs量子ドット中の電子スピン偏極は、光励起後500 psでランダムに向いた核スピンとの超微細相互作用により、最初の1/3になるが、わずか100 mTの外部磁場の印加により4nsになりこの速い電子スピン緩和は抑制される。すなわち、わずか0.1Tの磁場で、核スピンの揺らぎの凍結する効果を見いだした。

＜2個の電子または正孔をドープされたInAs量子ドット中のスピン緩和＞[論文76*]

2個の電子、または2個の正孔をドープされたInAs量子ドットを含むGaAs障壁層を円偏光光励起すると、電子がドープされているときには負の円偏光度をもつ量子ドット発光、正孔がドープされているときには正の円偏光度をもつ量子ドット発光を示す。円偏光度の励起強度依存性、縦磁場依存性ともに、電子がドープされているときと正孔がドープされているときとで異なった特異な変化を示した。0.5T以下の弱磁場領域の円偏光度の縦磁場依存性はランダムに分布した核スピンによる超微細相互作用により電子におよぼす有効磁場により、電子スピンの緩和が支配されていることを示し、円偏光度の励起強度依存性はテトラオン（電子3(1)個と正孔1(3)個の複合系）の発光寿命に影響しているとして理解される。

＜電子ドープInP量子ドット中のサブミリ秒の電子スピン緩和時間＞ [論文70*,86*,90*]

量子情報処理には、光との整合性が良いIII-V族半導体量子ドット中の長いスピン緩和時間を持つ電子スピンが最も有用であろう。ナノ秒程度の発光寿命により時間の制約を受ける光生成電子に比べ、ドープされた電子のスピンを光によりそろえることができれば発光寿命がないので長いスピン寿命という点で有利である。実際、電子を1個ドープしたInP量子ドットの発光の円偏光度を計測し、電子のスピン偏極がサブミリ秒からミリ秒に達する寿命をもつことを見いだした。チャージチューナブル自己形成InP量子ドットを円偏光ピコ秒レーザーパルスにより準共鳴励起し、ファラディー配置で縦磁場を加え、偏光フォトルミネッセンスおよびその時間分解を系統的に研究した。原子核スピンの揺らぎの効果を抑えられる0.1Tの縦磁場下で、InP量子ドットの発光帯を円偏光で準共鳴励起すると、励起光エネルギーからストークスシフトが大きいエネルギー領域では、負の円偏光度（NCP）をもつ発光となる。発光ポンプ・プローブ法を用いた時間分解測定により、負の円偏光度$A_{NCP}$は、数百マイクロ秒の緩和時間で緩和していくことが明らかになった。減衰カーブは単純な指数関数ではないが、少なくとも100μs もの長い時間経過後でも co-pump と cross-pump の間に相当の差がある。その後の研究で電子スピン偏極は 1ms 程度まで保たれていることが示された。負の円偏光度は温度や磁場に依存し、磁場の増加、温度の上昇とともに緩和時間が短くなっていくのが明らかとなった。

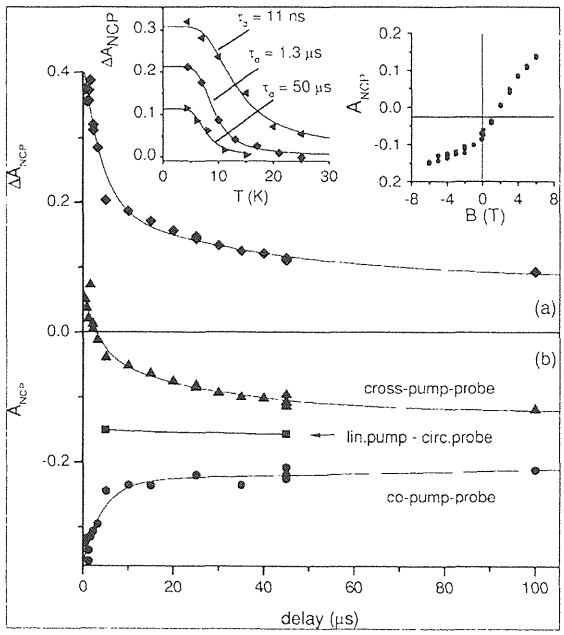


図10　電子がドープされたInP量子ドット中の発光の負の円偏光成分の時間依存性、温度依存性と磁場依存性

＜InP量子ドットにおける動的核スピン分極＞

動的核スピン分極がInP量子ドットにおいて起こっていることを2個の電子と1個の正孔からなるトリオンの負の円偏光発光を縦磁場下で観測することで確認できる。動的核スピン分極がおこると、電子スピンが感じる有効外部磁場$B_{eff}$は外部磁場$B$と有効核磁場　$B_N$の和として$B_{eff} = B + B_N$と表わされる。右（左）円偏光励起下でトリオンの発光の円偏光度を外部磁場$B$の関数と

して測定すると、図 11(a)の様に± $B_N$（励起強度 40 mW のとき～4.5 mT）で負の円偏光度が鋭く減少する半値半幅 15 mT の Lorentz 型の磁場依存性が得られる。右（左）円偏光で負の円偏光度が最小になる外部磁場が－（＋）にシフトすることから、有効核磁場 $B_N$ を相殺する外部磁場のとき、すなわち有効外部磁場が 0 のとき、負の円偏光度が最小になり、核スピンのゆらぎによる核磁場が 15mT であるとして図 11(a)は理解できる。図 11(b)に示すように、光照射強度の増加に比例して有効核磁場 $B_N$ は線形に増加し、比較的励起強度の強い 50mW でも、$B_N \cong 6mT$ であることは、InP 量子ドットにおける超微細相互作用は比較的弱いことを示している。

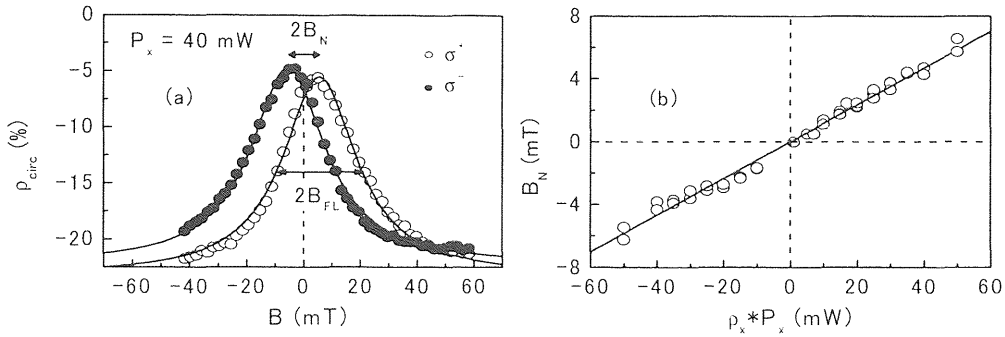


図 11　核スピン分極の効果

＜電子ドープ InP 量子ドット中の電子スピンのコヒーレンス時間＞

電子スピンのコヒーレンス時間は、ハンレ効果測定（横磁場下における円偏光度の磁場依存性）により求めた。光弾性変調器を用い円偏光度を 0.1%の精度で測定できるシステムを構築し、電子がドープされた InP 量子ドットにおいて準共鳴励起のもと、ハンレ効果測定を行った。図 12a は、準共鳴励起における発光スペクトル（実線は $I_+^+$、破線は $I_+^-$ を表す）と発光の円偏光度の検出波長依存性（●印）を示す。InGaP バリア層での励起では量子ドットの発光ピークにおいて 3.8%と正の円偏光度を示すが準共鳴励起では励起エネルギーからストークスシフト 60 meV 付近でレーザーの偏光度に対し負の円偏光度（NCP）を示す。また図 12b は、量子ドット発光ピーク波長におけるハンレ効果測定の結果を示す。ローレンツ型関数 $\rho(B)=\rho(0)/\{1+(\omega_L T_2^*)\}$（ラーモア周波数 $\omega_L=\mu_B gB/\hbar$、$T_2$*: スピン緩和時間、g: ランデの g 因子）を用いて、2 成分ローレンツ・フィッティングを行なった。ハンレ曲線の半値全幅より見積もって、速い成分では $gT_2^*$ =190 ps、弱磁場領域の遅い（鋭い）成分では 2.1 ns と求まった。速い成分の起源はホールのスピン緩和又は電子 2 つと正孔 1 つから構成されるトリオンの発光寿命によるもの、また遅い成分はドープされた電子のスピン緩和によるものと考えられる。図 12c の電圧依存性はこの鋭い NCP の成分とトリオン量子ビートの振幅が同じバイアスで起きていることを示し、量子ドットが電子を 1 個ドープされると、鋭い NCP が現れ、それがドープされた電子のスピン緩和によるものと同定できる。InP 量子ドットの電子の g-因子は 1.5 なので、$T_2$* =1.4 ns と導かれる。

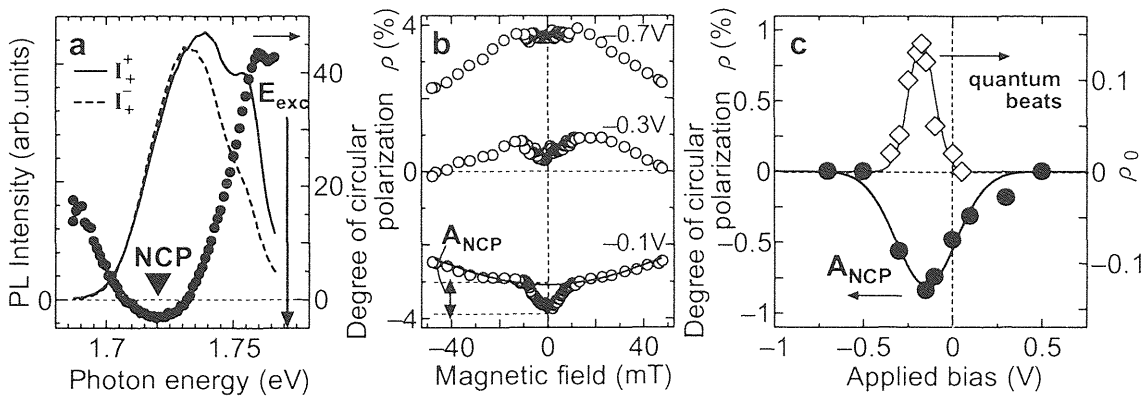


図 12 チャージチューナブル InP 量子ドットの発光の負の円偏光度とハンレ効果

＜超高分解能時間分解光誘起カー回転測定法の開発と単層量子ドット中のスピンダイナミクスの研究＞[論文80,88*]

単層量子ドット中の電子や正孔のスピンダイナミクスの研究を行うため、光弾性変調器、光ブリッジ型平衡フォトダイオードおよびロックイン増幅器を二段に直列に使うことにより、$5\times10^{-3}$度の角度分解能をもつ世界最高感度の時間分解カー回転測定系の建設に成功した。この測定系を単層の歪み誘起GaAs量子ドットにおいて、電子スピンのラーモア歳差運動が観測された。歳差運動周期から得られたg因子 $|g|\sim0.25$ は、すでに同一試料において報告のある発光量子ビート測定による結果と矛盾しない。また量子井戸におけるスピン緩和寿命よりも長い量子ドットのスピン緩和寿命が観測された。これはD'yakonov-Perel'機構の抑制によりスピン緩和が抑制されたと考えることが出来る。n-GaAs基板に作成された自己組織化InP量子ドットを用いた測定においては、観測されたラーモア才差運動の同期から$|g|\sim0.052$という正孔によると考えられる振動成分の観測に成功した。

2．5　超高感度ヘテロダイン検出フォトンエコーの開発と単層量子ドットへの応用

超高速レーザーパルスを用いたフォトンエコーは物質中の分極のコヒーレントな振る舞いを観測するのに極めて有用であり、物質中の励起子のコヒーレント緩和（位相緩和）や電子波束のコヒーレントな振動を観測するのに最適である。図13に示すようなヘテロダイン検出フォトンエコー測定法を開発した。この方法は、2光束のレーザーパルスに100MHz程度の2つの周波数が異なる高周波で変調をかけ、この周波数の結合周波数成分でフォトンエコー信号を検出する方式で従来のフォトンエコー測定に比べ1桁半の感度を有することが明らかになった。ヘテロダイン検出フォトンエコー測定法により、単層の量子井戸や積層された量子ドットの励起子のフォトンエコー信号が測定できるようになった。単層の歪み誘起GaAs量子ドットおよび電場をかけた単層のInP量子ドットのヘテロダイン検出フォトンエコー測定に成功し、前者では量子井戸に比べ量子ドットでは励起子のコヒーレンス時間が長く、励起子分子の束縛エネルギーが増大することを明らかにし、後者では電場により電子のドープ量を変えることでPauli Blocking効果、電場により正孔をトンネルで量子ドットから引き抜く過程による非マルコフ的減衰を初めて観測することに成功した。

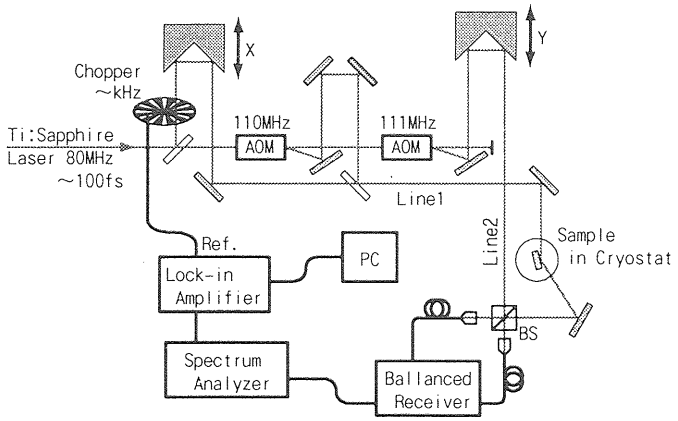


図13　超高感度ヘテロダイン検出フォトンエコー測定系

＜InP単層量子ドットのヘテロダインフォトンエコー＞[論文64*,69,81*,87]

電場を加えられたInP単層量子ドットにおいて共鳴光生成された正孔がトンネル効果で量子ドットから抜ける過程がヘテロダインフォトンエコーの時間特性で観測され、ノンマルコフ過程の反映した特異な非指数関数的減衰を示すことが明らかにされた。また、電荷のドープに伴うパウリブロッキングがフォトンエコー信号を消滅させることが明らかになった。

＜歪誘起GaAs量子ドットにおける励起子ー励起子分子量子ビート＞[論文65*,67,87,89*]

半導体中の励起子や励起子分子のような準粒子の束縛エネルギーは、低次元構造では電子や正孔が空間的に閉じ込められることによって、バルク結晶の時より大きくなることが予想される。量子井戸に局所的な歪（$\phi\sim90$nm）を加えることによって形成される歪誘起GaAs量子ドット試料を用いて、歪のない2次元的なGaAs量子井戸における励起子分子と、歪によって形成された0次元的量子ドット領域に閉じ込められた励起子分子の束縛エネルギーの直接的な比較を行った。図14 (a)に示すように、これら2つの領域は同一の試料中に存在し、発光エネルギーによって区別する事が出来る。

励起子分子の束縛エネルギーは、量子ビートの周期から決定され、それはヘテロダイン検出を利用した高感度時間分解四光波混合システムの開発によって初めて可能になった。図(b)に、厚さ 3.8nm の井戸内に作られた歪み誘起量子ドット試料の四光波混合信号を示す。信号には励起子分子の束縛エネルギーを反映した顕著なビートがみられる。一見して分かるように、その振動周期は 0 次元領域(SIQD)では、2 次元領域（QW）より短く、詳しく調べると振動数が 1.5 倍大きくなっている。この観測は、量子井戸の 2 次元的閉じ込めに横方向の面内閉じ込めを付与された量子ドットで、束縛エネルギーが 1.5 倍に増大したことを最も直接的な形で示す。

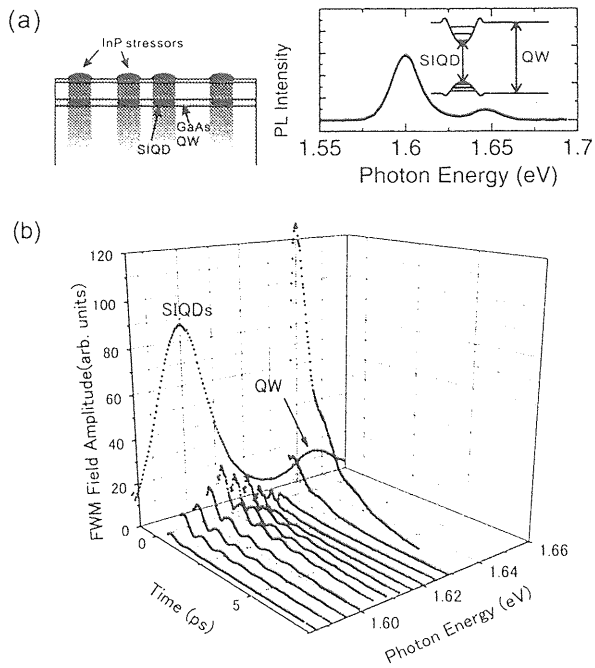


図 14　単層 GaAs 量子井戸と歪み誘起量子ドットにおけるフォトンエコー信号

## 3．研究の総括と今後の展望

本研究の主要な成果を列挙すると

1）量子ドットにおける励起子のコヒーレント緩和機構について統一的な描像を得た事、
2）量子ドットのエネルギー緩和におけるフォノンボトルネック効果を実験的に否定した事、
3）チャージチューナブル量子ドットを発見し、長い電子スピン緩和を明らかにした事、
4）超高感度ヘテロダイン検出フォトンエコーノ開発により単層量子ドットのコヒーレンス研究が可能になった事、

である。

このうち、原子様”から“イオン様”にまで特性を自由に変えられる系—チャージチューナブル InP 量子ドット—の発見は、本研究の後半の部分の研究方向を決定することとなった。今後、チャージチューナブル量子ドットを舞台にこの中の少数多体系のコヒーレンス、電子波束の運動、電子と核のスピン緩和を明らかにし、かつ制御する研究が進んでいくと期待できる。

数原子層のフォトンエコーが計測できるまでに進化した超高感度ヘテロダイン検出フォトンエコーは、今後、大幅に適用範囲を広げ、新しいレーザー分光学の発展になると期待している。

本稿で引用した研究代表者のグループの研究は、筑波大学大学院数理物質科学研究科・物理学系の奥野剛史博士、池沢道男博士および、何人かの大学院学生諸氏との共同研究である。特に、学位を取得されたJ. Zhao（趙家龍）、竹本一矢、西林一彦、菅野敦史各博士の寄与が大きい。また、多くの研究がA.V. Baranov, A.V. Fedorov, I.V. Ignatiev, S.Yu. Verbin, Ye Chen, V.K. Kalevich, T. Amand, B. Pal, S. Nair, H.-W. Ren,　杉崎満、阪東一毅、相原正樹、内山智香子各博士との共同研究として行われた。これらの各氏の研究協力に対し深く感謝したい。

# Ⅳ．発表論文集

以降は、発表論文リストの原著論文 1),4),7)～11),18),22),23),26),32),35),42),44)～46),49),51)～53),55),56),60),64),65),70),72),74)～76),81),82),86),88)～90)から構成されていますが、一部(下記 19 件)、著作権者(出版社、学会等)の許諾を得ていないため、筑波大学では電子化・公開しておりません。
なお、電子ジャーナルとして出版社から公開されており、契約している場合は全文を読むことができますので、下記のリンク先でご覧ください。

論文 1) DOI: 10.1002/(SICI)1521-3951(200104)224:3<613::AID-PSSB613>3.0.CO;2-X

論文 4) DOI: 10.1002/1521-3951(200103)224:2<461::AID-PSSB461>3.0.CO;2-V

論文 7) http://dx.doi.org/10.1143/jjap.40.1947

論文 8) http://dx.doi.org/10.1143/jjap.40.2084

論文 23) DOI: 10.1002/1521-396X(200204)190:2<547::AID-PSSA547>3.0.CO;2-8

論文 32) http://dx.doi.org/10.1016/S0022-2313(02)00617-8

論文 35) http://dx.doi.org/10.1016/S0022-2313(02)00444-1

論文 42) http://dx.doi.org/10.1016/S0038-1098(02)00327-7

論文 46) http://dx.doi.org/10.1143/jpsj.71.3052

論文 49) http://dx.doi.org/10.1143/jpsj.72.249

論文 51) http://dx.doi.org/10.1016/S1386-9477(02)00811-1

論文 52) http://dx.doi.org/10.1016/S1386-9477(02)00813-5

論文 56) http://dx.doi.org/10.1016/j.jlumin.2004.01.038

論文 64) http://dx.doi.org/10.1016/j.physe.2004.08.003

論文 65) http://dx.doi.org/10.1016/j.physe.2004.08.042

論文 72) DOI: 10.1002/pssa.200460324

論文 81) http://dx.doi.org/10.1143/jpsj.74.2933

論文 82) http://dx.doi.org/10.1143/jpsj.74.3082

論文 90) DOI: 10.1143/JPSJ.75.054702

# Fluorescence Intermittency in Self-Assembled InP Quantum Dots

Mitsuru Sugisaki,[1,*] Hong-Wen Ren,[1,†] Kenichi Nishi,[1,2] and Yasuaki Masumoto[1,3]

[1]*Single Quantum Dot Project, ERATO, JST, Tsukuba Research Consortium, 5-9-9 Tokodai, Tsukuba, Ibaraki 300-2635, Japan*
[2]*System Devices and Fundamental Research, NEC Corporation, 34 Miyukigaoka, Tsukuba, Ibaraki 305-8501, Japan*
[3]*Institute of Physics, University of Tsukuba, Tsukuba, Ibaraki 305-8571, Japan*

(Received 31 July 2000)

Fluorescence intermittency in InP self-assembled dots is investigated by means of far field imaging and single dot spectroscopy. Based on our observation that blinking dots are found in the vicinity of scratches and the blinking frequency is drastically enhanced under a near-infrared laser irradiation, we attribute the origin of the fluorescence intermittency to a local electric field due to a carrier trapped at a deep localized center in the $Ga_{0.5}In_{0.5}P$ matrix. The validity of this explanation is confirmed by a thermal activation-type behavior of the switching rate and artificial reproduction of the blinking phenomenon by an external electric field.

DOI: 10.1103/PhysRevLett.86.4883 PACS numbers: 71.35.–y, 61.46.+w, 73.21.–b, 78.66.Fd

Single quantum dot spectroscopy has revealed a lot of novel information hidden behind the inhomogeneously broadened photoluminescence (PL) band. One of the most interesting findings so far reported in quantum dot (QD) systems is the fluctuation of the PL peak energy and intensity with time, which would be unobservable in macroscopic studies. The former phenomenon, called as the spectral diffusion, is observed in CdSe [1–4] and InAlAs [5] QDs, where the PL peak energies from confined excitons and their LO sidebands fluctuate during the time of measurement. The latter phenomenon is referred to as the fluorescence intermittency or random telegraph signal, where the PL intensity switches between two or more discrete levels as the time goes by [1,5–9]. The spectral diffusion and the fluorescence intermittency are tentatively attributed to photoionization or mobile photoactivated nonradiative recombination centers. However, the detailed mechanism of the fluorescence intermittency is still under discussion, especially the location of the carriers during the blinking process and, more importantly, the origin of such large intensity changes have not been clarified yet.

In this Letter, we report on the origin of the fluorescence intermittency derived from a detailed optical study of self-assembled single InP QDs and show that the blinking is due to a local electric field generated by a carrier trapped by a deep localized center in the $Ga_{0.5}In_{0.5}P$ matrix. The validity of our model is confirmed by the thermal activation-type behavior of the switching rate. In addition, a strong enhancement of the blinking rate was observed when a near-infrared (near-IR) laser is irradiated together with a band-to-band excitation laser, which allowed us to estimate the energy level of the localized center. Notably, we clearly demonstrate how to reproduce all the features of the phenomenon artificially [10].

Self-assembled InP QDs sandwiched between two $Ga_{0.5}In_{0.5}P$ barriers 180 nm thick each were grown on a Si doped ($n^+$) GaAs (001) substrate using a metal-organic vapor phase deposition system [11]. For the single dot spectroscopic study, we adopted a confocal microphotoluminescence ($\mu$-PL) system [9]. The samples were set on a cold-finger of a liquid He flow-type cryostat. As the excitation light source, the 488 nm line of a continuous wave (CW) Ar-ion laser and a CW Ti:sapphire laser were used. The sample PL was collected using a microscope objective lens, and then the images were taken by a thermoelectrically cooled charge-coupled device (CCD) camera. For the $\mu$-PL measurements, the sample PL was analyzed using a 50 cm single monochromator and then detected by a liquid nitrogen cooled CCD camera.

Figures 1(a) and 1(b) show the $\mu$-PL images consecutively observed over the same area of the sample. Each bright spot corresponds to the PL from a single InP QD. As marked by the dotted circles, it was observed that some QDs exhibit the blinking phenomenon, i.e., the PL intensity switches randomly between a high efficiency state (hereafter referred to as "on") and a very weak state ("off"), while the PL from other QDs is stable. It should be mentioned that, even if a blinking QD is in the off state, the $\mu$-PL is not completely quenched, but weak $\mu$-PL remains.

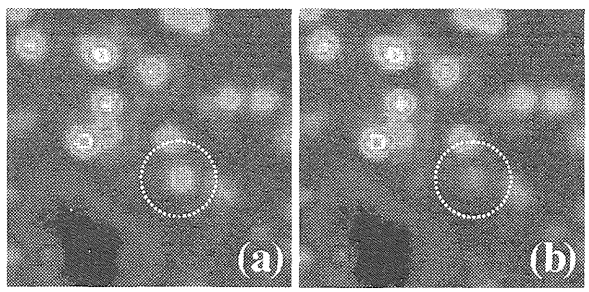


FIG. 1 (color). Microimages of a blinking InP QD in (a) on and (b) off states measured at 4 K with a 200 msec integration time. The observed area is 15 $\mu$m × 15 $\mu$m. The black region at the bottom left side of each image is a flaw on the sample surface, and thus the PL from the $Ga_{0.5}In_{0.5}P$ matrix is not observed in this region.

  

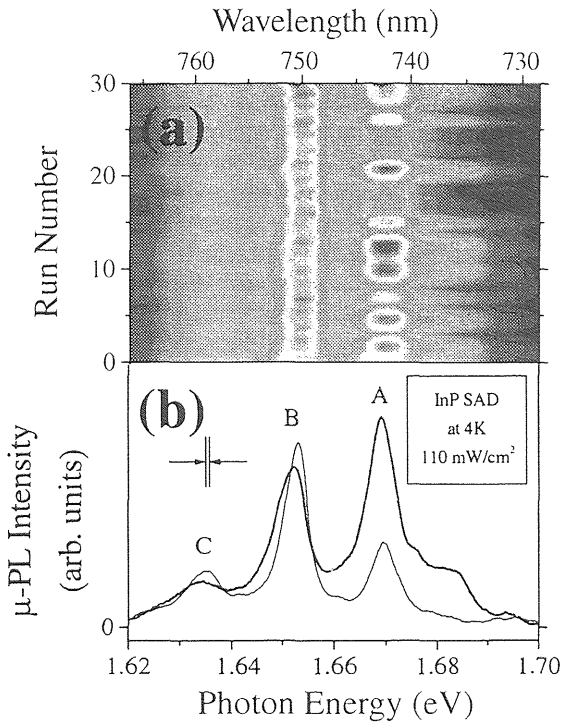


FIG. 2 (color). (a) Contour map made from $\mu$-PL spectra at 4 K of a blinking InP self-assembled dot (SAD) measured successively 30 times. (b) $\mu$-PL spectra of the on (thick red curve) and off (thin blue curve) states. Peak $A$ having the highest PL peak energy shows the large intensity change between the on and off states. Peaks $B$ and $C$ shift to the higher energy side when the system switches from the on state to the off state, while the intensity changes of these peaks are very small.

Figure 2(a) shows a contour plot of the $\mu$-PL spectra of a single blinking QD successively recorded 30 times with an individual integration time of 200 msec. It is found that not only the PL intensity but the $\mu$-PL spectrum also changes with time between the two types of spectra shown by the thick and thin curves in Fig. 2(b). Each of them corresponds to the $\mu$-PL spectrum when the blinking QD is in the on state and the off state, respectively. The PL peak denoted by $A$ shows a large intensity change between the on and off states. On the other hand, the PL bands $B$ and $C$ are almost unchanged in intensity, but the peak energies slightly shift to the higher energy side by a few meV when the state switches from on to off. This result indicates that the large intensity change observed in the $\mu$-PL images is mainly caused by the intensity change of the PL band having the highest PL peak energy. This also explains the weak PL in the off state, viz., some peaks change little when the state switches from on to off so that the $\mu$-PL intensity in the off state, though very weak, is not completely quenched as shown in Fig. 1(b).

In many cases a blinking QD was observed near a minor flaw on the sample surface; for instance, a small flaw is observed at the bottom left side in Fig. 1. It is thus reasonable to assume that there are many defect states near that point. Further, we found that new blinking QDs appeared after the surface of the sample was intentionally scratched by a needle. Therefore the fluorescence intermittency appears to be related to deep defect levels.

A possible mechanism for the switching between the on and off states can be modeled as follows. In the vicinity of some QDs there are localized deep levels due to defects. When a carrier is trapped by such a localized state, a local electric field generated by the trapped carrier is applied to the QD. In this case, the overlap of the wave functions of the confined electrons and holes is decreased. If the local field is much stronger, the confined carriers escape from the QD to the matrix. Therefore the $\mu$-PL intensity eventually becomes weak, and this is observed as the switching from the on state to the off state. The trapped carrier relaxes after a while by recombining with another carrier of opposite sign, mediated by phonons or through a photoreabsorption process. In this case, the local field by the trapped carrier disappears, and the system thus returns to the initial condition. This shows the switching from the off state to the on state [12].

In order to confirm the validity of the proposed model, we performed several additional experiments, which shed light on local trap centers and local electric fields. First, we measured the temperature dependence of the integrated $\mu$-PL intensity as shown in Fig. 3(a). If the switching is due to the trapping process of carriers, the trapping probability should be explained using a thermal activation model. As clearly seen, the switching becomes faster with the increase of the temperature. The average off times measured at various temperatures are summarized in Fig. 3(b). We found that the off period $t_{\mathrm{off}}(T)$ at temperature $T$ can be well reproduced using a thermal activation function,

$$t_{\mathrm{off}}(T) = \frac{t_{\mathrm{off}}(0)}{1 + a\exp(-E/k_{\mathrm{B}}T)}, \qquad (1)$$

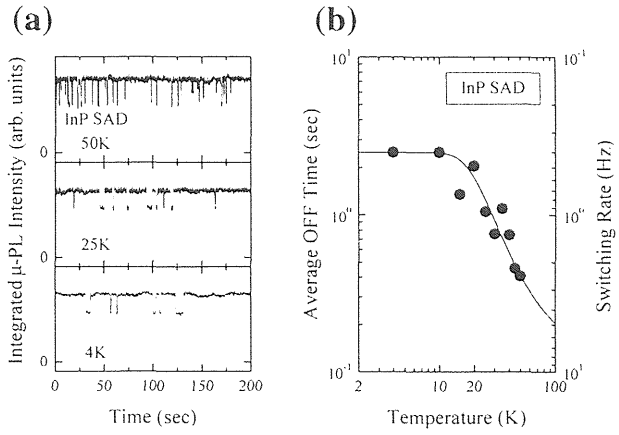


FIG. 3. (a) Time traces of the integrated $\mu$-PL intensity of a blinking QD measured at various temperatures. The switching rate becomes faster as the temperature is increased. (b) Log-log plot of the off duration as a function of temperature, which can be well explained by a thermal activation model written in Eq. (1), with $t_{\mathrm{off}}(0) = 2.5$ sec and $E = 7$ meV.

as shown by the solid line in Fig. 3(b), where $a$ is a constant and $E$ and $k_B$ denote the activation energy and the Boltzmann constant, respectively. This result strongly supports the existence of a localized trap center which is responsible for the switching phenomenon.

We then investigated the depth of the localized center. Figure 4(a) shows the integrated $\mu$-PL intensity under weak excitation by an Ar-ion laser. As shown in Fig. 4(b), we observed a drastic enhancement of the on-off switching rate when the QDs were resonantly excited by a near-IR (Ti:sapphire) laser of 1.75 eV in addition to the band-to-band excitation (Ar-ion) laser.

The switching rates which are defined as the reciprocal duration of the on and off periods are plotted in Fig. 4(c) as a function of the excitation energy of the near-IR laser. For comparison, the $\mu$-PL spectrum of the blinking QD is also shown. The broken and dotted lines show the switching rates of the on state and the off state, respectively, measured without the near-IR laser irradiation. When the near-IR laser energy is above 1.5 eV, the switching rates of the on and off states become 5 and 3 times faster, respectively, than those excited only by the band-to-band laser [16]. It should be mentioned that the enhancement can be observed even when the near-IR laser energy is below the lowest PL level of the InP QD because the near-IR laser can directly excite a carrier to the defect level in the $Ga_{0.5}In_{0.5}P$ matrix that is deeper than the confined exciton level in the InP QDs. The switching rates were almost independent of the excitation energy of the near-IR laser above 1.5 eV. When the near-IR laser energy is lower than 1.5 eV, however, the enhancement was not observed, and the switching rate was almost the same as that of Fig. 4(a). Hence we conclude that the localized center responsible for blinking has an excitation threshold energy of 1.5 eV [17,18].

Finally we checked the second key point of our model, namely, the local electric field, which is considered to cause a strong change in $\mu$-PL intensity. Figure 5(a) shows the contour map of the $\mu$-PL spectra of a normal single QD showing stable PL measured by applying a positive bias at the top of the sample. In order to perform this experiment, a semitransparent contact was fabricated by evaporating a 20 nm thick Au layer onto the sample surface. The PL observed at the higher energy side changes more sensitively than those observed at the lower energy side in intensity. As a result, the external electric field causes a fairly large change of the integrated $\mu$-PL intensity as shown in the inset in Fig. 5(b). The thick and thin curves in Fig. 5(b) were measured under the bias of 850 mV, which corresponds to a flat band condition (0 kV/cm), and about 10% weaker (750 mV = −3 kV/cm), respectively [19]. One can see that a small change of the electric field induces a drastic change of the $\mu$-PL spectra. One of the most important points in this study is that the change in intensity and peak energy of the $\mu$-PL spectra in the electric field qualitatively well reproduce the change of $\mu$-PL spectra between

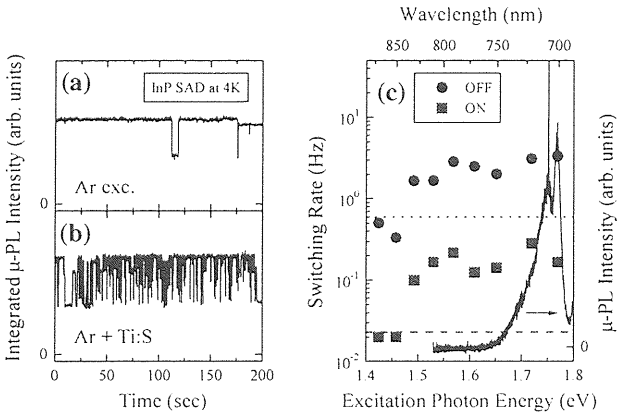


FIG. 4. (a) The integrated $\mu$-PL intensity versus time trace of a blinking QD under band-to-band (Ar-ion laser) excitation. (b) The blinking rate is drastically enhanced when a near-IR (Ti:sapphire) laser beam irradiates the sample simultaneously with a band-to-band excitation laser beam. (c) Plot of the switching rates of the on (squares) and off (circles) states. The broken and dotted curves show the switching rates of the on and off times, respectively, measured without the near-IR laser irradiation. For comparison, the $\mu$-PL spectrum of the blinking QD is also shown. The sharp line observed at 1.75 eV comes from the scattered light of the near-IR laser.

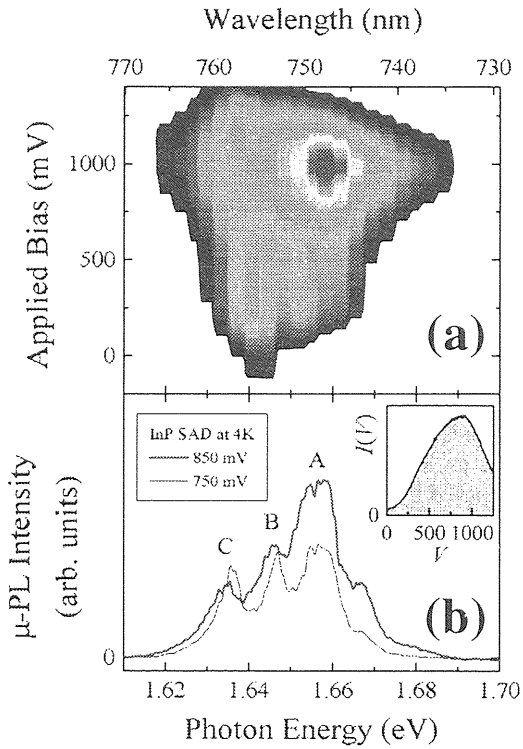


FIG. 5 (color). (a) Contour plot of the $\mu$-PL spectra in an external electric field. The PL intensity of the peak observed at the higher energy side is more sensitive to the field than those observed at the lower energy side. (b) $\mu$-PL spectra measured by applying a bias of 850 mV (the flat band condition, thick red curve) and 750 mV (thin blue curve), which qualitatively reproduce the $\mu$-PL spectra of the on and off states, respectively [compare with Fig. 2(b)]. Inset: Integrated $\mu$-PL intensity versus the applied bias.

the on and off states of a blinking QD shown in Fig. 2(b). That is, in Fig. 5(b), the PL peak $A$ observed at the higher energy side shows the largest change in intensity, and the PL peaks $B$ and $C$ shift to the higher energy side by a few meV keeping their PL intensities almost unchanged when the bias is changed from 850 to 750 meV. This fact is direct evidence supporting our model and brings us to the conclusion that the fluorescence intermittency is due to a local electric field induced by a trapped carrier near a single QD. Furthermore, we can estimate the distance between a blinking QD and a trap center from this result; if one assumes a static electric field in the sample layer and that one localized center can accept only one carrier, the distance is estimated to be 20 nm. This result indicates that the trap center located very close to (but spatially separated by a potential barrier from) the QD plays an important role in the blinking phenomenon.

In summary, we have studied the optical properties of the blinking self-assembled QDs. From the observation of the $\mu$-PL image and the temperature dependence of the switching rate, it has been shown that the blinking phenomenon is due to the trapping and subsequent delocalization processes of photoexcited carriers. Further, we have successfully demonstrated that the intensity changes and peak energy shifts observed in the $\mu$-PL spectra of a blinking QD can be well reproduced artificially by applying an external electric field, which indicates that the fluorescence intermittency is intimately related to a local electric field.

The authors thank Dr. S. V. Nair for many enlightening discussions and a critical reading of the manuscript. Stimulating discussions with Professor I. S. Osad'ko and Dr. J.-S. Lee are also acknowledged.

*Corresponding author.
Email address: mitsuru@ecf.utoronto.ca
Present address: Energenius Centre for Advanced Nanotechnology, University of Toronto, Haultain Building, 170 College Street, Toronto, Ontario, Canada M5S 3E3.
†Present address: Space Vacuum Epitaxy Center, University of Houston, 4800 Calhoun, Houston, TX 77204-5507.

[1] M. Nirmal, B. O. Dabbousi, M. G. Bawendi, J. J. Macklin, J. K. Trautman, T. D. Harris, and L. E. Brus, Nature (London) **383**, 802 (1996).
[2] S. A. Empedocles, D. J. Norris, and M. G. Bawendi, Phys. Rev. Lett. **77**, 3873 (1996); S. A. Empedocles and M. G. Bawendi, Science **278**, 2114 (1997).
[3] V. Türck, S. Rodt, O. Stier, R. Heitz, R. Engelhardt, U. W. Pohl, D. Bimberg, and R. Steingrüber, Phys. Rev. B **61**, 9944 (2000).
[4] J. Seufert, R. Weigand, G. Bacher, T. Kümmell, A. Forchel, K. Leonardi, and D. Hommel, Appl. Phys. Lett. **76**, 1872 (2000).
[5] H. D. Robinson and B. B. Goldberg, Phys. Rev. B **61**, R5086 (2000).
[6] M.-E. Pistol, P. Castrillo, D. Hessman, J. A. Prieto, and L. Samuelson, Phys. Rev. B **59**, 10 725 (1999).
[7] D. Bertram, M. C. Hanna, and A. J. Nozik, Appl. Phys. Lett. **74**, 2666 (1999).
[8] F. Koberling, A. Mews, and T. Basché, Phys. Rev. B **60**, 1921 (1999).
[9] M. Sugisaki, H.-W. Ren, S. V. Nair, J.-S. Lee, S. Sugou, T. Okuno, and Y. Masumoto, J. Lumin. **87–89**, 40 (2000).
[10] In order to confirm the reproducibility, every phenomenon reported here was examined at least more than three times using different QDs on different days.
[11] H.-W. Ren, M. Sugisaki, J.-S. Lee, S. Sugou, and Y. Masumoto, Jpn. J. Appl. Phys. **38**, 507 (1999).
[12] If one assumes that the trapping occurs through the Auger process [13] and if the Auger coefficient is the same order as that reported by Raymond *et al.* [14], the duration of the on period can be in the same order as our observation. As for the off period, the relaxation time of a single trapped electron observed in several systems is in the same order as the off period in our case [15]. We thus consider that our model is reasonable to explain the duration of the on and off periods.
[13] Al. L. Efros and M. Rosen, Phys. Rev. Lett. **78**, 1110 (1997).
[14] S. Raymond, K. Hinzer, S. Fafard, and J. L. Merz, Phys. Rev. B **61**, R16 331 (2000).
[15] See, for example, X. Jiang, M. A. Dubson, and J. C. Garland, Phys. Rev. B **42**, 5427 (1990); H. H. Mueller and M. Schulz, J. Appl. Phys. **83**, 1734 (1998); J. H. Scofield, N. Borland, and D. M. Fleetwood, Appl. Phys. Lett. **76**, 3248 (2000).
[16] The increase of the temperature by the near-IR laser irradiation is negligible (less than a few K) because the redshifts of the $\mu$-PL peak energies of the GaAs substrate and the $Ga_{0.5}In_{0.5}P$ matrix were not observed. Thus, the observed enhancement of the switching rates are *not* due to the increase of the temperature.
[17] The depth of the deep level that we observe is about 400 meV, which is close to the energy due to a Ga-vacancy defect and P-vacancy-related complexes; J. R. Dekker, A. Tukiainen, R. Jaakkola, K. Väkeväinen, J. Lammasniemi, and M. Pessa, Appl. Phys. Lett. **73**, 3559 (1998); Z. C. Huang, C. R. Wie, J. A. Varriano, M. W. Koch, and G. W. Wicks, J. Appl. Phys. **77**, 1587 (1995).
[18] Further, the anti-Stokes PL due to the deep states with energy 1.5 eV has recently been reported; I. V. Ignatiev, I. E. Kozin, H.-W. Ren, S. Sugou, and Y. Masumoto, Phys. Rev. B **60**, R14 001 (1999). The value is consistent with that observed in the current study.
[19] A single InP QD shows a $\delta$-function-like $\mu$-PL line under weak excitation [20]. Under the excitation shown in Fig. 5, since the number of the confined excitons is $\sim$10, the multiple $\mu$-PL lines are observed and the $\mu$-PL band width becomes broad due to the exciton-exciton interaction.
[20] M. Sugisaki, H.-W. Ren, S. V. Nair, K. Nishi, and Y. Masumoto, Solid State Commun. **117**, 435 (2001).

PHYSICAL REVIEW B, VOLUME 63, 033307

# Exciton-phonon coupled states in CuCl quantum cubes

Jialong Zhao,[1] Selvakumar V. Nair,[2] and Yasuaki Masumoto[1,2]
[1]*Institute of Physics, University of Tsukuba, Tsukuba, Ibaraki 305-8571, Japan*
[2]*ERATO Single Quantum Dot Project, Japan Science and Technology Corporation, Tokodai 5-9-9, Tsukuba, Ibaraki 300-2635, Japan*
(Received 12 May 2000; revised manuscript received 5 September 2000; published 29 December 2000)

The size dependence of excitonic states and vibrational modes in CuCl cubic quantum dots embedded in NaCl crystals was studied by means of site-selective persistent spectral hole burning spectroscopy. It is shown that the interaction of the longitudinal optical (LO) phonon with the exciton results in the formation of coupled exciton-phonon modes when the energy of the LO phonon approaches the energy spacings between the ground and excited states of the exciton. The energy anticrossings of the LO phonon modes with two higher optically allowed excited states of the exciton in CuCl QD's were clearly observed at confinement energies of about 10 and 6 meV, respectively. In addition, the linewidth of the LO phonon sideband in CuCl QD's in NaCl crystals was found to increase abruptly from 0.3 meV to about 1.2 meV at a confinement energy of about 23 meV, which appears to result from the exciton-phonon mixing of the LO phonon mode with the first excited state of the exciton. The experimental results are qualitatively understood by the LO phonon renormalization theory.

DOI: 10.1103/PhysRevB.63.033307 PACS number(s): 68.65.−k, 63.22.+m, 61.46.+w, 71.35.−y

Optical investigations on semiconductor quantum dots (QD's) or nanocrystals opened an exciting field of basic physics studies.[1,2] Studies of the size dependence of electronic and vibrational spectra as well as the exciton-phonon interaction in QD's are important for understanding their optical properties. The persistent spectral hole burning (PSHB) phenomenon is observed in many materials containing QD's, and PSHB provides a sensitive spectroscopic technique for the study of the size-dependent electronic states and vibrational modes in QD's.[3–10]

Since QD's containing only a few hundreds of atoms are like large molecules, the exciton formation in QD's would be expected to strongly influence the lattice vibrations. Recently, the LO phonon sidebands observed in the PSHB and photoluminescence spectra of spherical CuCl nanocrystals in glass showed an energy reduction of about 2 meV, compared with the energy of the LO phonon (25.6 meV) in the bulk crystals. The energy softening was described theoretically in terms of the phonon renormalization in the presence of a single exciton in spherical QD's.[8,11] Quantum beats of confined exciton-LO phonon complex were observed in CuCl nanocrystals and the reduction of LO phonon energy extracted from the quantum beat was interpreted in terms of LO phonon renormalization.[12] The studies of the excited-state phonons in QD's are still at an early stage and knowledge on the shape dependence of the LO phonon renormalization is lacking.

CuCl QD's embedded in NaCl crystals, unlike those in a glass matrix, show oscillatory fine structures in the inhomogeneously broadened $Z_3$ exciton absorption bands. These structures were assigned to the size-quantized $Z_3$ excitons confined in the CuCl QD's of cubic shape.[5,6,13] In this paper, we study the size dependence of the lattice vibrations in the excited states for CuCl cubic QD's in NaCl crystals by means of PSHB. We note that, unlike the conventional Raman scattering which involves the ground-state vibrational modes, the PSHB spectroscopy gives the information about phonon modes in the excited states.[8] The effect of the exciton formation on the lattice vibrations in the QD's was explored experimentally by tuning the size-dependent energy level spacings between the ground and excited states to be resonant with the LO phonon.

CuCl QD's used in the experiment were embedded in NaCl crystals. The NaCl crystals containing CuCl were grown by the transverse Bridgman method.[14] The size of the QD's was controlled by heat treatment with different temperature and time. The samples were directly immersed in superfluid helium at 2 K in an optical cryostat. A narrow-band dye laser pumped by the third harmonics of the output of a $Q$-switched $Nd^{3+}$: YAG laser (355 nm) was used as a pump source. The pulse duration and repetition were approximately 5 ns and 30 Hz, respectively. The spectral linewidth was about 0.014 meV. A halogen lamp was used as a probe source. The PSHB spectrum was measured as follows: First, the absorption spectrum was obtained and the sample was exposed to dye laser pulses to burn a persistent spectral hole at an excitation energy. Then, the absorption spectrum was measured again after the laser exposure was stopped. The absorption spectral change $-\Delta\alpha d$ is defined as the difference between the spectra before and after the laser exposure. The subsequent measurements were performed at the new position of the samples and not carried out at the position burnt previously. The transmitted light of the samples was detected by a liquid-nitrogen cooled charge-coupled device in conjunction with a 75-cm spectrometer involving an 1800 grooves/mm grating operated in the second order of diffraction. The spectral resolution of the experiment was about 0.13 meV.

Figures 1 and 2 show the absorption and PSHB spectra of two CuCl QD samples with different QD sizes at 2 K. Oscillatory fine structures are observed between 3.22 and 3.28 eV in the $Z_3$ exciton absorption bands as shown in Figs. 1(a) and 2(a), and are attributed to size-quantized exciton states in cube-shaped QD's.[5,6,13] As seen in Figs. 1(b) and 2(b), the main hole marked by $M$ coincides with the energy of the pump beam. The broad hole, referred as a pseudophonon-wing[15] with a Stokes shift of a few meV was

 

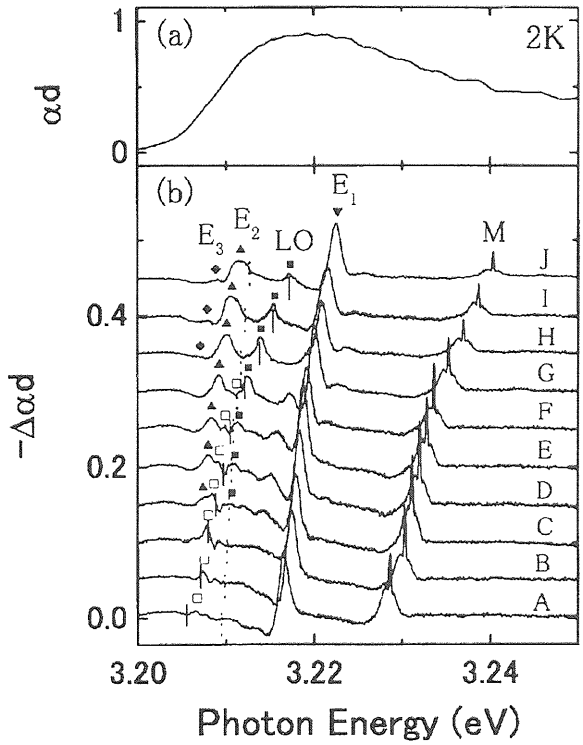


FIG. 1. Absorption (a) and PSHB spectra (b) of CuCl QD's with large size in NaCl crystals at 2 K. The excitation energies for spectra *A*, *B*, *C*, *D*, *E*, *F*, *G*, *H*, *I*, and *J* are 3.2287, 3.2303, 3.2311, 3.2320, 3.2329, 3.2336, 3.2353, 3.2370, 3.2387, and 3.2404 eV, respectively. The vertical dotted lines show the energies of the hole burning of the ground state $E_{1,1,1}$ under excitation of the excited state $E_{3,1,1}$ obtained from the relation $E_{3,1,1}-E_B=3.67(E_{1,1,1}-E_B)$. The vertical solid lines represent the energies of the LO phonon sideband holes calculated from $E_M-E_{LO*}$, where $E_{LO*}=23.1$ meV is the LO phonon energy in the excited state.

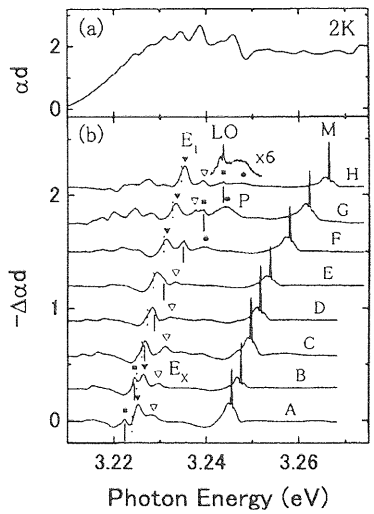


FIG. 2. Absorption (a) and PSHB spectra (b) of CuCl QD's with small size in NaCl crystals at 2 K. The excitation energies for spectra *A*, *B*, *C*, *D*, *E*, *F*, *G*, and *H* are 3.2454, 3.2474, 3.2496, 3.2517, 3.2538, 3.2580, 3.2623, and 3.2664 eV, respectively. The vertical dotted lines show the energies of the hole burning of the ground state $E_{1,1,1}$ under excitation of the excited state $E_{2,1,1}$ obtained from the relation $E_{2,1,1}-E_B=2(E_{1,1,1}-E_B)$. The vertical solid lines represent the energies of the LO phonon sideband holes calculated from $E_M-E_{LO*}$, where $E_{LO*}=23.1$ meV is the LO phonon energy in the excited state.

suggested to originate from the confined acoustic phonon-assisted absorption of the QD's.[16,17]

The Stokes shifts of the holes $E_1$, $E_2$, $E_3$, LO, and $P$ as a function of the exciton confinement energy are shown in Fig. 3. The confinement energies of the satellite holes, $E_{\text{hole}}-E_B$, where $E_{\text{hole}}$ is the photon energy of the hole and $E_B$ is the bulk $Z_3$ exciton energy ($E_B=3.2022$ eV at 2 K), were obtained from the PSHB spectra. According to the size dependence of the Stokes shift between the main hole and the satellite hole in the QD's, the exciton- and phonon-related holes can be distinguished. If an infinitely high potential barrier is assumed, the quantized exciton energy levels for a quantum cube are given by

$$E_{n_x,n_y,n_z}=E_B+\frac{\hbar^2\pi^2}{2M(L-a_B)^2}(n_x^2+n_y^2+n_z^2), \qquad (1)$$

where $M=2.3m_0$ is the translational mass of the bulk exciton and quantum numbers $n_x$, $n_y$, and $n_z$ take values 1, 2, 3, .... $L$ is the side lengths of the quantum cube and $L-a_B$ is used for the dead-layer correction. For a quantum cube the ground state $E_{1,1,1}$ and the first and higher excited states, $E_{2,1,1}$, $E_{2,2,1}$, $E_{3,1,1}$, $E_{2,2,2}$, and $E_{3,3,1}$, satisfy relations $E_{2,1,1}-E_B=2(E_{1,1,1}-E_B)$, $E_{2,2,1}-E_B=3(E_{1,1,1}-E_B)$, $E_{3,1,1}-E_B=3.67(E_{1,1,1}-E_B)$, $E_{2,2,2}-E_B=4(E_{1,1,1}-E_B)$, and $E_{3,3,1}-E_B=6.3(E_{1,1,1}-E_B)$. As seen in Figs. 1(b) and 2(b), the main hole burnt resonantly at the laser energy $E_M$ and the satellite hole $E_1$ almost obeys the equation $E_M-E_B=2(E_1-E_B)$. Thus, the dominant satellite hole $E_1$ is

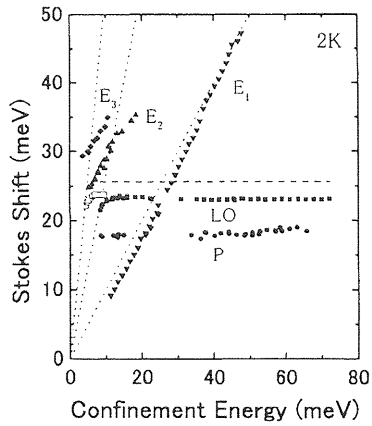


FIG. 3. Stokes shifts of the satellite holes $E_1$, $E_2$, LO, and $P$ in CuCl QD's in NaCl crystals as a function of the exciton confinement energy. The dashed line represents the energy of LO phonon in a bulk CuCl crystal. The dotted lines represent the size dependence of the energy spacings between the ground and excited states in the CuCl QD's on the quantum cube model.

from the hole burning of the ground state $E_{1,1,1}$ under excitation of the first excited state $E_{2,1,1}$ in the quantum cubes. Further, the holes marked by $E_2$ and $E_3$ in larger CuCl QD's are assigned to the hole burning of the exciton ground states under excitation of the excited states $E_{3,1,1}$,[5] and $E_{3,3,1}$, respectively. Strictly speaking, direct optical excitation of the first excited state $E_{2,1,1}$ in ideally cubic nanocrystals is forbidden and its oscillator strength should be zero. Therefore, the observation of the hole burning of the ground state under excitation of the first excited state suggests that the QD's are not ideal cubes.[5,6] Recently, the holes $E_1$ and $E_X$ observed in Fig. 2(b) were suggested to be from the hole burning of the exciton ground states under excitation of the degenerate first excited states $E_{2,1,1}$ and $E_{1,1,2}$ in nearly cubic CuCl quantum boxes.[18]

A pronounced nonresonant hole labeled by LO with a Stokes shift of 23.1 meV is located at the low-energy side of the main hole and is almost size-independent over a wide size range as shown in Fig. 3. From the size dependence, the hole is assigned to a LO phonon sideband of the exciton ground state, which is slightly smaller than the phonon energy of 23.5 meV in CuCl QD's in glass.[8] In addition, a broad hole denoted by $P$ with a Stokes shift of about 18 meV was observed in the PSHB spectra. The Raman spectrum of CuCl crystals in the transverse optical (TO) phonon regime is anomalous, consisting of a sharp [TO($\gamma$),~21.3 meV] and a broad [TO($\beta$),~18.7 meV] line at low temperature.[19,20] The Stokes shift of the hole $P$ measured in the PSHB spectra is close to the energy of the TO($\beta$). Therefore, the satellite hole $P$ may be from the optical absorption together with simultaneous emission of a TO($\beta$) phonon.

As seen in Figs. 1(b) and 2(b), the PSHB spectra are very complex because the hole burning of the ground states under excitation of various excited states was clearly observed at the lower energy side of the spectra, in contrast to the simple PSHB spectra of spherical CuCl QD's in glass.[8] We can easily demonstrate the LO phonon mixes with the excited states of the excitons in CuCl cubic QD's in NaCl crystals when the LO phonon is close to the energy differences between the ground and excited states. In the PSHB spectra of large CuCl QD's in Fig. 1(b), the holes $E_2$ and LO become close to each other when the dot size is increased. Then the LO phonon energy becomes small and the LO phonon mode clearly anticrosses with the optically allowed excited state $E_{3,1,1}$ of the exciton at an energy of about 3.212 eV. The Stokes shift of the hole $E_2$ is the energy difference between the ground state $E_{1,1,1}$ and the next optically allowed state $E_{3,1,1}$ in cubic QD's, and may be compared to the energy spacing between the ground state ($1S$) and the excited state ($2S$) in spherical nanocrystals, whose principal quantum number $n$ and angular momentum quantum number $l$ are taken as $n=1, l=0$, and $n=2, l=0$, respectively.[2] An anticrossing between the phonon sideband of the exciton ground state and the higher excited state $E_{3,1,1}$ is clearly observed at a confinement energy of about 10 meV in Fig. 3.

Further, it is noted that a sharp peak marked by an open square arises between holes $E_2$ and LO in spectra ranging from $G$ to $C$ in Fig. 1(b). The sharp peak becomes dominant with the increase of the dot size. The Stokes shift of the peak

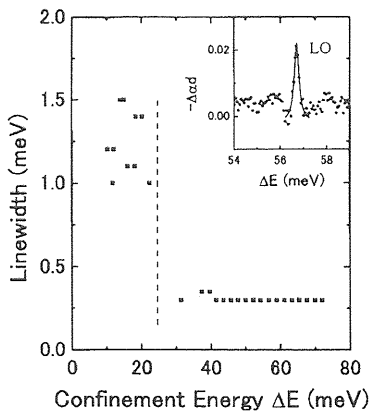


FIG. 4. Size dependence of the linewidth of LO phonons in CuCl QD's in NaCl crystals. The vertical dashed line shows the energy of the phonon that is equal to the energy spacing between the ground and the first excited state $E_{2,1,1}$. The inset shows the LO phonon sideband (closed circles) at the confinement energy of 56.7 meV and a Lorentzian fit (solid curve), respectively.

is about 23.7 meV and is not dependent on the dot size in the smaller QD's as shown in Fig. 3. Therefore, the peak is considered to be an LO phonon mode of CuCl QD's. The energy of the LO phonon mode is decreased rapidly when the dot size is further increased. As a result, the LO phonon mode shows a clear anticrossing with a higher optically allowed excited state $E_{3,3,1}$ of the exciton at a confinement energy of about 6 meV. The above result clearly shows that the renormalization of LO phonon exists in CuCl cubic QD's in NaCl crystals, resulting in clear anticrossings of the LO phonon mode of the exciton ground states with two higher optically allowed excited states, $E_{3,1,1}$, and $E_{3,3,1}$. The observed anticrossings are consistent with the renormalization theory of the LO phonon.[8,11]

In the following, we studied the change of the energy and the linewidth for the LO phonon when the LO phonon is resonant with the energy separation between the exciton ground state $E_{1,1,1}$ and the first excited state $E_{2,1,1}$, which may be considered to correspond to the ground state $1S$ and the first excited state $1P$ (quantum numbers $n=0$ and $l=1$) in spherical nanocrystals, respectively.[2] As seen in spectra $C$, $D$, and $E$ of Fig. 2(b), when the LO phonon is close to the energy difference between the ground state $E_{1,1,1}$ and the first excited state $E_{2,1,1}$, it is difficult to distinguish the holes $E_1$ and LO owing to broader width of the hole $E_1$. Thus, Fig. 3 does not show a clear energy anticrossing as the theory predicted.[11] However, it is found that the linewidth of the LO phonon is increased abruptly at a confinement energy of about 23 meV, as shown in Fig. 4. When the energy of the LO phonon in the small QD's is smaller than the energy difference between the ground state $E_{1,1,1}$ and the first excited state $E_{2,1,1}$, the LO phonon is very narrow and its linewidth is about 0.3 meV, as is shown in the enlarged spectrum $H$ of Fig. 2(b) and the inset of Fig. 4. The LO phonon becomes broad with a linewidth of about 1.2 meV in the spectra $A$ and $B$ of Fig. 2(b) after the phonon is resonant with the

energy difference between the ground state $E_{1,1,1}$ and the first excited state $E_{2,1,1}$. At the same time, it is noted that the intensity of the LO phonon sideband is enhanced near the exciton-phonon resonance.

In spherical QD's, the coupling of $l=1$ phonons with exciton $P$ states leads to a renormalization of the latter, as predicted in Ref. 11, but the $P$ states having a zero oscillator strength are not expected to show up in the PSHB spectrum. In the similar manner, the phonon sideband of the ground state in ideally cubic QD's can interact with the first excited-state $E_{2,1,1}$ with a zero oscillator strength. However, the PSHB experiment reported earlier[5,6] shows that the oscillator strength of the first excited state in CuCl QD's in NaCl crystals is not zero. Therefore, the coupling between the ground state $E_{1,1,1}$ and the first excited state $E_{2,1,1}$ through phonons of appropriate symmetry will cause a weak energy anticrossing that can be observed in the PSHB spectrum. Although we do not see a clear anticrossing of the LO phonon with the first excited state $E_{2,1,1}$, we interpret the observed broadening of the LO phonon sideband as due to exciton-phonon mixing. This interpretation is backed by the lineshape analysis of Zimin *et al.*[21] around the LO-phonon-exciton anticrossing region.

In conclusion, we have studied the LO phonon modes and exciton states in nearly cubic CuCl QD's in NaCl crystals by the PSHB spectroscopy. The exciton formation in the QD's has influenced the lattice vibrations, leading to a mixing of the LO phonon with the excitons near the exciton-phonon resonance. At larger sizes, the resonant mixing of the optically allowed excited states $E_{3,1,1}$ and $E_{3,3,1}$ of the exciton and the phonon modes shows clear anticrossing behaviors. At smaller sizes, the significant linewidth broadening of the LO phonon probably results from the mixing of the LO phonon with the exciton when the phonon is resonant with the transition between the ground and the first excited state. This indicates that the interaction of the LO phonons with excitons in QD's depends on the shape of QD's. Because the energy levels of the exciton excited states in nearly cubic QD's are more complex than those in spherical nanocrystals, further theoretical studies on the nearly cubic QD's are required to understand the interaction of the LO phonon with excitons in CuCl QD's in NaCl crystals.

One of the authors (J. Z.) sincerely thanks Dr. A. V. Fedorov, Dr. T. Mishina, Dr. T. Okuno, Dr. J. Qi, and Dr. M. Ikezawa for valuable discussions. This work was partially supported by the "Research for the Future" Program JSPS-RFTF 97P00106 from the Promotion of Science.

[1] A.D. Yoffe, Adv. Phys. **42**, 173 (1993).
[2] U. Woggon, *Optical Properties of Semiconductor Quantum Dots* (Springer, Berlin, 1997).
[3] K. Naoe, L.G. Zimin, and Y. Masumoto, Phys. Rev. B **50**, 18 200 (1994).
[4] Y. Masumoto, K. Sonobe, and N. Sakakura, J. Lumin. **72–74**, 294 (1997).
[5] N. Sakakura and Y. Masumoto, Jpn. J. Appl. Phys., Part 1 **36**, 4212 (1997).
[6] N. Sakakura, and Y. Masumoto, Phys. Rev. B **56**, 4051 (1997).
[7] For review see Y. Masumoto, J. Lumin. **70**, 386 (1996).
[8] L. Zimin, S.V. Nair, and Y. Masumoto, Phys. Rev. Lett. **80**, 3105 (1998).
[9] J. Valenta, J. Moniatte, P. Gilliot, B. Hönerlage, J.B. Grun, R. Levy, and A.I. Ekimov, Phys. Rev. B **57**, 1774 (1998).
[10] *Persistent Spectral Hole Burning: Science and Applications*, edited by W. E. Moerner (Springer-Verlag, Berlin, Heidelberg, 1988).
[11] S.V. Nair and Y. Masumoto, Jpn. J. Appl. Phys., Part 1 **38**, 581 (1999).
[12] H. Ohmura and A. Nakamura, Phys. Rev. B **59**, 12 216 (1999).
[13] T. Itoh, S. Yano, N. Katagiri, Y. Iwabuchi, C. Gourdon, and A.L. Ekimov, J. Lumin. **60–61**, 396 (1994).
[14] T. Itoh, Y. Iwabuchi, and M. Kataoka, Phys. Status Solidi B **145**, 567 (1988).
[15] J. Friedrich, J.D. Swalen, and D. Haarer, J. Chem. Phys. **73**, 705 (1980).
[16] S. Okamoto and Y. Masumoto, J. Lumin. **64**, 253 (1995).
[17] J. Zhao and Y. Masumoto, Phys. Rev. B **60**, 4481 (1999).
[18] J. Zhao, M. Ikezawa, A.V. Fedorov, and Y. Masumoto, J. Lumin. **87–89**, 525 (2000).
[19] M.L. Shand, H.D. Hochheimer, M. Krauzman, J.E. Potts, R.C. Hanson, and C.T. Walker, Phys. Rev. B **14**, 4637 (1976).
[20] A. Göbel, T. Ruf, C. Lin, M. Cardona, J. Merle, and M. Joucla, Phys. Rev. B **56**, 210 (1997).
[21] L. Zimin, S. V. Nair, and Y. Masumoto (unpublished).

PHYSICAL REVIEW B, VOLUME 63, 075316

# Phonon resonances in photoluminescence spectra of self-assembled quantum dots in an electric field

Ivan V. Ignatiev* and Igor E. Kozin
*Single Quantum Dot Project, ERATO, JST, Tsukuba Research Consortium, Tsukuba 300-2635, Japan and Institute of Physics, St.-Petersburg State University, St.-Petersburg, Russia*

Valentin G. Davydov,† Selvakumar V. Nair, Jeong-Sik Lee, and Hong-Wen Ren‡
*Single Quantum Dot Project, ERATO, JST, Tsukuba Research Consortium, Tsukuba 300-2635, Japan*

Shigeo Sugou
*Opto-electronics Research Laboratories, NEC Corporation, Tsukuba 305-0841, Japan and Single Quantum Dot Project, ERATO, JST, Tsukuba Research Consortium, Tsukuba 300-2635, Japan*

Yasuaki Masumoto
*Single Quantum Dot Project, ERATO, JST, Tsukuba Research Consortium, Tsukuba 300-2635, Japan and Institute of Physics, University of Tsukuba, Tsukuba 305-8571, Japan*

(Received 20 May 2000; revised manuscript received 11 September 2000; published 31 January 2001)

Phonon resonances observed in the photoluminescence (PL) spectra of InP and $In_{0.35}Ga_{0.65}As$ self-assembled quantum dots (QD's) in an external electric field are studied in detail. The resonances are shown to arise from fast phonon-assisted relaxation of hot carriers, and to become observable when the PL is quenched by nonradiative losses from excited states. A simple model is developed that considers tunneling of the carriers from the QD's into the barrier layer as the main process responsible for PL quenching in the presence of an electric field. From this model, the depth of the potential well for holes is estimated to be 10–20 meV for the InP QD's. The PL kinetics measurement is performed with a time resolution of 6 ps. Clear evidence of surprisingly fast carrier relaxation with emission of high-energy acoustic phonons is found. Further acceleration of the carrier relaxation is observed under strong optical pumping. We consider this effect to be caused by Auger-like carrier-carrier scattering processes. Acceleration of the relaxation observed at elevated temperatures is ascribed to stimulated phonon emission.

DOI: 10.1103/PhysRevB.63.075316 PACS number(s): 78.66.Fd, 63.22.+m, 78.47.+p, 73.21.−b

## I. INTRODUCTION

Quantum dots (QD's) attract much attention because of their unusual physical properties and promising prospects for application in device engineering. Three-dimensional carrier confinement gives rise to discrete energy levels with large spacings, provided that the QD's are sufficiently small. For this reason, QD's are often referred to as artificial atoms.[1] Realization of such artificial atoms in semiconductor heterostructures and their integration with conventional electronic and optical devices offer great potential for applications.[2–4] For optical applications, the main physical processes are the creation of carriers in the QD, their relaxation to the lowest-energy states, and radiative recombination.

The carrier relaxation process was studied extensively during the last decade because it mainly determines the luminescence efficiency of QD's.[5–12] At low temperature and weak excitation, the main relaxation mechanism is spontaneous emission of phonons by hot carriers. Though this point is evident, peculiarities of this process in QD's are not yet understood and have been widely discussed up to now.[13–23]

In polar semiconductors of interest, electrons and holes interact strongly only with the longitudinal-optical (LO) phonons. LO phonons produce an electric field to which the electrons and holes are sensitive as charged particles. The energy spectrum of the LO phonons is typically rather narrow, and can be roughly considered as a set of degenerate energy values. Therefore, fast relaxation occurs only in those QD's where the energy spacings are equal to the energy of one or several LO phonons. The carriers in other QD's have to relax via acoustic-phonon emission. This process is inherently slow because of the weak deformation potential interaction. This is well known for bulk materials, where the relaxation with emission of acoustic phonons is slower by two orders of magnitude than that with emission of LO phonons.[24] Theoretical considerations show that acoustic-phonon-mediated relaxation is further slowed down in QD's—this effect is commonly referred to as "phonon bottleneck."[5,6] Only phonons with wavelengths of the order of the QD diameter and an energy equal to an interlevel spacing may cause one-phonon relaxation. Although two-phonon relaxation is not so restricted, this process should be also slow because of weak electron-phonon interaction.[7]

It seems that some indication of the phonon bottleneck is found in a few experiments. The simplest experiment consists of the observation of the photoluminescence (PL) spectrum of a QD ensemble under an optical excitation slightly above the PL maximum. Sharp features (resonances) shifted by the LO-phonon energy from the excitation line were observed in the spectra of some samples.[13,14,16,18,20,25–27]

 

Other types of experiments apparently argue against the phonon bottleneck. The most important of these is the study of the rise time of the PL, that is determined by the relaxation of hot carriers to their lowest energy levels. These experiments show a fairly short rise time of a few or several tens of picoseconds in high-quality samples.[17,18] This observation contradicts theoretical predictions. However, in such experiments it is difficult to achieve both good spectral and time resolutions keeping a low excitation power. Therefore, it is not clear whether the observed fast relaxation is caused by LO-phonon emission, by acoustic-phonon emission, or by some other processes.

Many theoretical efforts have been put forward to explain fast carrier relaxation. Two-phonon processes involving LO $\pm$LA combination,[7] LO-phonon anharmonicity,[21] relaxation through continuum states,[22] and defect states[12,28,29] were considered to spread out the spectral region where the fast phonon-assisted relaxation is possible. In addition, an alternative mechanism of relaxation was proposed that considered carrier-carrier scattering (referred to as Auger-like processes).[8,11,30–32]

We recently proposed a powerful method to study carrier relaxation in QD's.[23] This method exploits the idea of artificially controlling PL quenching.[33–35] The PL quenching rate can be changed in a wide range by applying an external electric field to the sample. This allows one to study carrier relaxation by varying the ratio of the relaxation and PL quenching rates.

In this paper, we use this method to study phonon-assisted carrier relaxation in self-assembled QD's in more detail. We study the PL spectra and PL kinetics of heterostructures with InP and $In_{0.35}Ga_{0.65}As$ QD's in an electric field under quasiresonant excitation. We find that, for all heterostructures studied, a fast LO-phonon-assisted relaxation gives rise to LO resonances in the spectra of PL partially quenched by an electric field. The acoustic-phonon-assisted relaxation is not suppressed as strongly as predicted theoretically. The interaction with *high-energy acoustic phonons* is also fairly strong, and gives rise to a relatively fast relaxation which is only an order of magnitude slower than the resonant LO-phonon-assisted relaxation. We discuss a possible physical mechanism of the relatively strong interaction of an electron-hole pair with high-energy acoustic phonons. According to our results, we conclude that there is no phonon bottleneck effect in QD's, at least in the sense that it was proposed theoretically.

We present a model for a PL quenching mechanism in the presence of an electric field. The essential point of our model is the tunneling of carriers from QD's into the barrier layer. From a quantitative analysis of the experimental data, we evaluated the depth of the potential well for holes in InP QD's.

We also discuss an acceleration of the carrier relaxation due to carrier-carrier scattering and stimulated phonon emission. For this purpose, we study the PL spectra of samples in an electric field under strong optical pumping and at elevated temperatures.

## II. EXPERIMENTAL DETAILS

The sample with InP QD's was grown by gas-source molecular-beam epitaxy on an $n^+$ GaAs substrate. A 300-nm GaAs buffer layer containing a thin 3 $\times$(2-nm AlAs/10-nm GaAs) superlattice in the middle was grown at 600 °C to suppress dislocations. A thin (2 nm) AlAs layer on the buffer layer was grown to prevent compositional interdiffusion between GaAs and $In_{0.5}Ga_{0.5}P$ layers. One layer of InP QD's with a nominal thickness of 4 ML was grown between the 100-nm $In_{0.5}Ga_{0.5}P$ barrier layers. The growth rates were 0.5 ML/s for $In_{0.5}Ga_{0.5}P$, and 0.25 ML/s for InP. The interruption times used before and after the InP growth were 2 and 20 s, respectively. The areal density of the QD's is about $10^{10}$ $cm^{-2}$. This was determined by atomic force microscopy on a reference sample, grown in the same conditions without the top barrier layer. The average base diameter of the QD's is $\approx$40 nm and the height is $\approx$5 nm, as determined by cross-sectional transmission electron microscopy. The sample with $In_{0.35}Ga_{0.65}As$ QD's was grown by metal organic vapor phase epitaxy on the (711)B $n^+$ substrate. A QD layer with a nominal thickness of 4.5 MLs is embedded between 250- and 100-nm GaAs layers containing 2-nm AlAs layers as stop layers for photocreated carriers. The areal density of the QD's is about 5 $\times 10^9$ $cm^{-2}$. The average base diameter is $\approx$70 nm, and the height is $\approx$10 nm as determined by atomic force microscopy of the reference sample. The samples were provided with a semitransparent gold or indium tin oxide Shottky contact on the top surface, and with an Ohmic contact on the back surface.

The PL was excited selectively by a continuous wave (cw) Ti:sapphire laser within or slightly above the PL band of the QD's. This excitation is hereafter referred to as quasiresonant excitation. The pump power density was less than 100 $W/cm^2$. We checked that the PL intensity depended linearly on the excitation power within this range without any change of the PL spectrum. The spectral width of the laser line was less than 0.01 meV without any sidebands. The PL was dispersed by a double monochromator U1000 (focal length 1 m, numerical aperture 1:8, linear dispersion 0.36 nm/mm) with an extremely low background of scattered light ($10^{-14}$ at a distance of 3 meV from the laser line). The spectral resolution of the setup was approximately 0.15 meV. A photon counting system with a cooled GaAs or $In_{0.35}Ga_{0.65}As$ photomultiplier tube was used for detection of the PL signal.

The PL kinetics was studied using a picosecond Ti:sapphire laser with a pulse duration ranging from 1 to 5 ps, and a repetition rate of 82 MHz. In most experiments, we used a fairly low average pump power density of about 50 $W/cm^2$ to prevent the creation of more than one electron-hole pair in a QD per pulse. This allowed us to avoid relaxation due to carrier-carrier scattering. A 0.25-m double-subtractive dispersion monochromator (spectral resolution 0.5 nm) and a streak camera were used for accumulation of the signal in the selected spectral points. The time resolution of the setup was

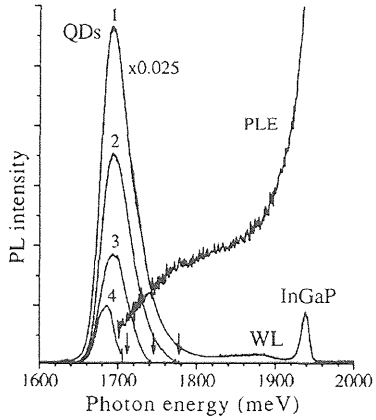


FIG. 1. The PL and photoluminescence excitation (PLE) spectra of the sample with InP QD's. PL spectrum 1 was recorded under $In_{0.5}Ga_{0.5}P$ band-to-band excitation. It is scaled by a factor 0.025. The PL bands of the $In_{0.5}Ga_{0.5}P$ barriers, the wetting layer, and the InP QD's are marked. PL spectra 2, 3, and 4 were recorded under quasiresonant excitation with photon energies indicated by arrows. The PLE spectrum was recorded by PL detection at $E_{PL}$ = 1700 meV.

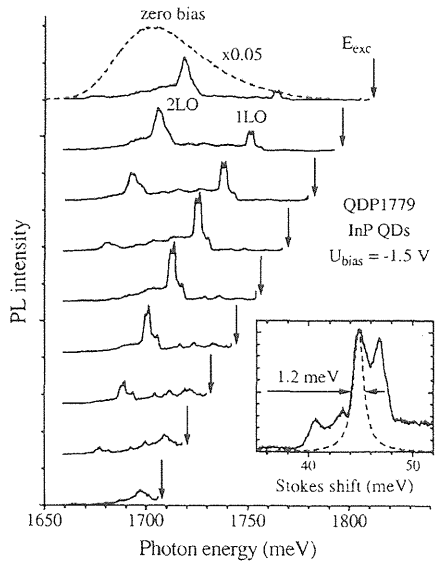


FIG. 2. PL spectra of the sample with InP QD's at different excitations indicated by arrows. $U_{bias} = -1.5$ V. The spectra are shifted vertically for clarity. The top curve, shown by a dashed line, is the spectrum at zero bias. It is scaled by a factor of 0.05. Inset: a part of the PL spectrum showing an LO resonance vs the Stokes shift. A fit of one of the peaks in the resonance by a Lorentzian is shown by dashed lines.

about 6 ps. Most measurements were done at a sample temperature 2 K to exclude any processes involving absorption or stimulated emission of phonons.

## III. EXPERIMENTAL RESULTS AND DISCUSSION

### A. PL spectra

The PL bands of the heterostructures recorded under nonresonant (barrier band-to-band) and quasiresonant excitation have a smooth profile without any sharp features. A typical spectrum of the sample with InP QD's is shown in Fig. 1. As seen, the most intense PL band in the spectrum is that of the QD's. The PL profile does not contain sharp features for any photon energy of excitation. The PLE spectrum is also smooth.

When a negative bias is applied to the sample surface, the integral PL intensity decreases. At the same time, the decrease of the PL in different spectral points is different and, as a result, pronounced resonances appear in the PL spectra. This behavior of the spectra was already discussed in Ref. 23. An example of the PL spectra of the InP QD's for various excitation energies is shown in Fig. 2. As seen, many resonances appeared in the spectra at negative bias. The most prominent resonance is shifted approximately from the excitation line by the LO phonon energy of the bulk InP crystal [$\hbar\omega_{LO}$=43.5 meV (Ref. 36)]. The energy positions of the resonances faithfully follow the photon energy of the excitation. Under the excitation at a high photon energy, a resonance shifted by $2\hbar\omega_{LO}$ (marked by 2LO in Fig. 2) is also observed. The relative intensity of the 1LO and 2LO resonances depends strongly on the excitation energy. The intensity of the resonances becomes weak when they leave a PL band measured at zero bias.

A few other weak resonances are visible in the spectral region between the excitation line and the 1LO resonance (hereafter referred to as the acoustic region of the spectrum), and also between the 1LO and 2LO resonances. Their energy shifts from the excitation line or the 1LO resonance line coincide with the energies of high-energy transverse acoustic (TA) and longitudinal acoustic (LA) phonons in InP crystal.

PL spectra of the sample with $In_{0.35}Ga_{0.65}As$ QD's are shown in Fig. 3. Without bias, the PL spectrum consists of two smooth maxima (see the inset), probably due to the existence of two sets of QD's with different sizes in this sample. A number of maxima (resonances) appear in the spectrum at negative bias. The most prominent resonances can be assigned to the GaAs- and InAs-like LO phonons of the $In_{0.35}Ga_{0.65}As$ QD's, because their energy shifts from the excitation line are close to the energy of the LO phonons in GaAs and InAs crystals, respectively. They are marked in Fig. 3 as $LO_G$ and $LO_I$. An intense resonance with a Stokes shift of about 20 meV can be assigned to LA phonons of an $In_{0.35}Ga_{0.65}As$ solid solution. A narrow peak with a Stokes shift of 33.2 meV, marked by * in Fig. 3, is probably due to the Raman scattering from the GaAs barrier layers, because the intensity of this peak does not depend on bias.

The LO-phonon resonances for all the samples have a rather complicated structure consisting of a few narrow peaks. A fit of each separate peak in the resonance by Lorentzians allows one to estimate the full width at half maximum (FWHM) to be about 1.2 meV for the InP QD's, as shown in the inset of Fig. 2. A similar fit of the $LO_G$ resonance in the spectra of the $In_{0.35}Ga_{0.65}As$ QD's (see Fig. 3) gives a FWHM of 0.5 meV.

Under positive bias, the PL intensity also starts to decrease. However, for $U_{bias}>0.7$ V, a strong increase of the

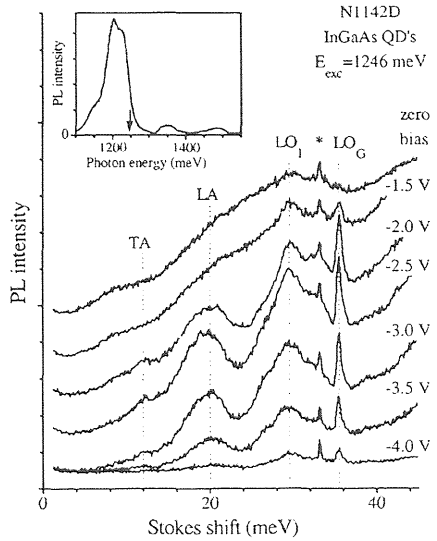


FIG. 3. The PL intensity vs the Stokes shift for the sample with $In_{0.35}Ga_{0.65}As$ QD's under different biases indicated against each curve. $E_{exc}$= 1246 meV. The spectra are shifted vertically for clarity. The energies of the resonances marked by TA, LA, $LO_I$, and $LO_G$ are 12, 20, 30, and 35.5 meV, respectively. Inset: PL spectrum of the sample without bias.

PL is observed. This effect is caused by the electric-current-induced radiative process, and is discussed elsewhere.[37]

### B. Physical mechanism

Based on the presented data, we now discuss the physical mechanism responsible for the observed phonon resonances. Generally, a few processes are possible — resonant Raman scattering, phonon-assisted electron-hole recombination, phonon-assisted absorption, and phonon-assisted relaxation in the presence of nonradiative losses.

Resonant Raman scattering has a low efficiency, as observed, for example, by Sirenko *et al.* for a heterostructure with InP QD's.[38] Our experimental results, namely, the dependence of the phonon resonance intensities on the applied bias and the strongly variable ratio of the 1LO and 2LO resonance intensities depending on spectral position within the PL band, allow us to rule out resonant Raman scattering as the process responsible for the phonon resonances. This point is further supported by the long decay time of the QD emission at the phonon resonances and the strong temperature dependence of the resonance intensities, discussed below.

Phonon-assisted electron-hole recombination can be also ruled out, because the electron-phonon interaction is weak in these structures and is able to produce only very small phonon sidebands in the PL spectra.[39] In addition, the ratio of intensities of the one- and two-phonon sidebands must be almost independent of the photon energy of the excitation, in contrast to the observed behavior of the 1LO and 2LO resonances.

The phonon resonances in the spectra can also be caused by phonon-assisted absorption when an absorbed photon creates an electron and a hole in their ground states, and a phonon. The probability of this process is usually equal to that of the phonon-assisted PL, and is also small. It can be enhanced by a resonance with some direct (phononless) optical transition as is discussed in Ref. 40. The phonon-assisted absorption in the $In_{0.4}Ga_{0.6}As$ QD's was observed by Findeis *et al.*[41] We neglect this process in the following discussion.

We assume that the main process causing phonon resonances is the selective phonon-assisted relaxation of hot carriers in the presence of nonradiative losses. The appearance of phonon resonances due to this process can be explained as follows.[14] The quasiresonant excitation creates electrons and holes in the excited states. The QD's in the ensemble have slightly different sizes and shapes, and the interlevel energy spacing $\Delta E$ has some distribution. The spacing $\Delta E$ can well match the LO-phonon energy $E_{LO}$ only in some subset of the QD's. Carrier relaxation in these QD's is fast due to the high efficiency of this process with the emission of a LO phonon. The relaxation in the rest of the QD's occurs via emission of acoustic phonons i.e., much more slowly. If the electron or hole can efficiently leave the QD (this process is usually referred to as nonradiative losses) before relaxation via acoustic-phonon emission, the PL does not appear in any spectral point except the point where it is "saved" by fast LO-phonon-assisted relaxation. In the time-integrated PL spectrum, a narrow peak shifted from the excitation line by the energy of the LO phonon, $E_{LO}$, must be observed in this case. However, if there are no significant nonradiative losses, electrons and holes in *any* QD eventually relax to the lowest levels and recombine. In this case, the PL spectrum must reproduce the energy distribution of the lowest optical transition which usually has a bell-like smooth shape. Behavior of the spectra presented in Figs. 2 and 3 agrees with this scenario.

### C. Model

The dependence of the PL spectra on the electric field was qualitatively discussed in Ref. 23. Here we analyze this dependence quantitatively in the framework of the model schematically drawn in Fig. 4. We assume that the quasiresonance excitation generates an electron and a hole in excited energy levels labeled by $|1e\rangle$ and $|1h\rangle$, respectively.

The excited electron and hole may relax at different rates. However, the experimental data do not allow us to separate these processes. On the other hand, the observed narrow resonances (see Figs. 2 and 3) can be formed only by one-step relaxation of carriers, with the emission of a single phonon. This may be relaxation of one of the photocreated carriers with another one being created in its ground state,[42] or relaxation of an electron-hole pair as a correlated system. Therefore, we consider some effective relaxation rate from the excited state of the electron-hole pair to its ground state.

The relaxation process competes with the nonradiative losses. We assume that the external electric field activates the tunneling of the photocreated carriers from the QD into the barrier layer. The depth of the potential well for holes is usually smaller than that for electrons. As for InP QD's, it is

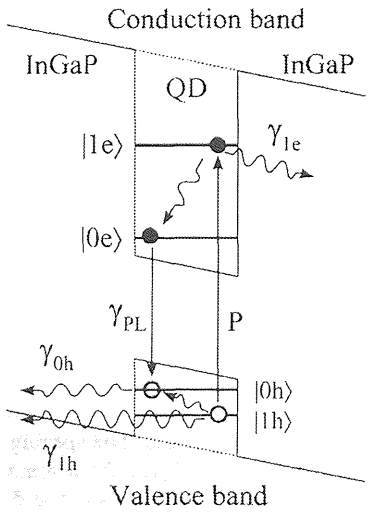


FIG. 4. A model of the PL quenching in the electric field. The vertical arrows marked by $P$ and $\gamma_{\mathrm{PL}}$ denote the pumping and radiative recombination processes, respectively. The relaxation of the hot carriers to their ground states is shown by the wavy arrows which are not labeled. The wavy arrows marked by $\gamma_{0h}$, $\gamma_{1h}$, and $\gamma_{1e}$ indicate tunneling of the hole from the ground and excited states, and of the electron from the excited state, respectively.

assumed that the holes are weakly localized in the dots or even in the surrounding material.[43,44] A real potential profile for carriers may be complicated due to strain and also due to composition fluctuations.[45] Nevertheless we assume for simplicity that the potential barrier for holes acquires a triangular shape in the electric field, as shown in Fig. 4.

In the semiclassical approach, the tunneling rate $\gamma_i(U)$ from the state $|i\rangle$ through a triangular barrier is given by the expression[46]

$$\gamma_i = \gamma_i^0 e^{-U_i/U}, \tag{1a}$$

with

$$U_i = (4/3e\hbar)\sqrt{2m^*}E_i^{3/2}d, \tag{1b}$$

where $m^*$ is the effective mass of a carrier, $E_i$ is the depth of the potential well for the carrier in state $|i\rangle$, and $d$ is the effective thickness of the insulating layer to which the bias is applied ($d \approx 0.5\mu$). Here we neglect the dependence of $E_i$ on $U$.

The well depth for electrons in the InP QD's is of about 200 meV, which prevents the electron from tunneling into the conduction band of the barrier layer at a moderate bias. However, the electrons may tunnel to deep levels that are present in the vicinity of the QD's even in high-quality heterostructures.[37,47,48] Analysis shows that the electron tunneling from the excited state $|1e\rangle$ affects the PL of the InP QD's at $U_{\mathrm{bias}} < -1$ V. To simplify our discussion, we describe the rate of this process, $\gamma_{1e}$, by the same equations (1). We also neglect variations of the carrier relaxation and optical transition probabilities in the electric field, a possible built-in electric field,[47] and intrinsic dipole moment of QD's.[45] All these effects influence the PL of the QD's much more weakly than the carrier tunneling.

The dynamics of the electron-hole pair populations $n_1$ and $n_0$ in the levels $|1\rangle$ and $|0\rangle$, respectively, are described in the framework of the model by the equations

$$\frac{dn_1}{dt} = P - (\gamma_r + \gamma_{1t})n_1,$$

$$\frac{dn_0}{dt} = \gamma_r n_1 - (\gamma_{\mathrm{PL}} + \gamma_{0t})n_0. \tag{2}$$

Here $\gamma_{\mathrm{PL}}$ is the rate of the electron-hole radiative recombination, $\gamma_r$ is the relaxation rate from state $|1\rangle$ to state $|0\rangle$, and $\gamma_{1t} = \gamma_{1h} + \gamma_{1e}$ and $\gamma_{0t} = \gamma_{0h}$ are the tunneling rates from the states $|1\rangle$ and $|0\rangle$, respectively.

For a cw excitation ($P$=const), the steady-state solution of Eq. (2) yields an expression for the bias dependence of the population of the radiative state $n_0$. As a result, the bias dependence of the PL intensity, which is proportional to $\gamma_{\mathrm{PL}}n_0$, is given by

$$I_{\mathrm{PL}}(U) = NP\frac{1}{(1+\gamma_{1t}/\gamma_r)}\frac{1}{(1+\gamma_{0t}/\gamma_{\mathrm{PL}})}, \tag{3}$$

where $N$ is the number of QD's which can emit light at a given spectral point under a given excitation.

The tunneling rates are equal to zero for zero bias [see Eqs. (1a) and (1b)]. Therefore, the PL intensity does not depend on the relaxation rate. This is why phonon resonances are not observed in the PL spectra in the absence of the electric field. In the presence of an electric field, Eq. (3) depends on the branching ratio of the relaxation and tunneling rates from the excited state $|1\rangle$. For slow acoustic-phonon relaxation, this ratio is larger and, therefore, the PL quenching is stronger than that for the fast LO-phonon relaxation.

To illustrate this behavior, in Fig. 5 we plot the bias dependence of the PL intensities for the sample with InP QD's at the LO resonance and also at the neighboring spectral point marked by 2AC in the inset of Fig. 5. The PL in the 2AC spectral point is contributed by those QD's in which the carriers have to relax with the emission of a few phonons because of the energy gap between the acoustic and LO phonons. The intensities $I_{\mathrm{LO}}(U)$ and $I_{2\mathrm{AC}}(U)$ at the LO and 2AC spectral points, respectively, are fitted by Eq. (3). The ratio of these intensities, normalized to unity at zero bias, may be used as a measure of the contrast of the features in the PL spectrum at strong bias. The bias dependence of this ratio is plotted in Fig. 5, and fitted by the equation

$$\frac{I_{\mathrm{LO}}(U)}{I_{2\mathrm{AC}}(U)} = \frac{(1+\gamma_{1t}/\gamma_{2\mathrm{AC}})}{(1+\gamma_{1t}/\gamma_{\mathrm{LO}})}, \tag{4}$$

that follows directly from Eq. (3). Here $\gamma_{\mathrm{LO}}$ and $\gamma_{2\mathrm{AC}}$ are relaxation rates with the emission of a LO phonon and two acoustic phonons, respectively. As is seen from the figure, the calculated curves reproduce the experimental values reasonably well. Thus, in spite of its simplicity, the model ad-

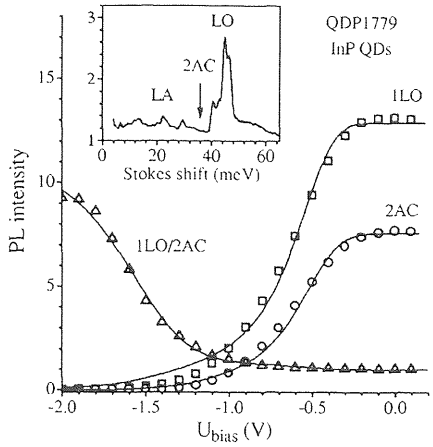


FIG. 5. Bias dependence of the PL intensities at the LO (squares) and 2AC (circles) spectral points and of their normalized ratio (triangles) for the sample with InP QD's. $E_{exc}=1771$ meV. Solid curves the fits by Eqs. (3) and (4). The fitting parameters for all the curves are $U_{1h}=2$ V, $U_{0h}=4$ V, $U_{1e}=16$ V, $\gamma^0_{1e}/\gamma^0_{1h}=3.8\times10^4$, $\gamma^0_{0h}/\gamma_{PL}=150$, $\gamma_{LO}/\gamma_{2AC}=12$, and $\gamma^0_{1h}/\gamma_{LO}=0.2$. Inset: the PL spectrum at $U_{bias}=-1.5$ V.

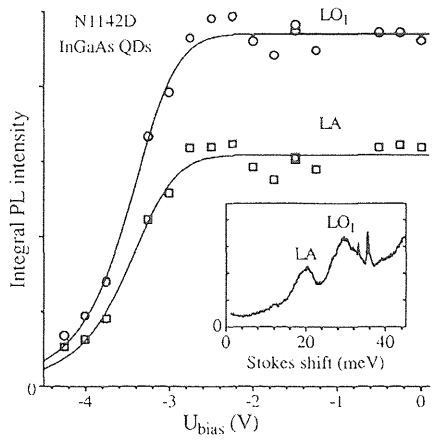


FIG. 6. Bias dependence of the PL intensity at the $LO_1$ (circles) and LA (squares) spectral points for the sample with $In_{0.35}Ga_{0.65}As$ QD's. The data are taken from the spectra presented in Fig. 3. Solid curves are fits by Eq. (3). The fitting parameters are $U_0=40$ V and $\gamma^0_0/\gamma_{PL}=9\times10^4$. Inset: PL spectrum at $U_{bias}=-3$ V.

equately describes, as a whole, the behavior of the PL intensity of the InP QD's versus the applied voltage.

From the fit, we have determined $U_{1h}=2$ V, $U_{0h}=4$ V, and $U_{1e}=16$ V. These values allow one to estimate the depth of the potential wells for carriers by means of Eq. (1b). The values $E_{0h}=13$ meV, $E_{1h}=9$ meV, and $E_{1e}=65$ meV were obtained using the heavy-hole effective mass,[49] $m^*_h=0.65m_0$, and the electron effective mass, $m^*_e=0.08m_0$, in the InP crystal.[50] Here $m_0$ is the electron mass. The obtained results show that the potential well for holes in InP QD's is small and positive, i.e., the holes are localized in the dots. This conclusion is further supported by the relatively high probability of optical transitions in the InP QD's, as discussed in Sec. III D.

The accuracy of the values of $E_{0h}$ and $E_{1h}$ is limited by many simplifications used in the model. We estimate an accuracy of about 50% by analysis of all sets of experimental data, as well as by comparing the results using various modifications of the described model. We would like to stress that the actual accuracy can be verified only by independent measurements of these values with a different technique.

We performed a similar analysis of the PL data for $In_{0.35}Ga_{0.65}As$ QD's presented in Fig. 3. The bias dependence of the $LO_1$ and LA resonances is shown in Fig. 6. Both dependencies are well fitted by the equation

$$I_{PL}(U)=P/(1+\gamma_{0t}/\gamma_{PL}), \tag{5}$$

accounting only for a tunneling from the radiative state $|0\rangle$. This means that tunneling from the excited state $|1\rangle$ at values of the bias used in our experiment is much slower than carrier relaxation with emission of $LO_1$ and LA phonons. Assuming that the hole tunneling process is responsible for PL quenching,[51] from the fit we can obtain the energy of the lowest hole state $E_{0h}=70$ meV. This value agrees with typical values considered for $In_{0.35}Ga_{0.65}As$ QD's.[4]

### D. Kinetics

Kinetic measurements of PL allow one to study the time evolution of the radiative state population $n_0$. The time resolution of our setup (6 ps) was enough to study the relaxation of the photocreated carrier in real time. We also performed a further verification of the model proposed above by analyzing the kinetics in the electric field.

Examples of the PL kinetics under quasiresonant excitation for two spectral points within the PL band are shown in Fig. 7. The kinetics consists of a relatively short rising part and a rather long decay. The PL leading edge is shorter than the time resolution of the setup for LO resonance and much longer for other spectral points, as shown in the inset. At negative bias, the decay becomes faster and the amplitude of the signal becomes smaller.

The time evolution of the PL intensity can be described by an equation that follows from Eqs. (2). Assuming that the excitation pulse is shorter than any other process under consideration, $P=P_0\delta(t)$, we obtain

$$I_{PL}(t)=I_0\{e^{-(\gamma_{PL}+\gamma_{0t})t}-e^{-(\gamma_r+\gamma_{1t})t}\}, \tag{6}$$

where

$$I_0=\gamma_r P_0/[(\gamma_r-\gamma_{PL})+(\gamma_{1t}-\gamma_{0t})].$$

The two terms of the Eq. (6) describe the decay and rise of the PL pulse, respectively.

The function $I_{PL}(t)$ given by Eq. (6) well fits the kinetics for the 2AC spectral point, as seen in Fig. 7. However, the behavior of the PL kinetics at LO resonance is more complicated. At zero bias, the fast and slow components of the PL rise are clearly seen. The kinetics is well fitted by

$$I_{LO}(t)=I_0\{e^{-(\gamma_{PL}+\gamma_{0t})t}-[\alpha e^{-\gamma_{LO}t}+(1-\alpha)e^{-\gamma_{ac}t}]e^{-\gamma_{1t}t}\}. \tag{7}$$

The slow PL rise component is probably due to multistep carrier relaxation with emission of acoustic phonons in some

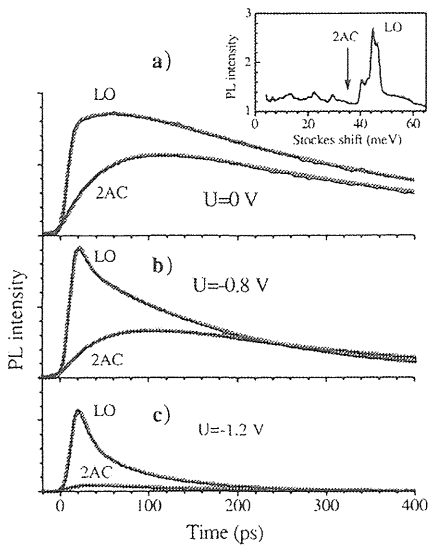


FIG. 7. PL kinetics of the sample with the InP QD's (thin solid line) for different biases at the LO and 2AC spectral points marked in the inset and a fit (thick gray line) by Eqs. (6)–(8) as discussed in the text. Values of the fitting parameters $\gamma_{\mathrm{PL}}+\gamma_{0t}=\tau_{\mathrm{PL}}(U)^{-1}$ and $\gamma_r+\gamma_{1t}=\tau_r(U)^{-1}$ for LO and 2AC kinetics, respectively, can be extracted from Fig. 8. Values of the other parameters for 2AC kinetics are $\gamma_{\mathrm{PL}}+\gamma_{0t}=(358\ \mathrm{ps})^{-1}$, $(230\ \mathrm{ps})^{-1}$, and $(104\ \mathrm{ps})^{-1}$ for $U=0$, $-0.8$, and $-1.2$ V, respectively. Values of the other parameters for LO kinetics are $\gamma_{\mathrm{ac}}+\gamma_{1t}=(43.3\ \mathrm{ps})^{-1}$ and $\alpha=0.67$ for $U=0$ V, and $\gamma_{\mathrm{ac}}+\gamma_{0t}=(9.9\ \mathrm{ps})^{-1}$ and $\beta=0.60$ for $U=-0.8$ V, and $\gamma_{\mathrm{ac}}+\gamma_{0t}=(11.8\ \mathrm{ps})^{-1}$ and $\beta=0.37$ for $U=-1.2$ V. Values of the parameter $\gamma_{\mathrm{LO}}+\gamma_{1t}$ is chosen to be $1\ \mathrm{ps}^{-1}$ for all biases. The fitting curves are convoluted with Gaussian with a FWHM of 6 ps. $E_{\mathrm{exc}}=1771$ meV. Inset: the PL spectrum at $U_{\mathrm{bias}}=-1.5$ V.

fraction $(1-\alpha)$ of the QD's. The carrier tunneling at negative bias compensates for this process, and another process causing a relatively fast PL decay component becomes observable [see Figs. 7(b) and 7(c)]. This process is probably the cascade relaxation of the carriers in "large" QD's in which the lowest-energy optical transition is redshifted relative to the given spectral point. In this case the PL kinetics is described by

$$I_{\mathrm{LO}}(t)=I_0\{[\beta e^{-\gamma_{\mathrm{ac}}t}+(1-\beta)e^{-\gamma_{\mathrm{PL}}t}]e^{-\gamma_{0t}t}-e^{-(\gamma_{\mathrm{LO}}+\gamma_{1t})t}\}, \tag{8}$$

where $\beta$ is the fraction of "large" QD's.

A good agreement of the fits with the PL kinetics allows one to determine the bias dependence of the PL decay time, $\tau_{\mathrm{PL}}(U)$, and the PL rise time, $\tau_{\mathrm{r}}(U)$. In Fig. 8 we show the bias dependencies of $\tau_{\mathrm{PL}}(U)$ for the LO resonance and of $\tau_{\mathrm{r}}(U)$ for the 2AC spectral point. According to Eqs. (6)–(8), they are described by the equations

$$\tau_{\mathrm{PL}}(U)=\frac{\tau_{\mathrm{PL}}}{1+\tau_{\mathrm{PL}}\gamma_{0t}}, \quad \tau_r(U)=\frac{\tau_r}{1+\tau_r\gamma_{1t}}. \tag{9}$$

The data in Fig. 8 are fitted by these functions using Eq. (1) for the tunneling rate, $U_0=4$ V determined above, and $U_1$ as a fitting parameter.[52] As seen, the fit with $U_1=5.5$ V well reproduces general behavior of the rise and decay times.

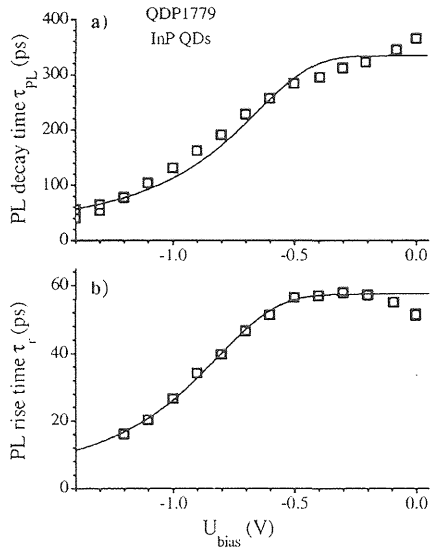


FIG. 8. Bias dependence of the PL decay time (a) and the PL rise time (b). Open squares represent the data obtained by fitting of the PL kinetics. Fits by Eqs. (9) are shown by solid lines. The fitting parameters are (a) $\tau_{\mathrm{PL}}=330$ ps, $\gamma_{0t}^0=0.2\ \mathrm{ps}^{-1}$, and $U_0=4$ V; and (b) $\tau_{\mathrm{r}}=58$ ps, $\gamma_{1t}^0=2.5\ \mathrm{ps}^{-1}$, and $U_0=5.5$ V.

As seen in Fig. 8(a), the PL decay time at small bias is about 300 ps. Experiments show that this time, as well as the PL intensity of the QD's, are almost independent of the sample temperature within several tens of K. This is an indication that PL decay is determined by radiative recombination of the electron-hole pair. This means that nonradiative losses of excitation at small bias are negligibly small. A smooth profile of the PL band of the QD's observed at any excitation energies (see Fig. 1) provides additional evidence of this conclusion. The obtained value of $\tau_{\mathrm{PL}}$ also agrees well with the model calculations of the radiative life time for disk-shaped QD's.[53] Thus we can speak about a relatively high probability of the optical transitions in InP QD's due to a good overlap of the electron and hole wave functions.

The PL rise time at the 2AC spectral point is about 60 ps at small bias [see Fig. 8(b)]. Similar kinetic measurements at acoustic resonances give a PL rise time that is approximately twice as small. The PL rise time at the LO resonance is shorter than our time resolution of 6 ps. A lower limit for this time can be deduced from the FWHM of the separate peaks of the LO resonances. It is about 1.2 meV for the InP QD's (see Fig. 2), that corresponds to a relaxation time of 0.6 ps. The corresponding value for $In_{0.35}Ga_{0.65}As$ QD's is about 1.5 ps.

### E. Acoustic-phonon resonances

The PL spectra of the biased samples as well as the PL kinetic data presented above demonstrate that the carrier relaxation with emission of high-energy acoustic phonons is efficient, in contradiction to theoretical predictions.[5,7] To make this contradiction evident, in Fig. 9 we plot the PL

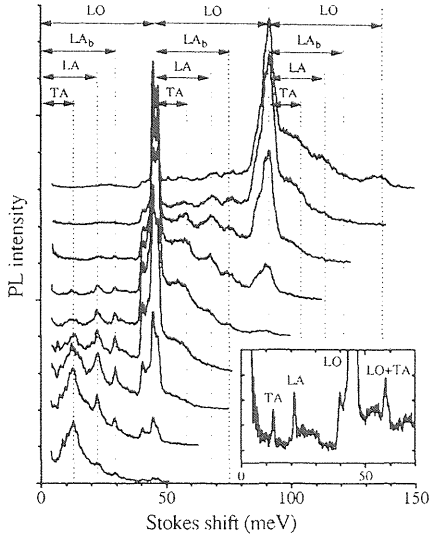


FIG. 9. The magnified PL spectra presented in Fig. 2 at different photon energies of excitation (from top to bottom) vs the Stokes shift. $U_{bias} = -1.5$ V. The spectra are shifted vertically for clarity. Similar phonon resonances in different spectra are marked by vertical lines. The arrows labelled "TA", etc., indicate the energy shift of the resonances from the laser line or 1LO or 2LO resonances. Inset: the PL spectrum at $U_{bias} = -2$ V vs the Stokes shift.

spectra presented in Fig. 2 versus the Stokes shift. It is seen that the various acoustic-phonon resonances are clearly observed not only between the laser line and the 1LO resonance, but also between the 1LO and 2LO resonances.

We cannot propose any quantitative description of the phenomenon, but there are a few points that, in our opinion, can be important for future modeling. The observed phonon resonances are caused by high-energy acoustic phonons. Acoustic phonons with such energy in the bulk crystal have a large momentum near the Brillouin zone boundary. This also holds with good accuracy for structures with QD's, because the confinement effect for the acoustic phonons in these samples may be considered weak due to the small difference between the elastic properties of the QD and the barrier material.

The interaction of a carrier with phonons of large momentum is efficient if the energy state of the carrier is characterized by the same momentum. The energy states of carriers in a QD are formed by a mixture of bulk states due to confinement. In other words, the wave function of the quantum-confined state in a QD is a linear combination of wave functions of various states in the Brillouin zone. To explain the observed resonances, we have to assume that this linear combination contains a considerable contribution from the large momentum states such as, for example, the states of the $L$ valley.

To support this assumption, we would like to note that the energy shift of the lowest electronic state in InP and $In_{0.35}Ga_{0.65}As$ QD's due to confinement is about a few hundred meV. This value is comparable with the energy separations of the minima in the $\Gamma$ and $L$ or $X$ valleys in these materials.[50] It should also be taken into account that the effective mass of electrons in valleys near the Brillouin zone boundary is large, and, hence, the energy shift of the states due to confinement is much smaller than that at the $\Gamma$ point. As a result, the energy separation between states of the $\Gamma$ and $L$ or $X$ valleys is decreased with the decreasing size of the QD. This may be the reason why the mixing of these states in the QD's is not small. A significant decrease of the energy separation between the $\Gamma$ and $L$ minima in InP QD's was observed by Menoni *et al.*[54] This decrease can also be induced by strain due to lattice mismatch of the QD's and surrounding material. An observation of the $\Gamma$-$X$ crossover under high pressure in the InP QD's (Ref. 55) and in the InAs QD's (Ref. 56) supports this assumption.

To model this situation it is necessary to go beyond the widely used effective-mass approximation that constructs QD energy states from Bloch functions in the neighborhood of the $\Gamma$ point. In fact, empirical pseudopotential calculations already showed the importance of $\Gamma$-$X$-$L$ valley mixing in QD's (see, for example, Ref. 57). Similar calculations for the structures studied in this work would be of interest.

Some experimental evidence of the above assumption seems to be provided by the spectrum shown in the inset of Fig. 9, where the TA, LA, and LO+TA resonances look like narrow peaks with a FWHM of about 2–3 meV. The formation of such narrow peaks is possible only if a small portion of the acoustic phonons causes a sufficiently strong relaxation. According to the above assumption, a selection of these acoustic phonons is caused by the wave-vector selection rule. It should be also taken into account that phonons with wave numbers near the Brillouin-zone boundary show small dispersions.

The interaction with the high-energy acoustic phonons may be also enhanced for two other reasons. The first is the small group velocity of the phonons that lengthens the interaction time. The second is the piezoelectric effect in these crystals that leads to long-range electric fields associated with acoustic phonons. Modeling these interactions at a large wave vector $q$ of phonons is the open problem.

### F. Auger-like processes

The phonon resonances discussed above can be observed under specific experimental conditions. The most important conditions are low PL efficiency, low power density of excitation, and low temperature. We can consider the data presented above as a illustrations of the resonances arising due to a decrease of the PL efficiency. In this section, we consider the *disappearance* of the resonances with increasing pump power.

We have measured the pump power dependence of the PL spectra and the kinetics of the biased sample QDP1779 with the InP QD's. 5-ps pulses, with a repetition period of about 12 ns, were used to increase the peak power of the excitation. The measured spectra are shown in Fig. 10. As seen, the acoustic-phonon resonances disappear and the LO resonance becomes barely observable under strong pumping. This fact means that the relaxation rate for *all interlevel spacings* becomes comparable to the LO-phonon-assisted relaxation rate. The PL kinetics reveals a steplike component of the PL rise

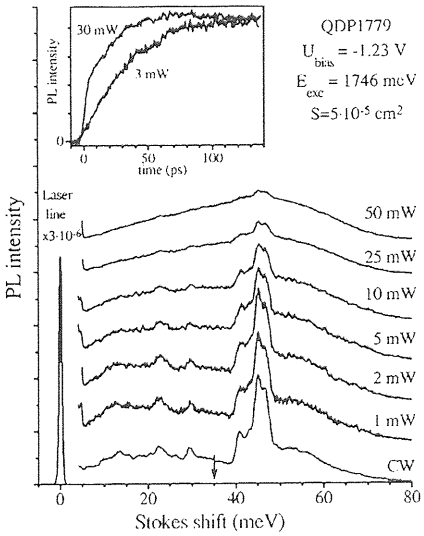


FIG. 10. PL spectra of the biased sample with InP QD's under cw excitation (bottom curve) and pulsed excitation with average power indicated against each curve. The laser spot area on the sample is $S=5\times10^{-5}$ cm$^2$; $E_{exc}=1746$ meV and $U_{bias}=-1.23$ V. An arrow marks the 2AC spectral point where the PL kinetics was measured. Inset: the PL kinetics under weak and strong excitations normalized at 130 ps.

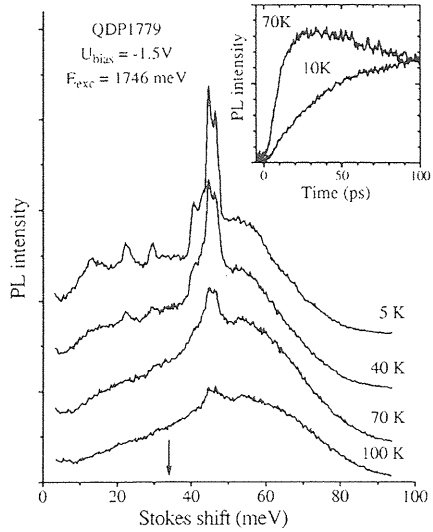


FIG. 11. PL spectra of the biased sample with InP QD's at different temperatures indicated near each spectrum. $E_{exc}=1746$ meV and $U_{bias}=-1.5$ V. The arrow indicates the spectral point at which the PL kinetics were measured. Inset: the normalized PL kinetics at temperatures indicated for each curve.

with an increase of the pumping (see the inset of Fig. 10), which also indicates an acceleration of the carrier relaxation.

The observed behavior of the PL spectra and kinetics can be explained by invoking Auger-like processes. The Auger-like process involved here is carrier-carrier scattering, in which one carrier loses its energy and the other one acquires it.[8,11,30–32] On the one hand, relaxation due to Auger-like processes should be fast because the carriers as charged particles interact with each other much more strongly than with phonons. On the other hand, this process is possible if separation between the energy levels for the first carrier coincides with that for the second one. In the case of the InP QD's, this condition can be easily fulfilled for electron-hole or hole-hole scattering, because of the large density of the high energy levels for holes. Also, the hole could be ejected out of the QD into the continuum of the barrier layer, so that the energy conservation condition is easily fulfilled.[30,31] It is evident that we should not expect any spectral features (resonances) due to relaxation via an Auger-like process. It is also evident that the efficiency of this process should depend on the number of carriers in the QD, because each carrier can be scattered by any other one. In the simplest model, the dependence on the pump power should be quadratic.

These features of the Auger-like process agree qualitatively with the experiment. Therefore, we can conclude that a strong pumping activates an alternative relaxation mechanism that is much faster than the acoustic-phonon-assisted relaxation. The Auger relaxation rate achieved in our experiments is comparable with the rate of the LO-phonon-assisted relaxation, that is about 1 ps$^{-1}$.

A quantitative analysis of the presented data is difficult because the absorption coefficient for the InP QD's at the laser line is unknown.[58] As a result, the number of photocreated electron-hole pairs in a QD cannot be estimated correctly. In addition, the observed pump power dependence of the PL intensity is more complicated than quadratic. The reason for this is probably some additional processes at strong pumping such as saturation of absorption that should lead to sublinear dependence, or saturation of deep levels that should lead to superlinear dependence.

### G. Thermostimulated relaxation

Another way to accelerate the carrier relaxation is to increase the sample temperature. Figure 11 depicts the PL spectra of the biased sample at a few elevated temperatures. It is clearly seen that phonon resonances become smaller relative to the structureless pedestal in the spectrum at $T=100$ K. The temperature increase at first destroys the lowest in energy phonon resonance (TA), then the other acoustic resonances, and finally the LO resonance.

This behavior is easy to understand. Heating of the sample creates phonons. These phonons can cause carrier relaxation due to stimulated emission of phonons into the same phonon modes. The number of phonons with small energy is always larger then that with high energy. Therefore, the stimulated emission is more efficient for low-energy phonons. The PL kinetics shown in the inset of Fig. 11 also demonstrates the shortening of the carrier relaxation time.

An important result is that the rate of relaxation at about 100 K becomes comparable to that of the LO-phonon-assisted relaxation, independent of the spectral point. Thus we can conclude that no retarded relaxation of the hot carriers in QD's should be expected at elevated temperatures. This result is important for device applications.

## IV. CONCLUSION

The present study of PL spectra of InP and $In_{0.35}Ga_{0.65}As$ QD's in an electric field allowed us to establish the nature of the observed narrow resonances. These are shown to arise due to a competition of the fast one-step relaxation of hot carriers with emission of an acoustic or LO phonon and nonradiative losses. For InP and $In_{0.35}Ga_{0.65}As$ QD's in an electric field, the nonradiative losses are mainly caused by hole tunneling from the QD's into the barrier layer.

We developed a model that quantitatively describes the bias dependence of PL intensity at the phonon resonances. This model allowed us to estimate the depth of the potential wells for holes in the studied heterostructures.

The proposed model was verified by the PL kinetic measurements for the samples with InP QD's. We found that the carrier relaxation is really fast with emission of not only LO phonons but also acoustic phonons. This result gives clear evidence of the relatively strong carrier-acoustic-phonon coupling in the QD's. We assume the main reason for this is a mixing of $\Gamma$ electronic states with the states with large momentum due to confinement of the electron in a QD.

We have also studied carrier relaxation in the presence of more than one electron-hole pair in a QD. Clear evidence is found for carrier-carrier scattering giving rise to acceleration of the relaxation. A similar effect was observed under heating of the sample where the acceleration of the relaxation is caused by stimulated phonon emission.

By careful analysis of the experimental data, we conclude that there is no phonon bottleneck effect in QD's, at least in the sense proposed in Refs. 5 and 6. Carrier relaxation with emission of acoustic or LO phonons is much faster than radiative recombination. Our experiments clearly show that phonon-assisted relaxation is the main channel for the carrier relaxation at low power density.

## ACKNOWLEDGMENTS

The authors wish to thank Dr. J. Qi and Dr. K. Nishi for sample preparation, and Dr. I. Gerlovin and Dr. V. Zapasskii for a fruitful discussion.

*Electronic address: ivan@paloma.spbu.ru

†Permanent address: Vavilov State Optical Institute, St.-Petersburg, Russia.

‡Present address: Space Vacuum Epitaxy Center, University of Houston, Houston, Texas 77204-5507.

[1] D. Gammon, Science **280**, 225 (1998).

[2] Y. Arakawa and A. Yariv, IEEE J. Quantum Electron. **QE-22**, 1887 (1986).

[3] D. Bimberg, M. Grundmann, and N. N. Ledenstov, *Quantum Dot Heterostructures* (Wiley, New York, 1999).

[4] M. Sugawara, *Self-Assembled InGaAs/GaAs Quantum Dots Semiconductors and Semimetals* (Academic Press, New York, 1999), Vol. 60.

[5] U. Bockelmann and G. Bastard, Phys. Rev. B **42**, 8947 (1990).

[6] H. Benisty, C. M. Sotomayor-Torrès, and C. Weisbuch, Phys. Rev. B **44**, 10 945 (1991).

[7] T. Inoshita and H. Sakaki, Phys. Rev. B **46**, 7260 (1992).

[8] U. Bockelmann and T. Egeler, Phys. Rev. B **46**, 15 574 (1992).

[9] U. Bockelmann, Phys. Rev. B **48**, 17 637 (1993).

[10] H. Benisty, Phys. Rev. B **51**, 13 281 (1995).

[11] A. L. Efros, V. A. Kharchenko, and M. Rosen, Solid State Commun. **93**, 281 (1995).

[12] P. C. Sercel, Phys. Rev. B **51**, 14 532 (1995).

[13] S. Fafard, R. Leon, D. Leonard, J. L. Merz, and P. M. Petroff, Phys. Rev. B **52**, 5752 (1995).

[14] R. Heitz, M. Grundmann, N. N. Ledentsov, L. Eckey, M. Veit, D. Bimberg, V. M. Ustinov, A. Yu. Egorov, A. E. Zhukov, P. S. Kop'ev, and Zh. I. Alferov, Appl. Phys. Lett. **68**, 361 (1996).

[15] K. Mukai, N. Ohtsuka, H. Shoji, and M. Sugawara, Phys. Rev. B **54**, R5243 (1996).

[16] K. H. Schmidt, G. Medeiros-Ribeiro, M. Oestreich, P. M. Petroff, and G. H. Döhler, Phys. Rev. B **54**, 11346 (1996).

[17] B. Ohnesorge, M. Albrecht, J. Oshinowo, A. Forchel, and Y. Arakawa, Phys. Rev. B **54**, 11532 (1996).

[18] M. Vollmer, E. J. Mayer, W. W. Rühle, A. Kurtenbach, and K. Eberl, Phys. Rev. B **54**, 17292 (1996).

[19] M. J. Steer, D. J. Mowbray, W. R. Tribe, M. S. Skolnick, M. D. Sturge, M. Hopkinson, A. G. Cullis, C. R. Whitehouse, and R. Murray, Phys. Rev. B **54**, 17 738 (1996).

[20] R. Heitz, M. Veit, N. N. Ledentsov, A. Hoffmann, D. Bimberg, V. M. Ustinov, P. S. Kop'ev, and Zh. I. Alferov, Phys. Rev. B **56**, 10 435 (1997).

[21] X. Q. Li, H. Nakayama, and Y. Arakawa, Phys. Rev. B **59**, 5069 (1999).

[22] Y. Toda, O. Moriwaki, M. Nishioka, and Y. Arakawa, Phys. Rev. Lett. **82**, 4114 (1999).

[23] I. V. Ignatiev, I. E. Kozin, S. V. Nair, H.-W. Ren, S. Sugou, and Y. Masumoto, Phys. Rev. B **61**, 15 633 (2000).

[24] V. F. Gandmacher and Y. B. Levinson, *Carrier Scattering in Metals and Semiconductors* (North-Holland, Amsterdam, 1987).

[25] M. Grundmann, R. Heitz, N. Ledentsov, O. Stier, D. Bimberg, V. M. Ustinov, P. S. Kop'ev, Zh. I. Alferov, S. S. Ruvimov, P. Werner, U. Gosele, and J. Heydenreich, Superlattice. Microstruct. **19**, 81 (1996).

[26] C. Guasch, C. M. Sotomayor-Torrès, N. N. Ledentsov, D. Bimberg, V. M. Ustinov, and P. S. Kop'ev, Superlattices. Microstruct. **21**, 509 (1997).

[27] A. V. Baranov, V. Davydov, H.-W. Ren, S. Sugou, and Y. Masumoto, J. Lumin. **87-89**, 503 (2000).

[28] D. F. Schroeter, D. J. Griffiths, and P. C. Sercel, Phys. Rev. B **54**, 1486 (1996).

[29] X.-Q. Li and Y. Arakawa, Phys. Rev. B **56**, 10423 (1997).

[30] M. Braskén, M. Lindberg, M. Sopanen, H. Lipsanen, and J. Tulkki, Phys. Rev. B **58**, R15993 (1998).

[31] S. Nair and Y. Masumoto, J. Lumin. **87-89**, 408 (2000); Phys. Status Solidi B **178**, 303 (2000).

[32] R. Ferreira and G. Bastard, Appl. Phys. Lett. **74**, 2818 (1999).

[33] F. Clérot, B. Deveaud, A. Chomette, A. Regreny, and B. Sermage, Phys. Rev. B **41**, 5756 (1990).

[34] K. H. Schmidt, G. Medeiros-Ribeiro, and P. M. Petroff, Phys. Rev. B **58**, 3597 (1998).

[35] I. E. Kozin, I. V. Ignatiev, H.-W. Ren, S. Sugou, and Y. Masu-

moto, J. Lumin. **87-89**, 441 (2000).
[36] E. Bedel, G. Landa, R. Charles, J. P. Redoulés, and J. B. Renussi, J. Phys. C **19**, 1471 (1986).
[37] I. Ignatiev, I. Kozin, H.-W. Ren, S. Sugou, and Y. Masumoto, Phys. Rev. B **60**, R14001 (1999).
[38] A. A. Sirenko, M. K. Zundel, T. Ruf, K. Eberl, and M. Cardona, Phys. Rev. B **58**, 12 633 (1998).
[39] R. Heitz, I. Mukhametzhanov, O. Stier, A. Madhukar, and D. Bimberg, Phys. Rev. Lett. **83**, 4654 (1999).
[40] V. Davydov, I. V. Ignatiev, I. E. Kozin, S. V. Nair, J.-S. Lee, H.-W. Ren, S. Sugou, and Y. Masumoto, Phys. Status Solidi B (to be published).
[41] F. Findeis, A. Zrenner, G. Bohm, and G. Abstreiter, Phys. Rev. B **61**, R10579 (2000).
[42] Optical transitions between the electron and hole states with different quantum numbers, e.g., $|0h\rangle$ and $|1e\rangle$, are forbidden only for highly symmetrical QD's. We cannot exclude these transitions from consideration for the studied QD's because of their low symmetry.
[43] C. Pryor, M.-E. Pistol, and L. Samuelson, Phys. Rev. B **56**, 10 404 (1996).
[44] M. Hayne, R. Provoost, M. K. Zundel, Y. M. Manz, K. Eberl, and V. V. Moshchalkov, Phys. Rev. B **62**, 10 324 (2000).
[45] P. W. Fry, I. E. Itskevich, D. J. Mowbray, M. S. Skolnick, J. J. Finley, J. A. Barker, E. P. O'Reilly, L. R. Wilson, L. A. Larkin, P. A. Maksym, M. Hopkinson, M. Al-Khafaji, J. P. R. David, A. G. Gullis, G. Hill, and J. C. Clark, Phys. Rev. Lett. **84**, 733 (2000).
[46] L. D. Landau and E. M. Lifshitz, *Quantum Mechanics*, 3rd ed (Pergamon, Oxford, 1977), Sec. 50.
[47] V. Davydov, I. Ignatiev, H.-W. Ren, S. Sugou, and Y. Masumoto, Appl. Phys. Lett. **74**, 3002 (1999).
[48] P. C. Sercel, Al. L. Efros, and M. Rosen, Phys. Rev. Lett. **83**, 2394 (1999).
[49] Size quantization can mix the heavy- and light-hole bands, which results in a change of the effective mass. This mixing leads to some uncertainty in the mass that should be used in the model. However the energies $E_i$, calculated using Eq. (1b) depends weakly (as $m^{-1/3}$) on the mass and cannot differ by more than 30% from the values given in the text.
[50] *Semiconductors, Intrinsic Properties of Group V Elements and III-V, II-VI, and I-VII Compounds*, edited by K.-H. Hellwege and O. Madelung, Landolt-Börnstein, New Series, Group III, Vol. 22, Pt. a (Springer-Verlag, Berlin, 1987), pp. 120, 191, and 351.
[51] We used the heavy-hole effective mass $m_{hh}=0.43m_0$. Actually, we cannot uniquely determine the type of carrier, electron or hole, which tunnels from the QD. In the case of electron tunneling, a similar estimation using the electron mass $m_e=0.05m_0$ gives rise to the energy of the lowest electron state $E_{0e}=140$ meV. This value can also be reasonable for the studied sample.
[52] We used a simple fit for the data in Fig. 8(b) because of limited time resolution.
[53] M. Sugawara, Phys. Rev. B **51**, 10 743 (1995).
[54] C. S. Menoni, L. Miao, D. Patel, O. I. Mic'ic', and A. J. Nozik, Phys. Rev. Lett. **84**, 4168 (2000).
[55] C. Ulrich, S. Ves, A. R. Goñi, A. Kurtenbach, K. Syassen, and K. Eberl, Phys. Rev. B **52**, 12 212 (1995).
[56] I. E. Itskevich, M. S. Skolnick, D. J. Mowbray, I. A. Trojan, S. G. Iyapin, L. R. Wilson, M. J. Steer, M. Hopkinson, L. Eaves, and P. C. Main, Phys. Rev. B **60**, R2185 (1999).
[57] H. Fu and A. Zunger, Phys. Rev. B **57**, R15 064 (1998); L. W. Wang, J. Kim, A. Zunger, *ibid.* **59**, 5678 (1999); L. W. Wang and A. Zunger, *ibid.* **59**, 15 806 (1999).
[58] We can roughly estimate the number of photocreated electron-hole pairs in an InP QD, $N_c$, under our experimental conditions, using the Fermi golden rule for an optical transition between the discrete energy states of a QD. We consider that the spectral width of the laser pulse is much larger than that of the optical transition, but is less than the spectral distance between the nearest optical transitions. The dipole moment of the optical transition was evaluated from the radiative lifetime determined experimentally for the lowest state of the electron-hole pair, assuming that this time is of the same order of magnitude for the first excited state. Our estimation gives $N_c=8$ for the case of the top curve in Fig. 10. Due to saturation of the absorption, the actual number of the carriers must be less.

RAPID COMMUNICATIONS

PHYSICAL REVIEW B, VOLUME 64, 201315(R)

# Complementary detection of confined acoustic phonons in quantum dots by coherent phonon measurement and Raman scattering

Michio Ikezawa, Tsuyoshi Okuno, and Yasuaki Masumoto
*Institute of Physics, University of Tsukuba, Tsukuba 305-8571, Japan*

Andrey A. Lipovskii
*St.-Petersburg State Technical University, Polytekhnicheskaja 29, St.-Petersburg, 195251 Russia*
(Received 11 July 2001; revised manuscript received 17 September 2001; published 2 November 2001)

Coherent acoustic phonon oscillation is observed in PbSe quantum dots embedded in phosphate glass by femtosecond pump-and-probe. The size dependence of the oscillation is investigated. Distinct low-frequency peaks are observed in Raman spectrum for the same samples. The size-dependence of the frequencies is well explained by elastic sphere model, but the observed modes are different to each other for coherent phonon and Raman scattering. Coherent phonon measurement and Raman scattering are found to give complementary information on confined acoustic phonons in this system.

DOI: 10.1103/PhysRevB.64.201315 PACS number(s): 63.22.+m, 78.47.+p

Semiconductor quantum dots (QDs) have attracted considerable attention in recent years.[1,2] Three-dimensional confinement of electrons to a nanometer-size space changes their continuous energy spectrum to discrete one. It not only modifies electronic state, but also modifies phonon spectrum to size-dependent discrete lines, and the electron-phonon interaction among them is thought to be changed also. The size-dependence of the exciton–phonon interaction in quantum dot has been the subject of extensive research. Experimental studies on the optical,[3,4] or acoustic[5–8] phonon modes in QDs have been carried out mainly by Raman scattering. Persistent spectral hole-burning (PSHB) spectroscopy was also successfully applied to QDs.[9,10] During the last decade, coherent oscillation of the confined vibrational modes became to be observable directly in time domain. There are some reports on the observation of coherent optical phonons in semiconductor QDs, CdSe QDs,[11] InP QDs,[12] etc. While the high energy optical phonon forms sidebands in optical spectrum, low energy acoustic phonon rather contributes to excitonic dephasing and homogeneous broadening,[13] which plays a crucial role in nonlinear device applications. Therefore a detailed understanding of the mechanism of generation and damping of confined acoustic phonon in QDs is important. Coherent oscillation of confined acoustic phonon in QDs was first reported by Krauss and Wise in 1997.[14] They observed temporal oscillation of the transmission in femtosecond pump-and-probe measurement on 3 nm PbS QDs dispersed in PVA (polyvinyl alcohol). They also measured Raman scattering of the same sample to compare with coherent phonon. However, as they mentioned in the paper, they were not able to systematically study the size-dependence, because size control in the polymer matrix was difficult. Therefore, the size-dependence of the relation between coherent acoustic phonon and Raman spectrum has not been not studied yet. In this Rapid Communication, we detect coherent acoustic phonon signal in QDs embedded in glass matrix with high sensitivity. We measured size-dependence of coherent phonon and Raman scattering. The complementary relation of these measurements was clearly shown.

For coherent phonon measurements, we performed femtosecond pump-and-probe. A mode-locked Ti:sapphire oscillator was used to produce pump and probe pulses, whose pulse width was about 30 fs. Center wavelength of the near transform-limited pulse was about 790 nm. A shaker was introduced into the pump beam path to modulate pump delay time at 80 Hz. The pump and probe beams were focused on the sample surface, and the transmitted probe beam were detected together with a reference beam by a pair of Si photodiodes to cancel the instability of the laser. The subtracted signal was led to a lock-in amplifier. To measure Raman spectra, a cw-Ti:sapphire laser pumped by an Ar-ion laser was used as an excitation source. A 1-m double monochromator with a photon counting system was used for detection. Samples used in this study were PbSe QDs grown in phosphate glass matrix.[15] The mean radius of all samples were estimated by Small-Angle X-ray Scattering (SAXS), and found to range between 1.4 nm and 3.5 nm. All experiments in this study were performed at room temperature.

An absorption spectrum of the sample with mean radius 2.9 nm is shown in Fig. 1(a). The time trace of pump-and-probe measurement is shown in Fig. 1(b). This is an expanded curve at the tail part of a large absorption change. A clear oscillatory component can be recognized superimposed on the absorption change of excitons. The oscillation period is about 2 ps, and the amplitude rapidly damps. We note that we detected coherent phonon signal by using a small pump delay modulation and lock-in technique, and that the data obtained here corresponds to the time derivative of ordinary transmission intensity. Therefore the signal in Fig. 1(b) can be fitted by a damped sine function, but it means that the corresponding phonon oscillation is expressed by a damped cosine function. The amplitude of the oscillation is in an order of $10^{-6}$ times the total probe intensity. In contrast, in QDs embedded in polymer matrix, PbS in PVA,[14] the modulation of probe intensity by the coherent confined acoustic phonon measured by time-resolved pump-and-probe was as large as $10^{-3}$ under almost equal excitation density to our experiment. It should be added that they did not observe coherent phonon signal in PbS in silicate glass matrix. It may

 

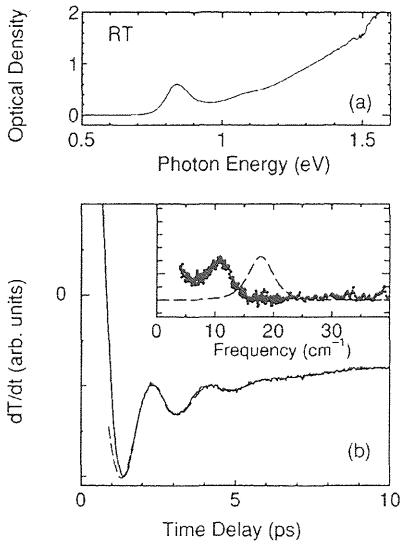


FIG. 1. (a) Absorption spectrum of PbSe QDs at RT. The mean radius is 2.9 nm. (b) Time-resolved transmission signal of the same sample at RT. An overdamped oscillation due to confined acoustic phonon is clearly observed. A dashed line represents the fitting by a damped sine function. In the inset, dots correspond to the Raman spectrum of the same sample. A dashed line is the Fourier transformed spectrum of the fitting curve for the coherent phonon signal.

be due to the weakness of the signal in glass matrix. Small modulation signal due to coherent acoustic phonon in QDs in glass matrix was also observed on PbTe QDs in glass.[16] This coherent phonon signal can be temporarily assigned to the confined acoustic phonon in the QDs because of its small frequency. Since the photon energy of the pump pulse is well above the first excited state of the sample, the pump pulses coherently excite all of QDs with various sizes in the size-distribution. Therefore a lot of QDs having different phonon frequencies contribute to the coherent phonon signal. The damping does not mean the real damping of the coherent oscillation of the confined phonon in each quantum dot, but dephasing due to the *inhomogeneous* broadening of the phonon frequency. As shown later, the damping constant is reasonably explained by the size-distribution. Figure 2 shows the size-dependence of pump-and-probe signal. The oscillation frequency increases with decreasing dot radius. It supports the assignment of the oscillation to the confined acoustic phonon whose frequency is known to be inversely proportional to the dot radius as seen later. Since the oscillatory component is weaker than the background due to the fast recovery of absorption change, it is difficult to separate phonon signal from the background. Therefore we obtained size-dependent frequency from the interval between the first and the second hump marked by a solid circle in the figure.

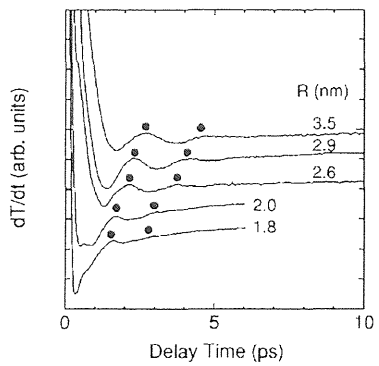


FIG. 2. Size-dependence of the coherent phonon signal. R is the mean radius of the PbSe QDs.

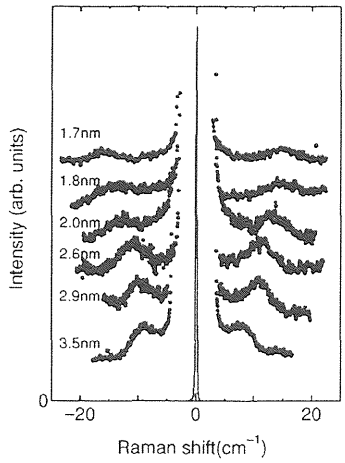


FIG. 3. Raman spectra for various size PbSe QDs at RT. Excitation laser was 750 nm. Size-dependent peaks were observed around 10 cm$^{-1}$.

To compare the coherent phonon with Raman scattering, Raman spectrum of 2.9 nm PbSe dots was measured by using 750 nm excitation laser. The results are displayed in the inset of Fig. 1(b) by dots. Fourier transformed spectrum of the fitting curve of the coherent phonon signal is also drawn in the inset of Fig. 1(b) by a dashed line. The peak position in the Raman spectrum is 11 cm$^{-1}$ and it does not coincide with the spectrum of the coherent phonon signal. There is no structure at 18 cm$^{-1}$ in the Raman spectrum. The size-dependence of Raman spectrum is shown in Fig. 3. The excitation laser was 750 nm. The spectral resolution was 1.4 cm$^{-1}$. Size-dependent low frequency peaks are clearly observed in the range from 8 cm$^{-1}$ to 16 cm$^{-1}$. With decreasing the dot size, the peak frequency increases and its width also increases, reflecting that the smaller dots have larger size-distribution. When we tried using an Ar-ion laser (514.5 nm) for excitation, the data was almost the same as 750 nm excitation. The peak frequencies in the Raman spectra are plotted as a function of dot radius by open circles in Fig. 4. For low frequency Raman spectrum, correction of the occupation number by Bose factor is needed in order to evaluate real phonon spectrum. The correction modifies the spectrum particularly in the very low frequency region, but does not strongly affect the peak position compared to the error bar under our experimental condition even for the largest dots. Solid circles in Fig. 4 represent the frequencies of the oscillation observed in the coherent phonon measurement. We can see the linear dependence of both frequencies on the inverse radius of dots, but the coherent phonon signal and the Raman signal seem to come from different confined

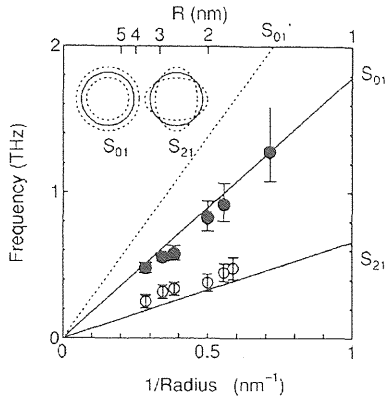


FIG. 4. Frequency of the coherent phonon and the Raman peak as a function of dot size. They are inversely proportional to the dot radius. Solid lines represent the calculation on the assumption that the stress at the dot boundary is zero, while a dashed line represents the calculation with rigid boundary condition. The inset represents the displacement in $S_{01}$ and $S_{21}$ spheroidal mode.

phonon modes in QDs. As is well known, vibration modes of a sphere with stress-free boundary condition were studied theoretically by Lamb.[17] According to their results, the vibrational mode is classified into two categories, spheroidal modes and torsional modes. Duval[18] derived the selection rule from the group theory that the mode observed in the first order Raman scattering was only spheroidal mode with $l=0$ or $l=2$. The lowest mode of $l=0$ spheroidal mode is known as *breathing mode*, where expansion and shrinkage of whole sphere occur. This mode is purely longitudinal, but $l=2$ is a mixed mode and have both longitudinal and transverse components. Displacements in these modes are illustrated in the inset of Fig. 4.

The frequencies of the spheroidal modes are expressed by $\nu_{ln}=\xi_{ln}V_l/R$, where $\xi_{ln}$ is a coefficient depending on the ratio of longitudinal ($V_l$) and transverse ($V_t$) sound velocities, and $R$ is the dot radius.[19] If we assume stress-free boundary condition, the numerator of the expression can be calculated by using bulk PbSe parameters. Finally, for the lowest spheroidal mode with $l=0$, the numerator, $S_{ln}=\xi_{ln}V_l$, is $S_{01}=1.79$, that is $\nu_{01}(\mathrm{THz})=1.79/R$ (nm). We can also try to assume *rigid* boundary condition where the lattice displacement at boundary is zero. This assumption was applied for the interpretation of the Raman spectrum on CdSe nanocrystals in glasses.[20] Under this assumption, the frequency of the spheroidal mode is shifted to higher frequency, $S_{01}'=2.76$. They are represented in Fig. 4 labeled $S_{01}$ and $S_{01}'$, respectively. The experimental data of the coherent phonon is well fitted by calculation based on the stress-free boundary condition. The assignment is supported by the phase of the observed coherent phonon signal. In coherent phonon measurement, the oscillation found to show cosine-like temporal behavior. In other words, the phonon amplitude is maximum at $t=0$ indicating the origin of instantaneous expansion by pump pulses. An instantaneous isotropic expansion occurs by the high density carriers impulsively excited by the femtosecond pump pulses, and the breathing mode oscillation starts. The oscillation modifies the optical spectrum of QDs through deformation potential. It causes small energy shift of the absorption spectrum synchronized with the oscillation, which led to the temporal change of the probe transmission we detected. On the other hand, the Raman peaks are assigned to $S_{21}$ mode. It is the lowest $l=2$ spheroidal mode. $S_{21}=0.66$ is deduced by assuming stress-free boundary condition. Small discrepancy may come from the fact that real PbSe is not exactly isotropic. The Raman active spheroidal modes ($l=0$ and $l=2$) can be distinguished by their polarization dependence.[18] $l=0$ mode can be observed only in the same polarization as the excitation polarization, while $l=2$ mode can be also observed in cross polarization. We examined polarization dependence of the low-frequency peak in Raman spectrum. The peak was observed under both parallel and cross-polarization detection. Therefore it is acceptable to assign these peaks to $l=2$ mode.

In this way, based on their size-dependence, the observed Raman peaks and the frequencies of coherent phonon are unambiguously assigned to the different phonon modes. In other semiconductor quantum dots, for example, CdSe QDs[20] and CdS QDs,[8] both $l=0$ and $l=2$ acoustic modes were observed in Raman spectrum unlike our results. The point is that in PbSe QDs the Raman scattering cannot detect the breathing mode, on the contrary, coherent phonon measurement mainly detects the breathing mode and could be useful as a complementary detection technique. We can find experimental results similar to ours in the research field of metal nanoparticles. The observed Raman peaks of acoustic phonon of Ag nanoparticles is mainly the $l=2$ mode,[21] while the observed coherent phonon oscillation corresponds to the $l=0$ mode.[22] Montagna and Dusi[23] deduced that the $l=0$ mode was not Raman active in nanoparticles with cubic Bravais lattice and for the (dipole-induced-dipole DID) scattering mechanism and explained why the $l=2$ mode dominated the Raman spectra of Ag nanoparticles. Since PbSe has NaCl-type crystal structure unlike CdS or CdSe where the crystal lattice is hexagonal, the same arguments as Ag nanoparticles may be applicable to the Raman spectra of PbSe QDs.

Let us explain the width of the power spectrum of the coherent phonon and Raman spectrum in the inset of Fig. 1(b). The size-distribution of the sample (2.9 nm) is estimated to be about 28% by the absorption spectrum in Fig. 1(a) and the relation between size and the first excited state energy which was previously reported.[24] The size-distribution also agrees to the estimation from SAXS data. It corresponds to a FWHM of 6 $cm^{-1}$ for $S_{01}$ mode and 2.9 $cm^{-1}$ for $S_{21}$ mode, and they reasonably agree with the observed width of 8 $cm^{-1}$ and 5.5 $cm^{-1}$.

The reason why the coherent phonon signal of QDs in glass is smaller than that of QD embedded in polymer matrix was not clarified. We cannot simply state that, compared to polymers, the hardness of the glass matrix surrounding QDs prevents them from vibrating acoustically and led to the small amplitude of the coherent phonon, because, as stated before, the stress-free coherent oscillation of QDs in glass was observed in our study. Therefore the combination of the QDs and glass should be relatively weak.

In Ref. 25, the 68 $cm^{-1}$ Raman peak on 2 nm PbS QDs in PVA was assigned to confined acoustic phonon mode with $l=0$. PbS is not so different from PbSe in elastic properties, but the frequency of the confined acoustic phonon is much larger. Moreover the size-dependence of the mode seems to be quite small, compared to the Raman spectrum on 3 nm PbS QDs,[14] and unlike our results, the coherent phonon signal reproduces the Raman spectrum in respect of the acoustic mode in this system. Thus we see that there are still more problems on the acoustic vibration of QDs in host matrix.

In conclusion, size-dependence of the confined acoustic phonon modes in PbSe QDs embedded in glass matrix was investigated by coherent phonon measurement and Raman scattering. The size-dependent frequency is well explained by stress-free elastic sphere model. It was found that coherent phonon experiment measures different confined acoustic modes from that in Raman scattering and is a useful tool to study confined phonon in QDs.

This work was supported by the Ministry of Education, Science, Sports and Culture, Grant-in-Aid for Encouragement of Young Scientists, 12740170, 2000, "Research for the Future" Program JSPS-RFTF 97P00106 from the Promotion of Science, project research of University of Tsukuba, Kurata Foundation (Japan), and INTAS foundation (EC). Authors are thankful to Dr. T. Mishina for fruitful discussion.

[1] A.D. Yoffe, Adv. Phys. **42**, 173 (1993).
[2] U. Woggon, *Optical Properties of Semiconductor Quantum Dots* (Springer, Berlin, 1997).
[3] M. Fujii, S. Hayashi, and K. Yamamoto, Appl. Phys. Lett. **57**, 2692 (1990).
[4] A. Tanaka, S. Onari, and T. Arai, Phys. Rev. B **45**, 6587 (1992).
[5] E. Duval, A. Boukenter, and B. Champagnon, Phys. Rev. Lett. **56**, 2052 (1986).
[6] N.N. Ovsyuk, E.B. Gorokhov, V.V. Grishchenko, and A.P. Shebanin, JETP Lett. **47**, 298 (1988).
[7] B. Champagnon, B. Andrianasolo, and E. Duval, J. Chem. Phys. **94**, 5237 (1991).
[8] A. Tanaka, S. Onari, and T. Arai, Phys. Rev. B **47**, 1237 (1993).
[9] S. Okamoto and Y. Masumoto, J. Lumin. **64**, 253 (1995).
[10] J. Zhao and Y. Masumoto, Phys. Rev. B **60**, 4481 (1999); J. Zhao, S.V. Nair, and Y. Masumoto, *ibid.* **63**, 033307 (2001).
[11] R.W. Schoenlein, D.M. Mittleman, J.J. Shiang, A.P. Alivisatos, and C.V. Shank, Phys. Rev. Lett. **70**, 1014 (1993).
[12] U. Banin, G. Cerullo, A.A. Guzelian, C.J. Bardeen, A.P. Alivisatos, and C.V. Shank, Phys. Rev. B **55**, 7059 (1997).
[13] M. Ikezawa and Y. Masumoto, Phys. Rev. B **61**, 12 662 (2000).
[14] T.D. Krauss and F.W. Wise, Phys. Rev. Lett. **79**, 5102 (1997).
[15] A.A. Lipovskii, E.V. Kolobkova, and V.D. Petrikov, Electron. Lett. **33**, 101 (1997); A. Lipovskii, E. Kolobkova, V. Petrikov, I. Kang, A. Olkhovets, T. Krauss, M. Thomas, J. Silcox, F. Wise, Q. Shen, and S. Kycia, Appl. Phys. Lett. **71**, 3406 (1997).
[16] E.R. Thoen, G. Steinmeyer, P. Langlois, E.P. Ippen, G.E. Tudury, C.H. Brito Cruz, L.C. Barbosa, and C.L. Cesar, Appl. Phys. Lett. **73**, 2149 (1998).
[17] H. Lamb, Proc. London Math. Soc. **13**, 51 (1882).
[18] E. Duval, Phys. Rev. B **46**, 5795 (1992).
[19] B. A. Alud, *Acoustic Fields and Waves in Solids* (Wiley, New York, 1973).
[20] L. Saviot, B. Champagnon, E. Duval, I.A. Kudriavtsev, and A.I. Ekimov, J. Non-Cryst. Solids **197**, 238 (1996).
[21] G. Mariotto, M. Montagna, G. Viliani, E. Duval, S. Lefrant, E. Rzepka, and C. Mai, Europhys. Lett. **6**, 239 (1988).
[22] N. Del Fatti, C. Voisin, F. Chevy, F. Vallée, and C. Flytzanis, J. Chem. Phys. **110**, 11 484 (1999).
[23] M. Montagna and R. Dusi, Phys. Rev. B **52**, 10 080 (1995).
[24] T. Okuno, Y. Masumoto, M. Ikezawa, T. Ogawa, and A.A. Lipovskii, Appl. Phys. Lett. **77**, 504 (2000).
[25] T.D. Krauss, F.W. Wise, and D.B. Tanner, Phys. Rev. Lett. **76**, 1376 (1996).

RAPID COMMUNICATIONS

PHYSICAL REVIEW B, VOLUME 65, 241312(R)

# Zero-field spin quantum beats in charged quantum dots

I. E. Kozin,[1,2] V. G. Davydov,[1] I. V. Ignatiev,[1,2] A. V. Kavokin,[3] K. V. Kavokin,[4] G. Malpuech,[3] Hong-Wen Ren,[1] M. Sugisaki,[1] S. Sugou,[1] and Y. Masumoto[1,5]

[1]*Single Quantum Dot Project, ERATO, JST, Japan*

[2]*Institute of Physics, St. Petersburg State University, St. Petersburg 198504, Russia*

[3]*LASMEA, Université Blaise Pascal-Clermont-Ferrand II, 63177 Aubière Cedex, France*

[4]*Ioffe Physico-Technical Institute, 26 Politekhnicheskaya, St. Petersburg 194021, Russia*

[5]*Institute of Physics, University of Tsukuba, Tsukuba 305-8571, Japan*

(Received 8 April 2002; published 14 June 2002)

Spins of resident electrons in charged quantum dots (QD's) act as local magnets inducing the Zeeman splitting of excitons trapped into dots. This is evidenced by the observation of quantum beats in the linearly polarized time-resolved photoluminescence of a biased array of self-assembled InP QD's. An external magnetic field is found to shorten the spin beats' decay time keeping constant the frequency of the beats. A model using the pseudospin formalism allows one to attribute the observed quantum beats to the radiative decay of hot trions having two electrons that occupy different energy levels in a QD.

DOI: 10.1103/PhysRevB.65.241312 PACS number(s): 73.21.La, 42.50.Md, 78.55.Cr, 78.67.Hc

The charged quantum dot (QD) is a peculiar quantum object exhibiting quite unusual optical properties.[1–7] If the neutral QD is an analog of an atom, the charged QD is an analog of an ion.[5] One should expect drastic alterations in the fine structure of the energy levels due to charging of the QD. Since the first observation of charged excitons in QD's,[1] they were studied in QD's with the electronic population controlled either by optical pumping[4] or by applying a bias.[3,6,7] The fine structure of charged excitons was studied by single-dot optical spectroscopy,[2–6] including experiments in magnetic fields.[2,5]

While the energy structure of QD's has been intensively studied, much less is known about coherent phenomena in QD's.[8–11] To the best of our knowledge, no experimental observations of coherent phenomena in charged QD's have been reported so far.

Here, we report on a new spin-related effect in charged QD's. We have observed spin quantum beats (QB's) in the *linearly polarized* photoluminescence (PL) of an InP QD ensemble under linearly polarized excitation, while circular-polarized components of PL under circular-polarized excitation have shown almost no modulation. This behavior cannot result from the splitting of excitonic levels into states corresponding to linear oscillators, such as those observed in Ref. 11. But it is typical for a Zeeman doublet which is split by a magnetic field. In our case, such a Zeeman-like splitting is observed in the absence of an external magnetic field. Moreover, an applied magnetic field suppresses the QB's caused by this splitting. We attribute this unexpected behavior to the peculiar spin structure of the three-particle complex (trion) formed by an excess (resident) electron located in the QD and a photocreated electron-hole pair.

We have studied heterostructures with single layers of InP self-assembled QD's embedded between $Ga_{0.5}In_{0.5}P$ barrier layers grown by gas-source molecular-beam epitaxy. The average diameter of QD's was about 40 nm with a height of about 5 nm. The details of the growth procedure and of the sample characterization are reported elsewhere.[12] In order to control the charge of QD's, a semitransparent Shottky contact has been fabricated on the top surface of the sample, and an ohmic contact has been attached onto the back surface. The total thickness of the undoped layers was about 0.5 $\mu$m. The PL was excited within the PL band of the QD's by (2–4)-ps pulses of a mode-locked Ti:sapphire laser, and detected at the selected energies near the maximum of the PL line [see inset in Fig. 1(a)] with a time resolution of 6 ps, using a 0.25-m subtractive-dispersion double monochromator and a streak camera. The measurements were done in linear and circular polarizations under normal light incidence. The temperature of the sample was 5 K.

Figure 1(a) shows the time-resolved PL kinetics excited by the linearly polarized light, and detected in the same (further referred to as parallel) linear polarization. The PL tran-

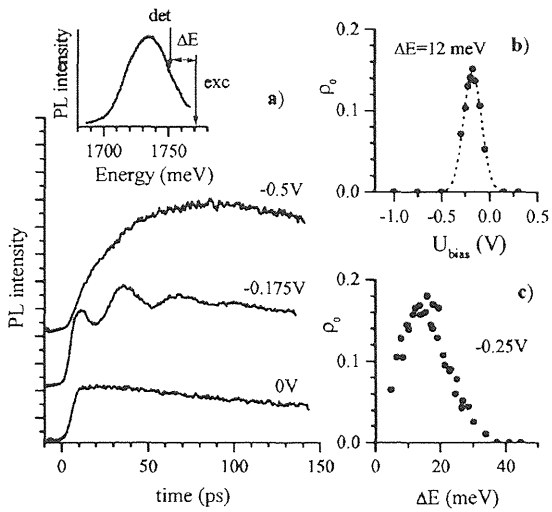


FIG. 1. (a) PL kinetics of the InP QD's in the linear polarization parallel to that of excitation at the spectral point, with Stokes shift between the excitation and detection energies of $\Delta E = 12$ meV for different bias. (b) Bias dependence of the QB amplitude $\rho_0$. Dashed line is the fit by a Gaussian with full width at half maximum $\Delta U = 0.22$ V. (c) QB amplitude $\rho_0$ versus the Stokes shift.

 

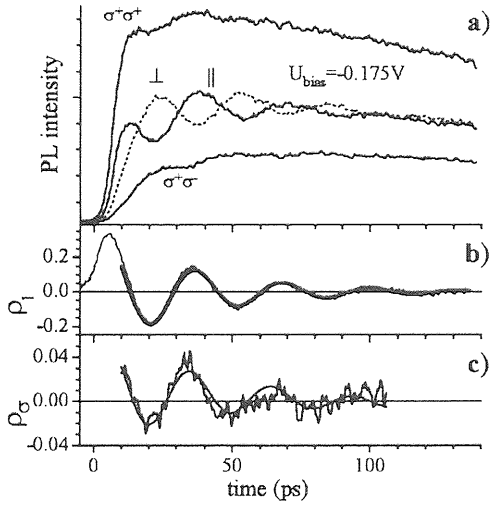


FIG. 2. (a) PL kinetics in the circular parallel ($\sigma^+\sigma^+$) and cross- ($\sigma^+\sigma^-$) polarizations, and also in the linear parallel ($\|$) and cross ($\perp$) polarizations. Applied bias $U_{bias}=-0.175$ V; Stokes shift $\Delta E=15$ meV. (b) Degree of linear polarization $\rho_l$ (noisy curve) and the fit (thick gray curve) by Eq. (1) with $\tau=30$ ps, $\omega=0.20$ ps$^{-1}$, and $\rho_0=0.2$. (c) Degree of circular polarization $\rho_\sigma$ (noisy curve) and the fit (solid curve) by Eq. (1) with the same values of $\tau$ and $\omega$ and $\rho_0=0.05$. Non-oscillating part of $\rho_\sigma$ is subtracted.

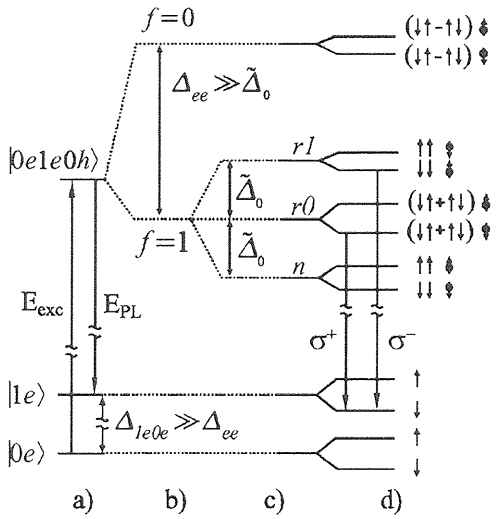


FIG. 3. Scheme of the optical transitions in a charged QD. The upper group of levels ($|0e1e0h\rangle$) represent the fine structure of a hot trion. Levels $|0e\rangle$ and $|1e\rangle$ are the states of the QD before absorption and after emission of a photon, respectively. $\uparrow$ and $\Uparrow$ indicate the electron and hole spins, respectively.

sients measured at the intermediate bias (of $-0.175$ V) show pronounced oscillations with a period of about 30 ps. Such oscillations are absent at zero electric field as well as in the strong-field limit [see Fig. 1(b)].

We assume that the oscillations appear in the case of optical excitation of the QD's containing *one* resident electron per dot. The presence of excess carriers in QD's under study at positive bias was evidenced in Refs. 15 and 16. The presence of the carriers can be easily checked by studying PL kinetics. Optical excitation creates an electron-hole pair in the excited state. The long rise time of the PL from the ground state of the electron-hole pair is governed by the relaxation time of the pair from the excited state and can be observed if there are no resident electrons in the QD's. This case is realized at strong negative biases as shown in Fig. 1(a). Extremely short rise times for small positive or zero bias evidence that, in this regime, the conduction-band ground state is occupied by an *extra electron* coming from the *n*-doped substrate or donors that are inevitably present in the system. At positive bias, each QD contains, on average, more than two resident electrons. Under strong negative bias, most of the dots are expected to be neutral, because of their field-induced depletion. The unusual QB's are observed at an intermediate negative bias [see Fig. 1(b)] where about a quarter of the QD's have single resident electrons, as will be shown below.

Figure 2(a) shows the time-resolved PL measured in the intermediate-field regime (bias of $-0.175$ V). The magnetic field is always zero. After excitation by a circularly polarized light ($\sigma^+$) and detection either in $\sigma^+$ or in $\sigma^-$ circular polarizations, we observe oscillations whose amplitude is quite weak compared to the value of the background signal in $\sigma^+$ polarization. The PL excited by linearly polarized light exhibits pronounced oscillations having opposite phases in parallel and cross polarizations (the cross polarization is orthogonal to the polarization of the incident light). These oscillations clearly manifest QB's between two eigenstates of the system corresponding to circularly polarized optical transitions. Fig. 2(b) shows the linear polarization degree of the PL: $\rho_l=(I_\parallel-I_\perp)/(I_\parallel+I_\perp)$, where $I_\parallel$ and $I_\perp$ are the PL intensities on the parallel and cross polarizations, respectively. It exhibits pronounced oscillations without any constant background, which can be well fitted by a function

$$\rho(t)=\rho_0\exp(-t/\tau)\cos(\omega t), \tag{1}$$

where $\rho_0$, $\tau$, and $\omega$ are fitting parameters. Amplitude of the QB's, $\rho_0$, is sensitive to the applied bias and to the shift between the energies of excitation and detection of the PL, as shown in Figs. 1(b) and 1(c), respectively.

The combination of a nearly constant circular polarization of PL under circularly polarized excitation and pronounced beats in linear polarizations is usually a signature of the Zeeman splitting of $\sigma^+$ and $\sigma^-$ polarized exciton states (to fit our experimental curves, a splitting of 0.12 meV would be required). We attribute the surprising Zeeman-like exciton splitting in the absence of an external magnetic field to the effect of *internal* exchange fields created by resident electrons in QD's.

We assume that a QD contains a resident electron in its ground state $|0e\rangle$. Optical excitation creates a hole in the ground state $|0h\rangle$ and an electron in the excited state $|1e\rangle$.[13] Under these conditions, the QD passes into the state $|0e1e0h\rangle$ shown in Fig. 3(a), which is a hot trion state. We consider hereafter the fine energy structure of the hot trion, where spins of the photocreated and resident electrons can be

parallel or antiparallel. The cold trion, created after the relaxation of the photoexcited electron to its ground state, has a trivial fine structure consisting of a single Kramers doublet, because spins of two electrons at the same energy level should be antiparallel, forming a singlet state. It is clear, therefore, that the cold trion cannot be responsible for the observed QB's.

The trion lifetime in the excited state is governed by the electron relaxation time. QB's are observed at relatively small Stokes shifts $\Delta E<30$ meV [see Fig. 1(c)], i.e., at energies of photocreated electrons (relative to their ground state), which are smaller than the LO phonon energy in the InP QD's, $E_{LO}=45$ meV.[14] The only way for such an electron to relax is to emit an acoustic phonon. This process takes several tens of picosecond.[14] Therefore the QB's can be observed within this time. This conclusion is in a perfect agreement with the data [see Fig. 2(b)].

The fine energy structure of the trion is governed by the exchange interaction of three particles. The electrons, being identical particles, interact with each other much stronger than each of them interact with the hole. This interaction forms the energy spectrum consisting of a singlet ($f=0$) and a triplet ($f=1$), where $\vec{f}=\vec{s}_1+\vec{s}_2$ is the total spin of the two electrons [see Fig. 3(b)]. One can assume that the singlet-triplet splitting $\Delta_{ee}$ in the InP QD's is of the same order of magnitude as that in the InAs QD's, where it has been estimated as 3.5 meV.[20]

The exchange interaction of an electron and a hole is well studied for excitons in quantum wells[17] and QD's.[18] It is known that the energy spectrum of the QD exciton consists of two doublets, one radiative and one nonradiative, with the splitting between them, $\Delta_0$, of the order of 0.1 meV. The in-plane asymmetry of QD's results in the further splitting of the radiative doublet described by the parameter $\Delta_1 \ll \Delta_0$. The splitting of the nonradiative doublet, $\Delta_2$, is much weaker. Since $\Delta_{ee} \gg \Delta_0$, one can consider the exchange interaction of the hole with two electrons in a trion as an interaction of the hole angular momentum $\vec{J}$ with the total spin of the two electrons $\vec{f}$. This is most conveniently done by choosing the spin states with $J_z=|+3/2\rangle$ and $J_z=|-3/2\rangle$ of the hole for the basic states of a pseudospin $j=1/2$, which we denote as $|-1/2\rangle$ and $|+1/2\rangle$, respectively.[17] Using the exciton pseudospin Hamiltonian from Ref. 17, we obtain

$$\hat{H}^{ex}_{hee}=2\tilde{\Delta}_0 f_z j_z+\tilde{\Delta}_1(f_x j_x-f_y j_y)+\tilde{\Delta}_2(f_x j_x+f_y j_y), \quad (2)$$

where $\tilde{\Delta}_{0,1,2}=(\Delta^{e1}_{0,1,2}+\Delta^{e2}_{0,1,2})/2$ and $\Delta^{ei}_{0,1,2}$ are the corresponding energy constants for the interaction of the hole with the $i$th electron.

A very essential point is that in Eq. (2) the heavy hole pseudospin $j=1/2$ interacts with an *integer* spin $f=0$, 1. As a result, the energy spectrum of the entire spin system obeys the Kramers theorem: in the absence of magnetic fields it consists of doublets which do not split further no matter how low the geometric QD symmetry becomes. The corresponding energy spectrum, shown in Fig. 3(c) for the case $\tilde{\Delta}_1=\tilde{\Delta}_2=0$, governs the polarization dynamics of PL.

Since the energy separation between the $f=0$ and $f=1$ level groups is greater than the exciting-pulse bandwidth, they can be considered separately. The $f=0$ doublet can yield no beats; therefore the analysis below will be concentrated on the $f=1$ group of levels. In this group, there are two radiative doublets and a nonradiative one, marked in Fig. 3(c) by $r_1$, $r_0$, and $n$, respectively.

Depending on the initial spin state of the resident electron, $s_z$, the circularly polarized light excites different trion states:

$$s_z=+1/2,\ \sigma^- \rightarrow |+1\rangle|+1/2\rangle,\ \sigma^+ \rightarrow |0\rangle|-1/2\rangle, \quad (3)$$

$$s_z=-1/2,\ \sigma^+ \rightarrow |-1\rangle|-1/2\rangle,\ \sigma^- \rightarrow |0\rangle|+1/2\rangle. \quad (4)$$

Here we have used the pseudospin notation $|f_z\rangle|j_z\rangle$.

As seen from Eqs. (3) and (4), only one state of the radiative doublets $r_0$ or $r_1$ can be excited by the circularly polarized light. The linearly polarized laser light coherently excites two states, one of them belonging to the $r_0$ doublet, and the other one to the $r_1$ doublet. For the case of $s_z=+1/2$, these two excited states are marked in Fig. 3(d) by arrows which denote the radiative transitions from these states.[19] Due to the energy separation of $r_0$ and $r_1$ doublets, radiative transitions from these states excited coherently should give rise to QB's at the frequency $\omega=\tilde{\Delta}_0/\hbar$. We believe that the observed QB's result from this coherent process.

Averaging the intensities of the polarized components of light over the spin states of resident electrons in the ensemble of QD's, we obtain an expression for the linear polarization degree:

$$\rho_l(t)\approx 4/5\cos(\omega t). \quad (5)$$

Equation (5) predicts a considerably larger amplitude of the QB's, $\rho_0=0.8$, than the maximum of the experimentally observed value [$\rho_0\approx 0.2$, see Figs. 1(b) and 1(c)]. The reduction of the beat amplitude is most likely caused by fluctuations in the occupancy of the QD's by resident electrons. The QD's containing no electron, or two electrons, evidently

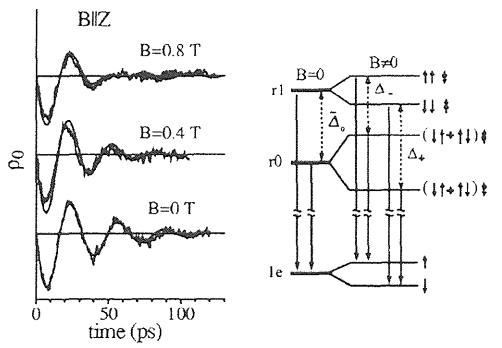


FIG. 4. QB's of trions (noisy curves) in magnetic field indicated against each curve and the fit (smooth curves) by function $\rho_l(B)=\rho_0\exp(-t/\tau)\cos(\omega t)\cos(\Delta\omega t)$ with $\tau=30$ ps, $\omega=0.20$ ps$^{-1}$, and $\Delta\omega=g\mu_B B/\hbar$, where $g=0.3$, for all the experimental curves. The scheme illustrates the difference of the beat energies, $\Delta_-$ and $\Delta_+$, in a magnetic field for spin $\uparrow$ and $\downarrow$ of the resident electron.

should not contribute to the beat signal, but they do contribute to the total PL signal, thus reducing the amplitude of the oscillating polarization degree.

A similar analysis can be done if an in-plane anisotropy is present. Coupling between the two radiative doublets, induced by the $\tilde{\Delta}_1$ term in Eq. (2), makes the polarization of corresponding radiative states slightly *elliptical*. Under these conditions, the circularly polarized light excites coherently both radiative doublets, resulting in the small-amplitude beats upon a constant background: $\rho_{\sigma} \approx 1 - 2\alpha^2[1 - \cos(\omega t)]$, where $\alpha \approx \tilde{\Delta}_1 / \tilde{\Delta}_0$.

One can see that the proposed model describes all the main qualitative features of the observed effect, namely, the QB's both in linear and circular polarizations at the same frequency, and the fact that the circular QB's are much weaker and are superimposed on a virtually time-independent background [see Figs. 2(b) 2 and 2(c)].

The model predicts also that the observed frequency of beats should not be sensitive to weak magnetic fields applied in the Faraday geometry (along $z$ axis). Indeed, the magnetic field splits the Kramers doublets as shown in the scheme in Fig. 4.[21] The energy separation between the optically excited states, $\tilde{\Delta}_0$, depends on the spin projection of the resident electron onto the magnetic field. For one projection (say $\uparrow$), $\tilde{\Delta}_0$ is *increased* by the value $\hbar\Delta\omega$, and for another projection ($\downarrow$) it is *decreased* by the same value, i.e. $\Delta_{\pm} = \tilde{\Delta}_0 \pm \hbar\Delta\omega$. Here $\hbar\Delta\omega = |g_h + g_e|\mu_B B$, where $g_e$ and $g_h$ are $g$ factors of the electron and the hole, respectively, $\mu_B$ is the Bohr magneton, and $B$ is the magnetic field. As a result, the average QB frequency of an ensemble of the QD's with non-polarized resident electrons is not shifted. While $\Delta\omega < 1/\tau$, the splitting results in an effective broadening of the frequency bandwidth of oscillations, which manifests itself in a more rapid damping. As seen from Fig. 4, the experimental polarization transients are well modeled by the calculations assuming $|g_h + g_e| \equiv g = 0.3$.

In conclusion, we have observed quantum beats with unusual polarization properties in the PL of InP QD's. The beats are shown to result from the peculiar spin structure of a hot trion formed by the electron-hole pair created by light and a resident electron.

The authors are grateful to A. Fedorov, I. Gerlovin, V. Kalevich, S. Nair, and A. Zrenner for fruitful discussions. This work was supported in part by RFBR and INTAS.

[1] T. Kawazoe and Y. Masumoto, Phys. Rev. Lett. **77**, 4942 (1996).
[2] M. Bayer *et al.*, Phys. Rev. B **60**, R8481 (1999).
[3] R.J. Warburton *et al.*, Nature (London) **405**, 926 (2000).
[4] A. Hartmann *et al.*, Phys. Rev. Lett. **84**, 5648 (2000).
[5] F. Findeis *et al.*, Phys. Rev. B **63**, 121309(R) (2001).
[6] J.J. Finley *et al.*, Phys. Rev. B **63**, 161305(R) (2001).
[7] D. Hessman *et al.*, Phys. Rev. B **64**, 233308 (2001).
[8] N.H. Bonadeo *et al.*, Science **282**, 1473 (1998).
[9] V.K. Kalevich *et al.*, Fiz. Tverd. Tela (St.Petersburg) **41**, 871 (1999) [Phys. Solid State **41**, 789 (1999)].
[10] J.A. Gupta *et al.*, Phys. Rev. B **59**, R10421 (1999).
[11] T. Flissikowski *et al.*, Phys. Rev. Lett. **86**. 3172 (2001).
[12] H.-W. Ren *et al.*, Jpn. J. Appl. Phys., Part 1 **38**, 2438 (1999).
[13] Due to the low symmetry of the QD's, such optical transitions are allowed.
[14] I.V. Ignatiev *et al.*, Phys. Rev. B **63**, 075316 (2001).
[15] I.V. Ignatiev *et al.*, Phys. Rev. B **60**, R14 001 (1999).
[16] Y. Masumoto *et al.*, Jpn. J. Appl. Phys., Part 1 **40**, 1947 (2001).
[17] E. L. Ivchenko and G E., *Superlattices and Other Heterostructures* (Springer Verlag, Berlin, 1995).
[18] R.I. Dzhioev *et al.*, Fiz. Tverd. Tela (St. Petersburg) **40**, 858 (1998) [Phys. Solid State **40**, 790 (1998)].
[19] All doublets are shown split to give an image of populated states and radiative transitions involved in the phenomenon discussed.
[20] E. Dekel *et al.*, Phys. Rev. B **61**, 11 009 (2000).
[21] Zeeman splitting of the $r1$ radiative doublet is $\delta_{r1}(B) = |2g_e + g_h|\mu_B B$, while the splitting of the $r0$ radiative doublet is $\delta_{r0}(B) = |g_h|\mu_B B$.

PHYSICAL REVIEW B 66, 075326 (2002)

# Interferometric coherence measurement of stress-induced $In_xGa_{1-x}As/GaAs$ quantum dots at the resonant-luminescence phonon sideband

A. V. Baranov,[1,2] V. Davydov,[1,*] A. V. Fedorov,[2,3] M. Ikezawa,[4] H.-W. Ren,[1,†] S. Sugou,[1,5] and Yasuaki Masumoto[1,4]
[1]*ERATO Single Quantum Dot Project, JST Corporation, Japan*
[2]*S. I. Vavilov State Optical Institute, 199034 St. Petersburg, Russia*
[3]*Venture Business Laboratory, University of Tsukuba, Tsukuba 305-8573, Japan*
[4]*Institute of Physics, University of Tsukuba, Tsukuba 305-8571, Japan*
[5]*OptoElectronics Research Laboratory, NEC Corporation, Tsukuba 305-8501, Japan*
(Received 10 September 2001; revised 4 April 2002; published 20 August 2002)

Dephasing of the lowest-energy electronic transition of $In_{0.1}Ga_{0.9}As/GaAs$ stress-induced quantum dots in inhomogeneously broadened system has been investigated by the interferometric double pulse excitation and time-integrated detection of optical-phonon sideband in their resonant-photoluminescence spectra. It was found that combination of the narrow phonon resonance and spectral filtering of the signals allow us to determine the dephasing time in inhomogeneously broadened ensemble of quantum dots. The dephasing time of about 100 ps at 2 K shows that a pure dephasing is still essential in the studied system, most likely, as a result of coupling of electronic excitations in quantum dots with optical phonons of surroundings via deformation potential.

DOI: 10.1103/PhysRevB.66.075326 PACS number(s): 78.47.+p, 42.50.Md, 63.22.+m

## I. INTRODUCTION

Semiconductor quantum dots (QD's) present a unique class of heterostructures possessing atomiclike discrete energy states and very narrow spectral lines due to three-dimensional quantum confinement. The homogeneous widths $\hbar\gamma_2$ about ~50 $\mu$eV were observed in photoluminescence (PL) spectra of single QD's of different types at low temperature.[1-3] A longest phase relaxation time of the fundamental exciton transition $T_2=1/\gamma_2$ of about 1.3 ns ($\hbar\gamma_2 \approx 0.5$ $\mu$eV) has been found by a photon-echo spectroscopy for weakly confined CuCl QD's in an NaCl matrix at 1 K (Ref. 4); $T_2$ of about 630 ps has been measured by a four-wave-mixing (FWM) technique for strongly confined $In_xGa_{1-x}As$ self-assembled QD's (SAQD's) at 7 K. Even for excited states, $T_2$ of ~40 ps has been measured by means of a wave-packet interferometry for a single QD formed by width fluctuation in a GaAs quantum well[6] (QW) and for $In_xGa_{1-x}As$ QD selected from a SAQD ensemble.[7] The low-temperature long coherence of the electronic state of QD's is very important for realization of efficient nonlinear optical processes in the QD systems and makes QD's a hopeful object for quantum computation and coherent information processing. Nevertheless, there is a lack of data on the dephasing time of inhomogeneously broadened QD systems fabricated by epitaxial growth, although they are most hopeful to be used in the optical device engineering. Because of low QD optical density, conventional methods of studying the systems, e.g. the FWM technique, may be used only for many layers of QD's (Ref. 8) or those in purposely prepared waveguides.[9,5] At the same time a technique of the wave-packet interferometry developed during the last few years looks very attractive for the study of the dephasing processes in the QD systems.[6,10,11]

This technique is based on interference of two coherent polarization waves excited by the two coherent pulse trains at the frequency $\omega_L$ resonant with an optical transition of the studied system. Optical responses of two level system that are proportional to the square of the polarization amplitude, e.g. absorption, will possess oscillations $N(\tau)=N(0)[1+s(\tau)\cos(\omega_L\tau)]$ with a change of a mutual delay $\tau$ between the pulses.[6,10,11] Because of intrinsic polarization decay, an amplitude of the oscillations $s(\tau)$ decays with a time constant of $T_2$. It is possible to obtain $T_2$ of the resonant states of mesoscopic semiconductor systems by the time-integrated detection of the related signal as a function of $\tau$. The signals of the resonant Rayleigh scattering,[11] the resonant fluorescence,[12] and the luminescence from low-lying electron state populated through the higher-energy state[6] have been analyzed to get the $T_2$ values. At the same time, it is known that signals corresponding to incoherent processes involving phonons of the system, e.g. resonant Raman scattering or optical-phonon sideband of the resonantly excited luminescence, also contain information about $T_2$ of the resonant electronic states of the system[13,14] and can be analyzed in the same manner. Although the Stokes-shifted signals allow us to simplify the study of the lowest-energy state coherence, since they are not masked by coherent stray light, such experiments have not been performed yet. For the studies of the QD systems, it is necessary to consider that most of real QD systems possess essentially inhomogeneous spectrum of electronic transitions. It is expected from general considerations that the inhomogeneity should result in shortening of the $s(\tau)$ decay observed in the time-integrated experiments. However, the lack of an adequate theoretical model describing the inhomogeneity effect on the time-integrated signals makes it difficult to derive intrinsic $T_2$ of interest.

In this work, we report the interferometric coherence measurement of the lowest-energy electronic state of stress-induced $In_{0.1}Ga_{0.9}As$ QD (SIQD) system by means of time-integrated detection of optical phonon lines in the resonant photoluminescence (RPL) spectra of QD's at 2 K. Relatively long dephasing time is expected for SIQD's as compared with other QD systems fabricated by epitaxial growth, e.g. self-assembled QD's.[15] The studied SIQD's system possesses essentially inhomogeneous spectrum of electronic transitions

 

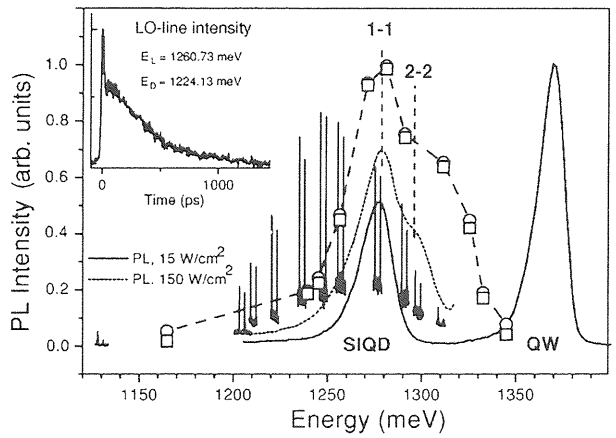


FIG. 1. Solid and dotted lines represent the PL spectra of the sample at 2 K in the region of the 1-1 and 2-2 transitions of SIQD's and the lowest transition of QW excited by a cw Ti:sapphire laser at 1822 meV with power densities of 15 and 150 W/cm$^2$, respectively. The pairs of narrow lines are the segments of the RPL spectra of SIQD's for different excitation energies $E_L$ at low excitation power limit. The different base levels of the segments represent the actual backgrounds of the RPL signals resulted from excitation of larger QD's. The open circles (squares) show the integral intensities of the LO- (TO-) phonon lines for different $E_L$, i.e. excitation spectra of the lines, therefore positions of the circles (squares) are shifted with respect to the relevant segments by the phonon energies. A dashed curve is a guide for eyes. Inset shows the time dependence of the LO-line intensity under 2-ps pulse excitation. $E_L$= 1260.73 meV and $E_D$= 1224.13 meV.

with full width at half maximum of ~20 meV. Basing on developed theoretical model describing time-integrated signals of the phonon-assisted secondary emission of inhomogeneously broadened system, we demonstrate that intrinsic dephasing time of the SIQD electronic transitions can be determined from the interferometric experiments with spectral filtering of the phonon-assisted RPL, when independent information on the phonon lifetime is available.

## II. SAMPLE AND ITS CHARACTERIZATION

SIQD's were prepared in an $In_{0.1}Ga_{0.9}As$ quantum well sandwiched between epitaxial GaAs barriers grown on a semi-insulating GaAs (001) substrate. A thickness of the $In_xGa_{1-x}As$ layer is 8 nm. The GaAs top barrier is 6.5 nm. SIQD's were formed by local strains caused by InP stressors grown in a Stranski-Krastanow mode on the top of the whole structure. The stressors are 60 nm in diameter, and 20 nm high and the areal density is $2\times10^9$ cm$^{-2}$. Details of the sample structure were published elsewhere.[16] Electronic energy structure in the SIQD's identified by the state-filling experiment at 2 K is typical for similar QD's.[17] The luminescence bands corresponding to the 1-1 transition (at 1277 meV) and the 2-2 transition (at 1296 meV) are shown in Fig. 1. A distinctive feature of the RPL spectra excited in the region of the low-energy transitions of SIQD's at 2 K is that pairs of narrow lines with the Stokes shifts of 33.60 meV and 36.55 meV, and half width at half maximum (HWHM) ($\hbar\Gamma_{PH}$) of about 60 $\mu$eV dominate the spectra (Fig. 1). The spectra were measured in a near backscattering geometry by the use of a continuous-wave (cw) Ti:sapphire laser and a 1-m double monochromator with combined spectral resolution of 10 $\mu$eV. Analogous pair of lines was found when the excitation photon energies $E_L$ of 1169 meV or 1345 meV were far from the transitions of SIQD's. The lines correspond to the off-resonant Raman scattering by the TO and LO phonons of GaAs.[18] A nonzero amplitude of the TO-phonon line comes from experimental imperfect backscattering geometry. Strong resonant enhancement of the line intensities is observed when $E_L$ falls in the region of the inhomogeneously broadened 1-1 and 2-2 transitions of SIQD's (Fig. 1). Simultaneously, the LO-phonon line becomes depolarized in contrast to the off-resonant case. The lowest-energy maximum in the excitation spectra of the lines corresponds to the 1-1 transition, whereas the higher-energy satellite is shifted by the LO- (TO-) phonon energy. The results clearly indicate that the zone center GaAs LO and TO phonons are effectively coupled with the low-energy electronic states of SIQD's giving rise to the narrow Raman-like lines. The conclusion is correct, whether the resonant Raman scattering or phonon sideband of the RPL are responsible for the lines in the cw spectra. However, for analysis of the time-integrated signals of the lines excited by a pair of 2-ps laser pulses, that will be described below, it is important to know the origin of the lines at the pulse excitation. A conventional time-resolved experiment by the use of a 2-ps laser-pulse excitation and an infrared streak camera with time resolution of about 30 ps showed that the phonon-assisted RPL makes main contribution to the LO- (TO-) line intensity. Indeed, an integral intensity of the slow (luminescence) component of the LO- (TO-) line signal excited in resonance with 1-1 transition (inset in Fig. 1) is essentially larger (> ten times) than that of the fast (Raman) component. It follows that at 2-ps pulse excitation the lines come mainly from the phonon-assisted annihilation of directly excited electron-hole pairs when SIQD's are excited in the region of the 1-1 transition (incoming resonance). At higher excitation energies, along with this process the annihilation of the pairs created by the optical-phonon-assisted absorption of the light can be responsible for the signal (outgoing resonance) as well as the excitation of the electron-hole pairs due to 2-2 transition followed by their relaxation to the lowest-energy states with emission of the LO(TO) phonon and consequent recombination.[19] At the same time, a broadband luminescence background observed in the RPL spectra at analogous incident photon energies (Fig. 1), most likely, arises due to the second process involving acoustic phonons of the system.

## III. INTERFEROMETRIC EXPERIMENT

In the interferometric coherence measurement (block scheme of the experimental setup is shown in Fig. 2), a modified Michelson interferometer has been used to form two coherent pulse trains with the same polarization and intensity separated by variable time delay $\tau$. The pulses were generated by a ~2-ps mode-locked tunable Ti:sapphire laser at a 82-MHz repetition rate. The pulse trains emerging from

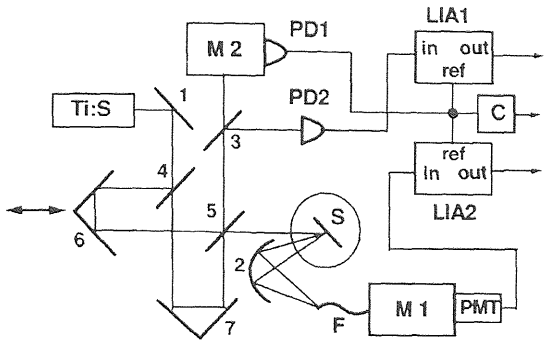


FIG. 2. Experimental setup: Ti:S represents picosecond mode-locked Ti:sapphire laser; $M$ represents monochromators; PD represents photodiodes; $S$ is the sample in the cryostat; $F$ is the fiber bundle; PMT represents photomultiplier; LIA represents lock-in amplifiers; C represents counter. 1,2 are the mirrors; 3–7 are the elements of the interferometer.

the interferometer illuminated the sample immersed in superfluid helium with the power density below the state-filling level. The luminescence was fed to a 1-m double monochromator ($M1$) equipped with an infrared photomultiplier. The monochromator served as a spectral filter that transmitted the luminescence at $\hbar\omega_D$ with bandpass $\hbar\Gamma_D$ determined by the slit width $W/2$. We used a continuously scanning interferometer instead of actively stabilized one commonly utilized in the coherent control experiments.[6,10,11] Then, the mutual time delay $\tau$ is slowly varied in time $t$ by the relation $\tau=2vt/c$, where $v$ is the scanning speed of an interferometer retroreflector, $c$ is the light speed, and the time-integrated luminescence signal $N(\tau)$ is described by

$$N(\tau)/N(0)=1-s(\tau)\cos(\omega\tau)=1-s(\tau)\cos(\omega' t), \quad (1)$$

where $\omega'=2\omega v/c$. The minus sign comes from the odd number of reflections of this beam off the interferometer's beamsplitters. The detected signals $N(\tau)$ oscillate with low frequency $f=\omega'/2\pi$ of about several tens hertz that allows one to use a lock-in technique in order to directly record the envelope of the oscillations $s(\tau)$ containing information about $T_2$ with improved signal-to-noise ratio. For example, $f=50$ Hz corresponds to $\omega=\omega_L=1.946\times10^{15}$ s$^{-1}$ ($E_L=1277$ meV) at experimentally used $v$ of $2.4\times10^{-3}$ cm/s. Continuously scanning the interferometer, we took the data triggered by the ac component of the signal of the photodiode (PD1) placed behind the output slit of an auxiliary monochromator ($M2$). It extracted a narrow spectral component at the energy of $\hbar\omega_r=\hbar\omega_L$ corresponding to the spectral maximum of another laser-pulse beam emerging from the interferometer. The coherence length of the component was found to be ~8 cm that enabled us to measure $\tau$ in time scale up to 200 ps. The PD1 signal $N_r(t)\sim\cos(\omega' t)$ served as a reference to the two lock-in amplifiers (LIA's). One of them (LIA2) collected the luminescence signal $N(\tau)$, and the second one (LIA1) was used for simultaneous recording of the pulse autocorrelation $a(\tau)$ utilizing the signal from the second photodiode (PD2) directly illuminated by the light beam from the interferometer. The amplitudes of the

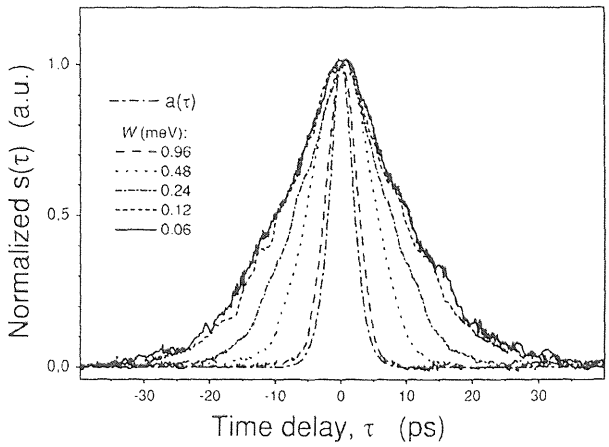


FIG. 3. Envelopes $s(\tau)$ of the time-integrated signals of the LO-phonon-assisted RPL for different values of the spectral selection bandpass $W$ (in energy units). The mean photon energy of the incident pulses, $E_L=1260$ meV is in the region of the 1-1 transition of SIQD's and the detection energy $E_D=E_L-\hbar\Omega_{LO}=1233.4$ meV corresponds to the maximum of the LO-phonon band. $a(\tau)$ is the laser-pulse autocorrelation. Full spectral width of the LO-phonon line, $2\hbar\Gamma_{PH}=120$ $\mu$eV.

corresponding LIA outputs are proportional to $s(\tau)$ and $a(\tau)$. The high stability of the interferometer and the scanning velocity $v$ allowed us to obtain the good signal-to-noise ratio with an accumulation time constant up to several seconds (the uncontrolled jitter of the relative phase between the excitation pulses was determined to be within 0.2-rad rms) and measure the $\omega_L$ values with accuracy of 0.5%.

## IV. RESULTS AND DISCUSSION

In Fig. 3 the envelopes $s(\tau)$ of the time-integrated signals of the LO-phonon-assisted RPL are shown for different values of the spectral selection bandpass $W$ (in energy units). The mean photon energy of the incident pulses, $E_L=1260$ meV is in the region of the 1-1 transition of SIQD's and the detection energy $E_D=E_L-\hbar\Omega_{LO}=1233.4$ meV corresponds to maximum of the LO-phonon band. It was initially found that $N(\tau)$ oscillates with frequency of $\omega_L$ that is a result of the interference in the absorption channel.[10,12,20] As seen from Fig. 3, the time trace of $s(\tau)$ dramatically depends on $W$. With the decrease of $W$ down to a value of about $2\hbar\Gamma_{PH}$, the $s(\tau)$ width monotonically increases, and does not depend on bandpass below this limit (Fig. 3). Analogous measurements for the TO-phonon line show the same results. Keeping in mind a different bandpass dependence of the resonantly excited coherent and incoherent secondary radiation,[11,12,21] we have studied the effect of the spectral filtering on the time trace of $s(\tau)$ for other excitation-detection conditions: detection of the laser light elastically scattered from the sample, $E_D=E_L$, and detection of the broad luminescence base in the vicinity ($\varepsilon=\pm3$ meV) of the LO- (TO-) phonon lines ($E_L=1280$ meV, $E_D=E_L-\hbar\Omega_{LO(TO)}+\varepsilon$). The luminescence background is observed at $E_L$ above the energy of the 1-1

transition (see Fig. 1). For the elastically scattered light, the decrease of $W$ resulted in the continuous increase of the width of $s(\tau)$ due to interference of two coherent pulses passed through the monochromator, as it was expected. For the luminescence base, the $s(\tau)$ was found to be independent of $W$ and to agree with $a(t_D)$ within experimental errors. Such features of the signal are typical for the luminescence from an optical transition populated through photoexcited higher-energy states with continuous spectrum, e.g., at excitation in the free-carrier continuum of the bulk semiconductor and detection of the exciton emission.[12] In our case it is, most likely, caused by a large inhomogeneous distribution of energy separation between the lowest and higher exciton levels in the SIQD system analogously reported for the self-assembled InAs QD's.[22] Then, though the detected luminescence comes from the lowest-energy states selected by the filter, these states are populated from the higher-energy quasicontinuum state through intraband relaxation mediated by acoustic phonons with continuous energy spectrum. Thus, $W$ dependence of $s(\tau)$ for the phonon-assisted RPL signal quite differs from those for other signals.

In order to explain the unusual $W$ dependence of the phonon-assisted RPL signal and to determine what information on relaxation constants of the SIQD's can be obtained from the signal analysis, we carried out theoretical analysis of a spontaneous phonon-assisted secondary radiation.[23] The spectral-selected time-integrated signal excited by two coherent pulse trains has been calculated for an inhomogeneously broadened system with two electronic states by the use of perturbation theory for the generalized master equation.[24] Electron-phonon interaction was considered in the adiabatic approximation. One phonon mode with fixed frequency was taken into account since, accordingly to our experimental data, the zone-center GaAs optical phonons contribute mainly to the interaction. The inhomogeneity width was supposed to be much broader than the spectral width of the laser pulses, which is in turn much more than the relaxation rate constants of the system quantum states taken into consideration and smaller than frequencies of the optical phonons. These assumptions hold for the studied SIQD system.

Then the signal of the secondary radiation for incoming resonance averaged over the transition frequency is determined by

$$N(\tau)=\frac{8\pi\beta}{\gamma_1}\sigma^2\Gamma_D^2F(\Delta_{0L})\times\int_{-\infty}^{\infty}dx\frac{1}{x^2+\Gamma_D^2}\frac{1+K(\tau)\cos[(x+\omega_D+\Omega)\tau]}{[(x-\delta_D)^2+\sigma^2]^2},\tag{2}$$

where

$$K(\tau)=\frac{\hat{\gamma}_2}{\gamma_2}e^{-(2\gamma_2+\gamma_{ph}/2)\tau}+\frac{\gamma_1}{2\gamma_2}e^{-\gamma_{ph}\tau/2},\tag{3}$$

$\Delta_{0L}=\omega_0-\omega_L$, $\delta_D=\omega_L-\omega_D-\Omega$, $\omega_0$ is the central frequency of distribution $F(\Delta_{0L})$ for electronic transitions in the inhomogeneous system, $\omega_L$ is the carrier frequency of laser pulses with spectral width $\sigma$, $\omega_D$ and $\Gamma_D$ are the frequency and bandpass of the spectral filter, $\beta$ is the constant, $\Omega$ is the optical-phonon frequency, $\gamma_2=\gamma_1/2+\hat{\gamma}_2$, $\gamma_2$ and $\hat{\gamma}_2$ are the coherence loss rate constants due to the full and pure phase disruptions, and $\gamma_1$ and $\gamma_{ph}$ are the inverse lifetimes of electronic population and phonon. The expression has been derived for exponential laser pulses ($\sim\exp[-\sigma|t|]$) and a Fabry-Perot spectral filter.

In the case of exact resonance $\delta_D=0$,

$$\begin{aligned}N(\tau)=\frac{8\pi\beta}{\gamma_1}\sigma^2\Gamma_D^2F(\Delta_{0L})\Bigg[&\frac{1}{\Gamma_D(\sigma-\Gamma_D)^2(\sigma+\Gamma_D)^2}\times\{1+K(\tau)e^{-\Gamma_D\tau}\cos[(\omega_D+\Omega)\tau]\}\\&-\frac{1}{\sigma(\sigma-\Gamma_D)^2(\sigma+\Gamma_D)^2}\{1+K(\tau)e^{-\sigma\tau}\cos\omega_L\tau\}\\&-\frac{1}{2\sigma^3(\sigma-\Gamma_D)(\sigma+\Gamma_D)}\{1+K(\tau)(1+\sigma\tau)e^{-\sigma\tau}\cos\omega_L\tau\}\Bigg].\end{aligned}\tag{4}$$

If $\Gamma_D\gg\sigma$, then

$$N(\tau)=\frac{4\pi\beta}{\gamma_1}\frac{1}{\sigma}F(\Delta_{0L})\{1+K(\tau)(1+\sigma\tau)e^{-\sigma\tau}\cos\omega_L\tau\}.\tag{5}$$

Since $\sigma\gg2\gamma_2+\gamma_{ph}/2$ by assumption, $K(\tau)\simeq1$ and $s(\tau)=(1+\sigma\tau)\exp(-\sigma\tau)$, i.e., it coincides with the laser-pulse autocorrelation $a(\tau)$. It is easy to show that the conclusion is fulfilled for any shape of the pulses.

If $\Gamma_D\ll\sigma$, then

$$N(\tau)=\frac{8\pi\beta}{\gamma_1}\frac{\Gamma_D}{\sigma^2}F(\Delta_{0L})\times[1+K(\tau)e^{-\Gamma_D\tau}\cos[(\omega_D+\Omega)\tau]].\tag{6}$$

Importantly the decay of the signal is independent of the laser-pulse shape and the cosine amplitude $s(\tau)=K(\tau)e^{-\Gamma_D\tau}$ [see Eq. (1)]. Moreover, the decay rate of $s(\tau)$ monotonically decreases with $\Gamma_D$ and $s(\tau)$ tends to $K(\tau)$ at $\Gamma_D\ll2\gamma_2+\gamma_{ph}/2$ that holds for any kind of spectral filter. Just in this limit, direct information about relaxation constants of interest can be obtained from the $s(\tau)$ analysis. Since the signal does not depend on the pulse shape, it is reasonable to assign it to a free-polarization one[25] that consists of two components in accordance with Eq. (3).[26] First of them decaying with $2\gamma_2+\gamma_{ph}/2$ and proportional to the pure dephasing $\hat{\gamma}_2$ can be attributed to the phonon-assisted RPL. Such definition is in accordance with the phonon-assisted RPL of inhomogeneously broadened system at monochromatic cw excitation, where a spectral width (HWHM) of the related line is $2\gamma_2+\gamma_{ph}/2$ and amplitude is proportional to $\hat{\gamma}_2$. It is the term that contains information about the intrinsic dephasing constant $\gamma_2$ of the resonant transitions. Second

term decays with $\gamma_{ph}/2$ and could be assigned to the resonant Raman scattering. When $\gamma_2 \gg \gamma_1/2$, the luminescence term dominates the time-integrated signal that decays with $2\gamma_2 + \gamma_{ph}/2$, i.e. it contains information on the coherence decay of the resonant electronic transitions.

Let us consider a correspondence between the limitation of the model and our experimental data. The direct time-resolved experiment at picosecond excitation on the SIQD system shows that the luminescence dominates the Stokes-shifted signal. The condition of exact resonance $\delta_D = \omega_L - \omega_D - \Omega = 0$ is fulfilled with accuracy close to $\Gamma_D$. The observed $W$, or $\Gamma_D$ dependence of $s(\tau)$ is qualitatively evident from Eqs. (5) and (6): $s(\tau)$ tends to $a(\tau)$ and $K(\tau)$ in the limits of broad and narrow spectral bandpasses, correspondingly. Although the values of $\gamma_2$ and $\gamma_{ph}$ are *a priori* unknown for the SIQD's as well as the exact value of $\Gamma_D$, it is reasonable to think that at saturation condition found experimentally for $W$ smaller than about 0.1 meV the inequality of $\Gamma_D \ll 2\gamma_2 + \gamma_{ph}/2$ approximately holds. Physical meaning of the spectral selection in the interferometric experiment is analogous to that in conventional cw experiments, where bandpass of the filter should be smaller than spectral width of the measured line in order to get a correct value of the width. As a result, the spectral-selected time-integrated signal is described by a single exponential decay

$$s(\tau) = e^{-(2\gamma_2 + \gamma_{ph}/2)\tau}. \quad (7)$$

Therefore, the inhomogeneous broadening of the electronic transitions gives rise to the $\gamma_{ph}$ term in decay of $s(\tau)$ and $\gamma_2$ can be determined if $\gamma_{ph}$ is known from independent measurements, e.g., from the off-resonant Raman-scattering experiment.

The wave-packet interferometry experiment on a single QD controlled the coherent status and measured $\gamma_2$ for the excited but not for the exciton ground state of QD.[6] At the same time the analysis of the signal of the phonon-assisted RPL under resonant excitation of the lowest-energy transition allows to determine dephasing constant for the exciton ground state of QD. For the SIQD system, it corresponds to excitation at the low-energy side of the related PL band (1-1 transition). We measured $s(\tau)$ for the LO line at $E_L$ in this region ($E_L = 1234$, 1244, 1260, and 1270 meV) at spectral bandpass corresponding to the saturation limit. Typical $s(\tau)$ for $E_L = 1234$ meV is shown in Fig. 4(a). It was found that $s(\tau)$ were well described by the monoexponential decay. Fitting of the curves by the use of Eq. (7) allows us to get the $\gamma = 2\gamma_2 + \gamma_{ph}/2$ values. As is seen in Fig. 4(b), $\hbar\gamma$ is practically constant of about 60 $\mu$eV with $\hbar\gamma = 55 \pm 5$ $\mu$eV for the lowest incident photon energy of 1234 meV. A set of precise independent off-resonant Raman measurements of the GaAs LO-phonon linewidth performed on the same sample at 2 K by the use of a 1064.2-nm cw radiation of a $Nd^{+3}:YVO_4$ laser gave us the $\hbar\gamma_{ph}$ value of $85 \pm 10$ $\mu$eV. The value was found by a standard deconvolution of LO-phonon signal with Lorentzian LO-phonon line and Gaussian apparatus response measured in the same experiment by the use of the incident light. Then we can determine the $\hbar\gamma_2$ value for the lowest-energy excitonic transition as $\hbar\gamma_2 = \hbar(\gamma - \gamma_{ph}/2)/2 \approx 6.3 \pm 1.5$ $\mu$eV that corresponds to the dephasing time value $T_2$ of $100 \pm 25$ ps.

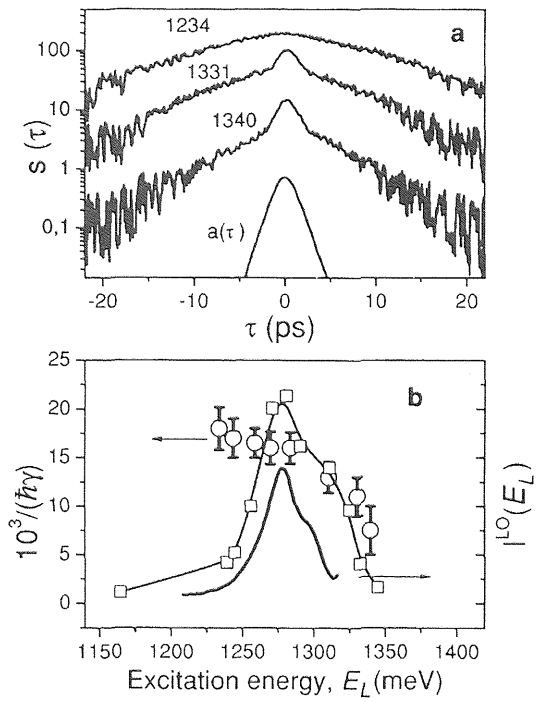


FIG. 4. (a) A semilogarithmic plot of the LO-line signal $s(\tau)$ for several $E_L$ (shown in a unit of meV). The curves are vertically displaced for clarity. Narrow spikes on the top of some curves are well described by $a(\tau)$ and are related to the broad luminescence base. (b) Open circles correspond to the $\gamma$ values determined from monoexponential fitting of $s(\tau)$ for different $E_L$ ($\hbar\gamma$ is shown in a unit of $\mu$eV). Note, only for $E_L \leq 1270$ meV the $\gamma$ values are described by $2\gamma_2 + \gamma_{ph}/2$, see the text. Relevant portions of the PL spectra of SIQD's (solid line) and the excitation spectrum of the LO-phonon line, $I^{LO}(E_L)$ (open squares, dashed line) are shown for comparison.

At higher $E_L$ (in the overlapping region of the 1-1 and 2-2 transitions and in the region of the 2-2 transition) the $s(\tau)$ time traces become narrower [Fig. 4(a)]. A spike related to the thermalized luminescence background and well described by $a(\tau)$ appears on the top of the curves, which indicates that processes involving electronic states different from lowest one additively contribute to the signals. Analysis of the signal becomes much complicated because of unknown contribution of other processes involving optical phonons. In this case, the signal $s(\tau)$ cannot be described by the above-mentioned simple model. Most likely, the shortening of the $s(\tau)$ decay is caused by an increasing contribution of the next excited state with higher $\gamma_2$ to the signal owing to overlapping of the 1-1 and 2-2 transition energies for different SIQD's.

The low temperature $T_2$ of the lowest exciton state in $In_{0.1}Ga_{0.9}As$ SIQD's is longer than that of the HH exciton in single GaAs QW by an order of magnitude[11,27] and than $T_2$ of the excited states in single QD.[6,7] However, it is shorter compared with highest known $T_2$ in CuCl QD's (Ref. 4) and

$In_xGa_{1-x}As$ SAQD's.[5] Comparison with recombination lifetime of the lowest exciton state ($T_1$ is about 300 ps, $\hbar\gamma_1 = 2.2$ $\mu$eV) found in direct time-resolved experiment shows that pure dephasing processes ($\hbar\hat{\gamma}_2 = 5.2$ $\mu$eV) are essential for the lowest-energy transition in the studied SIQD's even at $T = 2$ K. The fact is in a qualitative accord with the FWM data on III-V semiconductor SAQD's at ~5–7 K where the pure dephasing either governs the total dephasing rate of the exciton fundamental transition[8] or its rate is comparable with the depopulation one.[5] A quantitative discrepancy between our and cited data as well as mechanisms governing the pure dephasing in the QD's systems is still subject for discussion. A comparative analysis of temperature dependences of depopulation and dephasing rates is normally used for clarification of dephasing processes in QD's usually treated in the framework of theory of crystal defects.[28,29] The simplest case is two-level systems with radiative limited depopulation rate and pure dephasing rate caused by an elastic phonon scattering. The optical-phonon contribution is negligible at temperatures up to few tens of Kelvin due to the reduction of the phonon population.[30] Then acoustic phonons with continuous energy spectrum govern the pure dephasing rate resulting in its $T^7$ dependence.[31] A presence of the exciton fine structure with characteristic energy gap $\Delta\varepsilon$, that is an inherent property of most QD systems, causes qualitatively other temperature dependence: in addition to the elastic phonon scattering, transitions between levels of the structure with emission and absorption of the acoustic phonons will contribute to $\gamma_2$ via both the $\gamma_1$ and $\hat{\gamma}_2$ temperature dependences. In high-temperature limit $\Delta\varepsilon < k_BT$, $\gamma_1$ and $\hat{\gamma}_2$ will be proportional to $T$ and $T^2$, respectively. In opposite limit $\gamma_1$ is temperature independent for transitions with emission of the phonons and $\gamma_1 \sim \exp(-\Delta\varepsilon/k_BT)$ for transitions with absorption of the phonons, while $\hat{\gamma}_2 \sim \exp(-\Delta\varepsilon/k_BT)$ for both absorption and emission. Just this process was concluded to be responsible for the low-temperature total dephasing rate in $In_xGa_{1-x}As$ SAQD's,[5] where the linear temperature dependence of $\gamma_2$ has been observed in the range of 5–40 K. The high-temperature limit holds for this type of QD's where $\Delta\varepsilon$ are in the range of few hundred $\mu$eV.[32] The same linear dependence has been observed for $In_xAl_{1-x}GaAs$ SAQD's.[8] It follows that main contribution to the temperature dependence of $\gamma_2$ comes from that of $\gamma_1$. At the same time, physics of pure dephasing remains not quite clear since predicted dependence of $\hat{\gamma}_2 = aT^2 + bT^7$ was not detected despite the fact that measured values of $\hat{\gamma}_2$ were comparable with or more than those of $\gamma_1$. In studied $In_xGa_{1-x}As$ SIQD's relative contribution of $\hat{\gamma}_2$ to total dephasing rate is even greater than that found in Ref. 8 and we suppose that the $\gamma_2$ temperature-dependence measurements performed for this system will allow one to look inside the physics of the low-temperature pure dephasing in QD's.

## V. CONCLUSION

In conclusion, we show that dephasing time of lowest electronic transition of QD's in inhomogeneously broadened ensemble can be determined from analysis of time-integrated signal of optical-phonon-assisted RPL excited by two coherent pulse trains. Spectrally selected phonon-assisted RPL signals as a function of mutual delay between the pulses were analyzed in the framework of a theoretical model developed for the inhomogeneously broadened system with two electronic states and adiabatic electron-phonon interaction. It has been shown that spectral selection of the luminescence is necessary condition in order to get information on dephasing constant of the electronic transition in inhomogeneously broadened systems and an optical-phonon dephasing rate additively contributes to decay of the signal. The interferometric measurements have been carried out for $In_{0.1}Ga_{0.9}As/GaAs$ SIQD system by the use of 2-ps pulse trains. Characteristic property of studied SIQD's was found to be coupling of their low-energy electronic excitations with optical phonons of GaAs barriers or substrate that gives rise to analyzed phonon sideband of resonant luminescence under cw and pulse excitation. Dephasing rate of the lowest exciton state of the studied SIQD's of $6.3 \pm 1.5$ $\mu$eV ($T_2 = 100 \pm 25$ ps) has been found from the interferometric data by the use of appropriate fitting procedure and independent off-resonant Raman data on dephasing rate of zone-center bulk GaAs optical phonon.

The time-integrated signals of the phonon-assisted RPL can be used for the lowest-state coherence measurements of any inhomogeneously broadened systems with the narrow optical-phonon resonances in their RPL spectra. Importantly these data and analogous data obtained for phononless RPL signal allow one to get complete information on electron and phonon dephasing of the systems. It is worth noting that in the absence of the inhomogeneous broadening, e.g. for single QD, the time-integrated signals of the phonon-assisted RPL give information exclusively about $\gamma_2$.

## ACKNOWLEDGMENTS

The measurement system was constructed, based on an enlightening discussion with Dr. T. Mishina, which the authors deeply appreciated. The authors gratefully acknowledge Professor V. V. Ovsyankin for helpful and stimulating discussions. Two of us (A.V.B. and A.V.F.) are grateful to the RFBR, Grants Nos. 02-02-17311 and 01-02-17060, and INTAS, Grants Nos. 01-2100 and 01-2331, for partial financial support during this work.

*Permanent address: S.I. Vavilov State Optical Institute, 199034 St. Petersburg, Russia.

†Present address: Space Vacuum Epitaxy Center, University of Houston, Houston, TX 77204-5507.

[1] D. Gammon, E. S. Snow, B. V. Shanabrook, D. S. Katzer, and D. Park, Phys. Rev. Lett. **76**, 3005 (1996).

[2] Y. Toda, O. Moriwaki, M. Nishioka, and Y. Arakawa, Phys. Rev. Lett. **82**, 4114 (1999).

[3] K. Leosson, J. R. Jensen, J. M. Hvam, and W. Langbein, Phys. Status Solidi B **221**, 49 (2000).
[4] M. Ikezawa and Y. Masumoto, Phys. Rev. B **61**, 12 662 (2000).
[5] P. Borri, W. Langbein, S. Schneider, U. Woggon, R. L. Sellin, D. Ouyang, and D. Bimberg, Phys. Rev. Lett. **87**, 157401 (2001).
[6] H. H. Bonadeo, J. Erland, D. Gammon, D. Park, D. S. Katzer, and D. G. Steel, Science **282**, 1473 (1998).
[7] H. Htoon, D. Kulik, O. Baklenov, A. L. Holmes, Jr., T. Takagahara, and C. K. Shih, Phys. Rev. B **63**, 241303 (2001).
[8] D. Birkedal, K. Leosson, and J. M. Hvam, Phys. Rev. Lett. **87**, 227401 (2001).
[9] P. Borri, W. Langbein, J. Mørk, J. M. Hvam, F. Heinrichsdorff, M.-H. Mao, and D. Bimberg, Phys. Rev. B **60**, 7784 (1999).
[10] A. P. Heberle, J. J. Baumberg, and K. Köhler, Phys. Rev. Lett. **75**, 2598 (1995).
[11] S. Ceccherini, F. Bogani, M. Gurioli, and M. Colocci, Opt. Commun. **132**, 77 (1996).
[12] M. Gurioli, F. Bogani, S. Ceccherini, and M. Colocci, Phys. Rev. Lett. **78**, 3205 (1997).
[13] H. Stolz, *Time-Resolved Light Scattering from Excitons* (Springer-Verlag, Berlin, 1994).
[14] M. U. Wehner, M. H. Ulm, D. S. Chemla, and M. Wegener, Phys. Rev. Lett. **80**, 1992 (1998).
[15] A. S. Bracker, J. G. Tischler, D. Gammon, and B. Z. Nosho, Phys. Status Solidi B **224**, 133 (2001).
[16] H.-W. Ren, S. Nair, K. Nishibayashi, J.-S. Lee, S. Sugou, and Y. Masumoto, J. Electron. Mater. **29**, 520 (2000).
[17] H. Lipsanen, M. Sopanen, and J. Ahopelto, Phys. Rev. B **51**, 13 868 (1995).
[18] P. Y. Yu and M. Cardona, *Fundamentals of Semiconductors*, 2nd ed. (Springer, Berlin, 1999).
[19] R. Heitz, I. Mukhametzhanov, O. Stier, A. Madhukar, and D. Bimberg, Phys. Rev. Lett. **83**, 4654 (1999).
[20] M. Woerner and J. Shah, Phys. Rev. Lett. **81**, 4208 (1998).
[21] J. H. Eberly and K. Wódkiewicz, J. Opt. Soc. Am. **67**, 1252 (1977).
[22] R. Heitz, M. Veit, N. N. Ledentsov, A. Hoffmann, D. Bimberg, V. M. Ustinov, P. S. Kop'ev, and Zh. I. Alferov, Phys. Rev. B **56**, 10 435 (1997).
[23] A.V. Fedorov, A.V. Baranov, and Y. Masumoto, Opt. Spectrosc. **93**, 52 (2002).
[24] K. Blum, *Density Matrix Theory and Applications* (Plenum Press, New York, 1981).
[25] L. Allen and J. H. Eberly, *Optical Resonance and Two-level Atoms* (Wiley, New York, 1975).
[26] It should be noted that the signal is caused by spontaneous radiation and qualitatively different from that of free polarization well known in spectroscopy of transient coherent processes.
[27] K. Leo, E. O. Göbel, T. C. Damen, J. Shah, S. Smitt-Rink, W. Schäfer, J. F. Müller, K. Köhler, and P. Ganser, Phys. Rev. B **44**, 5726 (1991).
[28] S. Schmitt-Rink, D. A. B. Miller, and D. S. Chemla, Phys. Rev. B **35**, 8113 (1987); L. Besombes, K. Kheng, L. Marsal, and H. Mariette, *ibid.* **63**, 155307 (2001).
[29] T. Takagahara, Phys. Rev. B **60**, 2638 (1999).
[30] A. V. Uskov, A.-P. Jauho, B. Tromborg, J. Mork, and R. Lang, Phys. Rev. Lett. **85**, 1516 (2000).
[31] D. J. Diestler and A. H. Zewail, J. Chem. Phys. **71**, 3103 (1979); **71**, 3133 (1979).
[32] M. Bayer, A. Kuther, A. Forchel, A. Gorbunov, V. B. Timofeev, F. Schafer, J. P. Reithmaier, T. L. Reinecke, and S. N. Walck, Phys. Rev. Lett. **82**, 1748 (1999).

PHYSICAL REVIEW B 66, 235309 (2002)

# External-field effects on the optical spectra of self-assembled InP quantum dots

Mitsuru Sugisaki,[1,2,*] Hong-Wen Ren,[1,3] Selvakumar V. Nair,[1,2] Kenichi Nishi,[1,4] and Yasuaki Masumoto[1,5]

[1]*Single Quantum Dot Project, ERATO, Japan Science and Technology Corporation, Japan*

[2]*Centre for Advanced Nanotechnology, University of Toronto, Haultain Building, 170 College Street, Toronto, Ontario M5S 3E3, Canada*

[3]*Applied Optoelectronics Incorporation, 13111 Jess Pirtle Boulevard, Sugar Land, Texas 77478*

[4]*Photonic and Wireless Devices Research Labs., NEC Corporation, 34 Miyukigaoka, Tsukuba, Ibaraki 305-8501, Japan*

[5]*Institute of Physics, University of Tsukuba, Tsukuba, Ibaraki 305-8571, Japan*

(Received 8 May 2002; revised manuscript received 24 September 2002; published 12 December 2002)

The effects of external electric and magnetic fields on InP self-assembled quantum dots (QDs) were investigated by means of single dot spectroscopy. By systematically changing a bias applied to the sample, successive energy shifts of the photoluminescence (PL) peaks from excitons and biexcitons due to the quantum confined Stark effect were clearly observed. The quadratic Stark coefficient was evaluated to be of the order of $10^{-31}$ $Fcm^2$. The energy separation of the PL peaks arising from the excitons and biexcitons changed with the applied electric field, reflecting a slight difference of the Stark coefficient between the exciton and biexciton states. The existence of permanent dipole moments was also revealed in both the exciton and biexciton states. The spatial separations between the electrons and holes along the growth direction in a QD were estimated to be 7 Å for the exciton state, and 8 Å for the biexciton state. Further, the diamagnetic shift and the Zeeman splitting of the exciton states were clearly observed in a magnetic field. It was found that the diamagnetic coefficient gradually decreases on decreasing the QD size. A simple qualitative model can explain that this result is due to competition between quantum confinement and magnetic confinement.

DOI: 10.1103/PhysRevB.66.235309 PACS number(s): 78.67.Hc, 71.35.−y, 73.61.Ey, 75.75.+a

## I. INTRODUCTION

Zero-dimensional (0D) semiconductor structures or quantum dots (QDs), which are often referred to as artificial atoms, have attracted considerable interest recently due to their potential for applications and fundamental physics interest. From the basic physics point of view, one of the very interesting topics is experimental measurements of the wave functions on the confined electrons and holes. While a direct mapping of the wave functions is rather difficult, quantities that directly relate to the extent and shape of the electron and hole densities can be obtained by optical measurements in the presence of external fields.

In almost all presently available QD samples, the photoluminescence (PL) energy separation between the exciton and biexciton states is much smaller than their macroscopic PL bandwidth caused by the fluctuations in their size and shape. In order to eliminate the ambiguity due to these size-shape fluctuations, the observation of a single QD is very important. Since the QDs show very sharp PL lines reflecting the density of states of a 0D system, it is expected that even very small changes of their electronic energies can be easily measured.

By observing single QDs, important information and interesting phenomena hidden behind the inhomogeneous distribution have been clarified, such as many carrier effects,[1–3] charged excitons,[4,5] strong optical anisotropy,[6–8] fluorescence intermittency,[9,10] and photon anti-bunching.[11–13] In order to observe a signal from a single QD, it is important to reduce the number of QDs to be excited and probed. The QDs have to be well separated from each other in comparison with the spatial resolution of the detection microscope system. Among the various 0D systems investigated so far, the QDs formed thorough the Stranski-Krastanow (S-K) growth mode are most suitable for the study of a single QD because the QDs can be fabricated in a single layer. In the present work, we employed InP S-K QDs to explore their optical properties in the external fields.

The optical properties of single QDs in external fields have been investigated theoretically and experimentally by several groups. For example, the effects of electric field in a wide variety of QD systems have been reported in Refs. 5 and 14–24. Since each electronic state (e.g., one exciton, biexciton, and their excited states) shows a different energy shift with respect to the applied electric field,[16,21,22] detailed $\mu$-PL measurements are necessary to obtain information on the wave functions of these states. In quantum wells, Thilagam has theoretically shown that the energy shifts have a different magnitude between the exciton and biexciton states.[25] Such a study of QD systems would be interesting.

When an external electric field $F$ is applied, quadratic energy shifts of the exciton states $E(F)$ are observed by the Stark effect:

$$E(F)=E_0-pF-\beta F^2, \tag{1}$$

where $E_0$ is the energy for $F=0$. In most III-V bulk semiconductors, the linear coefficient $p$ is very small.[26–28] Recently, Fu has theoretically predicted a nonzero value of $p$ due to the existence of a permanent dipole moment in spherical QDs.[29] However, it is still very small, typically $\sim 1e\cdot$Å in QDs of a few tens of nm in size. On the other hand, in the case of the S-K QDs having pyramidal or lens shapes (e.g.,

 

$Al_xIn_{1-x}As$,[17] InAs,[18,21,22] and $In_xGa_{1-x}As$,[5,23]), it has been clarified that there exists a large permanent dipole moment. Patanè *et al.* have pointed out that the localization of the electron is above the hole in $In_xGa_{1-x}As$.[23] In other InAs QD samples, however, the confined holes are localized above the electrons in the QDs,[18,22] which is opposite to that predicted by theoretical calculations. The discrepancy between the experiments and theoretical calculations is considered to be due to nonuniform indium composition in real systems.[19] It is thus important to examine the existence of a permanent dipole moment and its direction in QDs of other materials. Furthermore, a permanent dipole moment in a biexciton state has never been carefully studied.

Turning our attention to the magneto-optical effects, magnetic field has historically been employed to artificially generate confined states in bulk semiconductors. In low-dimensional semiconductors, the excitonic states in a magnetic field are characterized by three energy scales: the lateral-size quantization energy, the exciton effective Rydberg energy, and the magnetic confinement energy. The magnetic length $\lambda$, which is equivalent to the cyclotron radius, is defined by

$$\lambda = \sqrt{\frac{\hbar}{eB}}, \tag{2}$$

where $e$ and $B$ are the electronic charge and the magnetic field, respectively. The magnetic length characterizes the scale of magnetic confinement. We can estimate $\lambda$ to be 26 nm at 1 T and 8 nm at 10 T. Since the semiconductor QDs have sizes of a few tens of nm, the magnetic length is comparable to the sizes of typical QDs in this magnetic field range. Therefore, it is interesting to investigate the competition between magnetic confinement and quantum confinement in QDs.

The exciton states show Zeeman splittings and diamagnetic shifts in a magnetic field. In many cases, these changes are much smaller than the inhomogeneous broadening of the PL band.[30–32] In addition, when the lateral quantization and the Coulomb attraction are increased by decreasing the QD size, the magnetic confinement becomes less important, leading to a smaller diamagnetic shift. It is thus necessary to investigate PL from single QDs. The PL from single QDs in the magnetic field has been reported by several groups.[1,32–37] Bayer *et al.* have observed a systematic decrease in the PL peak energy shift with decreasing size in large QDs fabricated from deep etched quantum wells, and related it to the transition from 2D to 0D.[38] On the other hand, the diamagnetic coefficient has almost a constant value in very small QDs.[32] It will be interesting to study these quantities in the intermediate size regime using QDs of different sizes.

Here we present the optical response of the InP single QDs in external electric and magnetic fields. From the optical measurements we extract the quadratic Stark coefficients of excitons and biexcitons. Our results reveal the existence of permanent dipole moments in both exciton and biexciton states. Further, the size dependence of the diamagnetic coefficients is discussed.

## II. EXPERIMENTAL DETAILS

The samples used in this study were prepared by means of metal-organic vapor phase epitaxy (MOVPE), as described in detail in Ref. 39. Self-assembled InP QDs sandwiched between two insulating $Ga_{0.5}In_{0.5}P$ barriers of 180 nm thickness each were grown on a Si doped ($n^+$) GaAs (001) substrate. In order to apply a dc bias to the sample, an $n$-$i$-Schottky diode structure was fabricated by depositing a semi-transparent gold layer of 20 nm thickness onto the sample surface.

As the excitation light source of the optical measurements, the 488 nm line of a continuous wave Ar-ion laser was used. For the single dot spectroscopic study in an electric field, a confocal micro-photoluminescence ($\mu$-PL) system was adapted.[3] The samples were set on a cold-finger of a liquid He flow-type cryostat and cooled down to 4 K. The unfocused laser beam with a diameter of $\sim$5 mm was irradiated on the sample surface to achieve a uniform excitation intensity. The sample PL was collected using a microscope objective lens with a numerical aperture of 0.42. A pinhole was placed on the image plane of the microscope to select a single QD. The spatial resolution of this system is better than 2 $\mu$m.

In order to measure the $\mu$-PL spectra by a conventional macroscopic configuration using a superconducting split-coil magnet up to 10 T, the QDs were confined in small mesas.[32] Micro-patterns were drawn on the sample surface by means of photolithography. Most part of the sample surface was chemically etched by $HCl:H_2O=2:1$ at 30 °C leaving behind small portions of size about $3\times3\,\mu m^2$. The spatial separation between the mesas is 100 $\mu$m. One of the mesas was selected by setting a pinhole of diameter 100 $\mu$m on the sample.

In both measurements in the electric field and the magnetic field, the PL signal was analyzed using a 50 cm single monochromator, and then detected by a charge coupled device camera cooled by liquid nitrogen. The spectral resolution of the detection system was better than 300 $\mu$eV.

## III. RESULTS AND DISCUSSION

### A. $\mu$-PL spectra from a single QD

Figure 1 shows the excitation power dependence of the $\mu$-PL spectra of a single InP QD measured without applying an external field. Under very weak excitation of less than $P=1$ mW/cm$^2$, a single sharp PL line denoted by X was observed at $\sim$1.671 eV. When the excitation power was slightly increased, a new line XX indicated by the arrow was observed at the lower energy side of X. The inset in Fig. 1 plots the $\mu$-PL intensities of the PL lines X and XX by closed and open circles, respectively.

It is instructive to analyze these results using a simple rate-equation model. The probability of the formation of an $N$-exciton state in a QD can be written as[3]

$$f_N = \frac{\alpha^N}{N!}e^{-\alpha}, \tag{3}$$

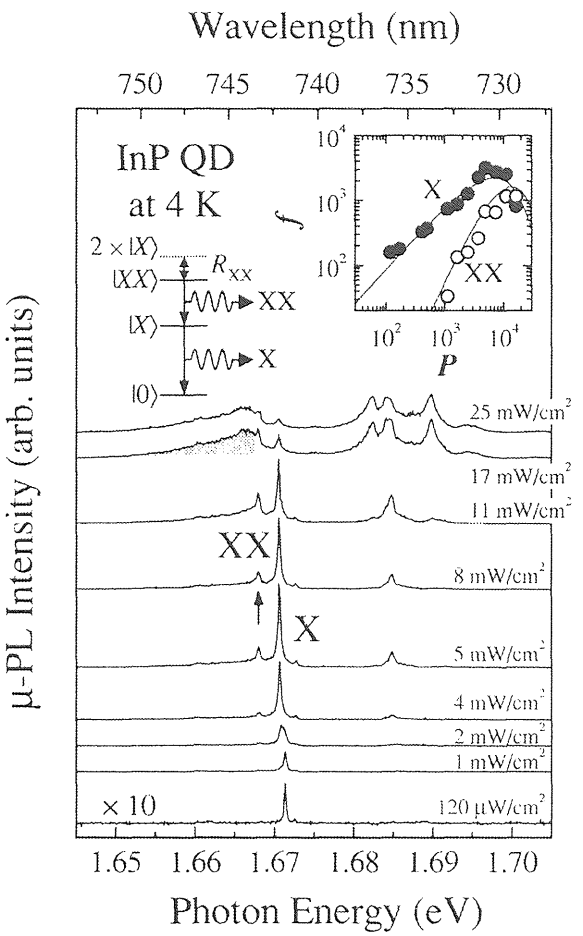


FIG. 1. Excitation power dependence of the $\mu$-PL spectra from a single InP QD without an external field. The PL peaks denoted by X and XX come from confined excitons and biexcitons, respectively. The PL from more than three excitons is observed around 1.685 eV and below the biexciton peak (shaded area). Inset: the PL intensities $f$ of X and XX lines as a function of the excitation power density $P$ in $\mu$W/cm$^2$ units. The solid curves are fitted by Eq. (3).

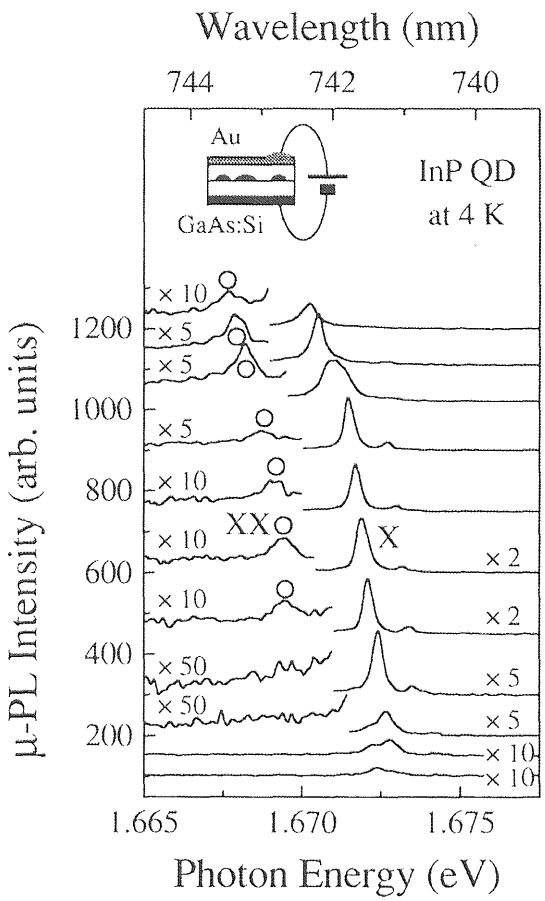


FIG. 2. Effect of an external electric field on the $\mu$-PL spectra of the QD shown in Fig. 1. The excitation power density is 8 mW/cm$^2$. The offset of each spectrum along the ordinate shows the bias applied to the sample. The applied field direction is schematically shown in the inset. With decreasing applied bias, the PL peaks from excitons (X) and biexcitons (XX) show blue shifts.

where $\alpha$ stands for the exciton generation rate that is proportional to the excitation power $P$. As shown by the solid curves, the experimentally observed excitation power dependence of the PL lines X and XX are both well reproduced using a single parameter $\alpha$. It is thus concluded that the PL lines X and XX arise from the radiative decay of single excitons ($N=1$) and biexcitons ($N=2$) in their ground states, respectively, i.e., X line comes from the transition of the confined exciton $|X\rangle$ to the ground state $|0\rangle$, while XX line reflects the transition from the biexciton state $|XX\rangle$ to the exciton state $|X\rangle$ (see the schematic drawn in Fig. 1). Since the exchange interaction in III-V QDs is very small, the energy separation of the PL peaks X and XX indicates the biexciton binding energy $R_{XX}$. In the case of InP QDs, a typical value of the biexciton binding energy is about 3 meV,[3] which is a few times larger than that of bulk InP.[40] When the excitation power was more than $\sim$15 mW/cm$^2$, the PL intensity of the lower-energy side shoulder of XX became strong (shaded area in Fig. 1). We consider that this shoulder originates from many exciton states, i.e., the exciton complexes composed from more than three electron-hole pairs. The PL from the confined excitons in the excited states was observed at $\sim$1.685 eV, i.e., the energy separation between the ground and first excited states is about 14 meV. First, the effect of an external electric field on the exciton and biexciton states was studied using this QD.

### B. Quantum confined Stark effect

Figure 2 shows a series of the $\mu$-PL spectra of the InP QD measured by systematically changing an external electric field. In this figure, the offset of each spectrum along the vertical direction indicates the applied electric field in mV units. The field was taken as positive when the field lines point from the Au contact on the surface to the GaAs substrate (see the schematic shown in Fig. 2). The excitation power was kept at 8 mW/cm$^2$ throughout the experiments. The PL peak from the biexciton XX is clearly observed as denoted by the open circles, in addition to the main PL line X from the exciton.

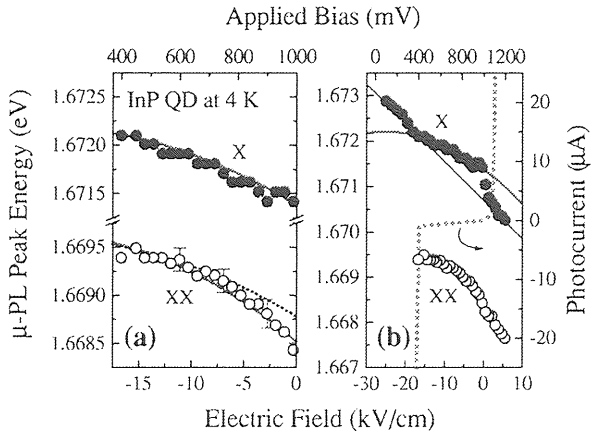


FIG. 3. PL peak energies of excitons (X, closed circles) and biexcitons (XX, open circles) as a function of applied electric field. The thick solid curves are fitted by Eq. (1). The quadratic Stark coefficient of the biexciton has a 40% larger value than that of the exciton. When the same value was assumed, a good fit was *not* obtained as shown by the thin dotted line in Fig. 3(a). The thick dotted curve in Fig. 3(b) is the photocurrent measured under the Ar laser irradiation of 8 mW/cm$^2$. When the photocurrent is small, the peak energy shows a quadratic shift with respect to the electric field, while it shows a linear shift (thin solid line) when the photocurrent is large. The magnification of Fig. 3(b) is shown in Fig. 3(a), where the photocurrent is very small.

The PL spectrum measured under the open circuit situation was reproduced when the applied bias was about 1000 mV.[41] The distinct blue shifts of the $\mu$-PL lines from the exciton and biexciton were observed with the decrease of the applied bias. Note that when the applied bias is less than 1000 mV, the electric field through the $Ga_{0.5}In_{0.5}P$ and InP layers is negative, i.e., the field lines point from the substrate to the surface. Further, the PL intensities of the excitons and biexcitons became weak as the applied bias was decreased.

Figure 3 shows the PL peak energies from the exciton X and biexciton XX shown in Fig. 2 as a function of the electric field by closed and open circles, respectively. Figure 3(b) shows the PL peak energies when the field was changed over a range wider than that in Fig. 3(a). The photocurrent $I$ measured under the Ar laser irradiation is also plotted by the thick dotted curve in Fig. 3(b). Since the photocurrent is zero when the applied bias is $\sim$1000 mV, the valence and conduction bands are flat at this point, which is consistent with the result mentioned above. The photocurrent is very small between $-17$ and 0 kV/cm ($|I|<1\,\mu$A), while the photocurrent abruptly increases outside of this region. When the photocurrent is large, the influence of the inflow of the carriers into the QDs from the electrode and the substrate has to be taken into consideration, which causes the increase of the sample temperature (Ohmic heating) and the formation of charged excitons as briefly discussed below. We therefore discuss the energy shift of the PL peaks for electric fields between $-17$ and 0 kV/cm as the first step in our analysis.

Figure 3(a) shows the magnification of Fig. 3(b). As shown by the solid lines, the transition energies $E(F)$ of the exciton X and the biexciton XX are well fitted by Eq. (1). It was found that the linear coefficient $p$ has a nonzero value, which implies the existence of a nonzero permanent dipole moment in these QDs. In other words, the centers of gravity of the confined electron and hole wave functions are spatially separated along the growth direction. We find that $p$ is positive, i.e., the holes are located near the base of the QD, while the electrons are distributed above the holes.

We note that the direction of the electron-hole alignment is consistent with the recent theoretical calculations on InP QDs.[42] The calculations show that holes tend to be localized closer to the base of the QD for two reasons: (*i*) the presence of the wetting layer at the base that pulls the hole towards it and (*ii*) the strain profile in the barrier region above the QD that shifts the valence band edge to lower energies, pushing the hole into the base of the QD. On the other hand, the electron density is more spread out in the QD because of the lighter mass of the electrons and the dilational strain in the barrier lowering the conduction band edge in the barrier material. Similar results have also been reported for InAs QDs without indium segregation.[15,19] The existence of a nonzero permanent dipole moment has been experimentally observed in exciton states of several kinds of QDs as mentioned above. However, in most InAs QD samples, the sign of the dipole moment is opposite from what we observe. It is believed that the reversal of the electron-hole spatial distribution in InAs/GaAs QDs is due to nonuniform indium distribution.

From the fittings, we evaluated the permanent dipole moment $p$ for the excitons to be $p_X=1.0\times10^{-28}$ Cm and that for the biexcitons to be $p_{XX}=1.4\times10^{-28}$ Cm. We note that in Eq. (1), $p$ indicates the $z$ component (the growth direction) of the dipole moment

$$p=\sum q_i z_i, \tag{4}$$

where $q_h=+e$ for a hole and $q_e=-e$ for an electron. We can therefore estimate the electron-hole spatial separation $d=\langle|z_e-z_h|\rangle$ along the $z$ axis to be $d_X=7$ Å for the excitons.[43] Noting that the observed PL energy for the biexciton is the difference between the biexciton and exciton states (see the schematic drawn in Fig. 1), the dipole moment of the biexciton state is $p_{XX}+p_X=2.4\times10^{-28}$ Cm. Again, from Eq. (4), this corresponds to an average electron-hole separation of $d_{XX}=8$ Å for the biexcitons. To the best of our knowledge, this is the first report on a nonzero permanent dipole moment in a biexciton state.

Regarding the quadratic Stark coefficient $\beta$ for the biexcitons, the fit was *not* good when the same value as that for the excitons is assumed [dotted curve in Fig. 3(a)]. The best fit was obtained when a 40% larger value than that for the excitons was employed [solid curve in Fig. 3(a)]. We evaluated the Stark coefficient for the excitons to be $\beta_X=2.1\times10^{-31}$ Fcm$^2$ and that for the biexcitons to be $\beta_X=2.9\times10^{-31}$ Fcm$^2$.[44]

When the electric field is either $F<-17$ kV/cm or $F>0$ kV/cm, a considerable amount of photocurrent flows in the sample as shown by the dotted curve in Fig. 3(b). The PL peak X from the confined exciton no longer shows a quadratic energy shift, but shifts linearly with the field. The en-

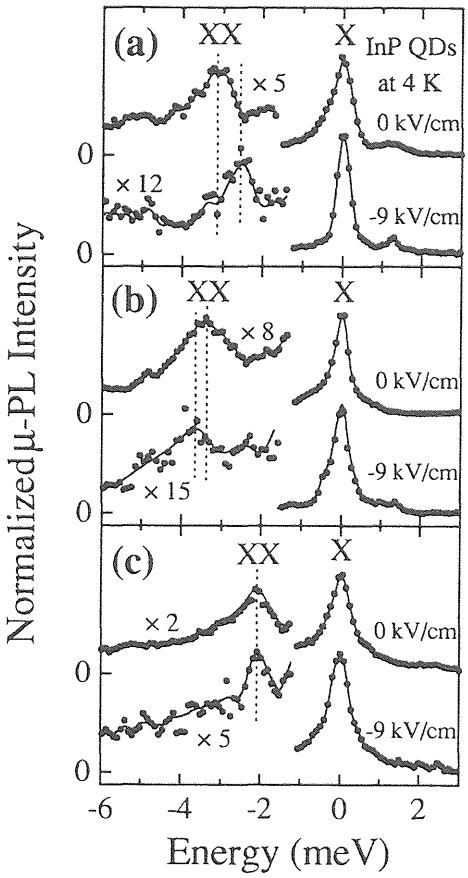


FIG. 4. $\mu$-PL spectra of three QDs with and without an applied electric field. The origins of the abscissas are taken at the PL peaks of the confined exciton lines X. The lower-energy-side peaks of the exciton lines come from the biexcitons XX. The energy separations between the exciton and biexciton lines differ from dot to dot in an electric field, reflecting the variation of the quadratic Stark coefficients. The PL peak energies of the excitons at zero electric field are (a) 1.671 eV, (b) 1.715 eV, and (c) 1.652 eV, respectively.

ergy shift becomes large on both sides of the small photocurrent region. The larger energy shift is not due to the increase of the sample temperature because an increase in the sample temperature results in a redshift of PL peak.[45] However, the PL peak shifts to the higher energy side when the field is $F < -17$ kV/cm. Instead, this large energy shift can be explained as follows: when the photocurrent is large, the probability of the trapping of the excess carriers into the QDs is enhanced, where the carriers are supplied from the electrode and the substrate. The excess carriers form coupled states with the excitons, resulting in new excitations, namely charged excitons. Unlike the excitons which are electrically neutral, the charged excitons are more sensitive to the electric field. Since the probability of the formation of the charged excitons is high when the electric field is either below $-17$ kV/cm or above 0 kV/cm and since the charged excitons are considered to be sensitive to the electric field, the energy shift becomes larger than that in the small photocurrent region.

We then investigated the optical responses of the exciton and biexciton states using several QDs in the same sample. Figure 4 shows the $\mu$-PL spectra when the field is $F = 0$ kV/cm (flat band condition) and $F = -9$ kV/cm. The sharp main PL peak of each spectrum shown in Fig. 4 comes from excitons and the small peak observed at the lower energy side arises from biexcitons. The abscissa shows the energy shift from the confined exciton state. The PL peak energies of the excitons are (a) 1.671 eV, (b) 1.715 eV, and (c) 1.652 eV. The spectra shown in Fig. 4(a) were measured using the QD shown in Figs. 1–3. As mentioned above, the permanent dipole moment has a nonzero value and the quadratic Stark coefficient of the biexcitons has a larger value than that of the exciton in this QD. Eventually, the energy separation between the PL peaks from the excitons and biexcitons becomes small when a negative field is applied.

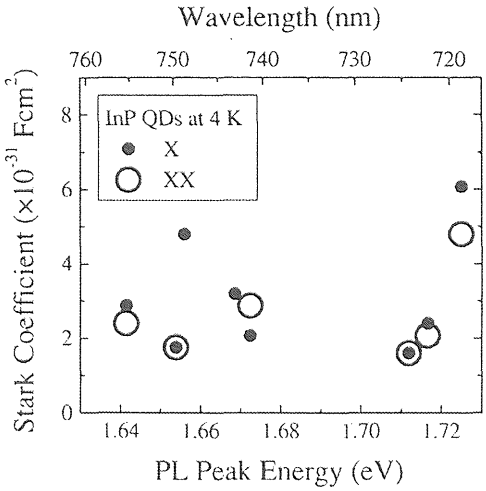


FIG. 5. Plots of quadratic Stark coefficients of excitons (X, closed circles) and biexcitons (XX, open circles) as a function of the PL peak energies at zero electric field.

The magnitude of the quadratic Stark coefficients of the excitons and biexcitons differs from dot to dot. For example, the energy separation of the PL peaks from the excitons and biexcitons becomes large in some QDs when the negative bias is applied as shown in Fig. 4(b), while the separation is almost constant in other QDs as shown in Fig. 4(c).

Figure 5 plots the quadratic Stark coefficients of the excitons and biexcitons examined in several QDs. We found that in most of the QDs $\beta$ ranges between $1 \times 10^{-31}$ and $6 \times 10^{-31}$ Fcm$^2$. The PL peak energy reflects the size of QDs. We note that $\beta$ measures the polarizability of the QDs apart from a constant. In very thin quantum wells, Barker and O'Reilly have theoretically concluded that the polarizability increases with the width.[19] A similar dependence may be expected in QDs. However, a systematic change with respect to the PL peak energy (i.e., the QD size) was not observed in InP QDs within the resolution of our experimental setup. The fluctuation of the values is probably due to a slight difference in shape of each QD.[46]

### C. Magnetic and quantum confinement

Figure 6 shows the comparison of the excitation power dependence of the PL spectra obtained by the (a) macro-

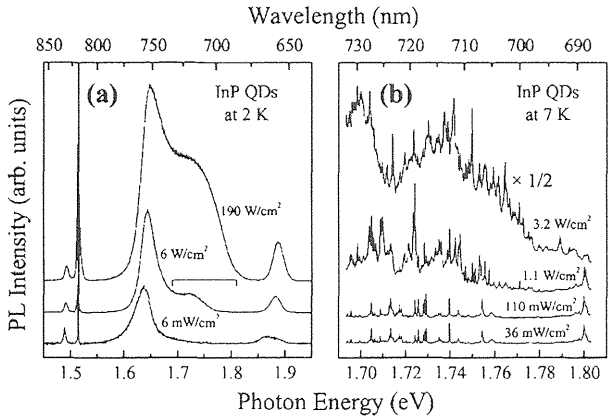


FIG. 6. Comparison of PL spectra of (a) as grown and (b) mesa samples under various excitation powers. The square bracket in Fig. 6(a) shows the energy region shown in Fig. 6(b). The state filling effect was significant when the excitation power was above ~1 W/cm$^2$.

scopic and (b) microscopic methods. For the measurements, (a) the as-grown sample and (b) the QDs in a small mesa were used. The bracket of Fig. 6(a) indicates the energy region shown in Fig. 6(b). In the macroscopic observations, the state filling effects, i.e., a broadening and a high energy shift of the PL band, were not observed when the excitation power density was lower than about 1 W/cm$^2$. We note that the excitation threshold of the state filling in the sample shown in Fig. 6 is higher than that in Fig. 1, because the areal density of the QDs in Fig. 6 is high. In the $\mu$-PL spectra (b), the number and energies of the PL peaks are the same between the excitation powers of 110 and 36 mW/cm$^2$. This indicates that most of the PL peaks come from the confined excitons in the ground state when the excitation power is below ~100 mW/cm$^2$. The magnetic field effects on the $\mu$-PL spectra were measured under weak excitation of 100 mW/cm$^2$ as a beginning of the magnetic PL study.

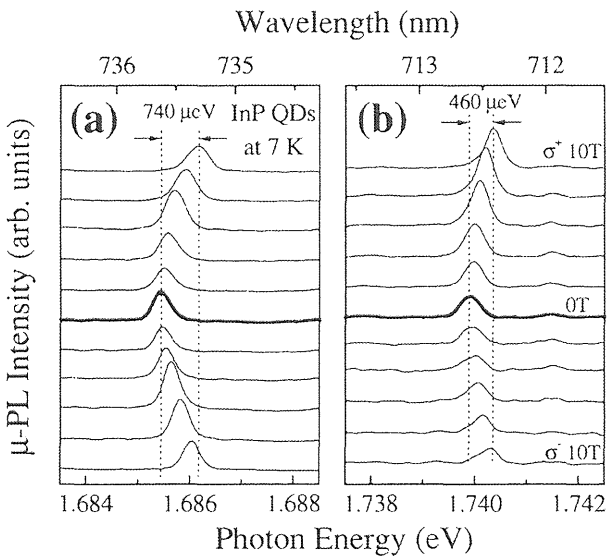


FIG. 7. Two examples of the PL energy shifts in a magnetic field. Measurements were performed in the Faraday configuration ($\boldsymbol{k}\|z\|\boldsymbol{B}$). The shifts in the magnetic field measured for the $\sigma^+$ polarization are larger than those for the $\sigma^-$ polarization. The PL peaks which appear at the lower energy side at zero field show a large energy shift in the magnetic field.

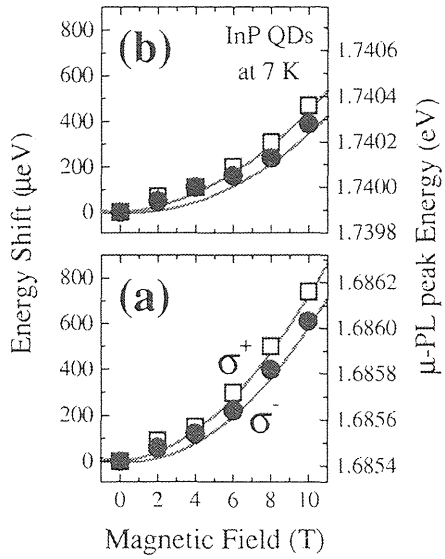


FIG. 8. Plots of the PL peaks shown in Figs. 7(a) and 7(b). The peaks denoted by the open squares were observed for $\sigma^+$ polarization, while those denoted by the closed circles correspond to $\sigma^-$ polarization. Note that the maximum values of the ordinates are the same, 900 $\mu$eV in both Figs. 8(a) and 8(b). The PL peak energies are well fitted by Eq. (5) as shown by the solid curves.

Figure 7 shows two sets of the $\mu$-PL spectra from two individual QDs measured under various magnetic field strengths. The measurement was performed in the Faraday configuration ($\boldsymbol{k}\|z\|\boldsymbol{B}$): the magnetic field $\boldsymbol{B}$ was applied normal to the sample surface, and the directions $\boldsymbol{k}$ of the photo-excitation and PL detection are parallel to the magnetic field. Here $z$ indicates the growth direction. The thick curves are the $\mu$-PL spectra at 0 T. The upper five curves shows data for $\sigma^+$ circular polarization, while the lower five curves correspond to $\sigma^-$ polarization. Since the photo-excitation was made above the band gap energy of the $Ga_{0.5}In_{0.5}P$ matrix, the polarization of the excitation laser beam caused no significant change of the $\mu$-PL spectra. The PL peaks show blueshifts on increasing the magnetic field. In all measured PL peaks, the energy shift was greater for $\sigma^+$ than for $\sigma^-$.

The PL peak energies in Figs. 7(a) and 7(b) are plotted as a function of the applied magnetic field in Figs. 8(a) and 8(b), respectively. The peaks denoted by open squares were observed for $\sigma^+$ polarization, while those denoted by closed circles were for $\sigma^-$ polarization. We note that the maximum values of the ordinates are the same, 900 $\mu$eV in both Figs. 8(a) and 8(b). The PL peaks observed at the lower energy side show a larger energy shift with the field than those observed at the higher energy side. The PL peak energies are well fitted by

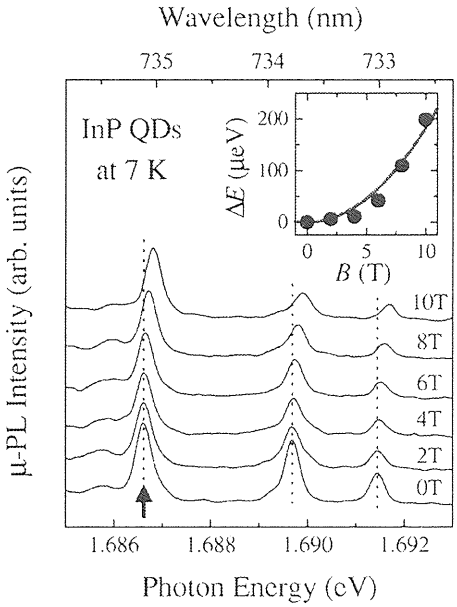


FIG. 9. $\mu$-PL spectra measured in the Voigt configuration ($k \| z \perp B$). The energy shift $\Delta E$ of the PL peak indicated by the arrow is shown in the inset by the closed circles as a function of the magnetic field $B$. The PL peak shows a quadratic shift as shown by the solid curve.

$$E(B) = E_0 \pm \tfrac{1}{2}\mu_B g^* B + \gamma_2 B^2, \tag{5}$$

where $E_0$ is the zero-field transition energy, $\mu_B$ is the Bohr magneton, and $g^*$ is the effective $g$-value of the confined exciton.[47] The coefficient $\gamma_2$ of the quadratic term in Eq. (5) is called as the diamagnetic coefficient, which is the main interest for the following part of the article.

The magnetic field effect on the $\mu$-PL spectra was also studied in the Voigt configuration ($k \| z \perp B$) as shown in Fig. 9. In this measurement, a polarizer was not set in the optical path because of the weak signal.[48] All PL peaks shift to the higher energy side with the increase of the magnetic field. The energy shift of the PL peak indicated by the arrow (1.6866 eV at 0 T) is shown in the inset by the closed circles. Again, the PL peak energies can be well fitted using a quadratic function as shown by the solid curve.

The diamagnetic coefficients evaluated from the experimental results shown in Figs. 7–9 are summarized in Fig. 10. In the experiments, several PL peaks were examined in the Faraday (closed triangles and circles) and Voigt (open lozenges) configurations. The data denoted by the closed triangles (Faraday configuration) and open lozenges (Voigt configuration) was measured under weak excitation of $\sim 100$ mW/cm$^2$, while those denoted by the closed circles (Faraday configuration) were measured under strong excitation of $\sim 300$ mW/cm$^2$. Some PL peaks appear when the excitation is slightly increased. The PL peaks denoted by the closed circles were not observed under weak excitation. Therefore, these PL peaks observed under strong excitation may come from the excited states or the ground state with low PL efficiency. A large difference in the diamagnetic coefficients was, however, not observed between the PL peaks

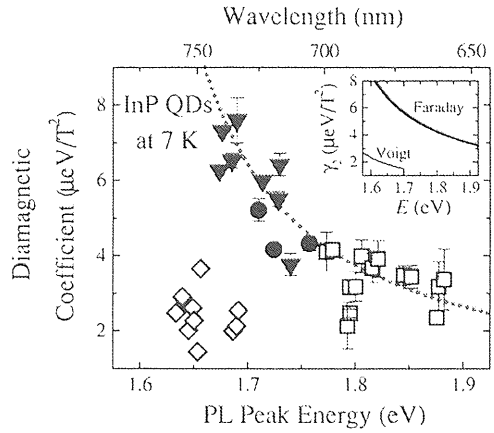


FIG. 10. Plots of the diamagnetic coefficients $\gamma_2$ measured in the Faraday (closed triangles and circles) and Voigt (open lozenges) configurations as a function of the PL peak energy $E$ at 0 T. The data denoted by the closed triangles (Faraday configuration) and open lozenges (Voigt configuration) were measured under weak excitation of $\sim 100$ mW/cm$^2$, while those denoted by the closed circles (Faraday configuration) were measured under strong excitation of $\sim 300$ mW/cm$^2$. The open squares were measured in the Faraday configuration using QDs grown by means of GS-MBE (from Ref. 32). The dotted curve is a guide to the eyes. Inset: Plots of the model calculation using Eq. (8). The experimental results observed in the Faraday (thick curve) and Voigt (thin curve) configurations are qualitatively well reproduced.

that appear under strong and weak excitations. The open squares were measured using QDs grown by means of gas-source molecular beam epitaxy (GS-MBE, for details, see Ref. 32). A systematic decrease of the diamagnetic coefficient was found with the increase of the detection energy when measured in the Faraday configuration. In other words, the diamagnetic coefficient decreases with decreasing QD size. The diamagnetic coefficient asymptotically approaches a constant value of $\sim 3$ $\mu$eV/T$^2$. This is almost the same as the value measured in the Voigt configuration. When the size of QDs becomes very small, the diamagnetic coefficient should finally approach the value of bulk $Ga_{0.5}In_{0.5}P$ due to the leakage of the exciton wave function.[49] However, the minimum value of the diamagnetic coefficient obtained in this study is $\sim 3$ $\mu$eV/T$^2$, which is much smaller than the diamagnetic coefficient in bulk $Ga_{0.5}In_{0.5}P$.[50] We thus consider that the small value is due to the strong confinement in small InP QDs.

In the Faraday configuration ($B \| z$), the magnetic fields confines the carriers in the $x$-$y$ plane, while they are confined in the $y$-$z$ plane in the Voigt configuration ($B \| x$). Therefore, the diamagnetic coefficient measured in the Faraday configuration reflects the wave function along the lateral direction ($x$ and $y$), while that measured in the Voigt configuration reflects the wave function along the growth direction $z$. Due to the flat shape of the QD, the quantum confinement along the $z$ direction is stronger than that along the $x$-$y$ direction, and thus the exciton wave function is already shrunk significantly along the $z$ direction even at 0 T. In this case, an additional confinement by the magnetic field is less effective. This ex-

plains why the diamagnetic coefficient is smaller when observed in the Voigt configuration.[51]

The diamagnetic coefficient can be written as

$$\gamma_2 = \frac{e^2\langle\rho^2\rangle}{8\mu}, \tag{6}$$

where $e$, $\sqrt{\langle\rho^2\rangle}$, and $\mu$ are the electronic charge, the effective exciton size, and the reduced mass, respectively. We note that the wave functions of the electrons and holes are assumed to have the same size. The effective exciton size due to the magnetic confinement can be estimated using this relationship.

The size dependence of the diamagnetic coefficient in the Faraday configuration is qualitatively understood as follows. In a strong confinement regime, the confined exciton energy $E$ and the QD radius $R$ have the relation

$$E = E_B + \frac{\hbar^2\pi^2}{2\mu R^2}, \tag{7}$$

where $E_B$ is the band gap energy of the bulk InP ($E_B = 1.42$ eV at liquid helium temperature[52]) and the second term is the confinement energy. In Eq. (7), the shape of the QD is assumed to be spherical for simplicity. The effective exciton radius is considered to be comparable with the QD size. Thus, we finally obtain the relation

$$\gamma_2 \simeq \frac{a}{E - E_B}, \tag{8}$$

with $a = (\hbar e\pi/4\mu)^2$. In the case of InP, $a = 1.7 \times 10^{-6}$ eV$^2$/T$^2$ is obtained when we use $m_{hh} = 0.56m_0$ ($m_0$ is the free electron mass) for the heavy hole and $m_e = 0.08m_0$ for the conduction electron to estimate the reduced exciton mass,[52]

$$\mu = \left(\frac{1}{m_{hh}} + \frac{1}{m_e}\right)^{-1}. \tag{9}$$

Despite the simplicity of this model, it explains our experimental results in the Faraday configuration very well, as shown by the thick curve in the inset in Fig. 10. The diamagnetic coefficient $\gamma_2$ gradually decreases as the observation energy $E$ increases, which is consistent with the experiment. Further, since the height of the QDs is about a quarter of the base diameter,[8,39] the diamagnetic coefficient when measured in the Voigt configuration is expected to be four times smaller than that in the Faraday configuration. Based on this model, the calculated result of the diamagnetic coefficient in the Voigt configuration is also shown by the thin curve in the inset in Fig. 10. Again, the agreement between the experiment and the model is fairly good. Therefore, we conclude that the gradual reduction of the diamagnetic coefficient with the QD size reflects the decrease of the effective exciton size due to the strong quantum confinement in the QDs.

## IV. SUMMARY

We have studied the optical properties of the InP QDs in the presence of external electric and magnetic fields. The quantum confined Stark shifts of both the exciton and biexciton states were clearly observed. The quadratic Stark coefficient was evaluated to be of the order of $10^{-31}$ Fcm$^2$, and it varies slightly from dot to dot. It was found that the energy separation of the PL peaks between the exciton and biexciton states changes with the applied bias, reflecting a small difference of the Stark coefficient of these states. We find that the exciton and biexciton states have a nonzero permanent dipole moment. The average spatial separation of the electron and hole wave functions along the growth axis was evaluated to be about 7 Å for excitons and 8 Å for biexcitons. We also found that the holes are located closer to the base of the QDs compared to the electrons. The experimental results are consistent with reported theoretical calculations.

Zeeman splitting and diamagnetic shift of the exciton state were also clearly observed by the magnetic PL measurements of single InP QDs. We found that there is a systematic decrease of the diamagnetic coefficient with decreasing size of the QDs. The diamagnetic coefficient measured in the Voigt configuration was small compared to that measured in the Faraday configuration. We concluded that the gradual reduction of the diamagnetic coefficient with the QD size reflects the decrease of the effective exciton size due to the quantum confinement.

## ACKNOWLEDGMENTS

The authors thank Professor H. E. Ruda of the University of Toronto for his encouragement to summarize this work. Close collaboration with Dr. J.-S. Lee is also acknowledged.

*Corresponding author; Email: mitsuru.sugisaki@utoronto.ca
Present address: Department of Physics, Graduate School of Science, Osaka City University, 3-3-138 Sugimoto, Sumiyoshi-ku, Osaka 558-8585, Japan.

[1] A. Kuther, M. Bayer, A. Forchel, A. Gorbunov, V.B. Timofeev, F. Schäfer, and J.P. Reithmajer, Phys. Rev. B **58**, 7508 (1998).
[2] F. Findeis, A. Zrenner, G. Böhm, and G. Abstreiter, Phys. Rev. B **61**, R10579 (2000).
[3] M. Sugisaki, H.-W. Ren, S.V. Nair, K. Nishi, and Y. Masumoto, Solid State Commun. **117**, 435 (2001).
[4] A. Hartmann, Y. Ducommun, E. Kapon, U. Hohenester, and E. Molinari, Phys. Rev. Lett. **84**, 5648 (2000).
[5] F. Findeis, M. Baier, A. Zrenner, M. Bichler, G. Abstreiter, U. Hohenester, and E. Molinari, Phys. Rev. B **63**, 121309(R) (2001); M. Baier, F. Findeis, A. Zrenner, M. Bichler, and G. Abstreiter, *ibid.* **64**, 195326 (2001).
[6] D. Gammon, E.S. Snow, B.V. Shanabrook, D.S. Katzer, and D. Park, Science **273**, 87 (1996).
[7] T. Kümmell, R. Weigand, G. Bacher, A. Forchel, K. Leonardi, D. Hommel, and H. Selke, Appl. Phys. Lett. **73**, 3105 (1998).
[8] M. Sugisaki, H.-W. Ren, S.V. Nair, K. Nishi, S. Sugou, T. Okuno, and Y. Masumoto, Phys. Rev. B **59**, R5300 (1999); M. Sugisaki, H.-W. Ren, K. Nishi, and Y. Masumoto, Solid State Commun. **117**, 679 (2001).

[9] As a review article, S.A. Empedocles, R. Neuhauser, K. Shimizu, and M.G. Bawendi, Adv. Mater. **11**, 1243 (1999).
[10] M. Sugisaki, H.-W. Ren, K. Nishi, and Y. Masumoto, Phys. Rev. Lett. **86**, 4883 (2001), and references therein.
[11] P. Michler, A. Kiraz, C. Becher, W.V. Schoenfeld, P.M. Petroff, L. Zhang, E. Hu, and A. Imamoğlu, Science **290**, 2282 (2000).
[12] C. Santori, M. Pelton, G. Solomon, Y. Dale, and Y. Yamamoto, Phys. Rev. Lett. **86**, 1502 (2001).
[13] V. Zwiller, H. Blom, P. Jonsson, T. Tsegaye, E. Goobar, M.-E. Pistol, L. Samuelson, and G. Björk, Appl. Phys. Lett. **78**, 2476 (2001).
[14] H. Gotoh and H. Ando, J. Appl. Phys. **82**, 1667 (1997).
[15] K. Chang and J.-B. Xia, Solid State Commun. **104**, 351 (1997).
[16] W. Heller, U. Bockelmann, and G. Abstreiter, Phys. Rev. B **57**, 6270 (1998).
[17] S. Raymond, J.P. Raynolds, J.L. Merz, S. Fafard, Y. Feng, and S. Charbonneau, Phys. Rev. B **58**, R13415 (1998).
[18] P.W. Fry, I.E. Itskevich, D.J. Mowbray, M.S. Skolnick, J.J. Finley, J.A. Barker, E.P. O'Reilly, L.R. Wilson, I.A. Larkin, P.A. Maksym, M. Hopkinson, M. Al-Khafaji, J.P.R. David, A.G. Cullis, G. Hill, and J.C. Clark, Phys. Rev. Lett. **84**, 733 (2000); P.W. Fry, I.E. Itskevich, S.R. Parnell, J.J. Finley, L.R. Wilson, K.L. Schumacher, D.J. Mowbray, M.S. Skolnick, M. Al-Khafaji, A.G. Cullis, M. Hopkinson, J.C. Clark, and G. Hill, Phys. Rev. B **62**, 16784 (2000).
[19] J.A. Barker and E.P. O'Reilly, Phys. Rev. B **61**, 13840 (2000).
[20] H. Gotoh, H. Kamada, H. Ando, and J. Temmyo Appl. Phys. Lett. **76**, 867 (2000).
[21] I.E. Itskevich, S.I. Rybchenko, I.I. Tarkakovskii, S.T. Stoddart, A. levin, P.C. Main, L. Eaves, M. Henini, and S. Parnell, Appl. Phys. Lett. **76**, 3932 (2000).
[22] W.-H. Chang, T.M. Hsu, C.C. Huang, N.T. Yeh, and J.-I. Chyi, Phys. Status Solidi B **224**, 89 (2001); T.M. Hsu, W.-H. Chang, C.C. Huang, N.T. Yeh, and J.-I. Chyi, Appl. Phys. Lett. **78**, 1760 (2001).
[23] A. Patanè, A. Levin, A. Polimeni, F. Schindler, P.C. Main, L. Eaves, and M. Henini, Appl. Phys. Lett. **77**, 2979 (2000).
[24] D. Hessman, J. Persson, M.-E. Pistol, C. Pryor, and L. Samuelson, Phys. Rev. B **64**, 233308 (2001).
[25] A. Thilagam, Phys. Rev. B **56**, 4665 (1997).
[26] D.A.B. Miller, D.S. Chemla, T.C. Damen, A.C. Gossard, W. Wiegmann, T.H. Wood, and C.A. Burrus, Phys. Rev. Lett. **53**, 2173 (1984).
[27] I. Bar-Joseph, C. Klingshirn, D.A.B. Miller, D.S. Chemia, U. Koren, and B.I. Miller, Appl. Phys. Lett. **50**, 1010 (1987).
[28] X.B. Mei, W.G. Bi, C.W. Tu, L.J. Chou, and K.C. Hsieh, J. Vac. Sci. Technol. B **14**, 2327 (1996).
[29] H. Fu, Phys. Rev. B **65**, 045320 (2002).
[30] S. Nomura, L. Samuelson, M.-E. Pistol, K. Uchida, N. Miura, T. Sugano, and Y. Aoyagi, Appl. Phys. Lett. **71**, 2316 (1997); S. Nomura, L. Samuelson, C. Pryor, M.-E. Pistol, M. Stopa, K. Uchida, N. Miura, T. Sugano, and Y. Aoyagi, Phys. Rev. B **58**, 6744 (1998).
[31] B. Kowalski, S. Nomura, C. Pryor, Y. Aoyagi, N. Carlsson, M.-E. Pistol, P. Omling, L. Samuelson, and W. Seifert, Phys. Rev. B **58**, 2026 (1998).
[32] M. Sugisaki, H.-W. Ren, K. Nishi, S. Sugou, T. Okuno, and Y. Masumoto, Physica B **256-258**, 169 (1998).
[33] S.W. Brown, T.A. Kennedy, D. Gammon, and E.S. Snow, Phys. Rev. B **54**, R17339 (1996); D. Gammon, A.L. Efros, T.A. Kennedy, M. Rosen, D.S. Katzer, D. Park, S.W. Brown, V.L. Korenev, and I.A. Merkulov, Phys. Rev. Lett. **86**, 5176 (2001).
[34] Y. Toda, S. Shinomori, K. Suzuki, and Y. Arakawa, Appl. Phys. Lett. **73**, 517 (1998); Y. Toda, S. Shinomori, K. Suzuki, and Y. Arakawa, Phys. Rev. B **58**, R10147 (1998).
[35] M. Bayer, A. Kuther, F. Schäfer, J.P. Reithmaier, and A. Forchel, Phys. Rev. B **60**, R8481 (1999).
[36] M. Bayer, O. Stern, A. Kuther, and A. Forchel, Phys. Rev. B **61**, 7273 (2000).
[37] I.E. Itskevich, S.T. Stoddart, S.I. Rybchenko, I.I. Tarkakovskii, L. Eaves, P.C. Main, M. Henini, and S. Parnell, Phys. Status Solidi A **178**, 307 (2000).
[38] M. Bayer, S.N. Walck, T.L. Reinecke, and A. Forchel, Phys. Rev. B **57**, 6584 (1998).
[39] H.-W. Ren, M. Sugisaki, J.-S. Lee, S. Sugou, and Y. Masumoto, Jpn. J. Appl. Phys., Part 1 **38**, 507 (1999).
[40] S. Charbonneau, L.B. Allard, A.P. Roth, and R.T. Sudersena, Phys. Rev. B **47**, 13918 (1993).
[41] The height of the Schottky barrier is consistent with the former report: S.D. Kwon, O.K. Kwon, B.-D. Choe, H. Lim, and J.Y. Lee, J. Appl. Phys. **78**, 2482 (1995).
[42] S.V. Nair, J. Shumway, and A. Zunger, Proceedings of the APS March meeting (Seattle, 2001).
[43] It has been pointed out that the electron and hole are spatially separated in multi-stacked InP QDs; In this case, the center of the wave function of the hole exists outside of the QDs: M. Hayne, R. Provoost, M.K. Zundel, Y.M. Manz, K. Eberl, and V.V. Moshchalkov, Phys. Rev. B **62**, 10324 (2000); M. Hayne, M. Maes, V.V. Moshchalkov, Y.M. Manz, O.G. Schmidt, and K. Eberl, Appl. Phys. Lett. **79**, 45 (2001); Such a large separation was, however, not observed in the single-layered InP QDs used in this study. The separation is much smaller than the QD size.
[44] Besombes *et al.* have recently observed the Stark shift of the neutral and charged exciton states in CdTe QDs. They found that each state has different value of the Stark coefficient: L. Besombes, K. Kheng, L. Marsal, and H. Mariette, Phys. Rev. B **65**, 121314(R) (2002).
[45] M. Sugisaki, H.-W. Ren, S.V. Nair, J.-S. Lee, S. Sugou, T. Okuno, and Y. Masumoto, J. Lumin. **87-89**, 40 (2000).
[46] It should be mentioned that we have measured the Stark shift under both weak (less than 0.1 excitons/dot) and strong (about 1 exciton/dot) excitation conditions to examine the effect from excess carriers on both inside and outside of the QDs. However, a significant difference was not observed in the Stark coefficients.
[47] We have measured several samples and found that the Zeeman splitting $\Delta E_{\pm} = \mu_B g^* B$, which reflects the effective $g$ -value, is scattered over a wide range from 200 to 800 $\mu$eV at 10 T. A systematic change of the Zeeman splitting was not observed, which is the same as the case of the InAs QDs in the (Al) GaAs matrix.[34] More details of the Zeeman splitting will be discussed elsewhere.
[48] Bayer *et al.* has reported a fine splitting in the Voigt configuration in $In_xGa_{1-x}As$ QDs, where the splitting is much smaller than that observed in the Faraday configuration.[36] In our case, however, such a splitting was not observed probably because of the small $g$-value in InP QDs.

[49] K.L. Janssens, F.M. Peeters, and V.A. Schweigert, Phys. Rev. B **63**, 205311 (2001).

[50] The diamagnetic coefficient of bulk $Ga_{0.5}In_{0.5}P$ strongly depends on the direction of the magnetic field due to the formation of the $Cu-Pt_B$ ordered domains. The value also depends on the degree of ordering. When the field is applied along the (100) direction, the diamagnetic coefficient is $\sim 10\ \mu eV/T^2$, which is much larger than the value in the InP QDs studied here: P. Ernst, Y. Zhang, F.A.J.M. Driessen, A. Mascarenhas, E.D. Jones, C. Geng, F. Scholz, and H. Schweizer, J. Appl. Phys. **81**, 2814 (1997); U. Kops, P.G. Blome, M. Wenderoth, R.G. Ulbrich, C. Geng, and F. Scholz, Phys. Rev. B **61**, 1992 (2000).

[51] We note that the small energy shift in the Voigt configuration has also been reported in GaAs/AlAs quasi-0D excitons and macroscopically in InAlAs/AlGaAs S-K QDs: A. Zrenner, L.V. Butov, M. Hagn, G. Abstreiter, B. Böhm, and G. Weimann, Phys. Rev. Lett. **72**, 3382 (1994); P.D. Wang, J.L. Merz, S. Fafard, R. Leon, D. Leonard, G. Medeiros-Ribeiro, M. Oestreich, P.M. Petroff, K. Uchida, N. Miura, H. Akiyama, and H. Sakaki, Phys. Rev. B **53**, 16458 (1996).

[52] *Landolt-Börnstein, Numerical Data and Functional Relationships in Science and Technology,* edited by O. Madelung, M. Schluz, and H. Weiss, New Series, Vol. 17a (Springer-Verlag, Berlin, 1982).

PHYSICAL REVIEW B 66, 235312 (2002)

# Fine structure and spin quantum beats in InP quantum dots in a magnetic field

I. A. Yugova* and I. Ya. Gerlovin†
*Institute of Physics, St.-Petersburg State University, St.-Petersburg, 198504, Russia*

V. G. Davydov, I. V. Ignatiev,‡ I. E. Kozin,§ H. W. Ren,¶ M. Sugisaki,** S. Sugou,†† and Y. Masumoto‡‡
*Single Quantum Dot Project, ERATO, JST, Japan*

(Received 13 March 2002; revised manuscript received 27 June 2002; published 16 December 2002)

The paper reports on quantum beats observed in the photoluminescence kinetics of a single layer of the InP self-assembled quantum dots in a magnetic field. It is found that the beats arise only after removal of excess charges from the quantum dots by an external electrical bias. The quantum beats are shown to be related to the interference of the excitonic fine-structure states split by the magnetic-field. The dependences of the beat characteristics on the magnetic-field strength and orientation are studied. Theoretical analysis based on a model spin Hamiltonian has allowed us to describe adequately the shape of the oscillating component of the signal. We have determined the values of the electron $g$-factor components and estimated the spread and the mean value of the hole $g$ factor, as well as of the electron-hole exchange splitting parameters.

DOI: 10.1103/PhysRevB.66.235312 PACS number(s): 73.21.−b, 71.70.Ej, 78.55.Cr, 78.67.Hc

## I. INTRODUCTION

Spin dynamics of carriers and excitons in the low-dimensional semiconductor heterostructures attracts nowadays a particular interest in view of potential feasibility of the logic and computer memory elements based on the effects of optical spin orientation.[1–3] The most promising, in this respect, are the structures with quantum dots (QD's) whose spin states are characterized by a high stability.[4] The main drawback of such structures is a large inhomogeneous broadening of their energy states, resulting from a strong spread of the QD parameters. The inhomogeneous broadening hampers getting information about spin-related structure of the excitonic states (fine structure) and makes impossible analysis of the spin dynamics. The inhomogeneous broadening can be eliminated using the single QD spectroscopy technique.[5–7] This technique, however, provides information about individual QD's rather than about the ensemble as a whole.

An efficient way to determine the ensemble-averaged fine-structure parameters is considered to be detection of the quantum beats (QB's) associated with interference between the spin states. This method is attractive due to its ability to detect small splittings (fractions of meV) hidden within inhomogeneously broadened excitonic transitions. The quantum beats technique is widely used for studying the fine structure and Zeeman splitting in quantum wells and superlattices.[8–13]

One could expect that the QB technique may be also successfully applied to studies of QD's. Indeed, there are several publications where the QB's in QD's were observed. But these observations were made only under specific experimental conditions. In particular, in the absence of the magnetic field, the beats between the exciton fine-structure states, split by the anisotropic exchange interaction, were observed in Ref. 16. Another example is the QB's between the fine-structure sublevels of the negatively charged exciton (trion).[17] Besides, the beats related to the free-electron spin precession in a transverse magnetic field were detected in Refs. 14 and 15. At the same time, no information about the QB's between the Zeeman sublevels of the excitonic states in QD's is available in the literature.

Until recently, the reasons why observation of the spin beats in QD's are hampered were obscure. As a rule, the absence of the QB's is associated with a great spread of the Zeeman splittings in the inhomogeneous ensemble of QD's. In our opinion, however, there is one more, perhaps not less important, reason related to the fact that QD's in most structures are charged. This circumstance was pointed out by many authors.[5,6,17–20] Even the presence of a single excess charge drastically complicates the excited-state fine structure.[17] As a result, the polarized light excites several, rather than only two, sublevels split by the magnetic field. In this case, the beats at different frequencies interfere and the oscillations of the resulting signal virtually vanish, which was observed experimentally.[17] So, observation of the QB's on the fine-structure Zeeman components is possible only in the ensemble of neutral QD's.

In this paper, we report on a study of kinetics of resonance photoluminescence (PL) of the InP QD's in a magnetic field. We have found that discharging the initially charged QD's by an external electric field, indeed, gives rise to strong QB's. Polarization characteristics of these beats differ from standard characteristics of the beats in the excitonic Zeeman doublet. The frequency of the beats was found to be dependent on the magnetic-field orientation. A theoretical analysis of the experimental data performed with the use of a model spin Hamiltonian has allowed us to identify the fine structure of the excitonic states in the system under study, to determine the longitudinal and transverse components of the electronic $g$ factor, and to estimate the spread of the hole $g$ factor and electron-hole exchange interaction parameters.

## II. EXPERIMENTAL DETAILS

We studied a heterostructure with a single layer of the InP QD's sandwiched between the $In_{0.5}Ga_{0.5}P$ barrier layers. The sample was grown by the gas source molecular-beam epitaxy

 

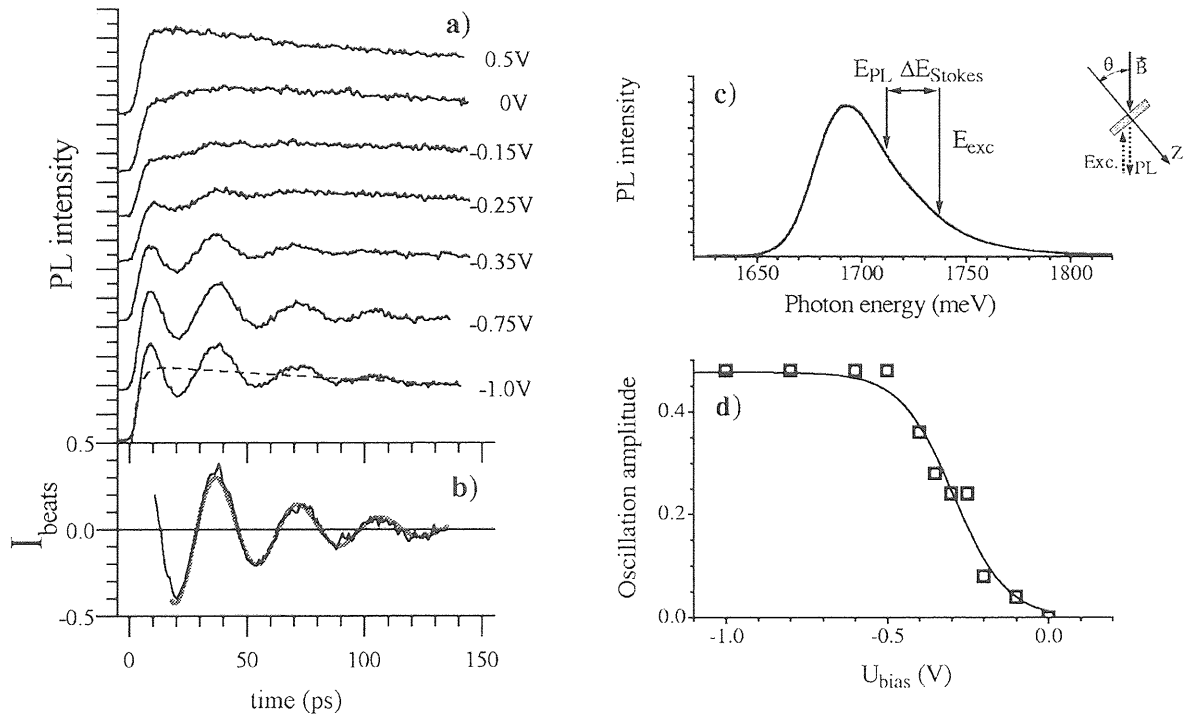


FIG. 1. (a) PL kinetics in the circular co-polarization for different biases applied to the top surface of the sample, indicated against each curve. $B=2$ T, $\theta=40°$, $\Delta E_{Stokes}=44.5$ meV. The dashed line shows fitting of the smoothly varying background by function (2) with the parameters $\tau_r=2.8$ ps, $\tau_{PL}=456.6$ ps. (b) Oscillating part of the PL signal normalized to $I_s$ (noisy curve) and its fitting by formula (1) (thick gray line). (c) PL spectrum of the QD's. The arrows show the photon energies for the exciting and detected light spaced by the Stokes shift $\Delta E_{Stokes}$. Geometry of the experiment is shown schematically in the inset. (d) Dependence of the beat amplitude $I_{beats}(0)$ on the bias (open squares) and the fitting by the function $y=y_0\{1-\mathrm{erf}[(U-U_{1/2})/(0.6\Delta U)]\}$ (solid line), where $U_{1/2}=U_0-\Delta U/2$, $U_0=-0.2$ V, $\Delta U=0.22$ V, and $\mathrm{erf}(x)$ is the error function. The values of the parameters $U_0$ and $\Delta U$ are taken from Ref. 17.

on an $n^+$ GaAs substrate. Details of the growth procedure and sample characterization are given in Refs. 21–24. The areal density of the QD's is about $10^{10}$ cm$^{-2}$. The average base diameter of the QD's is $\approx$40 nm and the height is $\approx$5 nm. To control the charge of the QD's, the sample was provided with a semitransparent indium tin oxide Shottky contact on the top surface and an Ohmic contact on the other one. The thickness of the undoped epitaxial layers, to which the electric voltage was applied, was about 0.5 $\mu$m.

In kinetic studies, the luminescence was excited by 3-ps pulses of a Ti:sapphire laser within the PL band (quasiresonant excitation) as shown in Fig. 1(c). The PL kinetics was measured with a time resolution of 6 ps using a 0.25-m subtractive double monochromator and a streak camera. The measurements were made in a cryostat with a superconducting magnet in the fields up to 7 T. The design of the cryostat allowed us to excite the sample and to detect its emission either along the magnetic-field direction (the Faraday configuration) or across the field (the Voight configuration). The PL was detected in the backscattering geometry as shown in the inset of Fig. 1. To study the beats at different angles $\theta$ between the growth axis $z$ of the structure and direction of the magnetic field $B$, the sample was rotated around the vertical axis.

## III. EXPERIMENTAL RESULTS

As has been shown experimentally, the PL pulse shape in a magnetic field is strongly affected by the applied bias. At zero and positive bias, the shape is smooth while at negative bias, the PL kinetics exhibits pronounced intensity oscillations as shown in Fig. 1(a). The oscillating part of the signal $I_{beats}$ can be determined by subtracting the smoothly varying background $I_s$ from the total signal $I_{PL}$ and normalizing to $I_s$: $I_{beats}=(I_{PL}-I_s)/I_s$. The oscillations can be well approximated by a simple equation,

$$I_{beats}(t)=I_{beats}(0)\exp(-t/\tau)\cos(\omega t), \qquad (1)$$

as shown in Fig. 1(b). Here, $I_{beats}(0)$, $\omega$, and $\tau$ are the amplitude, frequency, and decay time of the oscillations, respectively.

The background can be approximated by the function

$$I_s=I_0[\exp(-t/\tau_{PL})-\exp(-t/\tau_r)]. \qquad (2)$$

The parameters $\tau_r$ and $\tau_{PL}$ characterize the PL rise and decay times, respectively. The PL rise is related to relaxation of the hot photogenerated carriers to the radiative energy level. This process was studied in detail in Ref. 23. The PL decay results from radiative recombination of the electron-hole

pairs and nonradiative loss of the excitations. At negative bias, the nonradiative loss is due to the hole tunneling process as shown in Ref. 23.

The analysis of the experimental data has shown that the oscillation frequency as well as the oscillation decay time do not depend on the applied voltage. At the same time, the oscillation amplitude $I_{beats}(0)$ rapidly increases with increasing negative bias beginning from $U_0 = -0.15$ V, while at $U_0 < -0.5$ V the growth of the amplitude is saturated [see Fig. 1(d)]. We attribute this behavior of the oscillations to variations in the QD's charge state.

The InP QD's grown on the *n*-doped GaAs substrate are known to be usually charged.[20] The presence of the charges is related to the fact that the lowest electronic level of the QD's is positioned below the Fermi level of the doped substrate. Application of a negative voltage to the top surface of the sample removes the excess carriers from the dots and thus renders them neutral.[20,22] The magnitude of the voltage at which most dots become neutral depends on the mean size of the dots and equals, in the structure under study, $U_{bias} \leq -0.5$ V.[17] As seen from Fig. 1(d), the oscillation amplitude becomes the greatest exactly at this voltage. Such a correlation between the beat amplitude and the charge state of the QD's allowed us to conclude that observation of the QB's in a magnetic field is possible only for QD's with no excess charge. The presence of a finite interval $\Delta U$, in which the value of $I_{beats}(0)$ increases, is likely to be caused by a spread of heights of the potential barriers in the QD's ensemble.[25]

We studied behavior of the oscillations in different experimental conditions. The results of the study have shown that the oscillations are observed under excitation within or above the PL band of the QD's and under PL detection with the Stokes shifts, $\Delta E_{Stokes}$, up to $\Delta E_{Stokes} = 70$ meV. The oscillation *frequency* does not depend on the exciting photon energy and slightly decreases with decreasing photon energy of the detected PL. At the same time, the oscillation *amplitude* essentially depends on the Stokes shift between the PL and exciting light frequencies. The most intense oscillations are observed at the Stokes shift $\Delta E_{Stokes} = 45$ meV, which corresponds to the energy of the longitudinal optical (LO) phonons in the InP QD's.[23] All the data presented below are obtained for this value of the Stokes shift. The spectral dependence of the oscillation amplitude is discussed in detail elsewhere.[26]

Polarization characteristics of the oscillations appeared to be rather curious. It was found (see Fig. 2) that the most intense oscillations were observed under circularly polarized excitation with detection of the PL in the same polarization (co-polarized PL). Almost no oscillations were observed in the cross-polarized PL. Under the linearly polarized excitation, the oscillations in kinetics of the linearly co- and cross-polarized PL have the same phase. Their frequency coincides with that in circular polarization, but their amplitude is substantially smaller. It is noteworthy that the antiphase oscillations in the linear co- and cross- polarized PL, typical for the QB's of split Zeeman sublevels,[8,27] were not observed in our experiments.

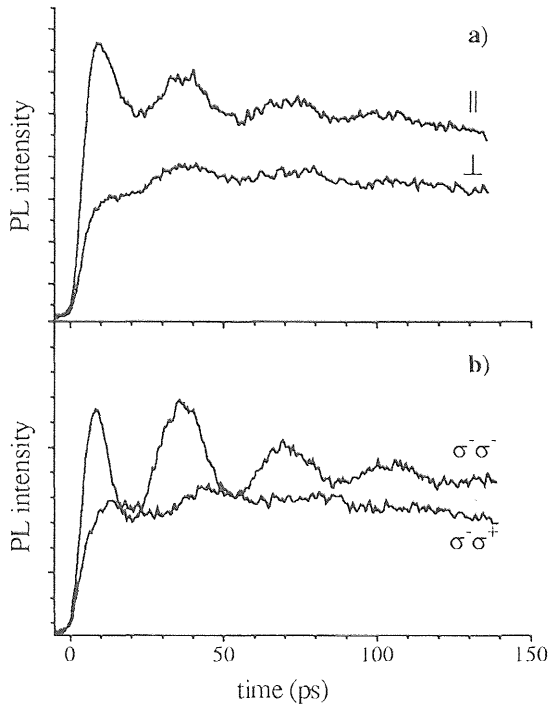


FIG. 2. PL kinetics in different polarizations (indicated against each curve). Symbols ∥ and ⊥ denote the co- and cross-linear polarizations, respectively; $\sigma^+$ and $\sigma^-$ denote circular polarization of the right and left helicities, respectively. In the case of circular polarization the first symbol denotes polarization of the excitation and the second the PL polarization. Experimental conditions are $B = 2$ T, $\theta = 40°$, $\Delta E = 45$ meV, and $U_{bias} = -0.75$ V.

To identify the nature of the oscillations, we studied the effect of the magnetic-field strength and orientation on the shape of the oscillations. Figure 3 shows dependence of the oscillations on the magnetic-field strength. One can easily see that an increase in the field is accompanied by an increase in the frequency of the oscillations. Fitting the oscillating part of the signal by Eq. (1) has allowed us to find that, in the range of 1–4 T, the oscillation frequency is directly proportional to the field strength as shown in Fig. 3(b). In the fields below 1 T, the period of the beats becomes longer than the decay time, and the oscillation frequency cannot be determined.

The behavior of the oscillations versus the magnetic-field orientation is found to be highly unusual. In the Faraday configuration ($\theta = 0°$), typical for observation of the Zeeman splitting in low-dimensional structures,[8,27,28] the oscillations are totally absent both in the linear and circular polarizations. Deviation of the magnetic field from the $z$ axis is accompanied by appearance of the oscillations [see Fig. 4(a)]. Within the range of the angles $20° < \theta < 60°$, the oscillation amplitude virtually does not depend on the angle, while at higher $\theta$, the amplitude substantially decreases. The oscillation frequency essentially increases with increasing angle $\theta$, i.e., with increasing transverse component of the magnetic field, as shown in Fig. 4(b).

Since the oscillations described above are observed only

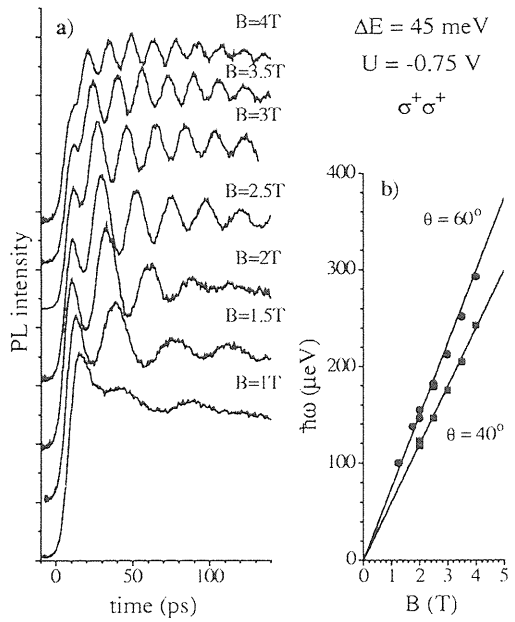


FIG. 3. (a) PL kinetics for different values of the magnetic field (indicated against each curve) for $\theta = 60°$. (b) Dependence of the oscillation frequency (in energy units) on the magnetic-field strength for two different angles $\theta$. The symbols are the experimental data and solid lines are the theoretical fits.

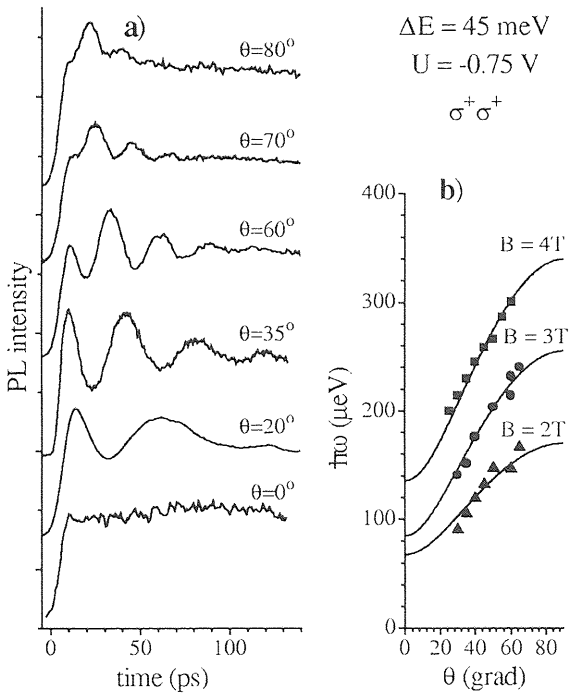


FIG. 4. (a) PL kinetics at different angles $\theta$ (indicated against each curve), $B = 2$ T. (b) Dependence of the oscillation frequency (in energy units) on the angle $\theta$ for three values of the magnetic field. Symbols are the experimental data and solid lines are the theoretical fits.

in the presence of a magnetic field, it is naturally to ascribe them to quantum beats between components of the excitonic fine structure split by the magnetic field. For analysis of the experimental data, we use the theoretical model of the excitonic fine structure, presented in the next section.

## IV. FINE-STRUCTURE MODEL

### A. Spin Hamiltonian

We analyzed characteristics of the fine-structure components using a theoretical model of the spin Hamiltonian of the electron-hole pair in a magnetic field similar to that presented in Refs. 28–30. Within the framework of this model, the Hamiltonian of spin states of the electron-hole pair in a bulk material can be presented in the form

$$H_{ex} = H_e + H_h + H_{e-h}. \tag{3}$$

The first term, $H_e$, describes the Zeeman splitting of the electronic states:

$$H_e = \mu_B g_e \sum_{i=x,y,z} S_{e,i} B_i, \tag{4}$$

where $\mu_B$ is the Bohr magneton, $g_e$ is the electron $g$ factor, and $S_{e,i}$ and $B_i$ are the Cartesian components of the electron spin and magnetic field, respectively. The second term, $H_h$, in Eq. (3) describes Zeeman splitting of the hole states:

$$H_h = -\mu_B \sum_{i=x,y,z} (kJ_{h,i} + qJ_{h,i}^3) B_i, \tag{5}$$

where $k$ and $q$ are the Zeeman splitting constants and $J_{h,i}$ is the $i$ component of total angular momentum of the hole. The last term in Eq. (3), $H_{e-h}$, describes exchange interaction between the electron and hole spins:

$$H_{e-h} = -\sum_{i=x,y,z} (aJ_{h,i} S_{e,i} + bJ_{h,i}^3 S_{e,i}). \tag{6}$$

Here, $a$ and $b$ are the spin-spin coupling constants.

In the InP-type semiconductors, the ground excitonic state is formed by an electron with the spin $S_e = \frac{1}{2}$ and a hole with the total angular momentum $J_h = \frac{3}{2}$. The size quantization along the growth axis $z$ realized in the quasi-two-dimensional systems (quantum wells and superlattices) is accompanied by splitting of the hole state into the light hole (LH) ($J_{h,z} = \pm\frac{1}{2}$) and heavy hole (HH) states ($J_{h,z} = \pm\frac{3}{2}$). The value of the splitting substantially exceeds typical Zeeman splittings in magnetic fields used.[31] This allows one to independently analyze the fine structure of the LH and HH excitons. As a rule, in the low-dimensional structures, the lowest energy state is that of the heavy hole. For this reason, the analysis presented below is restricted to the fine structure of the electron-HH pair or HH exciton.

The spin Hamiltonian of the HH exciton can be reduced to the fairly simple form[29]

$$H_{ex} = \sum_{i=x,y,z} [\mu_B (g_{e,i} S_{e,i} - g_{h,i} \tilde{S}_{h,i}) B_i - c_i S_{e,i} \tilde{S}_{h,i}], \tag{7}$$

where $\tilde{S}_h$ is the effective spin of the hole with the components $\pm\frac{1}{2}$ corresponding to the components $J_{h,z}=\mp\frac{3}{2}$, $g_{e,i}$, and $g_{h,i}$ are the components of the electron and hole $g$ factors, respectively, and $c_i$ is the spin-spin coupling constant. The relation of the quantities $g_{h,i}$ and $c_i$ with the coefficients $k$, $q$, $a$, and $b$ [see Eqs. (5) and (6)] is given by the formulas:

$$g_{h,z}=-3k_z-27q_z/4; \quad g_{h,x}=3q_x/2; \quad g_{h,y}=3q_y/2;$$

$$c_z=-3a_z-27b_z/4; \quad c_x=3b_x/2; \quad c_y=3b_y/2.$$

In the framework of the model under consideration, the eigenstates of the excitonic fine structure are characterized by projections of the total angular momentum of the exciton $\mathbf{J}=\mathbf{S_e}+\mathbf{J_h}$ upon the quantization axis. Accordingly, the states of the HH exciton $\{\varphi_i\}$ can be denoted as $|+1\rangle$, $|-1\rangle$, $|+2\rangle$, and $|-2\rangle$. In conformity with the selection rules, the optical transitions into the states with $J_z=\pm 1$ are allowed. The transitions into the states with $J_z=\pm 2$ are totally forbidden. The set of the states $\{\varphi_i\}$ specifies a basis of matrix representation of the HH-exciton spin Hamiltonian. In the absence of the magnetic field, the matrix of the HH-exciton spin Hamiltonian is determined only by the exchange interaction and can be represented in the form

$$H_{e-h}=\frac{1}{2}\begin{pmatrix} \delta_0 & \delta_1 & 0 & 0 \\ \delta_1 & \delta_0 & 0 & 0 \\ 0 & 0 & -\delta_0 & \delta_2 \\ 0 & 0 & \delta_2 & -\delta_0 \end{pmatrix}, \tag{8}$$

where $\delta_0=-c_z/4$, $\delta_1=-(c_x+c_y)/4$, and $\delta_2=-(c_x-c_y)/4$.

The matrix of the Zeeman part of the Hamiltonian can be simplified by assuming axial symmetry of the $g$ factor. Note that, for the shape of the QD's under study, the value of the $g$ factor is controlled mainly by confinement along the growth axis. For this reason, asymmetry of the confinement in the plane of the QD's should not noticeably affect the Zeeman splitting. For axial symmetry, the Zeeman part of the Hamiltonian has the form

$$H_e+H_h=H_{Zeeman}=\frac{\mu_B B}{2}\begin{pmatrix} -(g_{e,z}+g_{h,z})\cos\theta & 0 & g_{e,x}\sin\theta & g_{h,x}\sin\theta \\ 0 & (g_{e,z}+g_{h,z})\cos\theta & g_{h,x}\sin\theta & g_{e,x}\sin\theta \\ g_{e,x}\sin\theta & g_{h,x}\sin\theta & (g_{e,z}-g_{h,z})\cos\theta & 0 \\ g_{h,x}\sin\theta & g_{e,x}\sin\theta & 0 & -(g_{e,z}-g_{h,z})\cos\theta \end{pmatrix}, \tag{9}$$

where $\theta$ is the angle between the $z$ axis and direction of the magnetic field $\mathbf{B}$. In Eq. (9), we used the coordinate system in which $B_x=B\sin\theta, B_y=0, B_z=B\cos\theta$.

The Hamiltonian matrices (8) and (9) contain a large number of uncertain parameters: three components of the exchange splitting, $\delta_{0,1,2}$, two components of the electron $g$ factor, $g_{e,z}$ and $g_{e,x}$, and two components of the hole $g$ factor, $g_{h,z}$ and $g_{h,x}$. To reduce the number of independent parameters, we use several approximations based on our experimental data.

It was noted above (see Fig. 3 and comments therein) that the beat frequency is proportional to the magnetic-field strength. This may occur only when the Zeeman splitting, in the range of the magnetic field employed, substantially exceeds the exchange one. Therefore we can neglect the exchange splitting assuming that $\delta_{0,1,2}=0$.

We can additionally simplify the spin Hamiltonian by assuming a strong anisotropy of the hole $g$ factor in the system under study, $g_{h,z}\gg g_{h,x}$. This approximation is used by most authors who analyze Zeeman splitting of exciton spins in semiconductor heterostructures.[29,28] Thus, in the analysis of the beat frequency, we assume that $g_{h,x}=0$.

In the framework of the above approximations, the Hamiltonian matrices (8) and (9) contain only three free parameters $g_{e,z}$, $g_{e,x}$, and $g_{h,z}$. The energies of the Zeeman components can now be calculated analytically:

$$E_{1,2,3,4}=\pm\frac{\mu_B B}{2}\left[g_{h,z}\cos\theta\pm\left(g_{e,z}^2\cos^2\theta+g_{e,x}^2\sin^2\theta\right)^{1/2}\right] \tag{10}$$

The sign "−" inside the brackets corresponds to the states with energies $E_1$ and $E_2$ and the sign "+" to the states with energies $E_3$ and $E_4$.

The expressions for the wave functions obtained in an explicit analytical form are too cumbersome to be presented here.

### B. Quantum beats and fine structure

Before using the expressions obtained in the previous subsection for theoretical analysis of the experimental results, we have to determine what particular states of the excitonic fine structure are responsible for the observed beats. There are two types of beats that can be observed in the states of the HH exciton split by the magnetic field:[13]

(i) The beats between sublevels of the optically active doublet, which are revealed as antiphase oscillations of the PL intensity in the linear co- and cross polarizations;

(ii) The beats between the bright and dark sublevels mixed by transverse component of the magnetic field.

We start the discussion with the beats of the second type because the beats in our experiments were observed only in

tilted magnetic fields, i.e., in the presence of the transverse component of the field (see Sec. III).

*1. Beats between the bright and dark sublevels*

The transverse component of the magnetic field mixes states with different projections of the angular momentum, which makes transitions into optically inactive (dark) states partially allowed. In QD's, this effect was observed in Ref. 28. As follows from the Zeeman Hamiltonian matrix (9), the state $\varphi_1$ is mixed with the state $\varphi_3$, and the state $\varphi_2$ with $\varphi_4$. As a result, the circularly polarized light will simultaneously excite two components of the fine structure. In the absence of the spin relaxation, polarization of the PL from these components will reproduce polarization of excitation, and the PL intensity will oscillate with the frequency determined by the energy difference between these components. Thus under the $\sigma^+$ polarized excitation the beats between the states $\varphi_1$ and $\varphi_3$ will show up, while under the $\sigma^-$ polarized excitations, the beats between the states $\varphi_2$ and $\varphi_4$. In both cases, the beats should appear in the co-polarized PL.

The circular cross-polarized PL may appear only after the excitonic spin-flip process occurs.[8] Since the spin flip completely destroys the spin coherence, the beats of the above type cannot be observed in the cross-polarized PL.

The whole set of the features mentioned above (the presence of the beats in the circular co-polarized PL, their absence in the cross-polarized PL, and the necessity of the transverse component of the magnetic field) is present in the beats we observed (see Sec. III). Thus we can conclude that these beats are really related to the interference between the bright and dark states. The frequency of the beats is determined, in this case, by the energy difference between the relevant Zeeman components, i.e., by the quantity

$$\hbar\omega = E_1 - E_3 = \mu_B B(g_{e,z}^2 \cos^2\theta + g_{e,x}^2 \sin^2\theta)^{1/2}. \quad (11)$$

Equation (11) contains only longitudinal $g_{e,z}$ and transverse $g_{e,x}$ components of the electron $g$ factor. Partial contributions of the components depend on the tilt angle $\theta$. This makes it possible to unambiguously determine these components from the experimental data. For comparison with the experiment, we calculated dependences of the QB's frequencies, observed in the $\sigma^+$ polarization, on the angle $\theta$, and magnetic-field strength. The calculations were made using expression (11), with the quantities $g_{e,z}$ and $g_{e,x}$ regarded as fitting parameters. The results of the comparison of the theory and experiment are shown in Figs. 3(b) and 4(b). As is seen, one set of the parameters ($g_{e,z}=0.53$ and $g_{e,x}=1.43$) allows us to describe well all the experimental dependences.

An attempt to refine the model with allowance for the isotropic component of the exchange splitting $\delta_0$ has not been successful. It was found that introducing the exchange coupling $\delta_0 \leqslant 30$ $\mu$eV practically did not affect the results of the calculations. At greater $\delta_0$, the agreement between the calculated and experimental dependences was rapidly worsening. Based on these facts, we concluded that the exchange coupling energy in the structure under study does not exceed 30 $\mu$eV.

*2. Splitting of the bright doublet*

The experimental fact of absence of the beats between the bright doublet components in a longitudinal magnetic field (see Sec. III) needs to be specially discussed. It immediately follows from the spin Hamiltonian (8) that the longitudinal magnetic field splits the optically active doublet ($J_z=\pm 1$) into two components $E_1$ and $E_2$, with the splitting determined by the longitudinal component of the exciton $g$ factor, $g_z = g_{e,z} + g_{h,z}$: $\Delta E = \mu_B B g_z$. The coherent excitation of the split states with the linearly polarized light should give rise to quantum beats in the polarized PL at a frequency of $\omega = \delta E/\hbar$. Such beats are easily observed in the experiments with the GaAs quantum wells.[27,8]

The main reason for the absence of the beats in our case is, most likely, a large spread of the splittings of the bright doublet in the QD's ensemble. The spread may be predominantly caused by the spread of the longitudinal components of the excitonic $g$ factor. Indeed, according to the experimental data for single InP QD's obtained in Ref. 7, the spread of the longitudinal $g$ factor is very large and makes up $\Delta g_z = \pm 0.5$.

A result of the spread of the splittings should be destructive interference between the beat signals from different QD's. At small spread, such an interference leads to acceleration of decay of the beat signal (reversible dephasing).[32] If the spread substantially exceeds the mean value of the splitting, the beats cannot be observed and the degree of polarization of the PL decays smoothly in time. For the Gaussian spread of the splittings, the spread of the beat frequencies $\delta\omega$ and the decay time $\tau$ are connected by a simple relationship: $\delta\omega = 2/\tau$. In our experiments, we indeed observed the smooth decay of the degree of linear polarization in the longitudinal magnetic field. The decay time in the field $B = 1.5$ T makes up approximately 20 ps, which corresponds to the spread $\Delta g_z \approx 0.7$. This value is comparable with the one given in Ref. 7. The absence of the beats means that the mean value of $g_z$, in our sample, is significantly smaller than the spread, i.e., $\langle g_z \rangle < 0.7$.

Thus, due to the large spread of the excitonic $g$ factor, the beats between the Zeeman components of the bright doublet are not observed. At the same time, this spread does not prevent from observing the beats between the dark and bright states, described in the previous section. This apparent paradox can be easily explained with allowance for the fact that the splitting between the dark and bright components is controlled by the electron $g$ factor only [see Eq. (11)], whereas the splitting of the bright doublet is determined by the sum of the electron and hole $g$ factors. Hence it follows that the spread of the electron $g$ factor in the QD's under study is rather small and the main contribution to the spread of the excitonic $g$ factor is made by the hole $g$ factor. The reason for such a large spread of the hole $g$ factors calls for further investigation.

### C. Oscillation amplitude

The calculations fulfilled in the framework of the spin-Hamiltonian model has allowed us to determine not only the frequencies but also the whole shape of oscillations of the

polarized PL in the magnetic field. To describe the shape of the oscillations, we calculated the time-dependent matrix elements of optical transitions from the relevant states of the fine structure.

The eigenfunctions of the spin-Hamiltonian in a magnetic field of arbitrary orientation are linear combinations of the basis functions $\{\varphi_i\}=\{|+1\rangle, |-1\rangle, |+2\rangle, \text{ and } |-2\rangle\}$:

$$\psi_i=\sum_{j=1}^{4} a_{ij}\varphi_j. \tag{12}$$

The expansion coefficients $a_{ij}$ can be found by solving the stationary Schrödinger equation with Hamiltonian (8) and (9). The coherent pulsed excitation creates, at the initial moment, a linear superposition of the states $\psi_i$, whose subsequent evolution is described by the equation

$$\Psi(t)=\sum_{i=1}^{4} C_{0i}\exp(-iE_it/\hbar)\psi_i. \tag{13}$$

Here, $C_{0i}$ are the time-independent coefficients whose values are determined by the initial conditions of excitation.

In accordance with the selection rules for optical transitions, the $\sigma^+$ polarized light excites each of the eigenstates $\psi_i$ in proportion with the admixture of the basis function $|+1\rangle$. The mixing is determined by the coefficients $a_{ij}$ with $j=1$ in Eq. (12), so that the relationship $C_{0i}=a_{i1}^*$ is fulfilled.

The PL intensity in the $\sigma^+$ polarization $I_+$ is proportional to the matrix element of the optical transition squared:

$$I_+\propto|\langle\Psi(t)|\hat{d}|0\rangle|^2, \tag{14}$$

where $\hat{d}$ is the dipole moment operator and $|0\rangle$ is the ground state of the system. From Eqs. (13) and (14) and the expression for the coefficients $C_{0i}$ given above, we obtain the following expression for the PL signal (to within a constant factor):

$$I_+=\sum_{i}^{4}|a_{i1}|^4+2\sum_{i<k}^{4}|a_{i1}|^2|a_{k1}|^2\cos\left(\frac{E_i-E_k}{\hbar}t\right). \tag{15}$$

The first sum in Eq. (15) describes the smooth component of the signal $I_s$. It does not contain any time dependence since the model we use does not take into account relaxation processes. The oscillating part of the signal is described by the second sum in Eq. (15). In the framework of the above approximations, the only nonzero coefficients in this term, for the $\sigma^+$ polarized excitation, are $a_{1,1}$ and $a_{3,1}$.

Thus the expression for the beats intensity $I_{beats}$ (see definition in Sec. III) can be reduced to the form

$$I_{beats}=\frac{2R\sum_{i<k}^{4}|a_{i1}|^2|a_{k1}|^2\cos\left(\frac{E_i-E_k}{\hbar}t\right)}{\sum_{i}^{4}|a_{i1}|^4}\exp(-t/\tau). \tag{16}$$

The amplitude factor $R$ is introduced to take into account the loss of coherence in the process of relaxation of the photogenerated electron-hole pairs to the radiative energy level.[33] In addition, Eq. (16) contains a phenomenological exponential factor that takes into account the decay of the beats. Equation (16) allows us to determine the Zeeman splittings $E_i-E_k$ and decay constant $\tau$ from the experimental data.

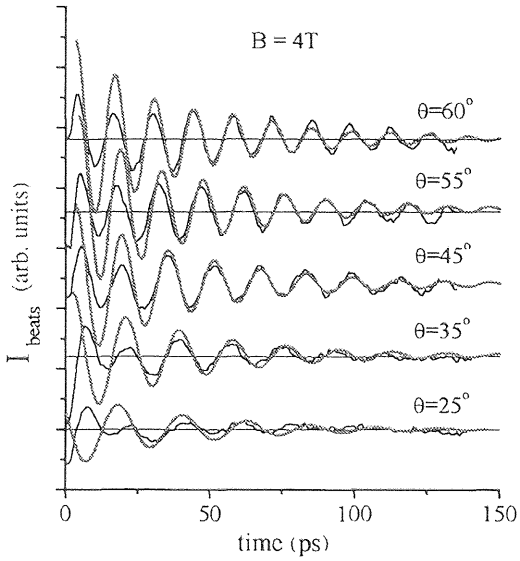


FIG. 5. Quantum beats in the InP QD's in a magnetic field of $B=4$ T. The noisy curves are the experiment and the thick gray lines are the calculations.

Analyzing our experimental data, we have found that the beat decay rate $1/\tau$ depends on orientation of the magnetic field. An increase in the angle $\theta$, i.e., a growth of the transverse component $B_x$, is accompanied by an increase in the beat decay rate. This effect is most likely to be related to the presence of a small transverse component $g_{h,x}$ of the hole $g$ factor. As follows from the spin Hamiltonian (9), the transverse component of the magnetic field, at a nonzero $g_{h,x}$, admixes each bright state to the both dark states, rather than only to one of them. As a result, the beats arise at several frequencies. The interference of these beats is revealed as a decay of the main harmonic. Since the value of the admixture is proportional to the square of the transverse component of the magnetic field, this effect should be observed only at large angles $\theta$.

Figure 5 shows an example of comparison of the experimental data with the results of calculations for the angles $\theta \leqslant 60°$ and magnetic field $B=4$ T. The calculations were made using formula (16) with allowance for an additional mixing of the states due to nonzero $g_{h,x}$. The value $g_{h,x}$ was used in the calculations as one more fitting parameter. It has been found that the best agreement with the experiment is achieved at $g_{h,x}=0.1$. It is important that all the experimental data obtained in the whole range of the magnetic-field strengths and for the angles $\theta\leqslant 60°$ can be well fitted using one set of the parameters: $g_{e,z}=0.53$, $g_{e,x}=1.43$, $R=0.8$, and $\tau=40$ ps. It should be emphasized that the estimated value of the $x$ component of the hole $g$ factor $g_{h,x}$ is small with respect to the electron $g$ factor. Therefore this component virtually does not affect the beat frequency.

A good agreement it is worth noting between the calculations and experimental data in spite of a limited number of parameters. A certain discrepancy between the calculations and experiments is observed only at the initial moment ($<10$ ps). This is probably related to the error of modeling of the smooth background upon extracting the beats from the total signal.[34]

It is surprising that the value $R$ is rather large. It means that about 80% of the coherence produced by the excitation is conserved after relaxation of the electron-hole pair to the radiative energy level. In this respect, the situation in the structure with quantum dots under study essentially differs from that in quantum wells, where, according to Ref. 13, the energy relaxation by more than 20 meV is accompanied by complete loss of the hole spin orientation. In our case, it is probably highly important that the relaxation occurs with emission of an LO phonon, and such a process is very fast. The relaxation with emission of acoustic phonons conserves a much smaller fraction of the coherence.[26]

The above set of the parameters makes it possible to adequately describe the shape of the oscillating signal at the tilt angles up to $\theta \leqslant 60°$. At larger angles, the oscillation amplitude sharply decreases (see Sec. III) and, to obtain agreement with the experiment, one has to significantly change the amplitude factor $R$. The reason for this effect invites further studies.

The proposed theory, as a whole, describes adequately the behavior of the beat amplitudes and frequencies at different values and orientations of the magnetic field. At the same time, a few questions remain open, calling for further research. First of all, the great difference between components of the electron $g$ factor, $(g_{e,x}-g_{e,z})\approx 0.9$, is fairly unusual. This value in quasi-two-dimensional heterostructures lies, as a rule, in the range of 0.1–0.2.[35,36] On the other hand, the value $g_{e,x}$ we obtained practically coincides with that of the electronic $g$ factor in the bulk InP.[37] Therefore we have to admit strong suppression of the longitudinal component of the electron $g$ factor in the InP QD's.

One more curious fact is that the exchange splitting in the structure under study is rather small, $\delta_0 < 30$ $\mu$eV. Our estimate of $\delta_0$ strongly differs from the value $\delta_0 \approx 100$ $\mu$eV found experimentally for the negatively charged exciton, trion, at the same QD's.[17] Such a strong difference between the exchange coupling in trion and in neutral exciton calls for special theoretical analysis.

## V. CONCLUSIONS

In this study, we observed quantum beats between Zeeman components of the fine structure of electron-hole pairs in the InP quantum dots. This proved to be possible after removal of excess charges upon application of negative electric bias to the top surface of the sample. It was found that the beats show specific polarization characteristics and depend in a nontrivial way on the magnetic-field orientation. Analysis of the experimental data within the framework of the spin-Hamiltonian model has allowed us to consistently explain the observed phenomena and to quantitatively describe the shape of the quantum beats signal. As a result, we have determined the values of the transverse and longitudinal components of the electron $g$ factor ($g_{e,z}=0.53$ and $g_{e,x}=1.43$) and estimated the exchange coupling ($\delta_0 < 30$ $\mu$eV). Based on the analysis of the experimental data, we came to the conclusion about a considerable spread of the hole $g$ factor ($\Delta g_h \approx 0.7$) and about nonzero value of the transverse component ($g_{h,x} \approx 0.1$) of the hole $g$ factor.

## ACKNOWLEDGMENTS

The authors wish to thank Professor V. Zapasskii, Dr. G. Kozlov, and Dr. K. Kavokin for a fruitful discussion.

*Electronic address: irina.yugova@pobox.spbu.ru

†Permanent address: Vavilov State Optical Institute, St.-Petersburg, 190034, Russia.

‡Permanent address: Institute of Physics, St.-Petersburg State University, St.-Petersburg, 198504, Russia.

§Permanent address: Institute of Physics, St.-Petersburg State University, St.-Petersburg, 198904, Russia.

¶Present address: Applied Optoelectronics Incorporation, Sugar Land, TX 77478.

**Permanent address: Faculty of Science, Osaka City University, Osaka 558-8585, Japan.

††Permanent address: Opto-Electronic Research Laboratory, NEC Corporation, Tsukuba, 305-8501, Japan.

‡‡Permanent address: Institute of Physics, University of Tsukuba, Tsukuba 305–8571, Japan.

[1] D.D. Awschalom and J.M. Kikkawa, Phys. Today **52**(6), 33 (1999).

[2] E. Pazy, I. D'Amico, P. Zanardi, and F. Rossi, Phys. Rev. B **64**, 195320 (2001).

[3] D. Loss and D.P. DiVincenzo, Phys. Rev. A **57**, 120 (1998).

[4] M. Paillard, X. Marie, P. Renucci, T. Amand, A. Jbeli, and J.M. Gerard, Phys. Rev. Lett. **86**, 1634 (2001).

[5] M. Baier, F. Findeis, A. Zrenner, M. Bichler, and G. Abstreiter, Phys. Rev. B **64**, 195326 (2001).

[6] M. Bayer, A. Kuther, A. Forchel, A. Gorbunov, V.B. Timofeev, F. Schäfer, J.P. Reithmaier, T.L. Reinecke, and S.N. Walck, Phys. Rev. Lett. **82**, 1748 (1999).

[7] M. Sugisaki, H.W. Ren, K. Nishi, S. Sugou, T. Okuno, and Y. Masumoto, Physica B **256-258**, 169 (1998).

[8] I.Ya. Gerlovin, Yu.K. Dolgikh, S.A. Eliseev, V.V. Ovsyankin, Yu.P. Efimov, V.V. Petrov, I.V. Ignatiev, I.E. Kozin, and Y. Masumoto, Phys. Rev. B **65**, 035317 (2002).

[9] S. Bar-Ad and I. Bar-Joseph, Phys. Rev. Lett. **66**, 2491 (1991).

[10] A.P. Heberle, W.W. Ruhle, and K. Ploog, Phys. Rev. Lett. **72**, 3887 (1994).

[11] R.E. Worsley, N.J. Traynor, T. Grevatt, and R.T. Harley, Phys. Rev. Lett. **76**, 3224 (1996).

[12] L. Sham, Science **277**, 1258 (1997).

[13] T. Amand, X. Marie, P. Le Jeune, M. Brousseau, D. Robart, J. Barrau, and R. Planel, Phys. Rev. Lett. **78**, 1355 (1997).

[14] J.A. Gupta, D.D. Awschalom, X. Peng, and A.P. Alivisatos, Phys. Rev. B **59**, R10 421 (1999).

[15] V.K. Kalevich, M.N. Tkachuk, P. Le Jeune, X. Marie, and T. Amand, Fiz. Tverd. Tela **41**, 871 (1999) [Phys. Solid State **41**, 789 (1999)].

[16] T. Flissikowski, A. Hundt, M. Lowisch, M. Rabe, and F. Henneberger, Phys. Rev. Lett. **86**, 3172 (2001).

[17] I.E. Kozin, V.G. Davydov, I.V. Ignatiev, A.V. Kavokin, K.V. Kavokin, G. Malpuech, H.W. Ren, M. Sugisaki, S. Sugou, and Y. Masumoto, Phys. Rev. B **65**, 241312(R) (2002).

[18] R.J. Warburton, C.S. Durr, K. Karrai, J.P. Kotthaus, G. Medeiros-Ribeiro, and P.M. Petroff, Phys. Rev. Lett. **79**, 5282 (1997).

[19] A. Hartmann, Y. Ducommun, E. Kapon, U. Hohenester, and E. Molinari, Phys. Rev. Lett. **84**, 5648 (2000).

[20] Dan Hessman, Jonas Persson, Mats-Erik Pistol, Craig Pryor, and Lars Samuelson, Phys. Rev. B **64**, 233308 (2001).

[21] H.-W. Ren, M. Sugisaki, S. Sugou, K. Nishi, A. Gomyo, and Y. Masumoto, Jpn. J. Appl. Phys., Part 1 **38**, 2438 (1999).

[22] Y. Masumoto, V. Davydov, I. Ignatiev, H.-W. Ren, and S. Sugou, Jpn. J. Appl. Phys., Part 1 **38**, 563 (1999).

[23] I.V. Ignatiev, I.E. Kozin, V.G. Davydov, S.V. Nair, J.-S. Lee, H.-W. Ren, S. Sugou, and Y. Masumoto, Phys. Rev. B **63**, 075316 (2001).

[24] Y. Masumoto, I.V. Ignatiev, I.E. Kozin, V.G. Davydov, S.V. Nair, H.-W. Ren, J.-S. Lee, and S. Sugou, Jpn. J. Appl. Phys., Part 1 **40**, 1947 (2001).

[25] In Ref. 17 it has been shown that at a voltage of $U = -0.2$ V each quantum dot contains, on average, one resident electron, the electron distribution being described by a Gaussian with a half width at half maximum of $\Delta U = 0.22$ V. With increasing negative voltage ($U < -0.2$ V), the number of neutral quantum dots increases, while with increasing positive voltage ($U > -0.2$ V), the number of multiply charged dots increases. Thus we can easily obtain the expression for the dependence of the number of uncharged quantum dots on the voltage, used to fit the data in Fig. 1(d).

[26] I.A. Yugova, V.G. Davydov, I.Ya. Gerlovin, I.V. Ignatiev, I.E. Kozin, M. Sugisaki, and Y. Masumoto, Phys. Status Solidi A **190**, 547 (2002).

[27] R.E. Worsley, N.J. Traynor, T. Grevatt, and R.T. Harley, Phys. Rev. Lett. **76**, 3224 (1996).

[28] M. Bayer, O. Stern, A. Kuther, and A. Forchel, Phys. Rev. B **61**, 7273 (2000).

[29] H.W. van Kesteren, E.C. Cosman, W.A.J.A. van der Poel, and C.T. Foxon, Phys. Rev. B **41**, 5283 (1990).

[30] E.L. Ivchenko and G.E. Pikus, *Superlattices and Other Heterostructures Symmetry and Optical Phenomena*, Springer Series in Solid-State Sciences Vol. 110 (Springer, Berlin, 1997).

[31] E.L. Ivchenko and A.A. Kiselev, Fiz. Tekh. Poluprovodn. **26**, 1471 (1992) [Sov. Phys. Semicond. **26**, 827 (1992)].

[32] H. Nickolaus, H.-J. Wunsche, and F. Henneberger, Phys. Rev. Lett. **81**, 2586 (1998).

[33] A possible reason for the decrease in the beats signal can also be incomplete orientation of spins of the electron-hole pair because of mixing of excited states of the light and heavy holes. As a result, e.g., under the $\sigma^+$-polarized excitation, the electrons, both with the spin $s = +1/2$ and with the spin $s = -1/2$, can be generated. A certain role can be also played by ellipticity of the exciting light arising upon oblique incidence of the beam upon the sample.

[34] The processes of formation of the secondary emission at the initial stages are rather complicated [see, i.e., W. Langbein, K. Leosson, J.R. Jensen, J.M. Hvam, and R. Zimmermann, Phys. Rev. B **61**, R10 555 (2000)] and may also result in behavior of the beats other than that described by Eq. (1).

[35] E.L. Ivchenko, Pure Appl. Chem. **67**, 463 (1995)

[36] A. Malinowski and R.T. Harley, Phys. Rev. B **62**, 2051 (2000).

[37] *Semiconductors, Intrinsic Properties of Group V Elements and III-V, II-VI, and I-VI Compounds*, edited by K.-H. Hellwege and O. Madelung, Landolt-Börnstein, New Series, Group III, Vol. 22, Pt. a (Springer-Verlag, Berlin, 1987).

PHYSICAL REVIEW B 68, 035333 (2003)

# Luminescence quantum beats of strain-induced GaAs quantum dots

Kazuhiro Nishibayashi, Tsuyoshi Okuno, Yasuaki Masumoto,* and Hong-Wen Ren†
*Institute of Physics, University of Tsukuba, Tsukuba, Ibaraki 305-8571, Japan*
(Received 11 March 2003; revised manuscript received 23 May 2003; published 30 July 2003)

Quantum beats of the strain-induced GaAs quantum dots were observed in the time-resolved photoluminescence in the magnetic field parallel and perpendicular to the growth direction. Quantum beats observed under the longitudinal magnetic field are caused by quantum interference of bright excitons showing Zeeman splitting. The oscillation period depends on the angle between the growth direction of the crystal and the magnetic field. Analysis based on the spin Hamiltonian for excitons explains the observed data and gives $g$ factors 0.51, 0.17, and 0.34 to the exciton, electron, and heavy hole, respectively. Quantum beats coming from electron Larmor precession were observed under the transverse magnetic field. The isotropic electron $g$ factor is observed in contrast to the anisotropic electron $g$ factor for the corresponding quantum well and is ascribed to the strain-induced opposite energy shift of heavy- and light-hole bands.

DOI: 10.1103/PhysRevB.68.035333 PACS number(s): 78.47.+p, 78.67.−n, 73.21.−b, 71.70.Ej

## I. INTRODUCTION

The semiconductor quantum dots (QDs), artificial atoms, have quantized energy levels characterized by orbital and spin angular momenta similar to atomic levels. Long optical coherence of exciton and spin in semiconductor quantum dots is expected to apply to quantum computation and quantum information processing.[1] Spin coherence time is known to be much longer than exciton coherence time in bulk and quantum structures.[2,3] Further, carrier spin relaxation is expected to be greatly suppressed by quantum confinement.[4] Nevertheless, study of spin-relaxation time and spin structures in quantum dots is still in the elementary stage. Therefore, new knowledge on the spin structure and the spin dynamics becomes important. Static and transient optical orientation, magneto-optic spectroscopy, spin-flip Raman scattering, and quantum beats have given us valuable information on spin-dependent energy levels of bulk and quantum well (QW) semiconductors. Especially, quantum beats are known to be an efficient method for studying a fine energy structure and spin dynamics of carriers in semiconductors[5] because they are not limited by the spectral resolution and hence give us finest energy splitting and because they also give us lower limit time of coherence between spin-split sublevels.

Quantum beats in semiconductor quantum structures under the magnetic field have been reported. Time-resolved pump-and-probe measurement revealed the electron and hole $g$ factors in quantum wells.[6] In the time-resolved luminescence measurement, quantum beats were observed under the resonant excitation of quantum wells.[2,7] Time-resolved luminescence revealed hole spin quantum beats.[8] Although many observations of quantum beats have been reported in quantum wells, the observations of quantum beats for quantum dots are limited.[9–12] This is ascribed to the large inhomogeneous broadening in the ensemble of quantum dots.

The utilization of stress caused by lattice mismatch between different semiconductors is an ideal method for fabrication of well-characterized quantum dots. Quantum dots are formed in a single quantum well by the stress modulation from the self-assembled islands fabricated on the surface. Self-assembled islands cause tensile strain perpendicular to the growth direction and therefore, the potential energies of the conduction band and valence band form additional harmonic potential wells laterally in the quantum well layer. Almost equally spaced quantum energy levels are observed and the formed quantum structures are called strain-induced quantum dots.[13–17] The strain-induced quantum dots have homogeneous size distribution in the growth direction and no defect at the interface. They have well-characterized quantum energy levels which are suitable for the precise optical study. In this paper we report the first, to the best of our knowledge, observation of two kinds of quantum beats coming from the Zeeman splitting of bright excitons and electron Larmor precession in strain-induced quantum dots.

## II. SAMPLES

The samples were grown by metal organic vapor phase epitaxy at 60 Torr on semi-insulating GaAs (001) substrates. Single GaAs-$Al_{0.3}Ga_{0.7}As$ quantum wells were grown. The thickness of the GaAs quantum well is 3.9 nm in one sample and 4.8 nm in another sample. The $Al_{0.3}Ga_{0.7}As$ top barrier layer was 9.6-nm thick. After the growth of the single quantum well, a 2.4-nm GaAs cap layer was grown. Finally, InP islands were formed by depositing four monolayer InP as stressors. The islands were ~90-nm wide and ~16-nm high. The areal density of the islands was $\approx 3\times 10^9$ $cm^{-2}$. An additional sample consisting of single quantum wells 2.4-nm, 4.8-nm, and 9.6-nm thick without InP stressors was also grown for the measurement of the well-width dependent $g$ factor of the electron.

## III. PHOTOLUMINESCENCE AND PHOTOLUMINESCENCE EXCITATION SPECTRA

Photoluminescence (PL) spectrum of the sample whose GaAs well width is 3.9 nm, excited at 2.33 eV by using a continuous-wave (cw) $Nd^{3+}:YVO_4$ laser is shown in the bottom panel of Fig. 1. The luminescence located at 1.64 eV

0163-1829/2003/68(3)/035333(6)/$20.00  

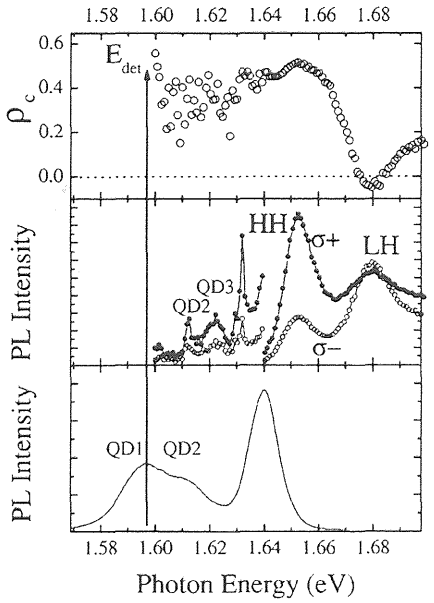


FIG. 1. Bottom panel: Photoluminescence (PL) spectrum of strain-induced GaAs quantum dots excited at 2 K with a cw $Nd^{3+}$:$YVO_4$ laser. The GaAs well width is 3.9 nm. Middle panel: Circularly polarized photoluminescence excitation spectra. The detected energy is set to the first excited state of the quantum dots, which is obtained from the luminescence measurement. Vertical scale is expanded by ten times between 1.60 eV and 1.64 eV. The closed (open) circles show the same (opposite) circular polarization as that of the excitation laser. Top panel: Degree of circular polarization $\rho_c$ of photoluminescence excitation spectrum.

is attributed to heavy-hole exciton recombination in the GaAs quantum well without modulation by stress. In the lower-energy region around 1.60 eV, the luminescence from strain-induced quantum dots is observed. In the figure, QD1 and QD2 denote the PL bands of the first and second excited states of dots, respectively, whose luminescence nonlinearity was reported previously.[17] The energy separation between the first and second excited states of dots is 16 meV which was also seen clearly in the nonlinear luminescence.[17] Circularly polarized photoluminescence excitation (PLE) spectrum was measured to specify the energy states of the dots more precisely. A tunable cw Ti:sapphire laser was used as an excitation source and its intensity was kept constant by an acousto-optic modulator. Circularly polarized light was made by a linear polarizer and a quarter-wave plate. The luminescence components of the same circular polarization as the excitation laser ($\sigma^+$) and its opposite ($\sigma^-$) were selectively measured by using another quarter-wave plate and a linear polarizer placed in front of a 1-m double monochromator. The luminescence intensity was measured by a liquid-nitrogen-cooled charge-coupled-device camera by changing the wavelength of the excitation laser.

The circularly polarized PLE spectra are shown at the middle panel of Fig. 1. The detected energy is set to the peak of the QD1 band (1.597 eV). Several structures are observed. The energy of the second excited state of the dots, QD2 in the bottom panel, agrees with the absorption structure QD2 in the middle panel and QD3 denotes the absorption by the third excited state of the dots. There is a sharp peak at 1.632 eV. The energy difference between this peak and the detected energy position is 35 meV which is equal to the longitudinal optical (LO) phonon energy of GaAs. Therefore, the origin of this peak is the luminescence through one LO-phonon relaxation. The peaks at 1.653 eV and 1.680 eV correspond to heavy-hole (HH) exciton and light-hole (LH) exciton in a quantum well, respectively. Clear difference is detected for $\sigma^+$ and $\sigma^-$ luminescence. The degree of circular polarization $\rho_c=(I_{\sigma^+}-I_{\sigma^-})/(I_{\sigma^+}+I_{\sigma^-})$ is as much as 0.4 at the LO-phonon peak, as is shown in the top panel of Fig. 1. When the HH state was excited, $\rho_c$ is 0.5, the highest value. When the LH state was excited, $\rho_c$ is negative and is $-0.05$. Based on the selection rule for the absorption and luminescence transitions by circularly polarized light,[18] negative polarization at the LH exciton of the quantum well and positive polarization at the HH exciton of quantum well show that quantum dot state is composed of the HH state while decrease of $\rho_c$ from 0.5 to 0.4 at the quantum dot state may contain the LH state of the quantum well.

## IV. EXCITON QUANTUM BEATS IN THE LONGITUDINAL MAGNETIC FIELD

The sample was mounted in a cryostat with a superconducting magnet at 5 K for the magneto-optic study. The direction of an external magnetic field is along the epitaxial growth direction. For the measurement of time-resolved photoluminescence, 2-ps pulses from a mode-locked Ti:sapphire laser were used for the excitation at the repetition rate of 82 MHz. The excitation and detection paths were along the magnetic field (Faraday configuration) and in opposite directions. The excitation pulses were linearly polarized. The luminescence components with linear polarization parallel ($\parallel$) or perpendicular ($\perp$) to that of the excitation laser were selected by a half wave plate and a linear polarizer. The luminescence was dispersed by a 25-cm subtractive-dispersion double monochromator and detected by a synchroscan streak camera. The typical time resolution of the system was $\sim$10 ps.

The excitation energy was carefully selected based on the PLE spectrum in Fig. 1. When the excitation energy is above the quantum well, the luminescence intensity of the QD1 band is high and most of quantum dots show luminescence, as is shown by a solid line in the inset of Fig. 2. This condition is not favorable for observation of the quantum beats because luminescence of quantum dots is inhomogeneously broadened. When the excitation energy is below the quantum well, the luminescence intensity of QD1 is reduced, because the light absorption by a selected ensemble of quantum dots is much weaker than the light absorption either by a quantum well or by a thicker barrier layer. However, in this case, narrow-band picosecond pulses site selectively excite an ensemble of quantum dots of almost the same size. The fast LO-phonon-mediated relaxation makes sharp sideband luminescence of site-selectively excited quantum dots. In the Faraday configuration, luminescence was detected at $E_{det}$ under

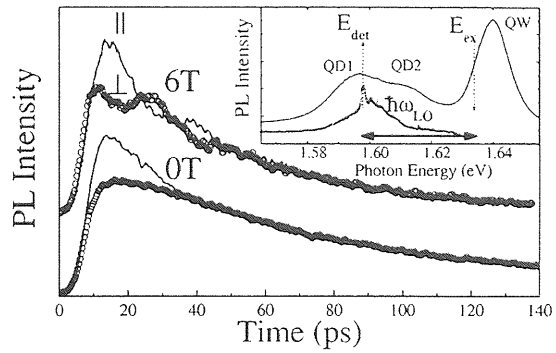


FIG. 2. Time-resolved photoluminescence profiles of strain-induced GaAs quantum dots (well width=3.9 nm) with co- and cross-linear polarization at 0 T and 6 T. The solid curves (circles) show the co-(cross-)linear polarization component of luminescence. The inset shows selectively excited luminescence spectrum (circles) and luminescence spectrum excited above the barrier (solid line). $E_{ex}$ and $E_{det}$ show the excitation and detection energies for time-resolved photoluminescence measurements (dotted arrows). The difference of these energies corresponds to the LO phonon.

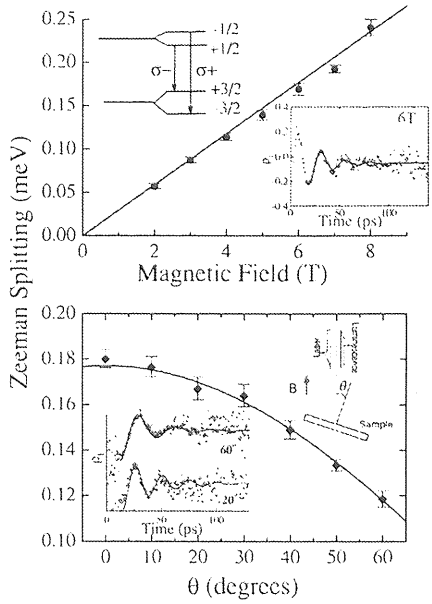


FIG. 3. Upper panel: The observed Zeeman splitting (closed circles) of strain-induced GaAs quantum dots (well width=3.9 nm) as a function of magnetic field $B$. The well-fitted straight line shows that $g$ factor is 0.51. The inset shows temporal change in the degree of linear polarization at $B=6$ T (open circles) and a fitting damped oscillation (a solid curve) with $2\pi/\omega=24$ ps and $\tau=20$ ps. A scheme shows optical transitions between Zeeman components of electrons and heavy holes composing the QD1 state. Lower panel: The angular dependence of the Zeeman splitting of strain-induced GaAs quantum dots at $B=6$ T (diamond) and its fitting by $\mu_B B(0.34\cos\theta+0.17)$. The inset shows the degree of polarization at $\theta=20°$ and $\theta=60°$. Fitted damped oscillations have parameters $2\pi/\omega=24.3$ ps and $\tau=30$ ps, for $\theta=20°$ and parameters $2\pi/\omega=34.5$ ps and $\tau=24$ ps, for $\theta=60°$.

the excitation at the QD1 energy plus the LO-phonon energy, $E_{ex}=E_{det}+\hbar\omega_{LO}$ (see the inset in Fig. 2).

Time traces of luminescence under magnetic field of $B=0$ T and $B=6$ T are shown in Fig. 2. The solid trace was measured at parallel linear polarization. The trace plotted by circles was measured at perpendicular polarization. At $B=0$ T, the polarization decay time is about 15 ps. The photoexcited electron-hole pairs immediately relax to the QD1 state by emitting LO phonon, and then they recombine. The intensity of parallel linear polarization component corresponds to the number of carriers that conserve the polarization memory in the LO-phonon relaxation. The difference of two curves shows that the initial degree of linear polarization $\rho_l=(I_{\parallel}-I_{\perp})/(I_{\parallel}+I_{\perp})$ is ~0.2. When a magnetic field is applied, a damping oscillation structure appears upon the decay profile. The parallel component at $B=6$ T decreases faster than that at $B=0$ T and is followed by damped oscillations. Still more dramatic changes were observed on the perpendicular linear component. After the quick rise around $t\sim12$ ps, the remarkable oscillation appeared. The parallel and perpendicular linear polarization traces are antiphase and they coincide after 60 ps. Excitataion by circular polarization did not induce the oscillation of luminescence. These polarization selection rules for the observation of the oscillation in the Faraday geometry suggest the quantum beat of bright excitons.[6] Linearly polarized light which is the superposition of right-handed and left-handed circularly polarized light excites both of the Zeeman-splitted bright excitons coherently and the quantum interference of the bright excitons shows quantum beat. Another excitonic quantum beat between bright exciton and dark exciton is observed for co-linear and co-circular polarization under the magnetic field tilted from the longitudinal direction and does not hold true in the observed quantum beat here.[12]

The degree of linear polarization was analyzed by varying the magnetic field. For the analysis, degree of linear polarization was fitted by formula $\rho_l=\exp(-t/\tau)\sin(\omega t)$, where $\omega$ means the angular frequency of the oscillation and $\tau$ means its damping time constant. The fitted result is displayed in the inset of the upper panel of Fig. 3 for the magnetic field of $B=6$ T. The solid curve is the fitted function with $2\pi/\omega=24$ ps and $\tau=20$ ps. The period of the beats decreased with increasing magnetic field. The energy splitting corresponding to inverse of the beat period is proportional to the magnetic field, as is shown in the upper panel of Fig. 3. The obtained splitting is much smaller than the laser linewidth (0.7 meV). From the absolute value of splitting and its linear dependence on the magnetic field, the beat is attributed to the quantum interference of bright excitons caused by the Zeeman splitting and the $g$ factor of bright excitons in the quantum dots is determined to be 0.51.

Further, the beat period was investigated in the Faraday configuration as a function of the angle between the magnetic field and the growth direction, as is shown at the lower panel of Fig. 3.

If the electron-hole exchange energy is much smaller than the electron Zeeman splitting,[19] the spin Hamiltonian of the electron-heavy-hole pair in the GaAs qunatum structures under a magnetic field gives the simple expression for the en-

ergy splitting of bright excitons, $E_1 - E_2 = \Delta E_{12}$, represented by[20]

$$\Delta E_{12} = \mu_B B(g_{h\parallel}\cos\theta + \sqrt{g_{e\parallel}^2\cos^2\theta + g_{e\perp}^2\sin^2\theta}), \quad (1)$$

where $g_{h\parallel}$ ($g_{e\parallel}$) is the $g$ factor of the hole (electron) for the magnetic field parallel to growth direction, $g_{e\perp}$ is the $g$ factor of the electron for the magnetic field perpendicular to the growth direction, and $\theta$ is the angle between the direction of magnetic field $B$ and the crystal growth axis, under the assumption that $g_{h\perp}$ is much smaller than $g_{h\parallel}$. The assumption is verified for the GaAs quantum well,[8] where $|g_{h\perp}|$ is measured to be 0.04 and is comparable to 1/50 of $g_{h\parallel}$. Because anisotropy is very large in GaAs quantum well, relation $g_{h\perp} \ll g_{h\parallel}$ is expected to hold for the strain-induced GaAs quantum dots where the lateral size is much larger than the height. As is shown in the following independent experiment in the Voigt configuration, electrons in the strain-induced GaAs quantum dots have isotropic $g$ factor $g_e$ and Eq. (1) is simplified to be $\Delta E_{12} = \mu_B B(g_{h\parallel}\cos\theta + g_e)$. By using the expression, the angle dependence of the energy splitting is well fitted, as is shown in the lower panel of Fig. 3. Here, we assumed that the lowest QD1 band mainly comes from heavy-hole exciton luminescence. The $g$ factors for exciton, electron, and hole obtained are 0.51, 0.17, and 0.34, respectively.

## V. ELECTRON QUANTUM BEATS IN THE TRANSVERSE MAGNETIC FIELD

Another type of quantum beats of the strain-induced GaAs dots coming from the electron Larmor precession was observed not only for the site-selective excitation of quantum dots but also for the excitation at the quantum well absorption in the Voigt configuration. The co- and cross-circular polarization components were selected by using a quarter-wave plate and were detected by the same experimental system that was used in the Faraday configuration. Under the high magnetic field above $B = 5$ T, the periodic oscillation appeared in the time trace, as is shown by the bottom traces (QD 0°) for strain-induced GaAs quantum dots (well width =3.9 nm) in Fig. 4. Here, the circularly polarized laser pulse excited the quantum dots and the LO-phonon sideband luminescence in the QD1 band was observed. The crystal-growth axis is perpendicular to the direction of the magnetic field and is parallel to the direction of the incident laser light. In the Voigt configuration, $\theta'$ denotes the angle between the crystal-growth axis and the direction of the incident laser light. Because of the circular polarization selection rule for the observation of the oscillation in the Voigt configuration, the periodic oscillation was thought to be originated from the quantum beat of electron Larmor precession. The electron Zeeman splitting $\Delta E_{e0°}$ is given by

$$\Delta E_{e0°} = g_{e\perp}\mu_B B. \quad (2)$$

We estimated $g_{e\perp}$ to be 0.17 by equating the oscillation period to $2\pi\hbar/g_{e\perp}\mu_B B$. The positive sign of this value is determined by knowing that the well-width dependent $g$ factor of electrons discussed in the following and that the electron $g$ factor monotonously increases with the decrease of the volume ratio of GaAs in GaAs-AlGaAs quantum structures from the electron $g$ factor of -0.44 in bulk GaAs.[21–25] Value $g_{e\perp}$ nicely agrees with the electron $g$ factor obtained in the Faraday configuration. The periodic oscillations were also observed in the luminescence time trace of the quantum well, as is typically shown by the second top traces (QW 0°) for a GaAs quantum well (well width=2.4 nm) in Fig. 4. The oscillation period for the quantum well was found to be shorter than that for the quantum dots in the same sample, although the quantum dots are formed in the quantum well by the strain. These results clearly show that $g_{e\perp} = 0.17$ for the quantum dots is smaller than $g_{e\perp} = 0.225$ for the quantum well in the same sample whose GaAs well width is 3.9 nm.

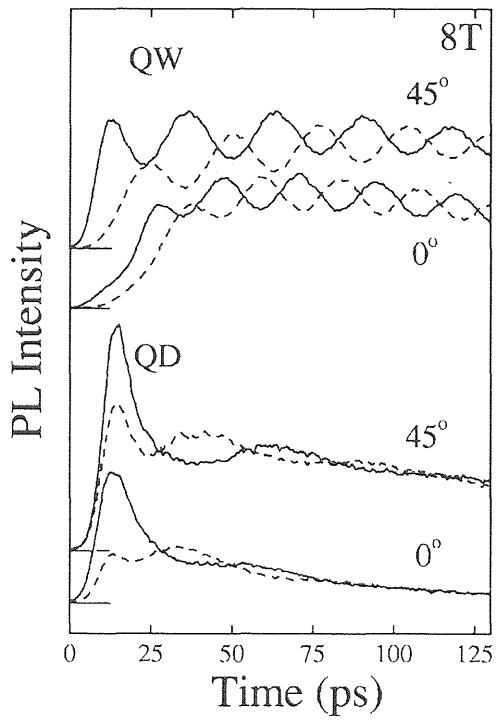


FIG. 4. Luminescence quantum beats of strain-induced GaAs quantum dots labeled by QD (well width=3.9 nm) and a GaAs quantum well labeled by QW (well width=2.4 nm) coming from electron spin precession observed in the Voigt configuration for $\theta' = 0°$ and 45° at $B = 8$ T. Solid and dashed lines show co- and cross-components of circular polarized luminescence.

For the measurement of the electron $g$ factor parallel to the sample growth direction ($g_{e\parallel}$), the crystal was rotated by 45°. The luminescence oscillations observed in this geometry are shown by the top traces (QW 45°) and the second bottom traces (QD 45°) in Fig. 4. Compared with the oscillation period observed at $\theta' = 0°$, the oscillation period observed at $\theta' = 45°$ is longer for the quantum well. On the other hand, the oscillation period does not change between $\theta' = 45°$ and $\theta' = 0°$ for the quantum dots. When the crystal is rotated to $\theta' = 45°$, the electron Zeeman splitting is given by[22]

$$\Delta E_{e45°} = \mu_B B\sqrt{(g_{e\parallel}^2 + g_{e\perp}^2)/2}. \quad (3)$$

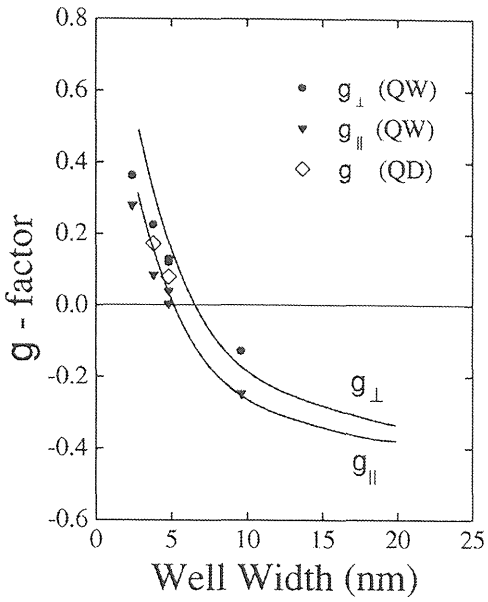


FIG. 5. Well-width dependence of the electron $g$ factor in strain-induced GaAs quantum dots and GaAs quantum wells. Electron $g$ factors $g_{\parallel}$ and $g_{\perp}$ were derived from quantum beats of electron Larmor precession for two angles between the magnetic-field and the crystal-growth direction, $\theta'=0°$ and $\theta'=45°$, in the Voigt configuration. Circles and triangles represent $g_{\perp}$ and $g_{\parallel}$ of electrons in quantum wells, respectively. Samples having two kinds of dots and three kinds of single quantum wells are used for the experiments. Diamonds represent $g$ factor of electrons in quantum dots. Solid lines show calculated $g_{\parallel}$ and $g_{\perp}$ of electrons in a single quantum well in the Kane model (Ref. 21).

From the measured oscillation period at $\theta'=45°$, $g_{e\parallel}$'s of quantum dots and a quantum well in the sample were derived by using Eq. (3) and the $g_{e\perp}$'s of electrons in quantum dots and a quantum well from the measured oscillation period at $\theta'=0°$. The $g_{e\parallel}$'s of quantum dots and a quantum well in the sample were 0.17 and 0.09, respectively, for the sample whose well width is 3.9 nm. The $g_{e\parallel}$ is equal to the $g_{e\perp}$ in quantum dots, although $g_{e\parallel}$ and $g_{e\perp}$ of a quantum well were different from each other. This indicates the isotropic $g$ factor for electrons in dots, in spite of anisotropic $g$ factor for electrons in the well in the same sample. Isotropic $g$ factor for electrons in dots was also observed in another strain-induced GaAs quantum dots formed in the GaAs well 4.8-nm thick. In two kinds of strain-induced GaAs quantum dots 3.9-nm or 4.8-nm high, electron $g$ factors in dots are average values of $g_{e\parallel}$ and $g_{e\perp}$ of electron in the same quantum wells, although $g_{e\parallel}$ and $g_{e\perp}$ of electron in the quantum wells strongly depend on the well width, as is shown in Fig. 5. Electron $g$ factors of GaAs quantum wells increase from a negative value to postive ones with the decrease in the well width. The observed well-width dependence agrees well with the previous reports.[22–24] The observed well-width dependence is well interpreted by the **k·p** perturbation theory.[21]

Anisotropic $g$ factor of electrons in quantum wells has been investigated extensively.[24] Its expression is given by the **k·p** perturbation theory and the physical origin for the anisotropic $g$ factor of conduction electron comes from the different optical selection rule for heavy hole to electron and light hole to electron transitions.[21] Anisotropic $g$ factors of conduction electron in GaAs quantum wells are described by[21]

$$g_{e\perp}-g_{e\parallel}=\frac{2p_{cv}^2}{m_0}\left[\frac{1}{E_g+E_{e1}+E_{hh1}}-\frac{1}{E_g+E_{e1}+E_{lh1}}\right], \tag{4}$$

where $p_{cv}$ is the transition matrix element between the valence band and the conduction band, $m_0$ is the bare electron mass, $E_g$ is the band-gap energy, and $E_{e1}$, $E_{hh1}$, and $E_{lh1}$ are size-quantized energies of electron, heavy hole, and light hole, respectively. The calculated anisotropic $g$ factor for electrons in quantum wells nicely explains the observed anisotropy. The anistropy is reduced if quantized energy of heavy hole and that of light hole approach each other in Eq. (4).

Strain effect on quantum wells can be analyzed by using the deformation potentials. The tensile strain formed by InP stressors on the $Al_{0.3}Ga_{0.7}As$ surface causes hydrostatic deformation potential $(2/3)\delta E_{hy}$ to the conduction electron, hydrostatic deformation potential $(1/3)\delta E_{hy}$ minus shear deformation potential $(1/2)\delta E_{sh}$ to the heavy hole, and hydrostatic deformation potential $(1/3)\delta E_{hy}$ plus shear deformation potential $(1/2)\delta E_{sh}$ to the light hole.[26] As a result, two-dimensional parabolic potential well is formed laterally in the well for electron, heavy hole, and light hole, and potential wells for light hole and heavy hole approach to each other. Based on parameters listed in Ref. 26, ratio $\delta E_{hy}/\delta E_{sh}$ is calculated to be 2.18. From the observed red-shift of the energy of strain-induced quantum dots from the energy of the heavy-hole exciton peak of the quantum well, $\delta E_{hy}-(1/2)\delta E_{sh}$ is evaluated to be 43 meV. Therefore, $\delta E_{hy}$ and $\delta E_{sh}$ are obtained to be 55.8 meV and 25.6 meV, respectively. Although the energy splitting between heavy hole and light hole in the quantum well is 27 meV which is seen at the middle panel of Fig. 1, the reduction in the energy splitting in strain-induced quantum dots is estimated to be $\delta E_{sh}=25.6$ meV. We believe the isotropic $g$ factor for the electron in the strain-induced GaAs quantum dots comes from the partial overlapping of the heavy-hole band and the light-hole band split once in the quantum well by the quantum confinement effect. Further study may be necessary to confirm the partial overlapping of the heavy-hole band and the light-hole band in the strain-induced GaAs quantum dots. In a spherical GaAs quantum dots, theory predicted the isotropic $g$ factor for the electron.[25] This is another possible explanation of the isotropic $g$ factor for the electron in the strain-induced GaAs quantum dots. However, we cannot simply use this theory because the shape of strain-induced GaAs quantum dots is far from the sphere and because the vertical confinement is much stronger than the lateral confinement. We consider this is a possible explanation but strain effect is much plausible in the strain-induced GaAs quantum dots. This problem needs further study.

## VI. CONCLUSIONS

In summary, two kinds of luminescence quantum beats of the strain-induced GaAs quantum dots were observed in the magnetic field parallel and perpendicular to the growth direction. Quantum beat of bright excitons showing Zeeman splitting and quantum beat coming from electron Larmor precession were observed. The oscillation period in the quantum beat of bright excitons observed under the longitudinal magnetic field depends on the angle between the growth direction of the crystal and the magnetic field. Analysis based on the spin Hamiltonian for excitons explains the observed data and gives $g$ factors 0.51, 0.17, and 0.34 to the exciton, electron, and heavy hole, respectively. Quantum beats coming from electron Larmor precession were observed under the transverse magnetic field. The isotropic electron $g$ factor is observed in the dots in contrast to the anisotropic electron $g$ factor for the corresponding quantum well and is ascribed to the strain-induced opposite energy shift of heavy- and light-hole bands. The quantum beats give us unique and fine information on not only spin structure but also energy structure of quantum dots.

## ACKNOWLEDGMENTS

Authors thank Dr. I. V. Ignatiev and Dr. S. Verbin at Institute of Physics, St.-Petersburg State University for the collaboration at the initial stage of the quantum beat measurements. This work was partially supported by Grand-in-Aid for Scientific Research No. 13852003 from the Ministry of Education, Sports, Culture, Science and Technology of Japan.

*Electronic address: shoichi@sakura.cc.tsukuba.ac.jp; URL http://www.first.tsukuba.ac.jp/~masumoto

†Present address: Applied Optronics Incorporation, 13111 Jess Pirtle Boulevard, Sugar Land, Texas 77478, USA.

[1] D. Loss and D.P. DiVincenzo, Phys. Rev. A **57**, 120 (1998).

[2] A.P. Heberle, W.W. Rühle, and K. Ploog, Phys. Rev. Lett. **72**, 3887 (1994).

[3] J.M. Kikkawa and D.D. Awschalom, Phys. Rev. Lett. **80**, 4313 (1998).

[4] A.V. Khaetskii and Y.V. Nazarov, Phys. Rev. B **61**, 12 639 (2000).

[5] J. Shah, *Ultrafast Spectroscopy of Semiconductors and Semiconductor Nanostructures* (Springer-Verlag, Berlin, 1996), p. 63.

[6] S. Bar-Ad and I. Bar-Joseph, Phys. Rev. Lett. **66**, 2491 (1991).

[7] T. Amand, X. Marie, P. Le Jeune, M. Brousseau, D. Robart, J. Barrau, and R. Planel, Phys. Rev. Lett. **78**, 1355 (1997).

[8] X. Marie, T. Amand, P. Le Jeune, M. Paillard, P. Renucci, L.E. Golub, V.D. Dymnikov, and L.E. Ivchenko, Phys. Rev. B **60**, 5811 (1999).

[9] V.K. Kalevich, M.N. Tkachuk, P. Le Jeune, X. Marie, and T. Amand, Phys. Solid State **41**, 789 (1999).

[10] T. Flissikowski, A. Hundt, M. Lowisch, M. Rabe, and F. Henneberger, Phys. Rev. Lett. **86**, 3172 (2001).

[11] I.E. Kozin, V.G. Davydov, I.V. Ignatiev, A.V. Kavokin, K.V. Kavokin, G. Malpuech, H.-W. Ren, M. Sugisaki, S. Sugou, and Y. Masumoto, Phys. Rev. B **65**, 241312(R) (2002).

[12] I.A. Yugova, I.Ya. Gerlovin, V.G. Davydov, I.V. Ignatiev, I.E. Kozin, H.W. Ren, M. Sugisaki, S. Sugou, and Y. Masumoto, Phys. Rev. B **66**, 235312 (2002).

[13] H. Lipsanen, M. Sopanen, and J. Ahopelt, Phys. Rev. B **51**, 13868 (1995).

[14] J. Tulkki and A. Heinamaki, Phys. Rev. B **52**, 8239 (1995).

[15] S. Grosse, J.H.H. Sandmann, G. von Plessen, J. Feldmann, H. Lipsanen, M. Sopanen, J. Tulkki, and J. Ahopelto, Phys. Rev. B **55**, 4473 (1997).

[16] R. Rinaldi, P.V. Giugno, R. Cingolani, H. Lipsanen, M. Sopanen, J. Tulkki, and J. Ahopelto, Phys. Rev. Lett. **77**, 342 (1996).

[17] K. Nishibayashi, T. Okuno, T. Mishina, S. Sugou, H.-W. Ren, and Y. Masumoto, Jpn. J. Appl. Phys., Part 1 **40**, 2084 (2001).

[18] C. Weisbuch, R.C. Miller, R. Dingle, A.C. Gossard, and W. Wiegmann, Solid State Commun. **37**, 219 (1981).

[19] The electron-hole exchange interaction $\delta$ was estimated by the magnetic-field-dependent electron quantum beat in the Voigt configuration. The electron Zeeman splitting $\Delta E_{e0^\circ}$ is given by $\Delta E_{e0^\circ} = \sqrt{\delta^2 + (g_{e\perp}\mu_B B)^2}$, if the electron-hole exchnage interaction $\delta$ is not neglected as shown in Eq. (2). Plotting the magnetic-field-dependent electron Zeeman splitting, we found that the electron-hole exchange interaction $\delta$ is smaller than 0.01 meV which is comparable with the electron Zeeman splitting at 1 T. The electron-hole exchnage interaction is negligibly smaller than the electron Zeeman splitting at 6 T.

[20] I.Ya. Gerlovin, Yu.K. Dolgikh, S.A. Eliseev, V.V. Ovsyankin, Yu.P. Efimov, V.V. Petrov, I.V. Ignatiev, I.E. Kozin, and Y. Masumoto, Phys. Rev. B **65**, 035317 (2001).

[21] E.L. Ivchenko and A.A. Kiselev, Fiz. Tekhn. Poluprovodn. **26**, 1471 (1992) [Sov. Phys. Semicond. **26**, 827 (1992)].

[22] P. Le Jeune, D. Robart, X. Marie, T. Amand, M. Brousseau, J. Barrau, V. Kalevich, and D. Rodichev, Semicond. Sci. Technol. **12**, 380 (1997).

[23] M.J. Snelling, E. Blackwood, C.J. McDonagh, R.T. Harley, and C.T.B. Foxon, Phys. Rev. B **45**, 3922 (1992).

[24] R.M. Hannak, M. Oestreich, A.P. Herberle, W.W. Rühle, and K. Köhler, Solid State Commun. **93**, 313 (1995).

[25] A.A. Kiselev, E.L. Ivchenko, and U. Rössler, Phys. Rev. B **58**, 16353 (1998).

[26] S.L. Chuang, Phys. Rev. B **43**, 9649 (1991).

PHYSICAL REVIEW B **68**, 113305 (2003)

# Longitudinal optical phonons in the excited state of CuBr quantum dots

Jialong Zhao,* Atsushi Kanno, Michio Ikezawa, and Yasuaki Masumoto
*Institute of Physics, University of Tsukuba, Tsukuba 305-8571, Japan*
(Received 12 May 2003; published 24 September 2003)

The size dependence of the longitudinal optical (LO) phonons in the excited state of CuBr quantum dots (QD's) in glass and NaBr crystals in the intermediate confinement regime was studied by means of persistent spectral hole burning spectroscopy. The phonon-exciton coupled states were clearly observed at a photon energy of about 2.993 eV when the LO phonon energy is close to the energy difference between the ground $1S$ and excited $1P$ states of CuBr QD's in glass. The energies of the LO phonons observed in smaller CuBr QD's in glass and NaBr crystals were determined to be about 18.6 and 17.6 meV, respectively, which are smaller than that of LO phonons in the bulk CuBr material. The energy softening of the LO phonons was explained in terms of the phonon renormalization.

DOI: 10.1103/PhysRevB.68.113305 PACS number(s): 68.65.−k, 63.22.+m, 61.46.+w, 71.35.−y

The elementary excitations of small quantum dots (QD's) containing a few hundreds of atoms are expected to modify the lattice vibrational frequencies due to the carrier confinement and resulting strong exciton-phonon interaction similar to the lattice vibrations in the excited state of many molecules and localized centers in solids.[1] The modification of the vibrational frequency in the electronic excited state of small-sized QD's is so unique that the QD's show a characteristic of the molecular nature. Recently, the energy softening of the longitudinal optical (LO) phonon by 8% was observed in persistent spectral hole burning (PSHB) and resonant photoluminescence spectra of 2.5-nm-radius CuCl QD's, typical QD's in the weak confinement regime.[2–4] In contrast to the 25.6-meV LO phonon in the ground state observed in Raman scattering and resonant photoluminescence spectra, a 23.5-meV LO phonon was observed in the excited state of CuCl QD's in glass by means of PSHB and resonant photoluminescence. The exciton-phonon coupled states were clearly observed as a result of strong Fröhlich interaction both in quantum spheres and quantum cubes when the energy of the LO phonon is close to the energy spacings between the ground and excited exciton quantum states.[2,4] The LO phonon softening in the excited state of CuCl QD's was also observed by means of quantum beats in the time domain[5] and two-photon-excited resonant luminescence in the spectral domain.[6] Theoretically, the energy softening was described in terms of the phonon renormalization in the presence of a single exciton in spherical QD's.[2,6,7] The theory predicted further the LO phonon renormalization in the excited QD's not only in the weak confinement regime but also in the strong confinement regime.[6,8]

Besides CuCl QD's,[9–13] CuBr QD's are another typical class of semiconductor nanomaterials for studying the quantum confinement effects of the exciton translational motion[14–17] and cataloged to the intermediate confinement regime on the basis of the ratio of the dot radius to the Bohr radius. LO phonon modes in the CuBr bulk material and QD's have been extensively studied by Raman scattering and site-selective luminescence spectra.[18–23] Up to now, the size-dependent excited states of the $Z_{1,2}$ excitons in CuBr QD's have not been studied yet. Fortunately, the PSHB phenomenon has been observed in CuBr nanocrystals,[24–26] and therefore it provides a sensitive site-selective tool for studying the size-dependent exciton states and phonon modes as well as the formed exciton-phonon coupled states in CuBr QD's.

In this Brief Report, we extend the study of phonon softening to QD's in the intermediate confinement regime from QD's in the weak confinement regime. We study in detail the LO phonons and exciton states for CuBr QD's embedded in glass and NaBr crystals in the weak and intermediate confinement regimes by means of PSHB spectroscopy. We successfully found the mixing of the LO phonon with exciton when the energy of the LO phonon approaches the energy spacings between the ground and excited states for CuBr QD's in glass and the energy softening of LO phonons experimentally for CuBr QD's in glass and NaBr crystals.

Samples used in the experiment were CuBr QD's embedded in glass or NaBr crystals. The average size of the QD's was estimated by small-angle x-ray scattering (SAXS) and transmission electron microscopy (TEM).[27] The samples were directly immersed in superfluid helium at 2 K in an optical cryostat. A narrow-band dye laser pumped by the third harmonics of the output of a $Q$-switched $Nd^{3+}$: YAG laser (355 nm) was used as a pump source. The pulse duration and repetition rate were 5 ns and 30 Hz, respectively. The spectral linewidth was about 0.014 meV. A halogen lamp was used as a probe source. The PSHB spectrum was measured as follows: First, the absorption spectrum was obtained and the sample was exposed to dye laser pulses to burn a persistent spectral hole at excitation energy. Then, the absorption spectrum was measured again after the laser exposure was stopped. The absorption spectral change $-\alpha d$ is defined as the difference between the spectra before and after the laser exposure. The transmitted light of the samples was detected by a liquid-nitrogen-cooled charge-coupled device in conjunction with a 75-cm spectrometer involving a 1800-grooves/mm grating operated in the first order of diffraction. The spectral resolution of the experiment for PSHB spectroscopy was about 0.3 meV.

Quantum size effect on the $Z_{1,2}$ exciton in CuBr QD's was observed in independent works, although the size dependence of the $Z_{1,2}$ exciton in CuBr QD's in glass, alkali halides, and polymers are slightly different from each

 

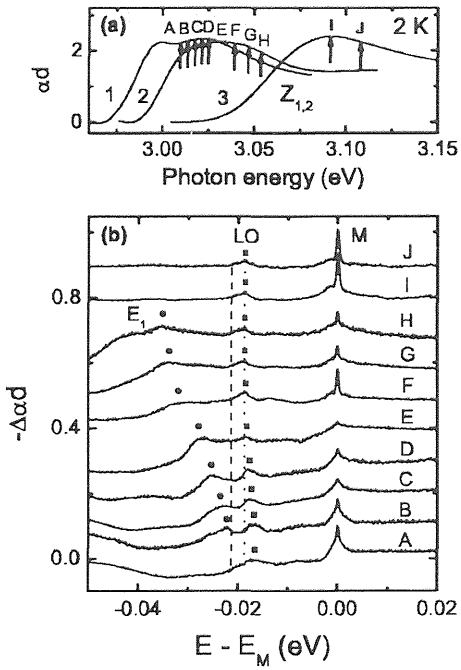


FIG. 1. Absorption (a) and PSHB spectra (b) of CuBr QD's in glass. The average radii for samples 1, 2, and 3 are 10.5, 5.0, and 2.4 nm. The excitation energies for spectra A, B, C, D, E, F, G, H, I, and J are 3.0094, 3.0130, 3.0167, 3.0203, 3.0242, 3.0388, 3.0463, 3.0537, 3.0916, and 3.1073 eV, respectively. The excitation density is 100 nJ/cm$^2$ and the exposure time is 5 min. The solid and dotted lines in (b) represent the energies of the LO phonons in the ground and excited states of the excitons in smaller CuBr QD's.

other.[14–17] We investigated the size dependence of the $Z_{1,2}$ exciton in CuBr QD's[27] and the relation is very close to that reported for CuBr QD's in glass,[17] which is phenomenologically described by a relation[17] $E_{n,l}=E_B+\hbar^2\pi^2\xi_{n,l}^2/(2MR^2)+A/R$, where $E_B=2.964$ eV is the $Z_{1,2}$ exciton energy of a bulk CuBr crystal at 2 K, $M=2.6\ m_0$ is the translational mass of the $Z_{1,2}$ exciton, $R$ and $a_B$ are the dot and the Bohr radius, $\pi\xi_{n,l}$ is the $n$th root of the spherical Bessel function of the $l$th order,[10,11] and $A$ is a factor. Theoretical treatment of QD's in the intermediate confinement regime shows that weak confinement model holds for the condition $R>4a_B$. On the simple weak confinement model, the size dependence of the energy spacing between the exciton states $1S$ and $1P$ in spherical CuBr QD's was simply estimated to be equal to the quantized energy of $1S$. In the following, we used this model because the anticrossing between LO phonon and $1S$-$1P$ energy split takes place in the large size region, $R>4a_B$.

The absorption and PSHB spectra of CuBr QD's in glass are shown in Figs. 1(a) and (b) at 2 K. As seen in Fig. 1(a), in comparison with the $Z_{1,2}$ exciton energy of the bulk CuBr, by decreasing the size of the QD's, the absorption band of CuBr QD's in glass is shifted to the high-energy side due to the quantum confinement effect. Further the exciton absorption band of bigger CuBr QD's in glass is found to be split into two peaks probably due to the strain effect. It is clearly noted that the $Z_{1,2}$ exciton absorption band of CuBr QD's is inhomogeneously broadened. This shows that the discrete nature of the exciton states and phonon modes is hidden under the inhomogeneously broadened absorption profile of the CuBr QD's due to the wide distributions in size and shape.

As seen in Fig. 1(b), a sharp main hole marked by M with asymmetric acoustic-phonon sidebands is burnt resonantly at the excitation energy. The energy of the LO phonon hole for smaller CuBr QD's was estimated to be about 18.6 meV. The energies of the LO and transverse-optical (TO) phonons in the bulk CuBr material are 21.1 and 17.0 meV, respectively, which were measured by Raman scattering.[18] Recently, by resonant Raman scattering,[19–22] the energy of LO phonon in the CuBr QD's in glass was measured to be 20.3 meV, which was almost the same as that of the bulk CuBr crystal. The energy of the LO phonon side bands for small 2.4-nm-radius CuBr QD's in glass was found to be lower than that of the bulk CuBr crystal by 2.5 meV (12%). The LO phonon softening observed in CuBr QD's by the PSHB spectroscopy is considered as the LO phonon renormalization in the presence of a single exciton in spherical QD's, in analogy with the LO phonon softening observed in CuCl QD's.[2–6] Phonons observed in the PSHB spectroscopy are unique, because it selectively probes the optical phonons in the electronic excited states as a pseudophonon wing at low temperatures.[2] On the other hand, resonant luminescence observes the optical phonons both in the electronic excited states and in the electronic ground state, and Raman scattering observes the optical phonons in the electronic ground state. The PSHB spectroscopy is superior to others. As seen in Fig. 1(b), a satellite hole marked by $E_1$ was observed in the PSHB spectra of larger size dots. The Stokes shift of the satellite hole is almost equal to half of the energy separation between the excitation photon energy and the bulk $Z_{1,2}$ exciton energy. It becomes small gradually when the dot size increases. Thus the satellite hole is considered to come from the hole burning of the ground state ($1S$) under excitation of the first excited state ($1P$) of the quantum confined excitons in the nearly spherical CuBr QD's.

Figure 2 shows the Stokes shifts of the LO phonon and satellite hole $E_1$ as a function of the photon energy of the satellite holes. As seen in Fig. 2, the holes $E_1$ and LO become close to each other when the dot size is increased. When the LO phonon energy of CuBr QD's in glass approaches the energy difference between the $1S$ and $1P$ exciton states, the LO phonon energy clearly shows an anticrossing with the Stokes shift of the hole $E_1$ at an energy of about 2.993 eV. We consider $1P$ exciton states can be excited and relaxed to $1S$ exciton state with the emission of LO phonon ($l=0$), because CuBr QD's are not perfectly spherical as shown in the TEM image. An anticrossing of the phonon energy with the energy separation between ground and excited state excitons is clearly observed in Fig. 2. The experimental result indicates that the interaction of the LO phonon with the exciton in CuBr QD's in glass results in the formation of the exciton-phonon coupled modes at exciton-phonon resonance, which is similar to those observed in CuCl QD's.[2–6] On the other hand, as seen in Fig. 2, the

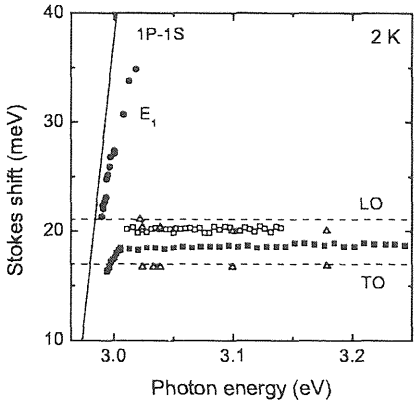


FIG. 2. Stokes shifts of the satellite holes $E_1$ (solid circles) and LO (solid squares) in CuBr QD's in glass as a function of photon energy of the satellite holes. The solid line shows the size dependence of the energy difference between exciton states $1S$ and $1P$. The dashed lines represent the energies of LO and TO phonons in a bulk CuBr crystal, respectively. The open squares and triangles show the energies of LO and TO phonons in CuBr QD's in glass, which were measured by Raman scattering (Refs. 19–22).

energies of LO phonons measured by PSHB spectroscopy are clearly smaller than those of LO phonons obtained by Raman scattering.[19–22]

The absorption and PSHB spectra of CuBr QD's in NaBr crystals are shown in Figs. 3(a) and (b) at 2 K. Unlike CuCl

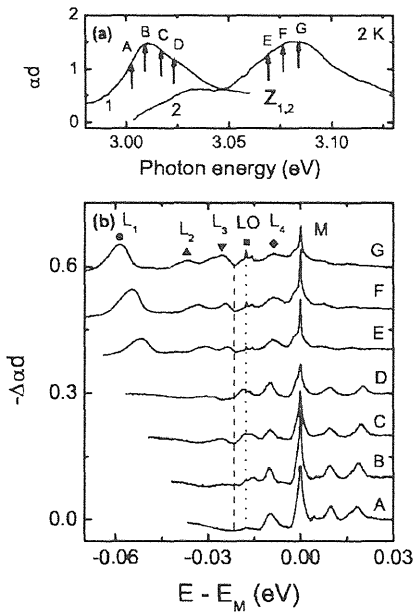


FIG. 3. Absorption (a) and PSHB spectra (b) of CuBr QD's in NaBr crystals. The average dot radii for samples 1 and 2 are 9.5 and 3.0 nm. The excitation energies for spectra A, B, C, D, E, F, and G are 3.0020, 3.0094, 3.0167, 3.0241, 3.0690, 3.0766, and 3.0843 eV, respectively. The excitation density is 100 nJ/cm$^2$ and the exposure time is 3 min. The solid and dotted lines in (b) represent the energies of the LO phonons in the ground and excited states of the excitons in smaller CuBr QD's.

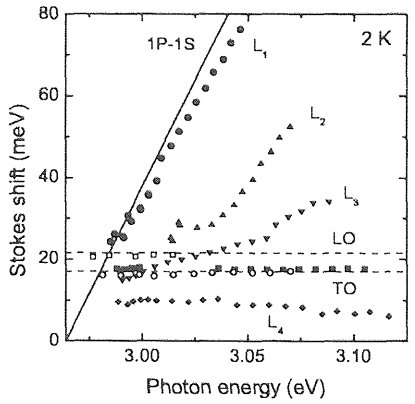


FIG. 4. Stokes shifts of the satellite holes $L_1$ (solid circles) and LO (solid squares) as a function of photon energy of the main hole structures. The solid line represents the energy spacing between the exciton states $1S$ and $1P$ in different sized CuBr QD's. The dashed lines show the LO and TO phonon energies in the bulk CuBr crystal. The open squares and circles show the energies of LO and TO phonons in CuBr QD's in NaBr crystals, which were measured by the site-selective luminescence.

QD's in NaCl crystals,[4,13] no clear oscillatory fine structure is observed in the absorption spectra of CuBr QD's in NaBr crystals. As seen in Fig. 3(b), many satellite holes are observed not only at the low-energy side but also at the high-energy side of the main hole M. The Stokes shift of the sharp LO phonon hole in CuBr QD's in NaBr crystals was determined to be about 17.6 meV, which is lower than the LO phonon energy in the bulk CuBr (21.1 meV) by 3.5 meV (17%) but larger than the TO phonon energy. As seen in Fig. 3(b), hole $L_1$ is a dominant satellite hole in the PSHB spectra. The Stokes shifts of the satellite holes $L_1$ and LO as a function of the photon energy of the satellite holes are plotted in Fig. 4. The Stokes shift of the hole $L_1$ is considered as the energy difference between the ground ($1S$) and excited ($1P$) states of the quantum confined exciton in CuBr QD's. If the energy of the LO phonon energy is close to the energy difference, the LO phonon is expected to mix with the excited state of the exciton, which should lead to the formation of the exciton-phonon coupled states. However, we have not observed the anticrossing behavior in large-sized CuBr QD's in NaBr crystals because we cannot distinguish many overlapped satellite and phonon holes. The exciton-phonon coupled states were clearly demonstrated only in CuCl QD's in NaCl crystals[4] and were not observed in CuBr QD's in NaBr crystals although the LO phonon softening was observed in both cases. Further, we measured the site-selective luminescence spectra of CuBr QD's in NaBr crystals at 2 K, in comparison with the energy change of the LO and TO phonons in CuBr QD's. Some exciton state-related and LO and TO phonon-assisted luminescence bands were clearly observed in the spectra. The energies of LO and TO phonons in CuBr QD's in NaBr crystals as shown in Fig. 4 are consistent with those in the bulk CuBr material.[18] In addition, it is noted that the many satellite holes from the exciton states were observed in CuBr QD's in NaBr crystals but not in glass, which are similar to those in CuCl QD's in NaCl crys-

tals and glass.[4,13] The reason for this difference possibly results from the QD shape-induced modification of the one-photon selection rules. The Stokes shifts of the satellite holes $L_2$ and $L_3$ may be related to the energy spacings between the higher exciton states in CuBr QD's with different dot size. However, the phonon-exciton coupled states could not be formed when the LO phonon energy of the ground exciton state $1S$ is close to these energy spacings.

In summary, we have studied the LO phonons in the excited state of CuBr QD's in glass and NaBr crystals. The phonon-exciton coupled states were clearly observed in CuBr QD's in glass when the LO phonon energy is close to the energy difference between the ground and the first excited states. The energy softening of the LO phonons observed in CuBr QD's was explained in terms of the phonon renormalization with the exciton. These observations of LO phonon softening together with our previous results in CuCl QD's indicate the universality of LO phonon softening in small-sized QD's.

One of the authors (J.Z.) would like to thank Dr. A. V. Fedorov and Dr. J. Qi for their valuable discussions. SAXS experiments were done by the approval of the Photon Factory (PF) Advisory Committee (Proposal No. 2002G218). This work was partially supported by a Grant-in-Aid for Scientific Research No. 13852003 from the Ministry of Education, Science, Sports and Culture of Japan.

*Present address: Institute of Physical Chemistry, University of Mainz, Welderweg 11, D-55099 Mainz, Germany.

[1] S. Nakajima, Y. Toyozawa, and R. Abe, *The Physics of Elementary Excitations* (Springer, Berlin, 1980).

[2] L. Zimin, S.V. Nair, and Y. Masumoto, Phys. Rev. Lett. **80**, 3105 (1998).

[3] A.V. Baranov, S. Yamauchi, and Y. Masumoto, J. Lumin. **87-89**, 500 (2000).

[4] J. Zhao, S.V. Nair, and Y. Masumoto, Phys. Rev. B **63**, 033307 (2001).

[5] H. Ohmura and A. Nakamura, Phys. Rev. B **59**, 12 216 (1999).

[6] A.V. Fedorov, A.V. Baranov, A. Itoh, and Y. Masumoto, Fiz. Tekhn. Poluprovodn. **35**, 1452 (2001) [Semiconductors **35**, 1390 (2001)].

[7] S.V. Nair and Y. Masumoto, Jpn. J. Appl. Phys., Part 1 **38**, 581 (1999).

[8] S.V. Nair, L. Zimin, and Y. Masumoto, *Proceedings of the 24th International Conference on Physics of Semiconductors*, VII-B-63, pdf no. 463, Jerusalem, 1998.

[9] A.I. Ekimov and A.A. Onushchenko, Fiz. Tekhn. Poluprovodn. **16**, 1215 (1982) [Sov. Phys. Semicond. **16**, 775 (1982)].

[10] A.D. Yoffe, Adv. Phys. **42**, 173 (1993).

[11] U. Woggon, *Optical Properties of Semiconductor Quantum Dots* (Springer, Berlin, 1997).

[12] A.I. Ekimov, Al.L. Efros, and A.A. Onushchenko, Solid State Commun. **56**, 921 (1985).

[13] N. Sakakura and Y. Masumoto, Phys. Rev. B **56**, 4051 (1997).

[14] T. Itoh, Y. Iwabuchi, and T. Kirihara, Phys. Status Solidi B **146**, 531 (1988).

[15] A.I. Ekimov, Al.L. Efros, M.G. Ivanov, A.A. Onushchenko, and S.K. Shumilov, Solid State Commun. **69**, 565 (1989).

[16] M. Oda, M. Shen, M. Saito, and T. Goto, J. Phys.: Condens. Matter **13**, 11 465 (2001).

[17] A. Nakamura, M. Ohta, S. Sasaki, and M. Takata, J. Lumin. **72-74**, 370 (1997).

[18] *Physics of II-VI and I-VII Compounds, Semimagnetic Semiconductors*, edited by O. Madelung, M. Schulz, and H. Weiss, Landolt-Börnstein, New Series, Group III, Vol. 17, Pt. b (Springer, Berlin, 1982).

[19] A.V. Fedorov, A.V. Baranov, and K. Inoue, Phys. Rev. B **56**, 7491 (1997).

[20] K. Inoue, A. Yamanaka, K. Toba, A.V. Baranov, A.A. Onushchenko, and A.V. Fedorov, Phys. Rev. B **54**, R8321 (1996).

[21] J. Valenta, J. Moniatte, P. Gilliot, B. Hönerlage, J.B. Grun, R. Levey, and A.I. Ekimov, Phys. Rev. B **57**, 1774 (1998).

[22] K. Inoue, A. Yamanaka, N. Tanaka, A.V. Baranov, and A.V. Fedorov, J. Korean Phys. Soc. **32**, S569 (1998).

[23] T. Itoh, Y. Iwabuchi, and M. Kataoka, Phys. Status Solidi B **145**, 567 (1988).

[24] Y. Masumoto, T. Kawazoe, and T. Yamamoto, Phys. Rev. B **52**, 4688 (1995).

[25] For the review see Y. Masumoto, J. Lumin. **70**, 386 (1996).

[26] *Semiconductor Quantum Dots: Physics, Spectroscopy and Applications*, edited by Y. Masumoto and T. Takagahara (Springer, Berlin, 2002).

[27] We carefully investigated the size of CuBr QD's in glass by means of either SAXS or TEM and the energy of the $Z_{1,2}$ exciton absorption peaks at low temperatures. The relation between the average radius of QD's, $R$, and the energy of the $Z_{1,2}$ exciton peaks $E$ is well expressed by a phenomenological equation: $E = B/R^2 + A$, where $A = 2.9989$ eV, $B = 0.598\,97$ eV nm$^2$, and $R$ is given in a unit of nm. The relation for CuBr QD's in NaBr was overlapped by that for CuBr QD's in glass.

PHYSICAL REVIEW B 68, 205318 (2003)

# Intraband carrier relaxation in quantum dots embedded in doped heterostructures

A. V. Baranov,* A. V. Fedorov, and I. D. Rukhlenko
*S. I. Vavilov State Optical Institute, 12 Birzhevaya Liniya, 199034 St. Petersburg, Russia*

Y. Masumoto
*Institute of Physics, University of Tsukuba, Tsukuba 305-8571, Japan*

(Received 7 April 2003; revised manuscript received 9 July 2003; published 21 November 2003)

The effect of bulk plasmon-LO-phonon excitations inherent to doped areas of semiconductor heterostructures upon the electronic dynamics of quantum dots spaced apart from the areas is studied. An effective mechanism of intraband carrier relaxation in quantum dots is proposed for such heterostructures. The mechanism involves interaction between the quantum dot carriers and the electric potential induced by bulk plasmon-LO-phonon modes of the doped areas. It is shown that the interaction opens two relaxation windows with the spectral positions and widths controlled, correspondingly, by the free-carrier concentrations and the bulk plasmon-LO-phonon mode dispersion of the doped areas. The relaxation rates related to the mechanism are calculated for quantum dots spaced apart by different distances $z_0$ from doped substrate (the area) with the different free-carrier concentrations $n_0$. The estimations carried out for InAs quantum dots and the GaAs substrate yield the relaxation rates of about $10^8$ $s^{-1}$ for $n_0 = 10^{18}$ $cm^{-3}$ and $z_0 = 100$ nm. The rates increase by two to three orders of magnitude with decreasing the distance down to 20 nm. A manifestation of the mechanism is shown for a system of self-assembled InAs/GaAs quantum dots separated by a distance of 100 nm from an $n$-doped GaAs substrate by means of the photoluminescence spectroscopy. From the experiment it has been found that $L^-$ and $L^+$ plasmon-LO-phonon modes of the GaAs substrate are involved in the intraband carrier relaxation in the quantum dots. The data are in good agreement with the theoretical predictions.

DOI: 10.1103/PhysRevB.68.205318 PACS number(s): 78.66.Fd, 63.22.+m, 71.35.Cc, 78.55.Cr

## I. INTRODUCTION

Rapid development of nanoengineering allows one to design quantum dot based nanoelectronic devices with a lot of structural components included doped semiconductor layers, connection elements, and substrates. The single electron transistors,[1] quantum bits,[2] memory storage cells,[3] and quantum dot lasers[4] are the typical examples of such devices. Since the quantum dots (QD's) are their major operating units, an intimate knowledge about energy and phase relaxation of the QD electronic subsystem is quite necessary to manufacture the high-performance devices. Up to now the main research efforts in this field have been directed to a study of relaxation processes caused by interactions with different elementary excitations localized inside the quantum dot or at its interface. For example, the effects of confined and interface optical phonons[5–10] and plasmons[11–13] on the QD electronic dynamics have been investigated. Several works have been devoted to study a multiphonon mediated relaxation involving longitudinal optical (LO) and acoustic phonons.[8,10,14,15] The defect-assisted multiphonon emission mechanism[16–18] has been proposed for an explanation of a fast carrier relaxation in quantum dots. Moreover, the Auger-like process[19,20] has been considered as another effective mechanism of intraband carrier relaxation.

In spite of the fact that the real QD based devices are the complicated heterostructures composed of many structure components (e.g., the host matrix, the quantum wells and wires, the capping, buffer, and wetting layers, etc.) there are relatively few studies of the QD electronic dynamics affected by interactions with the environment elementary excitations. Besides the interaction between QD electronic subsystem and barrier/matrix optical and acoustical phonons,[7,8,21–23] the influence of only nearest surroundings on the QD dynamics has been studied so far. For example, homogeneous broadening of optical transitions in self-assembled quantum dots caused by the elastic Coulomb collisions between carriers in wetting layer and in the dots[24] has been considered. The QD electronic dephasing caused by the charge fluctuations in an impurity state due to its recharging through the free-electron reservoir[2] have been investigated. It may be expected that not only free charges of environment but also plasmons and plasmon phonons which reside in doped heterostructure components will interact with the QD electronic subsystem. Evidently at close contact of the dots with the doped components the QD carriers will strongly interact with environment excitations accompanied by the electric fields. But in many cases such components, e.g., doped substrates, are remote from the quantum dots by several ten nanometers and strength of the interaction is a problem of question.

Simple electrostatic considerations show that the electric field induced by longitudinal bulk waves regardless of their nature (LO phonons, plasmons or plasmon-LO-phonon modes) cannot penetrate to materials with another dielectric permittivity.[25,26] However, it has been shown by the example of the LO phonons[27,28] that account of the phonon dispersion results in a rise of exponential tails of electric field in another material. The same situation is expected to take place in the case of the plasmons or plasmon-LO-phonon modes. Their dispersion plays a drastic role for understanding the physics of intraband carrier relaxation in quantum dots remote from doped material. It is due to the dispersion that electric fields induced by the longitudinal bulk waves can penetrate through interface and affect the QD electronic subsystem opening new relaxation channels.

In this work we develop a theoretical model of the QD

 

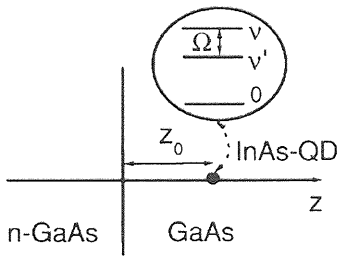


FIG. 1. A heterostructure considered in the model. Electron structure of quantum dot is shown schematically. $\Omega$ is the QD intraband transition frequency, $z_0$ is the distance between the doped semiconductor and dot.

carrier intraband relaxation via interaction between the carriers and the electric potential induced by the bulk plasmon-LO-phonon (PLP) modes of doped heterostructure components. We report experimental observation of the mechanism in system of InAs/GaAs self-assembled quantum dots (SAQD's). We show that the mechanism can be used for manipulation of electronic dynamics in QD based devices with $n(p)$-doped substrates.

## II. THEORETICAL MODEL

In order to understand a physical reason of coupling between the QD carriers and the bulk plasmon-LO-phonon modes of doped structural component we consider a simple model of heterostructure composed of two half-spaces filled by doped and undoped semiconductor with a plane interface (Fig. 1). The quantum dot is located at a distance $z_0$ from the doped material. To find the electric potential induced by the bulk PLP modes at the dot position we use an approach close to that which has been employed earlier[29] for description of the plasmon-photon modes in a single heterostructure. Such type of approach is based on the motion equations for all quasiparticles and fields under consideration. In our case the Bloch hydrodynamic equations describing the motion of an electron gas coupled with the electric field[29–31] is supplemented by the equation for dispersionless optical phonons:[26]

$$\frac{\partial \psi}{\partial t}=\frac{1}{2}(\nabla\psi)^2-\frac{e}{m}\varphi+\frac{1}{m}\int_0^n\frac{dp(n')}{n'}, \tag{1}$$

$$\frac{\partial n}{\partial t}=\nabla\cdot(n\nabla\psi), \tag{2}$$

$$\Delta\varphi=\frac{4\pi e}{\varepsilon_\infty}(n-N_0)+\frac{4\pi\alpha}{\varepsilon_\infty}\nabla\cdot\mathbf{u}, \tag{3}$$

$$\frac{\partial^2\mathbf{u}}{\partial t^2}=-\omega_T^2\mathbf{u}-\frac{\alpha}{\rho}\nabla\varphi, \tag{4}$$

where $\psi$ is the potential of the hydrodynamic velocity $\mathbf{v}=-\nabla\psi$ of the electron gas, $n$ is the density of free carriers with effective mass $m$, $\varphi$ is the self-consisted electric potential, $p(n)$ is the pressure-density relation of the carrier gas, $\mathbf{u}$ is the mechanical displacement field corresponding of optical phonons, $\alpha=\omega_T[(\varepsilon_0-\varepsilon_\infty)\rho/4\pi]^{1/2}$, $\varepsilon_0$ and $\varepsilon_\infty$ are the low- and high-frequency dielectric constants, $\rho$ is the reduced-mass density of a unit cell, $\omega_T$ is the limiting frequency of transversal optical phonons, and $N_0$ is the dopant concentration. In contrast to the polaritonic problem we take into account only the longitudinal electric field $\mathbf{E}=-\nabla\varphi$ and include to the Poisson equation [see Eq. (3)] an additional term that describes contribution of the phonon induced lattice polarization to the charge density. According to Eqs. (1)–(4) the fluctuations of electron gas density are coupled with the longitudinal optical phonons via the electric potential $\varphi$. It is easy to see that the phenomenological Lagrangian corresponding to Eqs. (1)–(4) has the following form:

$$L=\int d^3r\left[\frac{1}{2}\rho\dot{\mathbf{u}}^2-\frac{1}{2}\rho\omega_T^2\mathbf{u}^2-\alpha\nabla\varphi\cdot\mathbf{u}+\frac{\varepsilon_\infty}{8\pi}(\nabla\varphi)^2+mn\dot{\psi}\right.$$
$$\left.-\frac{1}{2}mn(\nabla\psi)^2+e\varphi(n-N_0)-n\int_0^n dn'\frac{p(n')}{n'^2}\right]. \tag{5}$$

The Lagrangian (5) allows us to define the appropriate Hamiltonian and by means of its diagonalization to introduce the eigen-PLP modes as well as an interaction between the electron subsystem of QD's and the PLP modes. Before proceeding to this program we simplify our problem using the usual linearization procedure.[29–31] As result, instead of Eqs. (1)–(4), a set of linear equations,

$$\frac{\partial\psi}{\partial t}=-\frac{e}{m}\varphi+\frac{\beta^2}{n_0}n, \tag{6}$$

$$\frac{\partial n}{\partial t}=\nabla\cdot(n_0\nabla\psi), \tag{7}$$

$$\Delta\varphi=\frac{4\pi e}{\varepsilon_\infty}n+\frac{4\pi\alpha}{\varepsilon_\infty}\nabla\cdot\mathbf{u}, \tag{8}$$

$$\frac{\partial^2\mathbf{u}}{\partial t^2}=-\omega_T^2\mathbf{u}-\frac{\alpha}{\rho}\nabla\varphi, \tag{9}$$

is obtained and the corresponding Hamiltonian is given by

$$H=\int d^3r\left[\frac{1}{2}\rho\dot{\mathbf{u}}^2+\frac{1}{2}\rho\omega_T^2\mathbf{u}^2+\alpha\nabla\varphi\cdot\mathbf{u}-\frac{\varepsilon_\infty}{8\pi}(\nabla\varphi)^2\right.$$
$$\left.+\frac{1}{2}mn_0(\nabla\psi)^2-e\varphi n+\frac{m\beta^2}{2n_0}n^2\right], \tag{10}$$

where $n_0=N_0$ is the uniform electron gas density in the undisturbed state and $\beta=[\hbar^2(3\pi^2n_0)^{2/3}/3m^2]^{1/2}$ is the speed of propagation of hydrodynamic disturbance in the electron gas.[29] In order to obtain the eigen-PLP modes we solved Eqs. (6)–(9) for the doped ($d$) and undoped ($u$) parts of heterostructure provided an equality to zero of the normal component of hydrodynamic velocity of electron gas $d\psi_d/dz|_{z=-0}=0$ as well as a continuity of the self-consisting electric potential $\varphi_d|_{z=-0}=\varphi_u|_{z=+0}$ and the normal component of electric displacement $\varepsilon_d(\omega)d\varphi_d/dz|_{z=-0}=\varepsilon_u(\omega)d\varphi_u/dz|_{z=+0}$, where $\varepsilon_i(\omega)=\varepsilon_{i\infty}(\omega^2-\omega_{iL}^2)/(\omega^2-\omega_{iT}^2)$ for $i=d$ or $u$, and $\omega_{iL}$ are the limiting frequencies of longitudinal optical phonons. Analy-

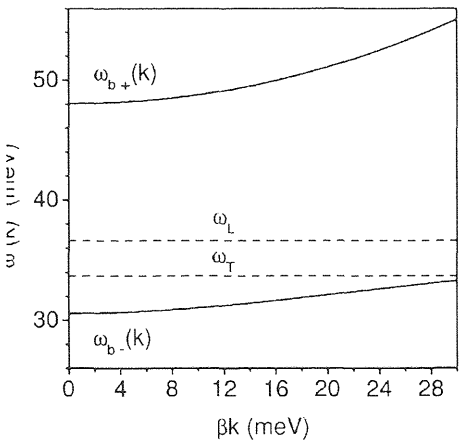


FIG. 2. The dispersion brunches for the bulk PLP modes in $n$-doped GaAs substrate with the concentration of free electrons equal $n_0 = 10^{18}$ cm$^{-3}$.

sis has shown that the bulk plasmon-LO-phonon modes occur if their wave vector $\mathbf{k}$ and frequency $\omega$ satisfy the inequality

$$\beta^2 k_z^2 = \omega^2 - \omega_p^2 \frac{\varepsilon_\infty}{\varepsilon(\omega)} - \beta^2 \mathbf{q}^2 > 0, \tag{11}$$

where $k_z$ is the normal component of $\mathbf{k}$, $\mathbf{q}$ is the projection of $\mathbf{k}$ onto the interface plane, $\omega_p = \sqrt{4\pi n_0 e^2/\varepsilon_\infty m}$ is the plasma frequency, and all material parameters correspond to the doped semiconductor. Then we obtain that the bulk plasmon-phonon modes have two branches of a dispersion relation (Fig. 2) with frequencies

$$\omega_{b\pm}^2(k) = \frac{1}{2}\{\omega_L^2 + \omega_p^2 + \beta^2 k^2 \pm [(\omega_L^2 + \omega_p^2 + \beta^2 k^2)^2 - 4\omega_p^2 \omega_T^2 - 4\omega_L^2 \beta^2 k^2]^{1/2}\}. \tag{12}$$

Obviously the upper branch of the plasmon-phonon modes is restricted from below by the condition $\omega_{b+}(k) \geqslant \omega_{b+}(0)$ while the lower branch is restricted by the double inequality $\omega_T > \omega_{b-}(k) \geqslant \omega_{b-}(0)$. Using the solution of Eqs. (6)–(9) and the Hamiltonian (10) we found a coupling energy $V(\mathbf{r}) = -e\varphi(\mathbf{r})$ between the QD electronic subsystem and the self-consisted electric potential $\varphi(\mathbf{r})$ induced by the PLP modes as

$$V(\mathbf{r}) = \sum_{\mathbf{k}} [V_{\mathbf{k}}(z) e^{i\mathbf{q}\cdot\mathbf{x}} b_{\mathbf{k}} + V_{\mathbf{k}}^*(z) e^{-i\mathbf{q}\cdot\mathbf{x}} b_{\mathbf{k}}^+], \tag{13}$$

where $b_{\mathbf{k}}(b_{\mathbf{k}}^+)$ is the annihilation (creation) operator of the plasmon-phonon mode and $\mathbf{x}$ is the coordinate in the interface plane. As for a function $V_{\mathbf{k}}(z)$, it has the simplest form when both parts of the heterostructure are filled by the same materials like the structure shown in Fig. 1. Then

$$V_{\mathbf{k}}(z) = V_k \cdot \begin{cases} \zeta_{\mathbf{k}} e^{ik_z z} + e^{-ik_z z} - \chi_{\mathbf{k}} \omega^2 e^{qz}, & z \leqslant 0, \\ \chi_{\mathbf{k}} \beta^2 k^2 e^{-qz}, & z > 0, \end{cases} \tag{14}$$

where

$$\zeta_{\mathbf{k}} = \frac{ik_z \delta(\omega) + q\gamma(\omega)}{ik_z \delta(\omega) - q\gamma(\omega)}, \quad \chi_{\mathbf{k}} = \frac{ik_z}{ik_z \delta(\omega) - q\gamma(\omega)}, \tag{15}$$

$$\gamma(\omega) = \frac{\omega_p^2}{2} \frac{\omega^2 - \omega_T^2}{\omega^2 - \omega_L^2}, \quad \delta(\omega) = \beta^2 k^2 + \gamma(\omega), \tag{16}$$

$V_k = [2\hbar m \gamma^2(\omega)/L^3 k^2 n_0 \omega \sigma(\omega)]^{1/2}$, $L^3$ is the normalized volume, $\sigma(\omega) = 1 + \omega_p^2(\omega_L^2 - \omega_T^2)/(\omega^2 - \omega_L^2)^2$, $\omega$ equals $\omega_{b+}(k)$ or $\omega_{b-}(k)$ depending on the considered PLP branch. The lower string of Eq. (14) shows that the self-consistent electric potential penetrates to the undoped part of the heterostructure and is responsible for the interaction between the QD electron subsystem and the plasmon-phonon modes. Moreover, as we mentioned above, the coupling vanishes for dispersionless PLP modes ($\beta = 0$).

Now, using the Fermi golden rule, we can calculate the intraband relaxation rates of QD electrons due to interaction with the doped semiconductor via electric potential induced by the plasmon-phonon modes. Supposing that temperatures are relatively small, $\omega_{b\pm}(k)/k_B T \gg 1$, we can restrict our consideration to only relaxation processes with emission of the PLP modes. Then, the rate of the intraband electron transitions depending on the intraband QD level spacing $\Omega = (E_\nu - E_{\nu'})/\hbar$, where $E_{\nu(\nu')}$ is the energy of initial (final) QD state with the quantum numbers $\nu(\nu')$ (see Fig. 1), is given by

$$W_{b\pm}^{(\nu',\nu)} = \frac{m\beta^2 q_\Omega^3}{\pi\hbar n_0} \int_0^1 \frac{d\tau e^{-2q_\Omega z_0 \tau} \tau \sqrt{1-\tau^2} f_{\nu',\nu}(\tau)}{1 + a(\Omega)(1-\tau^2)}, \tag{17}$$

where

$$q_\Omega = \frac{1}{\beta} \sqrt{[\Omega^2 - \omega_{b+}^2(0)][\Omega^2 - \omega_{b-}^2(0)]/(\Omega^2 - \omega_L^2)}, \tag{18}$$

$a(\Omega) = [\Omega\beta q_\Omega / \gamma(\Omega)]^2$, and the function $f_{\nu',\nu}(\tau)$ containing all information about QD parameters is

$$f_{\nu',\nu}(\tau) = A\upsilon_{\eta',\eta} |\langle \nu', \eta' | e^{-q_\Omega \tau (z - i|\mathbf{x}| \cos\psi)} | \nu, \eta \rangle|^2, \tag{19}$$

where $\psi$ is the angle between $\mathbf{q}$ and $\mathbf{x}$ vectors. The operation $A\upsilon_{\eta',\eta}$ in Eq. (19) implies the averaging over degenerate initial QD states $|\nu, \eta\rangle$ and summation over degenerate final QD states $|\nu', \eta'\rangle$, where $\eta$ and $\eta'$ are the quantum numbers related to the degenerated QD states. For example, for a spherical QD of the radius $R_0$ in the strong confinement regime,[32] i.e., when $R_{ex} > R_0$, where $R_{ex}$ is the bulk exciton Bohr radius for the QD material,

$$f_{n'l',nl}(\tau) = 2 \sum_{p=0}^{\infty} (2R_0 q_\Omega \tau)^{2p} \frac{(J_{n'l',nl}^{(p)} C_{l0,p0}^{l'0})^2}{(2p+1)!}, \tag{20}$$

where $nl(n'l')$ are the principle quantum number and angular momentum of initial (final) QD electronic states, $C_{lm,pt}^{l'm'}$ are the Clebsch-Gordon coefficients[33] governing the transition selection rules. The quantities $J_{n'l',nl}^{(p)}$ for a quantum dot with an infinitely high potential barrier ($E_0 \to \infty$) equal

$$J^{(p)}_{n'l',nl}=2\int_0^1 dx x^{2+p}\frac{j_{l'}(\xi_{n'l'}x)j_l(\xi_{nl}x)}{j_{l'+1}(\xi_{n'l'})j_{l+1}(\xi_{nl})}, \quad (21)$$

where $\xi_{nl}$ is the $n$th root of the spherical Bessel function of $l$th order $[j_l(\xi_{nl})=0]$. If the potential barrier $E_0$ is finite then

$$J^{(p)}_{n'l',nl}=2A_{n'l'}A_{nl}\left(B^{nl}_{n'l'}\int_0^1 dx x^{2+p}j_{l'}(\eta_{n'l'}x)j_l(\eta_{nl}x)\right.$$
$$\left.+C^{nl}_{n'l'}\int_1^\infty dx x^{2+p}k_{l'}(\zeta_{n'l'}x)k_l(\zeta_{nl}x)\right), \quad (22)$$

$$A_{nl}=[j_l^2(\eta_{nl})k_{l-1}(\zeta_{nl})k_{l+1}(\zeta_{nl})$$
$$-k_l^2(\zeta_{nl})j_{l-1}(\eta_{nl})j_{l+1}(\eta_{nl})]^{-1/2}, \quad (23)$$

$$B^{nl}_{n'l'}=k_{l'}(\zeta_{n'l'})k_l(\zeta_{nl}),C^{nl}_{n'l'}=j_{l'}(\eta_{n'l'})j_l(\eta_{nl}), \quad (24)$$

where $k_l$ is the modified spherical Bessel function, $\eta_{nl}=R_0(2m_1E_{nl}/\hbar^2)^{1/2}$, $\zeta_{nl}=R_0[2m_2(E_0-E_{nl})/\hbar^2]^{1/2}$, $m_1$ ($m_2$) is the electronic effective mass in the dot (surrounding media), the electronic energy $E_{nl}$ is determined by the secular equation[34]

$$m_2\eta_{nl}k_l(\zeta_{nl})j_l'(\eta_{nl})=m_1\zeta_{nl}k_l'(\zeta_{nl})j_l(\eta_{nl}). \quad (25)$$

Equation (17) describes two relaxation windows resulting from the intraband transitions with emission of the PLP modes of upper dispersion branch $\omega_{b+}(k)$ if $\Omega\geq\omega_{b+}(0)$ and those with emission of the PLP modes of lower dispersion branch $\omega_{b-}(k)$ if $\omega_T>\Omega\geq\omega_{b-}(0)$ (see Fig. 2). It is clearly seen that spectral positions of the windows depend on free-carrier concentration in doped structural component, and spectral widths of the windows and values of the relaxation rates are determined by the dispersion of the plasmon-phonon modes.

## III. EXPERIMENTAL RESULTS AND DISCUSSION

The discussed coupling of QD electronic subsystem with PLP modes of $n$-doped substrate and the intraband carrier relaxation mediated by these modes have been experimentally observed at 2 K in two systems of InAs/GaAs SAQD's with different parameters of electronic states. Two samples (A and B) were fabricated by MBE on a (001) surface of a Si-doped ($n_0\approx10^{18}$ cm$^{-3}$) GaAs substrate. In both cases a 100-nm GaAs buffer layer was grown. Then InAs of 1.8 monolayers (ML's) was deposited at 500 °C (480 °C) giving rise to lens-shaped QD's with diameter of ≈22 (18) nm, height of ≈10 (8) nm, and an areal density of ≈1.2 (2) $\times10^{10}$ cm$^{-2}$ for sample A (B). The thickness of a GaAs cap layer was 150 nm. The electronic energy structure of both quantum dot systems was found from their photoluminescence (PL) spectra in standard state-filling experiments[35] with excitation by a 514.5-nm line of $Ar^+$ laser. It was typical for lens-shaped InAs SAQD's (Ref. 36) with quasiequidistant spectra of interband inhomogeneously broadened (≈70 meV) transitions and peak energies of the lowest (0-0) transitions of ≈1228 meV (A) and ≈1321 meV (B). Insets in lower and upper panels in Fig. 3 show the PL spectra of

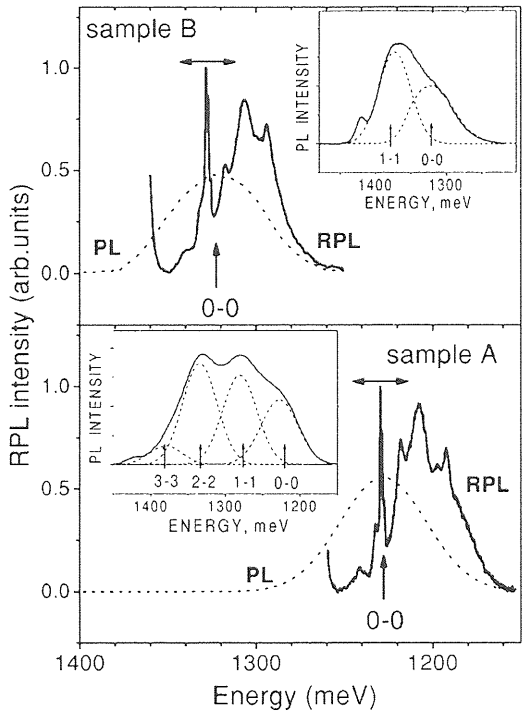


FIG. 3. The resonant photoluminescence (RPL) spectrum of InAs SAQD's in samples A (lower panel) and B (upper panel) excited in resonance with the 1-1 transition of quantum dots (1262 and 1361 meV, respectively). The position of the 0-0 photoluminescence (PL) band of the dots (dotted curve) is shown for comparison in both panels. The insets present the PL spectra of the samples measured in the state-filling experiments (see the text). A Gaussian line-shape fit is shown. The positions of the SAQD interband transitions (0-0, 1-1, etc.) are shown by arrows. The horizontal arrow bar shows the portion of spectrum which is under detailed analysis.

the samples at high excitation power and fitting of the PL spectra by a sum of Gaussians. The peak maximums correspond to the sequence of the QD interband transitions (0-0, 1-1, etc.). Energy gaps between peaks of the lowest and second transitions were about 53 meV (A) and 55 meV (B). Taking into account the inhomogeneous broadening of the transitions we concluded that the energies of the QD intraband level spacing[36] match those of the PLP modes expected for studied quantum dot heterostructures.

The secondary emission spectra of the samples were measured in the $x(y,y)z$ geometry, where $z$ is the growth direction of the InAs layer, by the use of a cw wavelength-tunable Ti:sapphire laser and a double monochromator equipped by a cooled InAs photomultiplier. The measurements were done at low pump power (<0.2 W/cm$^2$) when PL is only caused by recombination of the electrons and holes in their ground states. It was found that in accordance with earlier data[8,15,37] the PL spectra of the studied QD samples excited in resonance with high-energy QD transitions (hereinafter referred to as RPL spectra) are mainly formed by lines resulting from one- and multiphonon intraband carrier relaxation in the quantum dots. As an example, the RPL spectra of samples A and B excited in resonance with 1-1 transitions (the photon energies of 1262 and 1361 meV, respectively) are shown in

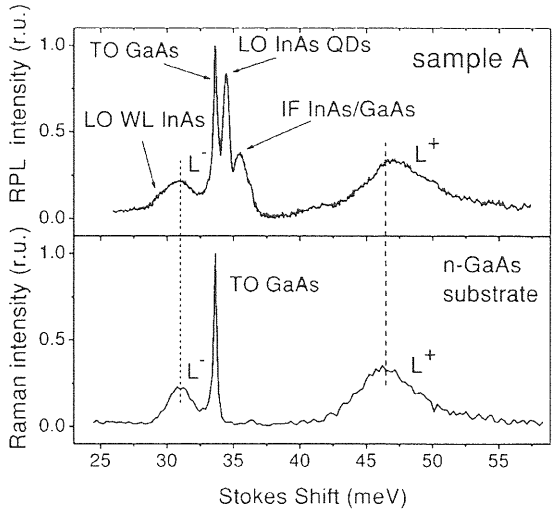


FIG. 4. Upper panel: Enlarged part of the RPL spectrum of sample A marked in Fig. 3 (lower panel) by the arrow bar plotted vs the Stokes shift. The background caused by the multiphonon lines was subtracted. Lower panel: The Raman spectrum of the $n$-doped GaAs substrate obtained from area of sample A with removed quantum dots. The spectrum has measured at the same excitation/detection conditions as the RPL one. The assignment of the lines in the RPL and Raman spectra is shown (see the text).

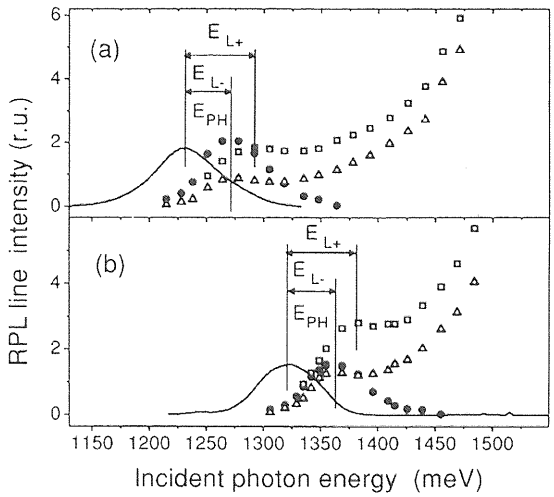


FIG. 5. Excitation profiles of the $L^+$ (open squares) and $L^-$ (open triangles) lines observed in the RPL spectra of samples A and B [(a) and (b), respectively]. The filled circles show the excitation profile of the intrinsic LO phonon line of InAs QD's. Solid curves show the positions of the QD 0-0 PL bands. $E_{PH}$, $E_{L^-}$, and $E_{L^+}$ are the energies of the LO phonons of InAs QD's, $L^-$ and $L^+$ PLP modes, respectively.

Fig. 3. To make an assignment of the RPL spectrum lines, the spectra were measured at different incident photon energies $E_{ex}$ covering the interband transition energies of QD's and were analyzed as a function of the Stokes shift, $E_{ex} - E_{RPL}$, where $E_{RPL}$ is the energy of photons detected in RPL experiments. The RPL spectra were fitted by a sum of Gaussians, that yields parameters of the overlapping lines.[8,15,37] It has been found that the Stokes shifts of the lines are invariable. This is a sign of phonon-assistant resonant photoluminescence. The lines of InAs wetting layer (WL), intrinsic LO phonons of InAs QD's, InAs/GaAs phonon interface mode (IF) with the Stokes shifts of 29.5, 34.3, and 35.5 meV, respectively, as well as their overtones and sum tones have been easily distinguished under analysis of the spectra. Assignment of the lines was carried out according to Ref. 7 where resonant photoluminescence spectra of the analogous InAs SAQD sample were studied. Further, we have analyzed in more detail the obtained RPL spectra in region of the Stokes shifts of 25–60 meV, as is shown in Fig. 3 by the arrow bars. This region of the spectrum after subtraction of background caused by the multiphonon lines is plotted vs Stokes shift in Fig. 4 (upper panel) for sample A. It is seen that except for the above mentioned phonon lines, the lines belonging to the zone-center bulk TO phonons and to the PLP modes, $L^-$, and $L^+$ (corresponding energies $E_{L^-}$ and $E_{L^+}$ are 31.1 and 46.7 meV, respectively) of $n$-doped GaAs (Ref. 38) appear to be in the spectra. The assignment of the $L^-$ and $L^+$ lines is based on comparison of the resonant photoluminescence spectra with Raman spectra of $n$-doped GaAs substrate. The Raman spectra were obtained from area of the sample with removed quantum dots at the same excitation/detection conditions as the RPL spectra. An example of the Raman spectrum is shown in Fig. 4 (low panel). The resonant photoluminescence spectra of sample B exhibited the same features. At first glance, the spectrum presented in the upper panel of Fig. 4 is a simple superposition of the phonon-assisted RPL spectrum of the quantum dots and Raman spectrum of the substrate. However, it was found that plasmon-LO-phonon lines in spectra of samples with QD's show unusual behaviors which indicate coupling between the substrate plasmon-phonon modes and electronic subsystem of the quantum dots.

We have plotted the integral intensities of the $L^-$ and $L^+$ lines of the samples with quantum dots as a function of the incident photon energy, so-called excitation profiles of the lines commonly used in resonant Raman spectroscopy. The excitation profiles of these lines in the RPL spectra of QD's are presented in Fig. 5 for samples A (a) and B (b) together with excitation profile of the intrinsic LO-phonon line of QD's. The positions of the 0-0 PL bands are shown in the same figure for comparison (solid curves). They indicate the energy spectra of inhomogeneously broadened lowest interband transitions of the QD ensembles. As can be seen, the excitation profile of the LO-phonon line of InAs QD's demonstrates single prominent peak blueshifted by the LO-phonon energy ($E_{PH}$) with respect to the 0-0 band. The excitation profiles of other phonon lines and their overtones demonstrated analogous shifts by the corresponding phonon or overtone energies. That is a signature of the fact that the phonon lines come from annihilation of the electron-hole pairs in the lowest energy state populated by the phonon-mediated intraband carrier relaxation from the directly photoexcited state. This process is described in detail in Refs. 12 and 35. In this case the intensity of the phonon lines excited by radiation with photon energy tunable in region of the higher-energy transitions of QD's follows the 0-0 PL band contour. It is just our case that can be seen if the excitation

profile in Fig. 5 will be shifted by the LO phonon energy to the red side. Evidently the analysis of the RPL line excitation profiles is equivalent to that of photoluminescence excitation spectra.

Let us discuss the excitation profiles of the $L^-$ and $L^+$ lines. As is well known,[39] in $n$-doped bulk GaAs the intensities of the $L^-$, and $L^+$ Raman lines have to increase monotonically with excitation energy approaching the GaAs band gap (pre-resonant Raman). However, except for this, we found that the excitation profiles of the $L^-$, and $L^+$ lines in spectra of different SAQD samples demonstrate pronounced resonances which are shifted by the $E_{L^-}$ and $E_{L^+}$ energies with respect to the corresponding 0-0 PL bands (see Fig. 5). This fact indicates that both the PLP modes of doped GaAs substrate are coupled with the QD electronic subsystem and are involved in the intraband carrier relaxation in quantum dot in the same manner as intrinsic phonons of quantum dot and its nearest surroundings. The observed plasmon-phonon lines are therefore superposition of the Raman signals from the substrate and the RPL signals from InAs SAQD's with comparable amplitudes at the maximum of the PLP line excitation profile. Importantly, the intraband carrier relaxation in the quantum dots induced by the plasmon-phonon modes is effective enough although distance between the substrate and QD layer is 100 nm long.

As is known,[15] the studied SAQD systems possess an inhomogeneously broadened spectrum of intraband transitions. In particular, light with definite photon energy in the region of the 1-1 transitions excites an ensemble of quantum dots with broad energy spectrum of intraband transitions to the lowest electron-hole states. Phonon-mediated intraband relaxation results in the RPL spectrum with the phonon related peaks. In other words, the RPL spectrum as a function of the Stokes shift can be considered as a spectrum of intraband relaxation rates. In the framework of our model we calculated a dependence of relaxation rate of the lowest energy intraband electronic transitions as a function of the intraband level spacing $\Omega$ (i.e., the spectrum of intraband relaxation rates). The calculations were performed for $z_0 = 100$ nm and different concentrations of the free electrons in region of $n_0 = 10^{18}$ cm$^{-3}$. Spherical quantum dot with infinite potential barrier was considered. A relation of $R_0 = \sqrt{\hbar(\xi_{11}^2 - \pi^2)/(2m_{QD}\Omega)}$ between the QD radius and $\Omega$, where $m_{QD}$ is the electronic effective mass in InAs, was used.

Figure 6 shows the results of calculation for $n_0 = 0.8 \times 10^{18}$ cm$^{-3}$ [solid line in Fig. 6(a)] in comparison with the experimental RPL spectrum of sample A [Fig. 6(b)] in the spectral region of interest. We see that the positions and widths $L^-$ and $L^+$ lines in the RPL spectrum are quite close to the calculated energy positions of relaxation windows with widths of several meV. The same correspondence has been observed for the RPL spectra of sample B. A little difference between $n_0$ of the substrate and its value used in the calculations may come from the fact that the optical phonon dispersion and/or retardation effects were not taken into account in our model. The relaxation rates for both PLP modes were estimated to be about $2 \times 10^8$ s$^{-1}$ in spite of the relatively long distance between the quantum dot and doped semiconductor. It is seen that observed features of the RPL spectra are in accordance with predictions of our theoretical model for the intraband carrier relaxation with emission of the plasmon-phonon modes. Indeed, as we have demonstrated by Eq. (17), the coupling between the QD electronic subsystem and plasmon-phonon modes via the self-consisting electric potential opens two relaxation windows corresponding to the QD interaction with the upper and lower PLP branches.

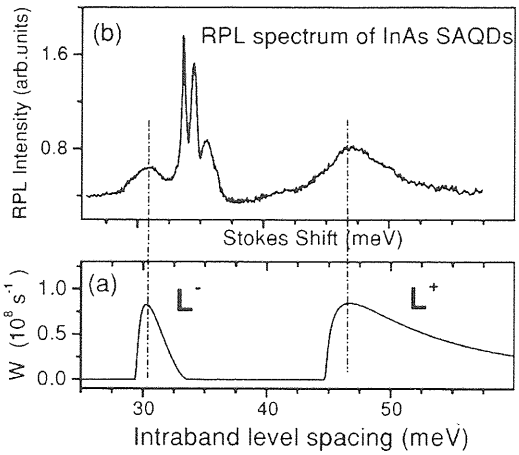


FIG. 6. Comparison between (a) calculated spectrum of relaxation rate $W$ and (b) relevant portion of the RPL spectrum of sample A, the same as shown in Fig. (4) (upper panel). The calculations based on Eq. (17) have been done for the lowest electronic intraband transitions in spherical InAs QD located at distance $z_0 = 100$ nm from $n$-doped GaAs substrate and dopant concentration of $n_0 = 0.8 \times 10^{18}$ cm$^{-3}$. $L^-$ and $L^+$ denote the relaxation windows corresponding to the PLP modes of GaAs substrate.

We would like to note that both the peak value and width of the relaxation windows are determined by the PLP

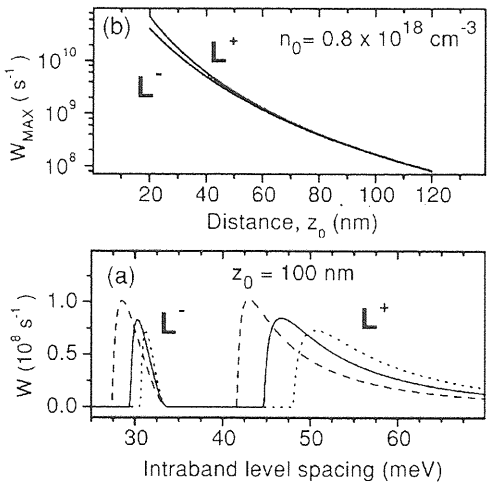


FIG. 7. (a) Calculated relaxation rate for lowest energy intraband electronic transitions $W$ in spherical InAs QD for different dopant concentration in GaAs substrate: $n_0 = 0.6 \times 10^{18}$ cm$^{-3}$, $n_0 = 0.8 \times 10^{18}$ cm$^{-3}$, and $n_0 = 10^{18}$ cm$^{-3}$ (dashed, solid, and dotted curves, respectively). A distance between the substrate and QD $z_0 = 100$ nm. (b) Peak value of the $W(W_{MAX})$ as a function of $z_0$ for $n_0 = 0.8 \times 10^{18}$ cm$^{-3}$.

mode dispersion, Eq. (12). At the same time, the spectral positions of the windows remarkably depend on the dopant concentration that is shown in Fig. 7(a) by the spectra of the relaxation rates calculated for different dopant concentrations ($n_0=0.6\times10^{18}$ cm$^{-3}$, $n_0=0.8\times10^{18}$ cm$^{-3}$, and $n_0=10^{18}$ cm$^{-3}$). The spectra demonstrate an 8-meV shift of the $L^+$ window with $n_0$. This fact is very important because the rates can be essentially varied by tuning of the PLP-mode windows to resonance or out of resonance with QD intraband transition energies by means of changing of $n_0$. Thus the switch on or switch off of the relaxation channels become possible. Such control of the intraband carrier dynamics will be especially effective in QD systems where inhomogeneous broadening of the intraband transitions is narrower than the window widths, in QD systems without such kind of broadening, and in a single QD. As for the efficiency of the relaxation process, our calculations show that with decrease of distance $z_0$ the peak values of the relaxation rates drastically increase [Fig. 7(b)] up to about $10^{11}$ s$^{-1}$ at $z_0=20$ nm. This value is comparable with rate of the Auger-like process of QD interband carrier relaxation.[20]

We believe the considered interaction has to be accounted for in design of QD based applications where $n(p)$-doped structural components of heterostructures spaced apart from the QD layers by ten or several ten nanometers are widely used. The concentration and distance dependencies of the coupling open promising opportunities for manipulation of QD electron dynamics in doped heterostructures. We would like to note that surface plasmon-LO-phonon modes of doped heterostructure components can be also involved in the intraband carrier relaxation in quantum dots. Consideration of this problem is in progress.

## ACKNOWLEDGMENTS

The authors thank Dr. S. Sugou and Dr. H.-W. Ren for growing samples studied in this work. The work was partially supported by the Single Quantum Dot Project, ERATO, JST, Japan which the authors deeply acknowledge. A.V.B. and A.V.F. are grateful to the RFBR (Grant No. 02-02-17311) and to the INTAS Program (01-2100 and 01-2331) for partial financial support of this work.

*Electronic address: baranov1@online.ru

[1] L. Guo, E. Leobandung, and S.Y. Chou, Science **275**, 649 (1997).
[2] T. Itakura and Y. Tokura, Phys. Rev. B **67**, 195320 (2003).
[3] K. Yano, T. Ishii, T. Sano, T. Mine, F. Murai, T. Hashimoto, T. Koboyashi, T. Kure, and K. Seki, Proc. IEEE **87**, 633 (1999).
[4] M. Dutta and M. A. Stroscio, *Advances in Semiconductor Lasers and Applications to Optoelectronics* (World Scientific, Singapore, 2000).
[5] X.-Q. Li and Y. Arakawa, Phys. Rev. B **57**, 12 285 (1998).
[6] X.-Q. Li, H. Nakayama, and Y. Arakawa, Phys. Rev. B **59**, 5069 (1999).
[7] F. Gindele, K. Hild, W. Langbain, and U. Woggon, Phys. Rev. B **60**, R2157 (1999).
[8] A.V. Baranov, V. Davydov, H.-W. Ren, S. Sugou, and Y. Masumoto, J. Lumin. **87-89**, 503 (2000).
[9] I.V. Ignatiev, I.E. Kozin, S.V. Nair, H.-W. Ren, S. Sugou, and Y. Masumoto, Phys. Rev. B **61**, 15 633 (2000).
[10] I.V. Ignatiev, I.E. Kozin, V.G. Davydov, S.V. Nair, J.-S. Lee, H.-W. Ren, S. Sugou, and Y. Masumoto, Phys. Rev. B **63**, 075316 (2001).
[11] P.A. Knipp and T.L. Reinecke, Phys. Rev. B **46**, 10 310 (1992).
[12] G. Biese, C. Schüller, K. Keller, C. Steinebach, D. Heitmann, P. Grambow, and K. Eberl, Phys. Rev. B **53**, 9565 (1996).
[13] S. Zanier, Y. Guldner, J.P. Vieren, G. Faini, E. Cambril, and Y. Campidelli, Phys. Rev. B **57**, 1664 (1998).
[14] T. Ioshita and H. Sakaki, Phys. Rev. B **46**, 7260 (1992).
[15] R. Heitz, M. Veit, N.N. Ledentsov, A. Hoffman, D. Bimberg, V.M. Ustinov, P.S. Kop'ev, and Z.I. Alferov, Phys. Rev. B **56**, 10 435 (1997).
[16] P.C. Sersel, Phys. Rev. B **51**, 14 532 (1995).
[17] D.F. Schroeter, D.F. Griffits, and P.C. Sersel, Phys. Rev. B **54**, 1486 (1996).
[18] X.-Q. Li and Y. Arakawa, Phys. Rev. B **56**, 10 423 (1997).
[19] U. Bockelman and T. Egeler, Phys. Rev. B **46**, 15 574 (1992).
[20] A.L. Efros, V.A. Kharchenko, and M. Rosen, Solid State Commun. **93**, 281 (1995).
[21] U. Bockelman and G. Bastard, Phys. Rev. B **42**, 8947 (1990).
[22] H. Benisty, Phys. Rev. B **51**, 13 281 (1995).
[23] A.V. Fedorov, A.V. Baranov, and Y. Masumoto, Solid State Commun. **122**, 139 (2002).
[24] A.V. Uskov, K. Nishi, and R. Lang, Appl. Phys. Lett. **74**, 3081 (1999).
[25] E. Evans and D.L. Mills, Phys. Rev. B **8**, 4004 (1973).
[26] N. Mori and T. Ando, Phys. Rev. B **40**, 6175 (1989).
[27] B.K. Ridley, Phys. Rev. B **49**, 17 253 (1994).
[28] F. Comas, C. Trallero-Giner, and M. Cardona, Phys. Rev. B **56**, 4115 (1997).
[29] R.H. Ritchie and R.E. Wilems, Phys. Rev. **178**, 372 (1969).
[30] L. Kleinman, Phys. Rev. B **7**, 2288 (1973).
[31] K.S. Srivastava and A. Tandon, Phys. Rev. B **39**, 3885 (1989).
[32] E. Hanamura, Phys. Rev. B **37**, 1273 (1988).
[33] D.A. Varshalovich, A. N. Moskalev, and V. K. Hersonskii, *Quantum Theory of Angular Moment* (World Scientific, Singapore, 1987).
[34] K. Vahala, IEEE J. Quantum Electron. **QE-24**, 523 (1988).
[35] S. Raymond, X. Guo, J.L. Merz, and S. Fafard, Phys. Rev. B **59**, 7624 (1999).
[36] A. Wojs, P. Hawrylak, S. Fafard, and L. Jacak, Phys. Rev. B **54**, 5604 (1996).
[37] K.H. Schmidt, G. Medeiros-Ribeiro, M. Oestreich, P.M. Petroff, and G.H. Döhler, Phys. Rev. B **54**, 11 346 (1996).
[38] A. Mooradian and A.L. McWhorter, Phys. Rev. Lett. **19**, 849 (1967).
[39] G. Abstreiter, M. Cardona, and A. Pinczuk, in *Light Scattering in Solids IV*, edited by M. Cardona and G. Guntherodt (Springer, Berlin, 1984).

# Optical Orientation Of Electron And Nuclear Spins In Negatively Charged InP QDs

S. Yu. Verbin[1,2], I. Ya. Gerlovin[3], I. V. Ignatev[1,2], and Y. Masumoto[4]

[1] *Institute of Physics and Venture Business Laboratory, University of Tsukuba, Tsukuba, 305-8571, Japan*
[2] *V.A.Fock Institute of Physics, St-Petersburg State University, 198504 St-Petersburg, Russia*
[3] *Vavilov State Optical Institute, St-Petersburg, Russia*
[4] *Institute of Physics, University of Tsukuba, Tsukuba, Japan*

**Abstract.** Light-induced spin orientation in negatively charged InP quantum dots is shown experimentally to be conserved for about 1 ms.

## INTRODUCTION

The long-term orientation of spin systems in semiconductor structures attract in recent years considerable attention as a promising way of recording and storage of optical information [1]. The most interesting, from this point of view, are the structures with quantum dots (QD), where, due to confinement of the carrier motion, the main spin-relaxation processes appear to be suppressed. According to theoretical estimates [2], the spin lifetime in such structures may reach units of ms and more. The so long lifetimes of the optically oriented electron spins in QDs have not been observed thus far. The longest lifetime of spin orientation (15 ns) was found experimentally in [3] in the studies of n-doped InAs QDs. In this communication, we present the results of experiments demonstrating conservation of the spin orientation for much longer time intervals.

## EXPERIMENT AND DISCUSSION

We studied kinetics of circularly polarized photoluminescence (PL) of the negatively charged InP QDs. It was found that the degree of circular polarization of the PL shows a slow component with a decay time of about 1 ns. The amplitude of the slow component was the greatest when each QD possessed, on average, a single resident electron. For the Stokes shift $\Delta E_{st} > 25$ meV, the degree of polarization was negative.

In conformity with conclusions of [3], the negatively polarized PL is emitted by QDs in which spins of the photoexcited and resident electrons are parallel. When the resident electron spin is preferentially oriented along that of the photoexcited electron, the amplitude of the degree of the negative circular polarization (NCP) should increase. Using the amplitude of the NCP as a measure for the degree of orientation of the electron spin, we have carried out a series of experiments to determine the spin orientation lifetime.

In the experiments, the PL was excited by two laser pulse trains obtained by splitting the beam of a mode-locked Ti:sapphire laser. One of these trains was shifted in time using an optical delay line. The time delay was about 1 ns. Polarizations of the beams could be varied independently.

Figure 1a shows the kinetics of the degree of polarization of the PL excited by the second (probe) beam for two different polarizations of the first beam considered as a pump. As is seen, passing from the co-polarized to cross-polarized pump results in more than two-fold decrease of the NCP created by the probe pulse. This means that the spin orientation created by the first beam is held till the moment of arrival of the second beam, i.e., for about 1 ns.

To strongly increase the time interval between the two beams, we used a mechanical chopper, which alternatively blocked the pump and the probe beams with a frequency of 120 Hz. A typical result of the experiment is presented in Fig. 1b. It is seen that the NCP of PL after probe pulse still reveals a well reproducible change, $\Delta\rho \approx 5\%$, caused by the change of polarization of the pump pulse. This result demonstrates in a straightforward way conservation of the spin orientation during the modulation period of units of ms.

CP772, *Physics of Semiconductors: 27th International Conference on the Physics of Semiconductors*,
edited by José Menéndez and Chris G. Van de Walle

So long conservation of the spin orientation is impossible without a stabilizing factor that suppresses the electron spin precession in random laboratory magnetic fields. In this case, the role of this factor is likely to be played by the fluctuating exchange field produced by nuclear spins [4]. To evaluate the fluctuations of the nuclear field, we have studied the behavior of the NCP at co- and cross-polarized pumping (with no chopper) in small transverse magnetic fields (Voigt configuration).

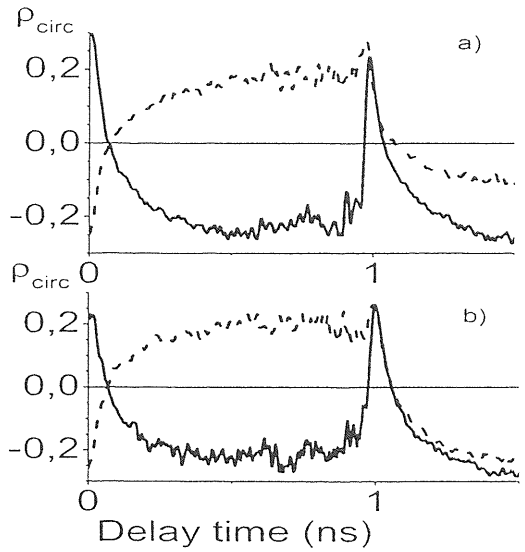


FIGURE 1. Kinetics of circular polarization degree at the two-pulse excitation: (a) without chopper, (b) with chopper blocking the beams alternatively. Solid (dashed) curves are for co- (cross-) polarized pump and probe beams.

The results of these studies are shown in Fig. 2. As one can see, dependences of the NCP on magnetic field, in the Voigt configuration, for the co- and cross-polarized pumping are strongly different. The difference between the values of the NCP for co- and cross-polarized pumping characterizes the spin orientation. Dependence of the degree of orientation on magnetic field is seen to be well described by a Lorentzian with a half-width of 0.01 T (curve 3 in Fig.2). According to conclusions of [4], this value corresponds to the mean value of the exchange field produced by fluctuations of the nuclear spins in the QD.

It follows from the above experimental data that the light-induced spin orientation in the negatively charged InP QDs is held during the time of about $10^{-3}$ s. This value exceeds by approximately 4 orders of magnitude the value of 150 ns, given in [5], which was considered until now a record value for semiconductor nanostructures.

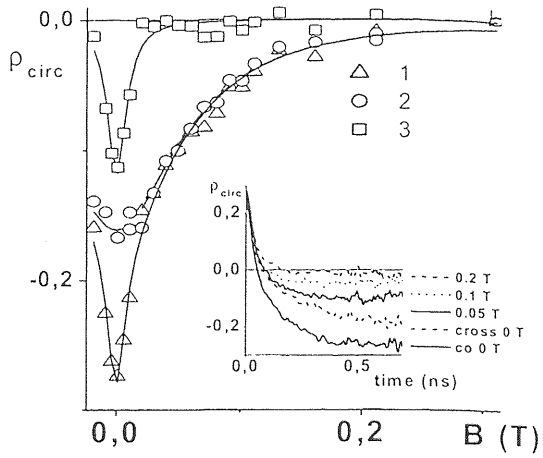


FIGURE 2. Dependences of NCP on trans-verse magnetic field: 1 is for co- and 2 for cross-polarized pump and probe, 3 is the difference between 1 and 2. Dots are experimental data, solid curves are fits by Lorentzians. Inset: kinetics of NCP at various magnetic fields.

## ACKNOWLEDGMENTS

Authors are thankful to Dr. K. Kavokin for fruitful discussions. The work is supported by Grant-in-Aid for Scientific Research on the Priority Area "Nanospintronics" (No. 16031203) from MEXT of Japan, by INTAS (1B 2167) and by RFBR (03-02-16858).

## REFERENCES

1. D.D.Awschalom J.M.Kikkawa, Phys.Today, **52**, 33 (1999).
2. A. V. Khaetskii, Yu. V. Nazarov, Phys. Rev. B, **61**, 12639 (2000)
3. S. Cortez, O. Krebs, S. Laurent, M. Senes, X. Marie, P. Voisin, R. Ferreira, G. Bastard,J-M. Gerard, T. Amand, Phys. Rev. Lett., **89**, 207401 (2002).
4. A. Merkulov, Al. L. Efros, M. Rosen, Phys. Rev. B, **65**, 205309 (2002)
5. R.I. Dzhioev, V.L. Korenev, B.P. Zakharchenya, D. Gammon, A.S. Bracker, J.G. Tischler, and D.S. Katzer, Phys. Rev. B **66**, 153409 (2002)

PHYSICAL REVIEW B **71**, 033314 (2005)

# Spin relaxation in CdTe quantum dots

Ye Chen, Tsuyoshi Okuno, and Yasuaki Masumoto
*Institute of Physics and Venture Business Laboratory, University of Tsukuba, Tsukuba, Ibaraki 305-8571, Japan*

Yoshikazu Terai,* Shinji Kuroda, and Koki Takita
*Institute of Material Science, University of Tsukuba, Tsukuba, Ibaraki 305-8573, Japan*
(Received 28 April 2004; revised manuscript received 28 September 2004; published 25 January 2005)

We have measured photoluminescence (PL) spectra and time-resolved PL in CdTe quantum dots under the longitudinal magnetic field up to 10 T. Circular polarization of PL increases with increasing magnetic field, while its linear polarization remains zero under linearly polarized excitation. This behavior cannot be explained by the anisotropic exchange interaction of excitons. Time-resolved PL measurements clarified that this behavior is caused by the suppression of spin relaxation induced by the longitudinal magnetic field. We believe that this behavior is related to the hyperfine interaction of electron spin with magnetic momenta of lattice nuclei.

DOI: 10.1103/PhysRevB.71.033314 PACS number(s): 78.66.Hf, 78.67.Hc, 78.20.Ls, 78.47.+p

The spin state of electrons in quantum dots (QDs) is considered as one of the most promising candidates for the implementation of spintronic and quantum information technologies.[1] A key challenge is to obtain long relaxation time of electron spin. The carrier spin-flip mechanisms, including exchange interaction, mixing between the conduction and valence band states through spin-orbit coupling, and spin splitting of the conduction band due to the lack of inversion symmetry,[2,3] have been studied in bulk and two-dimensional systems. In QDs, the discrete energy levels and the corresponding lack of energy dispersion lead to a predicted modification of the spin relaxation dynamics. In general, the D'yakonov and Perel' mechanism does not work in zero dimension because this spin-flip mechanism relies on translation invariance, which is already broken in QDs.[4] The electron spin relaxation mechanism connected with the spin-orbit interaction of carriers is strongly suppressed for localized carriers in QDs.[5] The absolute lack of energy states between QD energy levels is expected to inhibit not only the elastic processes of spin relaxation but also the inelastic ones such as phonon scattering. As a result, electron spin relaxation via interaction with nuclei becomes relatively important for localized electrons. Recently, Merkulov *et al.*[6] pointed out that the hyperfine interacting with nuclei may become the dominant mechanism of electron spin relaxation in quantum dots at low temperature. Although the hyperfine interaction has been demonstrated to induce the additional Zeeman splitting or polarization of electrons and exciton in QDs,[7,8] no direct experimental evidence has proved the importance of hyperfine interaction with nuclei responsible for spin relaxation in QDs up to now.

In this report, we investigated the spin relaxation mechanisms of carriers in CdTe QDs. We measured the magneto-photoluminescence (PL) spectra and time-resolved PL under the magnetic field with a Faraday configuration. An unusual magnetic field dependence of circular polarization was observed in steady-state PL spectra, which cannot be explained in the framework of anisotropic exchange interaction of excitons confined in an elongated QD. Time-resolved PL decay proved that the suppression of spin relaxation by the longitudinal magnetic field is the origin of this behavior. We believe that the spin relaxation of electrons localized in QDs is caused mainly by hyperfine interaction of electron spin with magnetic momenta of lattice nuclei. The hyperfine field is suppressed by the external longitudinal magnetic field.

The CdTe self-assembled QD was grown by molecular-beam epitaxy on a relatively thick (0.6–1.0 μm) ZnTe buffer layer formed on a GaAs (100) substrate.[9] The sample was not doped intentionally. Atomic force images show that the average size of CdTe QDs was ~20 nm in diameter and ~2.7 nm in height. The area density of the dots was $8\times10^{10}$ cm$^{-2}$. The PL and time-resolved PL measurements were performed in a magnetic field up to 10 T and at 10 K in a Faraday configuration. An optical parametric amplifier of a Ti:sapphire laser was used as an excitation source with a photon energy of 2.217 eV, corresponding to a quasi-resonance excitation of CdTe QDs. Circular and linear polarizations were obtained by using quartz wave plates and linear polarizers, respectively.

The representative PL spectra of our sample are shown in Fig. 1(a). In these measurements, the luminescence was collected under co-circular (the incident and emitted light with the same circular polarization) and cross-circular geometries (the incident and emitted light with counter-circular polarization). In order to study the intrinsic spin dynamics, the PL spectra were obtained by selectively exciting the sample with photon energy 2.217 eV slightly above the PL band of the QDs. The PL bands of the QDs have a smooth profile with two sharp features, $LO_1$ and $LO_2$ (24.5 and 19.5 meV, respectively), which are caused by fast relaxation of hot carriers with emission of LO phonons of ZnTe and CdTe.

At zero field, the PL band shows very weak circular polarization (7%). With increasing magnetic field the circular polarization of PL band increases. When the direction of magnetic field was reversed, the same results were obtained. We further measured the circularly polarized PL spectra under linearly polarized excitations at 4 T in Fig. 1(b). It confirms that no circular polarization was observed under linearly polarized excitation. Therefore, the circular polarization is not related to the thermalization between Zeeman split levels.

Figure 2 shows the circular polarization of the emission

 

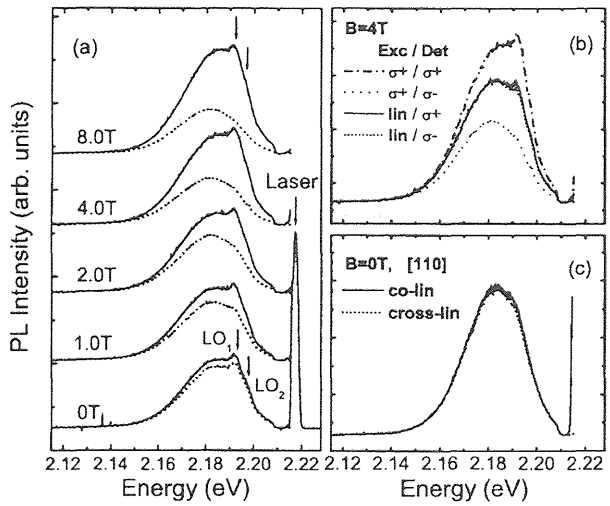


FIG. 1. Circularly polarized PL spectra (a) in co-circular (solid lines) and cross-circular (dotted lines) geometries, at various magnetic fields. (b) Circularly polarized PL spectra in four geometries at 4 T. Linearly polarized excitation gives the same intensity of right- and left-circularly polarized PL (lin/$\sigma^+$ and lin/$\sigma^-$, respectively). (c) Linearly polarized PL spectra in co- and cross-linear geometries along [110] direction.

peak as a function of magnetic field. The circular polarization is defined by $P=(I^+-I^-)/(I^++I^-)$, where $I^+$ and $I^-$ are the PL intensities under the co-circular and cross-circular geometries. It shows that the circular polarization increases with increasing the magnetic field and saturates at the high magnetic field above 6 T. The circular polarization of phonon replica $LO_1$ was also presented in the figure. Figure 1(a) shows that the phonon replica is not polarized at zero field, while it becomes strongly polarized in co-circular geometry with applying magnetic field.

This behavior is quite similar to the effect induced by the anisotropic exchange interaction of excitons. As we know,

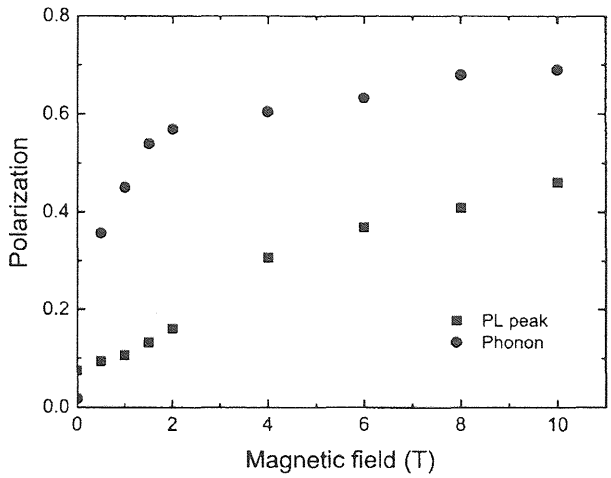


FIG. 2. Magnetic field dependence of the circular polarization of QDs emission peak and phonon resonance $LO_1$ in steady-state PL spectra.

the ground state of the e1-hh1 ($1s$) heavy-hole exciton in a zinc-blende quantum well is fourfold degenerate with the angular-momentum projection $M=s+j=\pm1,\pm2$ on the growth axis $z//[001]$ of the structure. The exchange interaction splits this state into a radiation doublet $|\pm1\rangle$ and two closely lying optically inactive singlets, which are a superposition of the $|\pm2\rangle$ states. In some QD structures, the symmetry is lowered and the exchange interaction is thus no longer isotropic.[10,11] The anisotropic exchange interaction splits the $|\pm1\rangle$ radiative doublet into two eigenstates labeled $|X\rangle=(|1\rangle+|-1\rangle)/(\sqrt{2})$ and $|Y\rangle=(|1\rangle-|-1\rangle)/(i\sqrt{2})$, linearly polarized along the [110] and [1$\bar{1}$0] directions, respectively. This anisotropic exchange splitting may originate from QD elongation and interface optical anisotropy.[12,13]

When the magnetic field was applied, and if the Zeeman splitting $\hbar\Omega_z=g\mu_B B$ is much larger than the exchange energy $\hbar\omega$, the QD exciton eigenstates are no longer the $|X\rangle$ and $|Y\rangle$ linearly polarized states, but the $|+1\rangle$ and $|-1\rangle$ circular ones. We thus expect to observe circularly polarized PL under $\sigma$-polarized excitation. This circular polarization was indeed observed by several groups in various nanostructure systems.[10–14] In our case, we did not observe any linear polarization at zero field under linearly polarized excitation along [110] and [1$\bar{1}$0] directions, as shown in Fig. 1(c). At higher field $B=4$ T, the PL spectra under linearly polarized excitation in Fig. 1(b) did not show circular polarization, which contradicts this model. We also checked the linearly polarized time-resolved PL under linearly polarized excitation along [110] and [1$\bar{1}$0] directions, and did not observe any polarization in the temporal profile. All these experimental results indicate that anisotropic exciton fine structure is not responsible for our results. Although the anisotropic exchange energy splitting was observed in elongated QDs, its absence is not strange in the isotropic QDs. Surrounding mixed crystal $Zn_xCd_{1-x}Te$ (Ref. 15) might induce isotropic inner core CdTe QDs.

Another possible explanation of the experimental results is that the circular polarization originates from the suppression of spin relaxation by the longitudinal magnetic field. Our results indicate that the spin relaxation time is very fast at zero field, and the spin orientation is practically destroyed during the electron lifetime. If we assume that the spin relaxation is suppressed by the longitudinal magnetic field, then the circular polarization of steady-state PL band increases with increasing magnetic field. We can use a common formula to estimate the spin relaxation time from the steady-state PL measurements:

$$P=\frac{P_0}{1+2\tau_r/\tau_s}. \quad (1)$$

Here, $P_0$ is the initial spin polarization, and $\tau_r$ and $\tau_s$ are the lifetime and spin relaxation time of carriers, respectively. The lifetime $\tau_r$ and the initial spin polarization $P_0$ use the values obtained from the time-resolved PL measurements, which will be discussed later. (The calculated spin relaxation rates from the steady-state PL polarization degree will be shown in Fig. 4.)

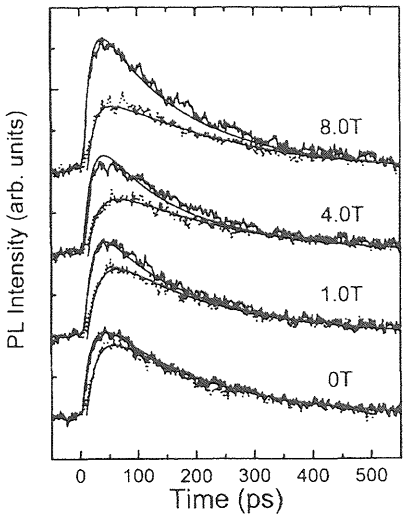


FIG. 3. Time dependence of the circularly polarized PL for co-circular (solid lines) and cross-circular (dotted lines) geometries at various magnetic fields (0–8 T) at 10 K. Smooth curves are fittings by a combination of a rise function and two exponential decay functions, whose decay times are related to $\tau_r$ and $\tau_s$.

The protuberant phonon structure observed in the cw luminescence band of QDs is formed by the competition between the phonon-mediated relaxation and nonradiative loss.[16] Further, in case of the circularly polarized luminescence, the competition between the phonon-mediated relaxation and spin relaxation is thought to determine the phonon structures in the cross-circularly polarized luminescence spectra. In this model, the assumption of suppression of spin relaxation can be used to explain the circular polarization of phonon structures simply. As is seen in Fig. 1(a), LO phonon structures in the cross-circular polarization geometry decrease with the increase of the magnetic field, while those in the co-circular polarization geometry does not change. This feature is explained by the assumption that spin flip time becomes longer than the time for the relaxation mediated by the LO phonon plus acoustic phonons with the increase of the magnetic field.

The time-resolved PL measurements confirmed the suppression of spin relaxation by external magnetic field. The temporal profiles of circularly polarized PL signal under the co-circular and cross-circular geometries at various magnetic fields are shown in Fig. 3. We can see clearly that the spin relaxation time becomes longer with increasing magnetic field. In order to investigate the spin dynamics and recombination process, we calculated the sum $(I^+ + I^-)$ and the difference $(I^+ - I^-)$ of the circularly polarized luminescence, where $I$ is the intensity of circularly polarized PL. The sum $(I^+ + I^-)$ is proportional to $\exp(-t/\tau_r)$, where $\tau_r$ is the lifetime. We obtained the lifetime at the maximum position of the PL band, $\tau_r = 190$ ps, which is independent of magnetic field. The time-dependent degree of circular polarization $P(t)$ is defined by $P(t) = (I^+ - I^-)/(I^+ + I^-)$. $P(t)$ is proportional to $\exp(-2t/\tau_s)$,[17] where $\tau_s$ is the spin relaxation time. The spin relaxation time can be estimated from the decay of $P(t)$. The obtained spin relaxation rates, $1/\tau_s$, are shown as a function

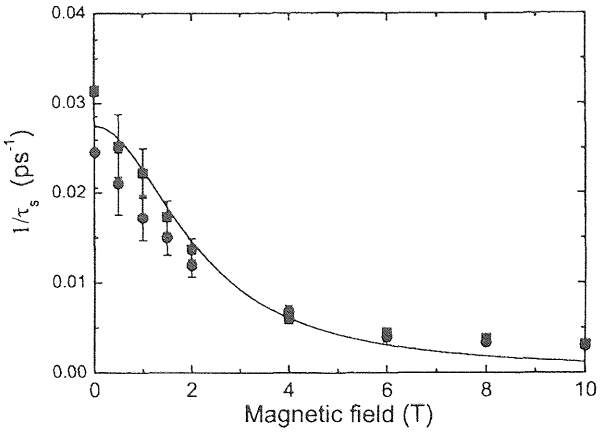


FIG. 4. Magnetic field dependence of the spin relaxation rate. The experimental values from time-resolved PL (circles) and the estimated values from steady-state PL spectra (squares) are shown together for comparison. The solid line is the theoretical fitting according to Eq. (2).

of magnetic field in Fig. 4 by circles. We can see that the measured spin relaxation rates are consistent with the estimated ones from steady-state PL spectra (squares). The discrepancy at low field may come from the fluctuation of laser power, or the difference of detected energies in PL and time-resolved PL measurements. The time-resolved PL measurements proved further that the unusual magnetic field dependence of circular polarization observed in steady-state PL measurements originates from the suppression of spin relaxation by the longitudinal magnetic field.

The spin relaxation rate is not affected remarkably by the magnetic field in the framework of anisotropic exchange interaction of exciton, as was reported by Paillard *et al.*[14] However, we observed that the spin relaxation rate decreases remarkably with the increase of the longitudinal magnetic field. Therefore, the model of the anisotropic exchange interaction of excitons cannot explain our results. We need to consider other possibilities. A suppression of spin relaxation by the external magnetic field has been reported for the case of spin relaxation of electrons localized at donors in bulk crystal.[18,19] These authors have found that spin relaxation of electrons localized in potential wells is caused mainly by hyperfine interaction of electron spins with magnetic momenta of lattice nuclei, the hyperfine magnetic field being randomly changed due to the hopping migration of electrons over localized states in the crystal. This mechanism should work for localized electrons in QDs. In a strong magnetic field, the nuclear hyperfine fields only perturb the precession frequency of the electron spin about the external magnetic field. As a result, the spin component parallel to $B$ is conserved, while the transverse spin component precesses with Larmor frequency. The dependence of the electron spin relaxation time $\tau_s$ on the longitudinal magnetic field can be described by the expression

$$\frac{1}{\tau_s} = \frac{1}{\tau_s(0)(1+\Omega^2\tau_c^2)}. \tag{2}$$

Here, $\tau_s(0)$ is the spin relaxation time under the zero magnetic field, $\Omega = g_e\mu_B B/\hbar$ is the precession frequency of the

electron spin in the field $B$, and $\tau_c$ is a characteristic time of the order of correlation time of the fluctuating magnetic field responsible for the spin relaxation. Here we used $\tau_c$ as a fitting parameter. If the nuclear field $B_N$ is present, the quantity in Eq. (2) is defined by the total field acting on the electron spin. By this formula, we can simulate the magnetic field dependence of spin relaxation time, which is in good agreement with the experimental data.

Merkulov *et al.* studied theoretically electron spin relaxation in InAs QDs and CdSe QDs via interaction with nuclear spins, and they proposed the hyperfine interaction is the dominant mechanism of carriers in these QDs.[6] They obtained the spin dephasing time on the order of 50–100 ps for InAs QDs, which is close to our data. Correspondingly, we think that the fast relaxation in CdTe QDs is due mainly to the hyperfine interaction with nuclei spin at zero field. The spin relaxation is suppressed by the external magnetic field. However, the hyperfine interaction constants in CdTe are not experimentally determined. Reliable quantitative calculation is difficult to obtain. In this material only a fraction of the nuclei (25% of the Cd ions) have magnetic moments, and they have spin $I=1/2$. As a result, the electron spin interaction with the nuclei in these QDs is weak. Although Merkulov *et al.* calculated the hyperfine interaction in nanocrystal CdSe QDs, the obtained spin dephasing time is around 1 ns, and longer than our data. Further theoretical and experimental work is needed to clarify the spin relaxation time for various materials.

In conclusion, we have measured the PL spectra and time-resolved PL in the CdTe/ZnTe QDs under a longitudinal magnetic field up to 10 T and at 10 K. An unusual magnetic field dependence of circular polarization was observed in steady-state PL spectra. However, we did not observe any linear polarization at zero field. This cannot be explained by the anisotropic fine structures of excitons. Time-resolved PL confirmed that electron spin relaxation is suppressed by the longitudinal magnetic field. We attribute it to the effect of nuclear field. We believe that the spin relaxation is determined mainly by the hyperfine interaction of electrons with nuclei. The Larmor precession of electron spin about the strong external magnetic field can suppress the precession about the internal hyperfine field, thus preserving the initial orientation of electron spins. We expect our experiments can help to understand the spin relaxation processes and to extend the relaxation time in CdTe QDs.

---

*Present address: Department of Materials Science, Osaka Prefecture University, Sakai, Japan.

[1] S. A. Wolf, D. D. Awschalom, R. A. Buhrman, J. M. Daughton, S. von Molnar, M. L. Roukes, A. Y. Chtchelkannova, and D. M. Treger, Science **294**, 1488 (2001).

[2] *Optical Orientation*, in Modern Problems in Condensed Matter Sciences Vol. 8, edited by F. Meier and B. Zakharchenya (North-Holland, Amsterdam, 1984).

[3] M. Z. Maialle, E. A. de Andrada e Silva, and L. J. Sham, Phys. Rev. B **47**, 15 776 (1993).

[4] M. I. D'yakonov and V. I. Perel', Zh. Eksp. Teor. Fiz. **60**, 1954 (1971) [Sov. Phys. JETP **33**, 1053 (1971)].

[5] A. V. Khaetskii and Y. V. Nazarov, Phys. Rev. B **61**, 12 639 (2000).

[6] I. A. Merkulov, Al. L. Efros, and M. Rosen, Phys. Rev. B **65**, 205309 (2002).

[7] D. Gammon, Al. L. Efros, T. A. Kennedy, M. Rosen, D. S. Katzer, D. Park, S. W. Brown, V. L. Korenev, and I. A. Merkulov, Phys. Rev. Lett. **86**, 5176 (2001).

[8] R. I. Dzhioev, B. P. Zakharchenya, V. L. Korenev, and M. V. Lazarev, Phys. Solid State **41**, 2014 (1999) [Fiz. Tverd. Tela (Leningrad) **41**, 2193 (1999)].

[9] Y. Terai, S. Kuroda, K. Takita, T. Okuno, and Y. Masumoto, Appl. Phys. Lett. **73**, 3757 (1998).

[10] D. Gammon, E. S. Snow, B. V. Shanabrook, D. S. Katzer, and D. Park, Science **273**, 87 (1996).

[11] E. L. Ivchenko, Pure Appl. Chem. **67**, 463 (1995); R. I. Dzhioev *et al.*, Phys. Solid State **40**, 790 (1998).

[12] S. Hameau, Y. Guldner, O. Verzelen, R. Ferreira, G. Bastard, J. Zeman, A. Lemaître, and J. M. Gérard, Phys. Rev. Lett. **83**, 4152 (1999).

[13] R. I. Dzhioev, H. M. Gibbs, E. L. Ivchenko, G. Khitrova, V. L. Korenev, M. N. Tkachuk, and B. P. Zakharchenya, Phys. Rev. B **56**, 13 405 (1997).

[14] M. Paillard, X. Marie, P. Renucci, T. Amand, A. Jbeli, and J. M. Gérard, Phys. Rev. Lett. **86**, 1634 (2001).

[15] T. Okuno, M. Nomura, Y. Masumoto, Y. Terai, S. Kuroda, and K. Takita, J. Phys. Soc. Jpn. **71**, 3052 (2002).

[16] I. V. Ignatiev, I. E. Kozin, V. G. Davydov, S. V. Nair, J. S. Lee, H. W. Ren, S. Sugou, and Y. Masumoto, Phys. Rev. B **61**, 15 633 (2000); **63**, 075316 (2001).

[17] R. J. Seymour and R. R. Alfano, Appl. Phys. Lett. **37**, 231 (1980).

[18] R. R. Parsons, Can. J. Phys. **49**, 1850 (1971).

[19] V. L. Berkovits, A. I. Ekimov and V. I. Safarov, Sov. Phys. JETP **38**, 169 (1974) [Zh. Eksp. Teor. Fiz. **65**, 346 (1973)].

# Direct Observation of the Electron Spin Relaxation Induced by Nuclei in Quantum Dots

P.-F. Braun,[1] X. Marie,[1,*] L. Lombez,[1] B. Urbaszek,[1] T. Amand,[1] P. Renucci,[1] V. K. Kalevich,[2] K. V. Kavokin,[2] O. Krebs,[3] P. Voisin,[3] and Y. Masumoto[4]

[1]*LNMO, INSA 135 Avenue de Rangueil, 31077 Toulouse CEDEX 4, France*
[2]*IOFFE Institute, Politeknicheskaya 26, St. Petersburg 194021, Russia*
[3]*Laboratoire de Photonique et Nanostructures, Route de Nozay, 91460 Marcoussis, France*
[4]*Institute of Physics, University of Tsukuba, Tsukuba 305-8571, Japan*

(Received 10 November 2004; revised manuscript received 17 December 2004; published 23 March 2005)

We have studied the electron spin relaxation in semiconductor InAs/GaAs quantum dots by time-resolved optical spectroscopy. The average spin polarization of the electrons in an ensemble of $p$-doped quantum dots decays down to 1/3 of its initial value with a characteristic time $T_\Delta \approx 500$ ps, which is attributed to the hyperfine interaction with randomly oriented nuclear spins. We show that this efficient electron spin relaxation mechanism can be suppressed by an external magnetic field as small as 100 mT.

DOI: 10.1103/PhysRevLett.94.116601 PACS numbers: 72.25.Fe, 72.25.Rb, 73.21.La, 78.47.+p

Spins of localized electrons in semiconductor quantum dots (QDs) are attractive for future spintronic and quantum information devices since they are not subject to the classical spin relaxation mechanisms known for free carriers [1–5]. Recent theoretical studies have predicted that the dominant mechanism of electron spin relaxation in QDs at low temperature is due to the hyperfine interaction with nuclear spins [6–8]. An electron spin in a quantum dot interacts with a large but finite number of nuclei $N_L \approx 10^3$–$10^5$ [4]. In the frozen fluctuation model, the sum over the interacting nuclear spins gives rise to a local effective hyperfine field $\mathbf{B}_N$ [6]. The electron spin can thus coherently precess around $\mathbf{B}_N$ [6,7]. However, the amplitude and the direction of the effective nuclear field vary strongly from dot to dot. The average electron spin $\langle \mathbf{S}(t) \rangle$ in an ensemble of dots will thus decay as a consequence of the random distribution of the local nuclear effective field. For the sake of simplicity, this spin dephasing mechanism on the QD ensemble is termed here "spin relaxation." Note that for repeated measurements on a single QD the hyperfine interaction has the same effect as for an ensemble of dots [6,7].

The spin dynamics of carriers in III-V or II-VI semiconductor QDs have been studied experimentally by different groups in recent years [9–20]. Spin relaxation times of the neutral exciton longer than 20 ns have been found in undoped QDs [13–15]. In $n$-doped QDs, hole spin relaxation times longer than 10 ns have been measured [16,17]. In all these experiments, no manifestation of the electron spin relaxation due to the interaction with nuclei has been observed for the following reasons: (i) In undoped QDs the photogenerated electron feels a strong effective magnetic field due to the exchange interaction with the hole [21]. This exchange field is much stronger than the effective hyperfine field of the nuclei, which thus plays a negligible role [22]. (ii) In the experiments performed on $n$-doped QDs the ground state luminescence corresponds to the radiative recombination of the negatively charged exciton $X^-$ formed by one hole, and a pair of electrons with opposite spins in a singlet state [23]. In this case, no effect of the hyperfine interaction with nuclei is expected since the total electron spin in the charged exciton is zero and the hole spin is only weakly coupled to the nuclear spins due to the $p$ symmetry of the hole Bloch function [24].

The ideal configuration to probe the electron spin relaxation mediated by nuclei in QDs with optical experiments presents itself in the form of positively charged excitons $X^+$ (consisting of one electron and two holes forming a spin singlet). As in the case of $X^-$, the exchange interaction between the electron and the two holes cancels in the $X^+$ ground state. The analysis of the circular polarization of the $X^+$ luminescence in $p$-doped QDs following a circularly polarized laser excitation will thus probe *directly* the spin polarization of the electron. A large spin polarization of the $X^+$ luminescence has indeed been observed recently in InAs/GaAs and GaAs/AlGaAs quantum dot photoluminescence (PL) spectra [25,26]. To the best of our knowledge the spin dynamics in $p$-doped QDs has, however, not been studied at low temperature so far.

In this Letter, we present measurements of the electron spin dynamics in $p$-doped InAs/GaAs quantum dots using optical orientation experiments. We find that the time dependence of the electron spin polarization exhibits two regimes: the polarization decays within the first 800 ps down to 1/3 of its initial value; it then remains stable with no measurable decay on the radiative lifetime scale. We also show experimentally that this efficient spin relaxation mechanism can be suppressed by the application of a small external magnetic field ($B \approx 100$ mT). We interpret these results as experimental evidence of electron spin relaxation mediated by the hyperfine interaction with nuclei in an ensemble of QDs. We have studied three modulation doped QD structures grown by molecular beam epitaxy on (001) GaAs substrates. Very similar results have been obtained for all three samples. We present here the experimental data obtained in one of them which consists of 10 planes of lens shaped self-assembled InAs/GaAs QDs separated by a 30 nm GaAs layer; a beryllium delta doping layer

 

is located 15 nm below each wetting layer (WL). The nominal acceptor concentration is $N_A = 15 \times 10^{10}$ cm$^{-2}$ per layer in this sample. The QD density is about $4 \times 10^{10}$ cm$^{-2}$ per plane. The observation of QD ground state PL under strictly resonant excitation (not shown here) proves that this structure contains on average less than two resident holes on the QD ground state. We have investigated the spin properties in these structures by continuous wave (cw) and time-resolved PL experiments. In the time-resolved experiments the samples are excited by 1.5 ps pulses generated by a mode-locked Ti-doped sapphire laser with a repetition frequency of 82 MHz. The time-resolved PL of the QD ground state is then recorded using an S1 photocathode streak camera with an overall time resolution of 30 ps. The excitation pulses are circularly polarized ($\sigma^+$). The luminescence intensity copolarized ($I^+$) and counterpolarized ($I^-$) with the excitation laser is recorded. The circular polarization degree of the luminescence is defined as $P_c = (I^+ - I^-)/(I^+ + I^-)$. In the following the arrows $\uparrow, \downarrow$ characterize the spin projection on the Oz growth axis of the electron ground states (labeled $S_c$), whereas $\Uparrow$ and $\Downarrow$ characterize the heavy-hole pseudospin in the valence ground state (labeled $S_v$) [18].

Figure 1(a) displays the cw PL spectrum of the QD ground states at $T = 10$ K. It is characterized by a full width at half maximum of about 50 meV due to the fluctuations of size, shape, and strain in the ensemble of dots. Figure 1(b) presents the circular polarization of the time-integrated PL after a circularly polarized picosecond excitation. The excitation energy is 1.44 eV; this corresponds to the photons absorption in the low energy part of the WL (because of the strain and the quantum confinement, this absorption corresponds to a heavy-hole-to-electron-like transition [18]). We measure a circular polarization degree of $\approx$19% of the QD ground state emission ($B_z = 0$). The excitation intensity is about 1 mW; this corresponds to the photogeneration of less than one electron-hole pair per QD. All three $p$-doped samples that we have studied present circular polarization degrees larger than 10%. In contrast, the same experiment performed in nominally undoped QD samples (not shown here) yields a very small polarization $P_c < 3\%$. This weak circular polarization in undoped QDs under these nonresonant excitation conditions is a direct consequence of the linearly polarized neutral exciton eigenstates due to the anisotropic exchange interaction (AEI) between the electron and the hole [13,14,27,28]. The measurement of a significant circular polarization in Fig. 1 is a strong indication of the successful chemical doping of the QD. For simplicity, we consider for the interpretation that (i) the dots contain a single resident hole and (ii) a single electron-hole pair is optically injected into the dot. Following excitation into the WL, it is commonly assumed that the electron spin does not relax during the capture and energy relaxation process in the QD, whereas the initial hole spin orientation is lost due to efficient spin relaxation processes in the WL [18,25,29]. The recorded PL in the $p$-doped QD samples corresponds essentially to the radiative recombination of positively charged exciton $X^+$ formed with a spin polarized electron and two holes with opposite spin [see Fig. 1(c)]: $|X^+\rangle = 1/\sqrt{2}(|\Uparrow, \Downarrow, \downarrow\rangle - |\Downarrow, \Uparrow, \downarrow\rangle)$.

Figure 2 displays the circular polarization dynamics of the QD ground state luminescence [same excitation conditions as Fig. 1(b)]. The inset presents the time evolution of the luminescence intensity components $I^+$ and $I^-$. The circular polarization dynamics in Fig. 2 presents two regimes. The polarization decays within the first 800 ps down to a value of about 12%, then it remains stable with no measurable decay on the radiative lifetime scale. We can infer that the spin relaxation in this second regime is longer than 10 ns. This specific circular polarization dynamics has been observed for any detection energy in the PL spectrum of the QD ground state ensemble. Moreover, we have measured similar kinetics in all the $p$-doped samples we have studied.

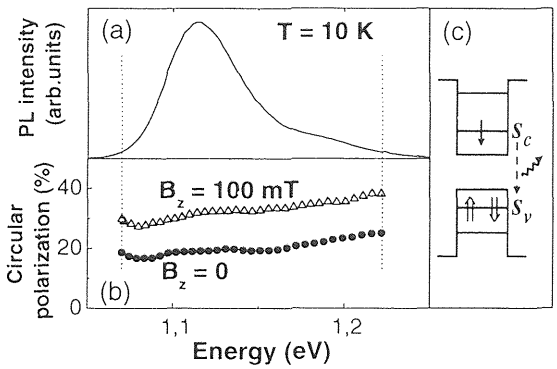


FIG. 1. (a) cw photoluminescence spectrum of the QD. (b) Circular polarization of the QD ground state luminescence for (●) $B_z = 0$ and (△) $B_z = 100$ mT. (c) Scheme of a positively charged exciton $X^+$ formed by a spin polarized electron and two holes with opposite angular momentum projection.

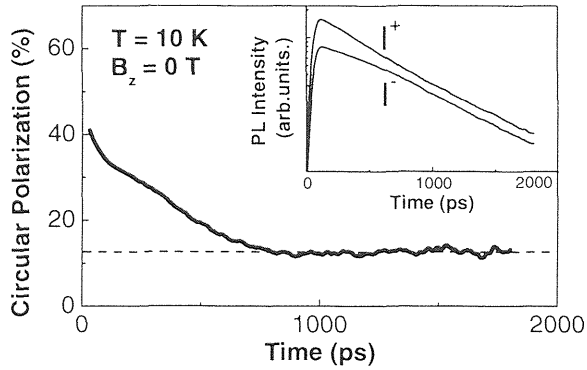


FIG. 2. Circular polarization dynamics of the QD luminescence after a circularly polarized $\sigma+$ laser excitation. Inset: Photoluminescence intensity copolarized $I^+$ and counterpolarized $I^-$ with the laser (semilogarithmic scale). The detection energy is centered at $E_{det} = 1.11$ eV.

All these results are in very good agreement with the predicted electron spin relaxation by nuclei [6–8]. The time dependence of the average electron spin due to the interaction with nuclei can be written as [6]

$$\langle \mathbf{S}(t) \rangle = \frac{\mathbf{S}_0}{3}\left\{1 + 2\left[1 - 2\left(\frac{t}{2T_\Delta}\right)^2\right]\exp\left[-\left(\frac{t}{2T_\Delta}\right)^2\right]\right\}, \quad (1)$$

where $\mathbf{S}_0$ is the initial spin, $T_\Delta = \hbar/(g_e \mu_B \Delta_B)$ is the dephasing time due to the random electron precession frequencies in the randomly distributed frozen fluctuation of the nuclear hyperfine field, $\mu_B$ is the Bohr magneton, and $g_e$ is the electron effective Landé factor. The dispersion of the nuclear hyperfine field $B_N$ is described here by a Gaussian distribution characterized by its width $\Delta_B$: $W(\mathbf{B}_N) \approx \exp[-(\mathbf{B}_N)^2/\Delta_B^2]$ [6]. It is clear from Eq. (1) that the time dependence of the average electron spin polarization exhibits two regimes. After a strong initial decay with a characteristic time $T_\Delta$, the average electron spin polarization is expected to reach a constant value of 1/3 of the initial polarization (inset of Fig. 3) [30]. The circular polarization measured in Figs. 1 and 2 corresponds mainly to the radiative recombination of $X^+$; i.e., it probes directly the spin relaxation of electron: $P_c(t) \approx \rho_e(t) = 2\langle S(t) \rangle$, where $\rho_e$ is the electron spin polarization. The initial value of the average electron spin polarization here is about $\rho_e(0) \approx 40\%$; $\rho_e(t)$ then drops down to about 1/3 ($\rho_e \approx 12\%$) of its initial value in agreement with the predictions of Eq. (1). After the initial drop, the average electron spin polarization remains stable on the radiative lifetime scale. Merkulov *et al.* calculated that the subsequent electron spin dephasing, which is the result of the variations of the nuclear field direction, occurs on a time scale typically 100 times longer than $T_\Delta$ [6]. Thus it cannot be observed on the radiative lifetime scale.

A key argument for the hyperfine interaction being responsible for the initial polarization decay comes from magnetic field dependent measurements. We have recorded the circular polarization dynamics of the QD ground state luminescence with a magnetic field applied along the Oz growth axis. Merkulov *et al.* and Semenov *et al.* predict that the electron spin dephasing induced by hyperfine interaction can be strongly suppressed in an external magnetic field [6,8,31]. The required magnetic field must be larger than $\Delta_B$, which is of the order of 10 mT [7], to ensure that the Zeeman interaction of the electron spin with the magnetic field is stronger than the interaction with the nuclei. We see in Fig. 1(b) that the time-integrated circular polarization is almost doubled at the peak of the spectrum when a magnetic field of $B_z = 100$ mT is applied. This strong increase in circular polarization for such a weak external magnetic field is very unusual in nonmagnetic semiconductors. Note that the Zeeman splitting energy of the electron in this weak magnetic field is at least 50 times smaller than $k_B T$ at $T = 10$ K [21]. Figure 3 displays the circular polarization dynamics of the QD ground state luminescence with magnetic fields $B_z = 100$ mT and $B_z = 400$ mT; the dynamics for $B_z = 0$ is also presented for comparison. By applying a field of $B_z = 100$ mT, we drastically increase the initial decay time to ≈4000 ps, as compared to ≈500 ps at $B_z = 0$. This pronounced effect of the small external magnetic field observed in Fig. 3 agrees very well with the expected influence of the external magnetic field on the QD electron spin relaxation by nuclei [6,8]. The effect observed here is similar to the suppression of the nuclear hyperfine interaction measured recently for localized electrons in lightly doped bulk *n*-GaAs [32,33].

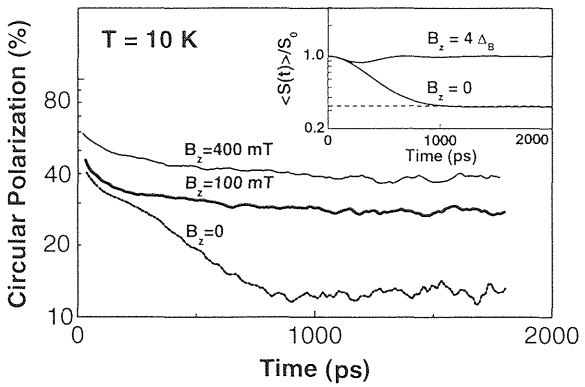


FIG. 3. Circular polarization dynamics of the QD ground state luminescence (semilogarithmic scale) for $B_z = 0$, $B_z = 100$ mT, and $B_z = 400$ mT. The inset displays the calculated time dependence of the average electron spin $\langle \mathbf{S}(t) \rangle / \mathbf{S}_0$ (see text).

We see in Fig. 3 that the time evolution of the circular polarization at $B_z = 400$ mT is very similar to the behavior at $B_z = 100$ mT [34]. The main difference is a small increase of the initial circular polarization, which is probably due to the effect of the magnetic field on the electron spin relaxation during its capture and energy relaxation inside the dot. We still observe a slow initial decay of the circular polarization in Fig. 3, whereas we expect a total suppression of the spin relaxation by nuclei for $B_z > 100$ mT (see inset) [6,8]. First, we have assumed up to now that the analyzed luminescence corresponds only to the radiative recombination of positively charged excitons $X^+$. This is an oversimplified description as neutral excitons $X^0$ or doubly charged excitons $X^{2+}$ can contribute to the recombination process since some of the dots contain zero or two holes before the optical excitation (the majority of the dots containing one resident hole). The slow initial decay observed in Fig. 3 for $B_z \neq 0$ could be due to the complex spin dynamics of $X^0$ or $X^{2+}$. Second, we have neglected in our interpretation the details of the spin-dependent energy relaxation inside the dots. In *n*-doped InAs/GaAs QDs it has been shown, in particular, that the strong AEI in the $X^-$ charged exciton hot triplet state plays a significant role in the spin dynamics [18,35]. In *p*-doped QDs a similar slow spin flip process mediated by the AEI in the $X^+$ hot triplet state could occur in the QD where the photogenerated and resident hole spins are parallel. This

effect may also contribute to the slow initial decay of the circular polarization in Fig. 3 for $B_z \neq 0$. As the anisotropic exchange energy in the hot triplet state is a few tens of $\mu$eV, the suppression of the AEI spin relaxation mechanism would require the application of magnetic fields of the order of a few Teslas. Note that in $n$-doped QDs the application of a field of $B_z = 100$ mT does not yield any measurable change in the PL circular polarization dynamics [36].

The initial decay time of the average electron spin polarization due to the interaction with nuclei can be estimated from Fig. 3 ($B_z = 0$). We find $T_\Delta \approx 500$ ps. Merkulov *et al.* showed that this dephasing time can be written as

$$T_\Delta = \hbar \left[ n^2 \sum_j I^j (I^j + 1)(A^j)^2/(3N_L) \right]^{-1/2}, \qquad (2)$$

where $N_L$ is the number of nuclei interacting with the electron in the QD, $A^j$ the hyperfine constant, $I^j$ the spin of the $j$th nucleus, and $n$ the number of nuclei per unit cell [6]. The sum goes over all the atoms in the primitive unit cell. We take for the hyperfine constants of As ($I^{\mathrm{As}} = 3/2$) and In ($I^{\mathrm{In}} = 9/2$) the values $A_{\mathrm{As}} = 47$ $\mu$eV and $A_{\mathrm{In}} = 56$ $\mu$eV, consistent with $n = 2$ [37]. For a typical dot size (base diameter $\approx 17 \pm 3$ nm, height $\approx 5 \pm 2$ nm) [38], we estimate that the number of nuclei in interaction with the electron is $N_L = N_0 \pm \Delta N_L \approx 6 \times 10^4 \pm 4 \times 10^4$ [6,7]. Equation (2) yields for an InAs dot $T_\Delta^{\mathrm{InAs}} \approx 450 \pm 170$ ps, in good agreement with the experimental value ($\approx$500 ps) if we consider (i) the great uncertainty on the determination of the number of nuclei $N_L$ interacting with the electron and (ii) the In/Ga interdiffusion which yields the formation of InGaAs dots rather than pure InAs dots [39]. From the experimental determination of the dephasing time $T_\Delta$, we can estimate the dispersion $\Delta_B$ of the nuclear hyperfine field $\mathbf{B}_N$. We find $\Delta_B = \hbar/(g_e \mu_B T_\Delta) \approx 28$ mT, assuming an electron $g$ factor of $|g_e| = 0.8$ as measured by Bayer *et al.* [21]. This value of $\Delta_B$ is consistent with the effect of the external magnetic field observed in Figs. 1(b) and 3. The external magnetic field $B_z = 100$ mT is about 4 times larger than $\Delta_B$. The inset of Fig. 3 presents the calculated average electron spin $\langle \mathbf{S}(t) \rangle / \mathbf{S}_0$ for $B_z = 0$ and $B_z = 4 \times \Delta_B$ ($\approx$100 mT) with the parameters $T_\Delta = 450$ ps and $\Delta_B = 28$ mT [6]. An additional Gaussian broadening of $(T_\Delta)^{-1}$ corresponding to the dot size variations $\Delta N_L/N_0 \approx T_\Delta \sigma (2 \ln 2)^{1/2}$ with a standard deviation of $\sigma \approx 0.8 (T_\Delta)^{-1}$ has been added to the calculation of Ref. [6] to take into account the fluctuations of $N_L$ from dot to dot. We clearly observe the quenching of the spin relaxation by nuclei through the application of a weak external magnetic field. In conclusion, we have investigated the spin dynamics of positively charged excitons in InAs/GaAs quantum dots by time-resolved photoluminescence. We have shown that the dominant electron spin relaxation mechanism at low temperature in QDs is due to the hyperfine interaction with nuclei. Although this efficient spin relaxation mechanism may strongly limit the performance of future spintronic devices, our measurements show that this spin relaxation can be suppressed by applying a magnetic field as small as 100 mT, provided, for example, by small permanent magnets.

We gratefully thank A. E. Zhukov and V. M. Ustinov for the sample growth.

*Electronic address: marie@insa-toulouse.fr

[1] A. Imamoglu *et al.*, Phys. Rev. Lett. **83**, 4204 (1999).
[2] R. Fiederling *et al.*, Nature (London) **402**, 787 (1999).
[3] M. Oestreich, Nature (London) **402**, 735 (1999); H. Ohno, Science **291**, 840 (2001).
[4] A. Imamoglu *et al.*, Phys. Rev. Lett. **91**, 17402 (2003).
[5] L. M. Woods *et al.*, Phys. Rev. B **66**, 161318(R) (2002).
[6] I. A. Merkulov *et al.*, Phys. Rev. B **65**, 205309 (2002).
[7] A. Khaetskii *et al.*, Phys. Rev. Lett. **88**, 186802 (2002).
[8] Y. Semenov *et al.*, Phys. Rev. B **67**, 73301 (2003).
[9] D. Gammon *et al.*, Science **277**, 85 (1997).
[10] J. A. Gupta *et al.*, Phys. Rev. B **59**, R10421 (1999).
[11] I. Ignatiev *et al.*, Physica (Amsterdam) **17E**, 361 (2003).
[12] R. Dzhioev *et al.*, Phys. Solid State **41**, 2014 (1999).
[13] M. Paillard *et al.*, Phys. Rev. Lett. **86**, 1634 (2001).
[14] A. S. Lenihan *et al.*, Phys. Rev. Lett. **88**, 223601 (2002).
[15] E. Tsitishvili *et al.*, Phys. Rev. B **66**, 161405 (2002).
[16] T. Amand *et al.*, Superlattices Microstruct. **32**, 157 (2002).
[17] T. Flissikowski *et al.*, Phys. Rev. B **68**, 161309 (2003).
[18] S. Cortez *et al.*, Phys. Rev. Lett. **89**, 207401 (2002).
[19] M. Kroutvar *et al.*, Nature (London) **432**, 81 (2004).
[20] K. Gundogdu *et al.*, Appl. Phys. Lett. **84**, 2793 (2004).
[21] M. Bayer *et al.*, Phys. Rev. Lett. **82**, 1748 (1999).
[22] S. I. Erlingson *et al.*, Phys. Rev. B **64**, 195306 (2001).
[23] R. J. Warburton *et al.*, Nature (London) **405**, 926 (2000).
[24] E. I. Gryncharova *et al.*, Sov. Phys. Semicond. **11**, 997 (1977).
[25] A. Bracker *et al.*, Phys. Rev. Lett. **94**, 047402 (2005).
[26] S. Laurent *et al.*, Acta Phys. Pol. A **106**, 185 (2004).
[27] T. Flissikowski *et al.*, Phys. Rev. Lett. **86**, 3172 (2001).
[28] W. Langbein *et al.*, Phys. Rev. B **69**, 161301 (2004); A. Tartakovskii *et al.*, Phys. Rev. Lett. **93**, 57401 (2004).
[29] T. Damen *et al.*, Phys. Rev. Lett. **67**, 3432 (1991).
[30] This plateau value is due to the fact that no relaxation occurs when the nuclear field component is oriented along the initial electron spin $\mathbf{S}_0$.
[31] In contrast, the decay of the components of the ensemble average spin polarization perpendicular to the applied magnetic field cannot be suppressed.
[32] J. S. Colton *et al.*, Phys. Rev. B **69**, 121307 (2004).
[33] R. I. Dzhioev *et al.*, Phys. Rev. B **66**, 245204 (2002).
[34] We did not observe any significant difference, within our experimental accuracy, in the spin dynamics at $B_z \neq 0$ for a $\sigma^+$ or $\sigma^-$ polarized excitation.
[35] K. V. Kavokin, Phys. Status Solidi (a) **195**, 592 (2003).
[36] S. Laurent *et al.* (to be published); S. Laurent, Ph.D. thesis, Université Paris 6, 2004, http://tel.ccsd.cnrs.fr.
[37] D. Paget *et al.*, Phys. Rev. B **15**, 5780 (1977).
[38] M. Paillard *et al.*, Appl. Phys. Lett. **76**, 76 (2000).
[39] The same calculation for GaAs dots of the same size yields $T_\Delta^{\mathrm{GaAs}} \approx 2550 \pm 950$ ps.

PHYSICAL REVIEW B 72, 045325 (2005)

# Optical spin polarization and exchange interaction in doubly charged InAs self-assembled quantum dots

V. K. Kalevich,[1,2,*] I. A. Merkulov,[1] A. Yu. Shiryaev,[1] K. V. Kavokin,[1] M. Ikezawa,[2] T. Okuno,[2] P. N. Brunkov,[1] A. E. Zhukov,[1] V. M. Ustinov,[1] and Y. Masumoto[2]

[1]*Ioffe Physico-Technical Institute, St. Petersburg 194021, Russia*

[2]*Institute of Physics, University of Tsukuba, Tsukuba 305-8571, Japan*

(Received 19 November 2004; revised manuscript received 29 April 2005; published 14 July 2005)

The work is an experimental study of optical spin polarization in InAs/GaAs quantum dots (QDs) with two resident electrons or holes. A capture of a photogenerated electron-hole pair into such a QD creates a negative or positive tetron (doubly charged exciton). Spin polarization was registered by the circular polarization of the QD photoluminescence (PL). The spin state was found to be radically different in the dots with the opposite sign of the charge. Particularly, under excitation in a GaAs barrier, the polarization of the ground-state PL is negative (relative to the polarization of exciting light) in the negatively charged QDs and positive in the positively charged QDs. With increasing excitation intensity, the negative polarization rises from zero up to a saturation level, while the positive polarization decreases. The negative polarization increases in weak magnetic fields applied in Faraday geometry; however, it is suppressed in strong fields. The positive polarization always increases as a function of magnetic field. We propose a theoretical model that qualitatively explains the experimental results.

DOI: 10.1103/PhysRevB.72.045325 PACS number(s): 72.25.Fe, 72.25.Rb, 73.21.La, 78.55.Cr

## I. INTRODUCTION

When one passes from three-dimensional to zero-dimensional objects, the role of different mechanisms of spin relaxation changes significantly. When analyzing different mechanisms of spin relaxation for the carriers localized in semiconductor quantum dots (QDs), it is convenient to use the analogy with the spin relaxation of deep paramagnetic centers.[1] The relaxation due to spin-orbital interaction gets suppressed,[2] while the exchange interaction intensifies and becomes anisotropic,[3,4] and the relaxation by nuclei also gets stronger.[5] An anisotropic exchange interaction of electrons and holes induced by the dot asymmetry can split the exciton radiative doublet and destroy spin polarization of QD excitons.[3,4] The anisotropic exchange can be strongly suppressed in charged QDs containing an odd number of carriers (including photocreated electron-hole pairs), since such QDs have half-integer spin and the anisotropic exchange does not split spin states due to the Kramers theorem.[6] Indeed, a long-living spin orientation has been observed in negatively charged InAs,[7] InP,[8] and ZnSe (see Ref. 9) QDs containing one or three resident electrons. As the Kramers theorem is not applicable to the complexes comprising an even number of particles, the question of the spin conservation in QDs with an even number of resident carriers remained, so far, open.

Generally, an analysis of the exchange interaction is significantly complicated by increasing the number of resident carriers in a QD. However, the situation is radically simplified in a QD with two resident carriers. The matter is that in such a QD the ground state of majority carriers is a singlet with a zero spin. Therefore, the exchange interaction of the four-particle complex (tetron) containing two resident carriers and a photoexcited electron-hole pair reduces to the exchange interaction of the photoexcited pair. The latter is the analog of an ordinary exciton. But in contrast with an ordinary exciton, in the tetron one of the particles coupled by the exchange interaction (hole or electron) is in the ground state, while the other one (electron or hole) is in the first excited state. This provides a possibility to study an exchange interaction of particles located at different orbital states. In this work, we study optical spin polarization in QDs with two resident electrons or holes.

## II. SAMPLES AND EXPERIMENTAL RESULTS

We studied the molecular-beam expitaxy (MBE) grown structures containing ten layers of self-assembled InAs/GaAs QDs separated by 30-nm-thick GaAs barriers. The dot density in a layer of about $0.5\times10^{11}$ cm$^{-2}$, base diameter of $\approx$15 nm, and height of $\approx$5 nm was found from the TEM studies (for review see, e.g., Refs. 10 and 11). The dots are positively or negatively charged due to delta doping by Si or Be, respectively. The delta-doping layers are located 15 nm below each QD layer. The dopant density was equal to the double QD density producing nominally two resident electrons or holes per dot on average. The MBE grown structure with a single layer of InAs QDs embedded into the middle of the *i* layer of the *n-i-n* GaAs matrix was also studied. GaAs barriers, cladding the *i* layer, are doped by Si with concentration of $2\times10^{16}$ cm$^{-3}$. In such structures, the QDs are filled with electrons.[12,13] The independent capacitance-voltage measurements[13] showed that on average two resident electrons occupy each QD at low temperature in the *n-i-n* structure.

The carrier spin polarization was created by optical pumping with circular polarized light.[14] A continuous wave tunable Ti:sapphire laser was used for excitation. The helicity of the exciting laser beam was alternated at 42 kHz using a quartz photoelastic modulator.[15,16] Changing the excitation

 

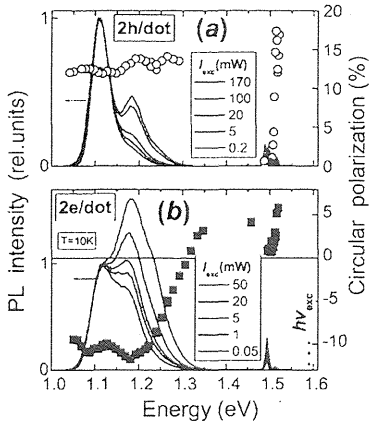


FIG. 1. PL (solid lines) and PL polarization spectra (○ and ■) of doubly positively (a) and negatively (b) charged delta-doped InAs QDs recorded at excitation into the GaAs barrier. $T=10$ K. Excitation energy $h\nu_{exc}$(eV): 1.653 (a), 1.59 (b). Excitation power $I_{exc}$(mW): 1 (○), 5 (■).

helicity at a high frequency precluded dynamical polarization of spins of lattice nuclei.[14,17] The spin polarization of charge carriers was determined by measuring the photoluminescence (PL) circular polarization degree, which is defined as $\rho=(I_+^+-I_+^-)/(I_+^++I_+^-)$, where $I_+^+$ and $I_+^-$ are the intensities of the $\sigma^+$ PL component under $\sigma^+$ and $\sigma^-$ pumping, respectively. To measure the PL circular polarization up to 1.4 $\mu$m, a highly sensitive polarization analyzer[16] with an InGaAsP photomultiplier and a two-channel photon counter synchronized with the quartz polarization modulator was used. For the measurements in a longitudinal magnetic field, the sample was inserted in a center of a superconducting solenoid with a warm bore. The measurements were done at 10 K.

PL and PL polarization spectra of the delta-doped QDs measured at excitation above the GaAs barrier are presented in Fig. 1. The solid lines in Fig. 1 show the PL spectra taken at different excitation intensities. The band centered at the 1.11 eV is the PL of the QD ground state. We suppose that the high-energy shoulder within the range of 1.16–1.21 eV is the radiation of the QD first excited state. With increasing excitation density, the shoulder grows due to the state-filling effect and even exceeds the ground-state PL in negatively charged dots. In positively charged QDs this effect is much less pronounced. This difference is most likely due to the following reasons. In InAs/GaAs QDs, the size quantization energy for electrons is much greater than for holes (50–70 meV against 5–10 meV between the ground and first excited states.[18,19]) Therefore, the visible "excited-state PL" is due to recombination of excited-state electrons. As in $n$-type QDs the ground state is filled with electrons, it takes lower pump power to have the excited electron level occupied for doubly negatively charged ($2e$) QDs than for doubly positively charged ($2h$) QDs. At high-excitation density, a weakly pronounced wing associated with the QD second excited state arises in the 1.22–1.26 eV range indicating that there are at least three electron shells in the QD conduction band. The radiation near the 1.5 eV comes from the GaAs barrier.

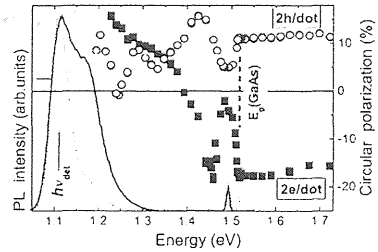


FIG. 2. PL and PL polarization excitation spectra of double-charged delta-doped InAs QDs. $T=10$ K. PL spectra of the positively (dotted line) and negatively (solid line) charged dots recorded at $h\nu_{exc}=1.653$ eV, $I_{exc}=0.2$ mW, and $h\nu_{exc}=1.59$ eV, $I_{exc}=0.05$ mW, respectively. PL circular polarization excitation spectra of the positively (○) and negatively (■) charged dots measured in the center of the ground-state PL band. $h\nu_{det}$(eV): 1.109 (○), 1.117 (■). $I_{exc}$(mW): 5 (○), 20 (■).

The PL polarization spectra of positively and negatively charged dots are shown in Fig. 1 by open circles and closed squares, respectively.

PL circular polarization excitation spectra for positively (○) and negatively (■) charged dots measured in the center of the ground-state PL band are shown in Fig. 2. One can see in Figs. 1 and 2 that the polarization spectra are radically different for positively and negatively charged dots. Under above-barrier excitation, the ground-state PL polarization remains practically constant within a wide range of excitation energies (1.52–1.73 eV) for both types of QDs, but it is negative for $2e$-QDs and positive for $2h$-QDs (see Fig. 2). This "sign rule" holds for excitation into the wetting layer also, but here the absolute value of polarization exhibits a strong nonmonotonous dependence on the excitation-photon energy, which is probably due to the splitting between heavy and light hole subbands in the wetting layer. Under excitation below the wetting layer (<1.38 eV), the PL polarization in $2e$-QDs becomes positive due to spin polarization of holes.[20]

In the following, we consider the case of above-barrier excitation. In this case the ground-state PL polarization is positive in positively charged dots and negative in negatively charged ones. To the contrary, the wetting-layer and barrier emissions are, of course, positively polarized for both types of QDs. This results in a crossover from negative to positive polarization in the PL spectra of negatively charged dots (at ~1.32 eV), as seen in Fig. 1.

The dependences of the ground-state PL polarization on excitation power and longitudinal magnetic field are also strongly different in negatively and positively charged dots. With increasing excitation intensity, the negative polarization rises from zero up to a saturation level, while the positive polarization always decreases, as shown in Fig. 3. We note that spectral dependences of $\rho$ and the dependence of $\rho$ on excitation power for doubly negatively charged QDs in a $n$-$i$-$n$ structure with one layer of InAs QDs (not shown here) are qualitatively similar to those shown in Figs. 1–3 for $n$-delta-doped dots.

Figure 4 shows that the negative polarization increases in weak magnetic fields applied in Faraday geometry, but strong fields suppress it. The positive polarization always increases as a function of magnetic field.

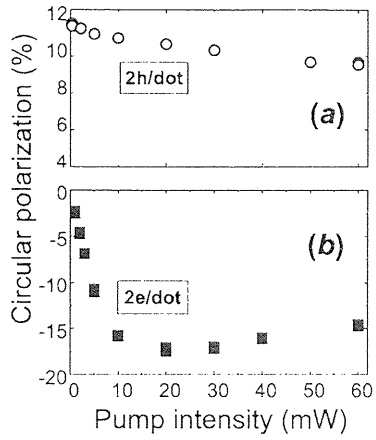


FIG. 3. Ground-state PL polarization vs excitation power for doubly positively (a) and negatively (b) charged InAs QDs. $T$ = 10 K. (a) $h\nu_{exc}$=1.722 eV, $h\nu_{det}$=1.109 eV. (b) $h\nu_{exc}$=1.59 eV, $h\nu_{det}$=1.117 eV.

## III. THEORETICAL MODEL AND DISCUSSION

### A. Qualitative explanation of the experimental results

We start with a qualitative explanation of one of the main results of this work, the observation of opposite signs of the circular polarization of the ground-state PL in doubly positively charged ($2h$) and doubly negatively charged ($2e$) QDs under excitation in the barrier. In our opinion, the main reason for this difference is the fact that photoexcited electrons coming to QDs from the GaAs barrier retain their initial spin polarization (50%), while holes completely depolarize before their capture into QDs.[21] This is a consequence of a strong difference of spin relaxation times of holes and electrons in bulk semiconductors.[14] As the ground-state PL of charged QDs is a result of recombination of a photoexcited carrier with a resident carrier of opposite charge and *zero* average spin polarization, one could expect *positive* polarization of the PL in positively charged QDs and *no polarization* of the PL in negatively charged QDs. In reality, however, the difference between positively and negatively charged QDs is even stronger, due to the anisotropic exchange (AE) electron-hole interaction, which results in *negative* PL polarization in negatively charged QDs.

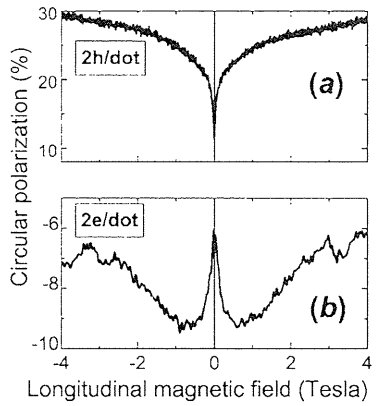


FIG. 4. Longitudinal magnetic field dependence of the ground-state PL polarization of doubly positively (a) and negatively (b) charged InAs QDs. $T$=10 K. Here, the sample with negatively charged dots is a $n$-$i$-$n$ structure with one layer of InAs QDs. (a) $h\nu_{exc}$=1.722 eV, $I_{exc}$=5 mW, $h\nu_{det}$=1.109 eV. (b) $h\nu_{exc}$=1.55 eV, $I_{exc}$=7 mW, $h\nu_{det}$=1.143 eV.

As shown earlier for excitons,[3,7,22,23] AE in an electron-hole pair results in a simultaneous spin-flip transition of the electron *and* the hole. In other words, AE provides a transfer of angular momentum between the electron and the hole. Note, however, that "transfer" does not imply "conservation" in this case; a portion of the angular momentum goes to the crystal lattice via the spin-orbit interaction, making it possible to match the electron spin 1/2 with the heavy hole spin 3/2. In particular, this feature of the AE results in a possibility of flip-flop transitions for electron-hole pairs both with antiparallel and parallel spins. In the former case, similarly to the usual electron-electron spin exchange, the hole acquires a portion of angular momentum of the same sign as that lost by the electron. In the latter case, both the electron and the hole lose their angular momentum to the crystal lattice, so that the portion of angular momentum gained by the hole is opposite in sign to that lost by the electron. The matrix elements of these two transitions ($\delta_b$ for the "bright" states with the total spin projection on the structure axis equal to $\pm 1$ and $\delta_d$ for the "dark" states with the spin projection $\pm 2$) are generally different.[23,24] If we now consider an ensemble of electron-hole pairs where the electrons are spin-polarized and the holes are not, we can readily see that the electrons are in any case losing their average spin via AE, while the holes can acquire spin polarization of the same sign as that of electrons (if $\delta_b > \delta_d$), of the opposite sign (if $\delta_b < \delta_d$), or remain with zero spin polarization (if $\delta_b = \delta_d$). Theoretically, all these situations can be realized in QDs[23,24]; however, experimental works published up to now indicate that in real QD structures $\delta_b \gg \delta_d$.[7,22,24] Therefore, one can expect the AE to result in a spin polarization of holes parallel to the initial polarization of electrons. According to the well-known optical selection rules,[14] the PL resulting from recombination of these holes with unpolarized resident electrons in negatively charged QDs has the helicity opposite to that of the exciting light. Such a "negative" PL polarization has been so far observed in singly negatively charged QDs.[7,22] As the capture of an electron-hole pair into a singly charged QD results in the formation of a trion whose ground state is a Kramers spin doublet not affected by the AE, intermediate states were invoked to explain the negative polarization. According to Ref. 22, the AE occurs in exciton before its binding with the resident electron. Cortez *et al.*[7] explain their experimental results by the AE in the excited triplet state of the QD trion. In doubly charged QDs, two resident carriers form a spin singlet that does not hinder the AE in the photoexcited electron-hole pair. This fact, together with experimentally documented fast capture of photoexcited carriers from the barrier into QDs, suggests that the negative PL polarization observed in our experiments is due to the AE *inside* the QD. The basic properties of this interaction, including the relation between $\delta_b$ and $\delta_d$, should remain the same as for excitons, though values of these constants may be different. A theoretical model we propose on the basis of this assumption repro-

duces all the main features of the observed phenomena, including the effects of magnetic fields and the dependence of the polarization on the excitation intensity both for positively and negatively doubly charged QDs. The model calculations are presented in Sec. III B. However, the main qualitative results of the model can be obtained without any mathematics.

Let us consider first the situation in $2e$-QDs. If photoelectrons come from the barrier with spin down ($\downarrow$), and photoholes come unpolarized (spin projection of the hole is $\Uparrow$ or $\Downarrow$), then $|+1\rangle$ ($\downarrow\uparrow\downarrow\Uparrow$) and $|-2\rangle$ ($\downarrow\uparrow\downarrow\Downarrow$) tetrons are formed with equal probability. By analogy with the corresponding exciton states, we will in the following refer to $|\pm 1\rangle$ tetrons as bright, and to $|\pm 2\rangle$ tetrons as dark, though both these doublets are radiative. The emission of the $|+1\rangle$ bright tetron has $\sigma^+$ polarization, while the $|-2\rangle$ dark tetron emits $\sigma^-$ light. As the AE is stronger in the bright tetron ($\delta_b \gg \delta_d$), its emission depolarizes faster, and therefore the net PL polarization is negative.

The magnetic field dependence of the polarization also finds its explanation in the different strength of the AE in bright and dark tetrons. Indeed, analogously to what has been observed earlier in excitons,[22] the longitudinal magnetic field suppresses flip-flop transitions generated by the AE and restores polarization of both bright and dark tetrons. Besides, due to weaker AE in the dark tetron, its polarization is restored in weaker fields, and the magnitude of the negative PL polarization increases. Further increase of the magnetic field also suppresses the depolarization of the bright trion, and as a result the net PL polarization goes to zero in high magnetic field. This explains the experimentally observed W-shaped magnetic field dependence of the PL polarization, shown in Fig. 4(b).

In $2h$-QDs, the polarization of bright and dark tetrons has the same (positive) sign. Therefore, the increase of polarization of each of the two types of tetrons in the magnetic field should be accompanied by a monotonous increase of positive polarization of their net PL, as indeed is observed experimentally [see Fig. 4(a)].

In order to explain the experimentally observed dependence of the PL polarization on the pump intensity (see Fig. 3), the model should be expanded to include the capture kinetics of photoexcited electrons and holes. Based on the results of Refs. 21 and 25, we assume that under above-barrier excitation electrons and holes are captured into QDs separately. Additionally, we suppose that a negatively charged QD first captures a hole and, only then, an electron (for positively charged dots the situation is opposite-an electron is captured first, then a hole). This assumption is based on a simple observation that a charged QD attracts particles of the opposite charge and repels like-charged ones and also on the experimental results of Ref. 26. An evident consequence is that the opposite-charge carrier lives for some time in the QD before the coming of the like-charge one; during this time interval, the QD contains not a tetron, but a trion. The stronger is pumping, the shorter is this time; at weak pumping, however, trions can exist for a long enough time to give a significant contribution into the photoluminescence. Therefore, the net PL of the QD ensemble is governed by trions at extremely low pumping and experiences a crossover to tetron-dominated regime at higher pump intensities (note that trion and tetron PL lines cannot be spectrally resolved in ensemble measurements). Now, as the ground-state trion PL has zero polarization for negatively charged QDs, and a polarization equal to that of photoexcited electrons in positively charged QDs, we can conclude that the net polarization as a function of pump intensity should be negative, increasing in the absolute value, in $2e$-QDs, and positive, somewhat decreasing, in $2h$-QDs. This behavior is indeed observed experimentally (see Fig. 3) and reproduced by model calculations in Sec. III B.

### B. Model calculations

#### *1. Negatively charged QDs*

We assume that the photogenerated electrons and holes are captured into the dots separately under the above-barrier excitation.[21,25] Further, we believe that a photohole is captured first, forming a trion, and then a photoelectron is trapped to the QD first excited state, yielding a tetron. In accordance with the spin projection of electron ($\uparrow$, $\downarrow$) and hole ($\Uparrow$, $\Downarrow$), we denote trion states as $\uparrow\downarrow\Uparrow$ and $\uparrow\downarrow\Downarrow$, $|+1\rangle$ and $|-1\rangle$ tetrons as $\downarrow\uparrow\downarrow\Uparrow$ and $\uparrow\uparrow\downarrow\Downarrow$, and $|+2\rangle$ and $|-2\rangle$ tetrons as $\uparrow\uparrow\downarrow\Uparrow$ and $\downarrow\uparrow\downarrow\Downarrow$. In the following, we will refer to $|\pm 1\rangle$ and $|\pm 2\rangle$ tetrons as bright and dark tetrons, respectively, in an analogy to bright and dark exciton states. though in fact both bright and dark tetron states are radiative and have equal oscillator strengths.

The photoexcited hole can recombine with the resident electron, either before or after the capture of a photoexcited electron.

The fraction of photons emitted by the QD with a photohole before capture of a photoelectron (trion emission) is

$$\nu = \frac{1}{1 + w\tau}, \tag{1}$$

where $\tau$ is the ground-state radiative lifetime; $w$ is an electron capture rate at the first excited level, which is proportional to the excitation intensity $I_{exc}$. The polarization of this light is equal to the hole polarization $P_h$.

The fraction of photons emitted by the QD with a photohole after capture of a photoelectron via recombination of the photohole with one of the resident electrons (tetron emission) is

$$\nu_b + \nu_d = \frac{w\tau}{1 + w\tau}, \tag{2}$$

where $\nu_b$ and $\nu_d$ are the fractions of bright and the dark tetrons, formed by one $s$ hole, two $s$ electrons, and one $p$ electron.

As the holes are captured unpolarized, we put the fractions of bright and dark tetrons equal to each other

$$\nu_b = \nu_d = \frac{1}{2}\frac{w\tau}{1 + w\tau}. \tag{3}$$

The net polarization of the QD emission is then given by the expression

$$\rho_{2e} = \nu P_h + \nu_b P_b + \nu_d P_d, \tag{4}$$

where $P_b$ and $P_d$ are average polarizations of bright and dark tetrons. The initial polarization of the PL from bright and dark tetron states is determined by the polarization of captured photoelectrons $P_{e0}$: $P_{b0}=-P_{d0}=P_{e0}$, so that $\rho_{2e}$ is initially equal to zero. It becomes nonzero due to unequal strength of the AE in the bright and dark tetron states, resulting in a disbalance of $P_b$ and $P_d$. In order to find these values at the moment of recombination, one should analyze the influence of the AE on the tetron spin state.

The AE interaction in the tetron, where the two electrons on the lowest level of size quantization are in a spin-singled state and therefore do not interact with other spins, is analogous to that in the exciton. The spin structure and dynamics of the QD exciton is well documented.[3,7,22–24,33,34] We will use the results of Refs. 22, 23, and 33 to analyze the polarization of tetron photoluminescence. This is done, briefly, as follows.

AE splits ground states of both the bright and the dark tetron into two levels with the wave functions being linear combinations of $+1/2$ and $-1/2$ states. This effect can be described by a two-level model with a pseudospin 1/2, reflecting the tetron polarization, and an effective magnetic field of the AE directed perpendicularly to the initial direction of the pseudospin ($z$ axis). An external magnetic field $B\|z$ splits pseudospin states with projections $+1/2$ and $-1/2$ onto the structure growth axis and for this reason, in this model, it is parallel to the initial pseudospin direction. A combined action of the two fields results in the pseudospin precession around their vector sum. Under a continuous-wave excitation of tetrons, they are characterized by a pseudospin vector averaged over time (taking into account the lifetime of the corresponding tetron state). The PL circular polarization, determined by the $z$ projection of this vector, is given by the following expressions:

$$P_b = P_{e0}\frac{1+(\Omega_{bz}\tau_b)^2}{1+(\Omega_{bz}\tau_b)^2+(\Omega_b\tau_b)^2},$$

$$P_d = -P_{e0}\frac{1+(\Omega_{dz}\tau_d)^2}{1+(\Omega_{dz}\tau_d)^2+(\Omega_d\tau_d)^2}, \tag{5}$$

similar to the formula for the electron mean spin in the Hanle effect in a tilted magnetic field.[14] Here $\tau_{b,d}$ is the hole lifetime in bright and dark tetrons, $\hbar\Omega_{bz,dz}=g_{b,d}\mu_B B$ and $\hbar\Omega_{b,d}=\delta_{b,d}$ are the Zeeman and anisotropic splittings of the bright and dark tetrons; $g_{b,d}$ is the $g$ factor of the bright or dark tetron and $\mu_B$ is the Bohr magneton.

Since the holes come from the barrier unpolarized ($P_h=0$), then

$$\rho_{2e} = \frac{P_{e0}}{2}\frac{w\tau}{1+w\tau}\left(\frac{1+(\Omega_{bz}\tau_b)^2}{1+(\Omega_{bz}\tau_b)^2+(\Omega_b\tau_b)^2} - \frac{1+(\Omega_{dz}\tau_d)^2}{1+(\Omega_{dz}\tau_d)^2+(\Omega_d\tau_d)^2}\right). \tag{6}$$

As, because of the symmetry of envelope wave functions, the ground-state hole recombines predominantly with one of the ground-state electrons, we may take the recombination times of bright and dark tetrons, $\tau_b$ and $\tau_d$, approximately equal to each other, and replace them with a unique tetron lifetime $\tau$. In this case, in zero external field

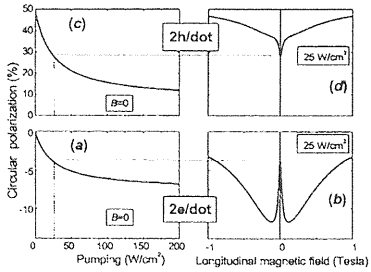


FIG. 5. Dependences of the PL circular polarization on the excitation intensity and longitudinal magnetic field in the double negatively and positively charged dots, calculated with Eqs. (6) and (8). The capture rate $w$ was calculated as $w=W/h\upsilon_{exc}N_{dot}$, where $W$ is the pump density and $N_{dot}$ is the dot density. The following parameters are used: $P_{e0}=0.5$, $\tau=0.5$ ns, $|g_b|=3$, $|g_d|=1.4$, $\delta_b=100$ $\mu$eV, $\delta_d=2$ $\mu$eV, $N_{dot}=5\times10^{10}$ cm$^{-2}$, $h\upsilon_{exc}=1.6$ eV. (a) and (c) $B=0$. (b) and (d) $W=25$ W/cm$^2$. See text for details.

$$\rho_{2e} = \frac{w\tau}{1+w\tau}\frac{P_{e0}}{2}\left(\frac{1}{1+(\Omega_b\tau)^2} - \frac{1}{1+(\Omega_d\tau)^2}\right). \tag{7}$$

Since $\delta_b \gg \delta_d$,[7,22,24] the second term in Eq. (7) exceeds the first one, and $\rho_{2e}$ is negative. The electron capture rate $w \propto I_{exc}$. So, $\rho_{2e} \propto I_{exc}$ at a weak pumping $w\tau \ll 1$ and goes to zero by decreasing the excitation intensity. With the excitation rise, the PL polarization achieves its maximal value that does not depend on the excitation intensity at $w\tau \gg 1$ and for a certain electron polarization $P_{e0}$ is determined by the ratio of anisotropic splittings of bright and dark tetrons $\delta_b$ and $\delta_d$ [see Fig. 5(a)].

In these calculations we have assumed that the values of excitonic $g$ factors measured in Ref. 30 ($|g_b|\approx3$, $|g_d|\approx1.4$) are suitable for our QDs also.

### 2. *Positively charged QDs*

We apply the same model to describe polarization in doubly positively charged dots. The difference is that now we assume that the photoelectron is captured first, forming a positively charged trion ($\downarrow\Uparrow\Downarrow$ or $\uparrow\Uparrow\Downarrow$). The subsequent capture of a photohole to the first excited state creates positively charged ($\downarrow\Uparrow\Downarrow\uparrow$ or $\uparrow\Uparrow\Downarrow\Downarrow$) and dark ($\downarrow\Uparrow\Downarrow\Downarrow$ or $\uparrow\Uparrow\Downarrow\Uparrow$) tetrons. Equations. (1)–(4) can be used to calculate the polarization, but now $\nu$ in Eq. (1) denotes the fraction of photons emitted by QDs with a photoelectron before the hole capture. Their polarization is $\rho=P_{e0}$. Respectively, $w$ is a hole capture rate at the first excited level. By changing the sign in the expression $P_d$ in Eq. (5) (because the emission of dark tetrons in $2h$-QDs is positively polarized), we obtain the following expression for the PL polarization in $2h$ dots, $\rho_{2h}=\nu P_{e0}+\nu_b P_b+\nu_d P_d$:

$$\rho_{2h} = P_{e0}\frac{1}{1+w\tau}\left(1+\frac{w\tau}{2}\frac{1+(\Omega_{bz}\tau_b)^2}{1+(\Omega_{bz}\tau_b)^2+(\Omega_b\tau_b)^2} + \frac{w\tau}{2}\frac{1+(\Omega_{dz}\tau_d)^2}{1+(\Omega_{dz}\tau_d)^2+(\Omega_d\tau_d)^2}\right). \quad (8)$$

$\rho_{2h}$ has the positive sign, because all the terms in Eq. (8) are positive. The maximal value of $\rho_{2h}$ is equal to the initial polarization of electrons, $P_{e0}$, which can be realized in the limit of weak pumping ($w \ll \tau^{-1}$). With increasing intensity $\rho_{2h}$ decreases and, at strong pumping ($w \gg \tau^{-1}$) saturates at a level [Fig. 5(c)] that is determined, in the absence of the external magnetic field, by the ratio $\delta_b/\delta_d$. The longitudinal magnetic field always enhances the PL polarization, resulting in a V-shaped dependence $\rho_{2h}(B)$ [see Fig. 5(d)]. The sharp increase of $\rho_{2h}(B)$ at weak fields and much more smooth increase at higher fields are due to restoration of optical orientation in dark and bright tetrons, respectively.

### C. Discussion

Dependences calculated for positively and negatively charged dots with the same set of parameters are shown in Fig. 5. One can see that the model calculation reflects all the main features of the experimental observations.

A W-shaped dependence of the negative PL polarization on the longitudinal magnetic field under above-barrier excitation has been observed earlier in singly charged *n*-doped InP quantum islands.[22] Though the PL of the negative trion was detected, the dependence $\rho(B)$ was explained via magnetic-field-induced restoration of the polarization of photoexcited excitons before their binding with the resident electron and formation of a trion. For the weak AE in the dark exciton to result in a considerable loss of polarization, the exciton needs the lifetime in the island of at least 200 ps.[22] This is possible in InP islands, having the lateral size 4–6 times larger than the exciton size (~100 A). However, this scenario is not realistic in our InAs/GaAs QDs, because the capture of photoexcited carriers in such QDs is very fast ($\lesssim$15 ps),[7,21] the dot size is comparable to the Bohr radius of the exciton, and, as a consequence, photoexcited and resident carriers immediately form a complex.

Further corrections to the model should involve multiexcitonic effects, which can be considerable at high excitation power. However, we believe that the essential features of the observed phenomena are captured by the simplest tetron model. Some other possible effects are discussed below.

#### *1. Electron spin relaxation due to hyperfine interaction*

In doubly negatively charged QDs, the photoexcited ($p$) electron is coupled with the lattice nuclei by hyperfine interaction (on the contrary, hyperfine interaction of holes with lattice nuclei is absent[27]), and its polarization can be destroyed as a result of a precession of its spin in a fluctuation of the effective nuclear field.[5] However, the isotropic part of its exchange interaction with the hole, which splits the spin states of the tetron into bright and dark doublets, suppresses the precession of the electron spin. An estimation with Eq. (7) of Ref. 5 gives the energy of the hyperfine interaction of an electron with the nuclear spin fluctuation $\delta_{eN} \sim 5$ $\mu$eV (we assume that in our samples an InAs QD contains $\approx 10^4$ nuclei, the spins and the hyperfine constants of indium and arsenic are equal to $I_{In}=9/2$, $I_{As}=3/2$, $A_{In} \approx 56$ $\mu$eV, $A_{As} \approx 46$ $\mu$eV, respectively).[28,29] We suppose that the exchange interaction between the $p$ electron and the $s$ hole in the tetron is of the same order as the exchange interaction in the ground ($s$-$s$) exciton state. The exchange splitting of bright and dark exciton states, $\delta_0$, is 100–600 $\mu$eV in InAs/GaAs QDs,[4,24,30,31] which is considerably higher than the hyperfine energy $\delta_{eN}$. Therefore, the electron spin-flip transitions due to the hyperfine interaction are suppressed in the negative tetron (a stabilization of the electron spin by the exchange interaction was earlier considered for the exciton in Ref. 32).

In a doubly positively charged QD, the photoelectron comes first and, before the hole capture, experiences the influence of the nuclear fluctuation. In this case, the degree of depolarization of electrons is determined by the relations of the dephasing time of the electron ensemble in fluctuation nuclear fields, $T_\Delta$, with the electron recombination time with resident holes, $\tau$, and the capture time of the hole, $w^{-1}$. The latter can vary within a wide range depending on the pump intensity. In the InAs QDs under study, $T_\Delta \approx 0.2$ ns,[35] $\tau \sim 1$ ns.[4,7,21] At weak pumping, when the hole capture rate is small, $T_\Delta$ is the shortest time, and the nuclear-induced electron spin dephasing may dominate. In this case, for zero external field, one can use Eq. (8) with the initial electron polarization $P_{e0}$ replaced by $P_{e0}/3$. This does not qualitatively change the calculated dependence of $\rho_{2h}$ on pump intensity, plotted in Fig. 5(c).

Magnetic fields should suppress the effect of nuclear fluctuations and, consequently, increase the electron polarization. Since the energies of the hyperfine interaction $\delta_{eN}$ and the AE in the dark tetron $\delta_d$ are comparable, suppression of both these interactions can give rise to a sharp increase of the PL polarization observed in weak magnetic field [Fig. 4(a)]. We would like to note that the suppression of nuclear fluctuations by a magnetic field should be more pronounced at weak pumping, where the depolarizing effect of nuclear fluctuations is stronger.

#### *2. Spin memory effects*

Our model does not consider the effects of "spin memory," i.e., of the spin polarization of resident electrons remaining after recombination of a polarized electron-hole pair in 2$e$-QDs. After recombination of the dark tetron, the QD remains with two electrons having the same spin direction (predominantly $\downarrow\downarrow$ in the case of $\sigma^+$ excitation). This is again a doubly charged QD and, as we suggested above, it should capture a hole first. Since photoexcited holes are not polarized, holes $\Uparrow$ and $\Downarrow$ can be captured with equal probabilities. The $\Uparrow$ hole forms a hot trion $\downarrow\downarrow\Uparrow$, emitting $\sigma^+$ light. However, AE of the $\Uparrow$ hole and each of the two $\downarrow$ electrons is strong and can transform the hot trion into the cold one with the spin configuration $\downarrow\uparrow\Downarrow$,[7] which lives long and emits $\sigma^-$ light increasing the negative PL polarization. A capture of the $\Downarrow$ hole forms a hot dark trion $\downarrow\downarrow\Downarrow$. The AE in such a trion would result in a cold trion $\downarrow\uparrow\Uparrow$, producing the $\sigma^+$ emission.

But the AE in dark trions is weaker than in bright ones; therefore, the net PL polarization of $\downarrow\downarrow$ QDs after a hole capture is, presumably, $\sigma^-$.

Before the hole capture, the two $\downarrow\downarrow$ electrons may be affected by the hyperfine interaction with a nuclear spin fluctuation, which would deflect their total spin from its initial direction. As a result, within the time comparable to the precession period of an electron spin in the nuclear-fluctuation field ($T_\Delta \approx 0.2$ ns),[35] these QDs, retaining the total spin of the two electrons equal to 1, will have zero projection of the total spin onto the structure growth axis (a more detailed consideration of this process will be published elsewhere). After the hole capture, such dots will give unpolarized emission.

Thus, the QDs with two spin-polarized electrons yield on average $\sigma^-$ light. As the relative number of such dots is small, their contribution should not considerably affect the PL polarization of the whole ensemble of QDs.

To summarize, we observed optical spin orientation in doubly negatively and positively charged quantum dots. We propose a theoretical model including separate capture of photoexcited electrons and holes from the barrier and the anisotropic exchange interaction in doubly charged excitons (tetrons). The model explains different signs of the circular polarization of the emission from the ground state of positively and negatively charged dots, as well as the polarization dependence on the pump intensity and the magnetic field in the Faraday geometry.

## ACKNOWLEDGMENTS

This work was partially supported by Nanoscience Special Project of University of Tsukuba, INTAS (Grant No. 1B 2167), RFBR, the Russian Academy of Sciences program, and Program of the Russian Ministry of Science and Technology. One of the authors (I.A.M.) thanks CRDF. The authors are grateful to R.I. Dhzioev, V.L. Korenev, M.M. Afanasiev, X. Marie, and T. Amand for useful discussions.

*Corresponding author. Fax: (+7)-(812)-2471017. Email address: kalevich@solid.ioffe.ru

[1] A. Abragam and B. Bleaney, *Electron Paramagnetic Resonance of Transition Ions* (Clarendon Press, Oxford, 1970).

[2] A. V. Khaetskii and Y. V. Nazarov, Phys. Rev. B **61**, 12639 (2000).

[3] R. I. Dzhioev, B. P. Zakharchenya, E. L. Ivchenko, V. L. Korenev, Yu. G. Kusraev, N. N. Ledentsov, V. M. Ustinov, A. E. Zhukov, and A. F. Tsatsul'nikov, JETP Lett. **65**, 804 (1997).

[4] M. Paillard, X. Marie, P. Renucci, T. Amand, A. Jbeli, and J. M. Gérard, Phys. Rev. Lett. **86**, 1634 (2001).

[5] I. A. Merkulov, Al. L. Efros, and M. Rosen, Phys. Rev. B **65**, 205309 (2002).

[6] I. E. Kozin, V. G. Davydov, I. V. Ignatiev, A. V. Kavokin, K. V. Kavokin, G. Malpuech, Hong-Wen Ren, M. Sugisaki, S. Sugou, and Y. Masumoto, Phys. Rev. B **65**, 241312(R) (2002).

[7] S. Cortez, O. Krebs, S. Laurent, M. Sénès, X. Marie, P. Voisin, R. Ferreira, G. Bastard, J.-M. Gérard, and T. Amand, Phys. Rev. Lett. **89**, 207401 (2002); T. Amand, B. Urbaszek, M. Sénès, P. Renucci, X. Marie, O. Krebs, S. Laurent, S. Cortez, P. Voisin, R. J. Warburton, B. D. Gerardot, P. M. Petroff, and J.-M. Gérard, Proceedings of PSSN2003, Kyoto, Japan (unpublished); http://www.ipc.kit.ac.jp/~takaghra/pssn.html

[8] I. V. Ignatiev, I. Ya. Gerlovin, M. Ikezawa, V. K. Kalevich, S. Yu. Verbin, and Y. Masumoto, Physica E (Amsterdam) **17**, 361 (2002).

[9] T. Flissikowski, I. A. Akimov, A. Hundt, and F. Henneberger, Phys. Rev. B **68**, 161309(R) (2003).

[10] D. Bimberg, M. Grundmann, and N. N. Ledentsov, *Quantum Dot Heterostructures* (Wiley, Chichester, 1999).

[11] V. M. Ustinov, A. E. Zhukov, A. Yu. Egorov, and N. A. Maleev, *Quantum Dot Lasers* (Oxford University Press, Oxford, 2003).

[12] V. K. Kalevich, M. Ikezawa, T. Okuno, A. Yu. Shiryaev, A. E. Zhukov, V. M. Ustinov, P. N. Brunkov, and Y. Masumoto, Phys. Status Solidi B **238**, 250 (2003).

[13] P. N. Brunkov, A. A. Suvorova, N. A. Bert, A. R. Kovsh, A. E. Zhukov, A. Yu. Egorov, V. M. Ustinov, A. F. Tsatsul'nikov, N. N. Ledentsov, P. S. Kop'ev, S. G. Konnikov, L. Eaves, and P. S. Main, Semiconductors **32**, 1096 (1998).

[14] *Optical Orientation*, edited by F. Meier and B. Zakharchenya, Modern Problems in Condensed Matter Sciences Vol. 8 (North-Holland, Amsterdam, 1984).

[15] S. N. Jasperson and S. E. Schnatterly, Rev. Sci. Instrum. **40**, 761 (1969).

[16] V. D. Kul'kov and V. K. Kalevich, Instrum. Exp. Tech. **24**, 1265 (1981).

[17] Alternating the helicity of the exciting light results in periodic change of the mean spin direction of photoexcited electrons. As the modulation period is much shorter than the longitudinal spin relaxation time of the nuclear spin, the nuclei cannot follow the rapidly changing direction of the electron spin, and no dynamical nuclear spin polarization develops.

[18] O. Stier, M. Grundmann, and D. Bimberg, Phys. Rev. B **59**, 5688 (1999).

[19] A. J. Williamson, L. W. Wang, and Alex Zunger, Phys. Rev. B **62**, 12963 (2000).

[20] V. K. Kalevich, M. Ikezawa, T. Okuno, A. Yu. Shiryaev, K. V. Kavokin, P. N. Brunkov, A. E. Zhukov, V. M. Ustinov, and Y. Masumoto, Physica E (Amsterdam) **21**, 1018 (2004).

[21] V. K. Kalevich, M. Paillard, K. V. Kavokin, X. Marie, A. R. Kovsh, T. Amand, A. E. Zhukov, Yu. G. Musikhin, V. M. Ustinov, E. Vanelle, and B. P. Zakharchenya, Phys. Rev. B **64**, 045309 (2001).

[22] R. I. Dzhioev, B. P. Zakharchenya, V. L. Korenev, P. E. Pak, D. A. Vinokurov, O. V. Kovalenkov, and I. S. Tarasov, Phys. Solid State **40**, 1587 (1998).

[23] G. E. Pikus and E. L. Ivchenko, *Superlattices and Other Heterostructures*, Springer Series in Solid-State Sciences Vol. 110 (Springer-Verlag, Berlin, 1995).

[24] M. Bayer, G. Ortner, O. Stern, A. Kuther, A. A. Gorbunov, A.

Forchel, P. Hawrylak, S. Fafard, K. Hinzer, T. L. Reinecke, S. N. Walck, J. P. Reithmaier, F. Klopf, and F. Schäfer, Phys. Rev. B **65**, 195315 (2002).
[25] M. Grundmann and D. Bimberg, Phys. Rev. B **55**, 9740 (1997).
[26] K. Gündogdu, K. C. Hall, Tomas F. Boggess, D. G. Deppe, and O. B. Shchekin, Appl. Phys. Lett. **84**, 2793 (2004).
[27] E. I. Gr'ncharova and V. I. Perel', Sov. Phys. Semicond. **11**, 997 (1977).
[28] M. Gueron, Phys. Rev. **135**, A200 (1964).
[29] D. Paget, G. Lampel, B. Sapoval, and V. I. Safarov, Phys. Rev. B **15**, 5780 (1977).
[30] M. Bayer, A. Kuther, A. Forchel, A. Gorbunov, V. B. Timofeev, F. Schäfer, J. P. Reithmaier, T. L. Reinecke, and S. N. Walck, Phys. Rev. Lett. **82**, 1748 (1999).
[31] B. Urbaszek, R. J. Warburton, K. Karrai, B. D. Gerardot, P. M. Petroff, and J. M. Garcia, Phys. Rev. Lett. **90**, 247403 (2003).
[32] D. Gammon, Al. L. Efros, T. A. Kennedy, M. Rosen, D. S. Katzer, D. Park, S. W. Brown, V. L. Korenev, and I. A. Merkulov, Phys. Rev. Lett. **86**, 5176 (2001).
[33] R. I. Dzhioev, H. M. Gibbs, E. L. Ivchenko, G. Khitrova, V. L. Korenev, M. N. Tkachuk, and B. P. Zakharchenya, Phys. Rev. B **56**, 13405 (1997).
[34] D. Gammon, Al. L. Efros, J. G. Tischler, A. S. Bracker, V. L. Korenev, and I. A. Merkulov, Chapter 6 in *Quantum Coherence, Correlation and Decoherence in Semiconductor Nanostructures*, edited by T. Takagahara (Academic Press, Amsterdam, 2002).
[35] An estimation with Eq. (11) of Ref. 5 gives $T_{\Delta} \approx 0.2$ ns for our InAs QDs.

PHYSICAL REVIEW B 72, 153302 (2005)

# Submillisecond electron spin relaxation in InP quantum dots

Michio Ikezawa, Bipul Pal, and Yasuaki Masumoto
*Institute of Physics, University of Tsukuba, Tsukuba 305-8571, Japan*

Ivan V. Ignatiev* and Sergey Yu. Verbin
*Institute of Physics, University of Tsukuba, Tsukuba 305-8571, Japan*
*and Institute of Physics, St.-Petersburg State University, St.-Petersburg, 198504, Russia*

Il'ya Ya. Gerlovin
*Vavilov State Optical Institute, St.-Petersburg, 190034, Russia*
(Received 12 July 2005; published 3 October 2005)

Light-induced orientation of electron spins in the negatively charged InP quantum dots is found to persist longer than 100 $\mu$s. We have proved experimentally that the long-lived orientation is due to slow relaxation of the electron spins rather than to the dynamic nuclear polarization effects.

DOI: 10.1103/PhysRevB.72.153302 PACS number(s): 78.67.Hc, 72.25.Fe, 73.21.La, 78.47.+p

In recent years, the long-lived spin orientation in semiconductor structures attracts increasing attention of researchers as a promising way of quantum information processing and storage.[1] The structures with quantum dots (QDs) in which the main processes of spin relaxation are suppressed due to confinement of the carrier are particularly advantageous in this respect. According to the theoretical estimates,[2] the electron spin lifetime in QDs can lie in the range of milliseconds or even seconds. This theoretical prediction has stimulated the studies of spin relaxation in low-dimensional structures.[3–8] The most exciting experimental results achieved in this field were the electron spin relaxation time $T_1 \geqslant 50$ $\mu$s, observed for the one-electron QD (Ref. 5) and $T_1 \sim 20$ ms observed for the InGaAs self-assembled QDs.[7,8] At the same time, a fundamental question arises associated with the origin of so long-lived spin polarization. Along with suppression of main spin relaxation processes in QDs, predicted theoretically,[2] persistence of the spin polarization can result from dynamic nuclear polarization[10–13] capable to conserve the electron spin for a long time. It should be particularly emphasized that the dynamic nuclear polarization is a very slow process which cannot realize fast recording of information. The role of nuclear polarization has not been discussed in Refs. 5, 7, and 8 and the question about origin of the long-lived spin orientation in semiconductor QDs is open so far.

In this paper, we present the experimental results showing that relaxation of the electron spin in InP QDs is indeed very slow and the lifetime of real spin memory in this system can exceed 100 $\mu$s. On the analysis of the experimental data we came to conclusion that so long-lived spin memory is not associated with the nuclear polarization. To study the electron spin memory, we used a modification of the known pump-probe technique with detection of the polarized photoluminescence signal (PL pump probe).[4,6,9] The method involves detection of the effect of a circularly polarized pump on polarization of the PL excited by a probe beam. The PL pump-probe method makes it possible to overcome the limitation of the experimental study of spin dynamics related to finiteness of the electron-hole pair lifetime. At the same time, this method allows one to retain the high sensitivity and spectral selectivity characteristic of the conventional PL techniques. For excitation of the PL we used a tunable Ti:sapphiere laser with the 2-ps pulse duration and the 82-MHz repetition rate.

The structure under study is described in Ref. 14. The lowest electron level in the QDs is close to the Fermi level of the doped substrate that allowed us to control the amount of the resident electrons in the QDs by means of an external voltage. Most measurements were done in a magnetic field parallel to the growth axis of the structure (longitudinal magnetic field) $B=0.1$ T. This, according to Ref. 15, makes it possible to suppress the effect of the nuclear field fluctuations on the electron spin orientation.

As an indication of the resident electron spin orientation, we used the effect of negative circular polarization (NCP) of PL of the charged InP QDs observed when the energy difference of the exciting and detected photons (Stokes shift) exceeds 30 meV [see inset in Fig. 1(a)]. The highest NCP value was obtained in the PL kinetics measured in real time by a streak camera with a Stokes shift of 45 meV [Fig. 1(a)]. The degree of polarization calculated in a standard way, $\rho=(I^+-I^-)/(I^++I^-)$, where $I^+$ ($I^-$) is the copolarized (cross-polarized) PL intensity, changes its sign in approximately 100 ps after the excitation and then comes to a negative steady-state value further referred to as the NCP amplitude [Fig. 1(b)].

The experiments have shown that the NCP amplitude strongly depends on the bias, $U_{\text{bias}}$, applied to the sample [right inset in Fig. 1(b)]. The greatest NCP is reached in a narrow bias window near $U_{\text{bias}} \approx -0.1$ V practically coincident with the range where, according to Ref. 14, the trionic quantum beats are observed. So we can conclude that it is the trionic states that are responsible for the arising NCP.

We suppose that the negatively polarized PL is emitted by QDs with parallel electron spins (see left part of the scheme in Fig. 2).[16] This spin configuration is possible under excitation with a large Stokes shift when the photoexcited and resident electrons occupy different energy states. In these dots, referred to as the *P*-type QDs, the direct relaxation of

 

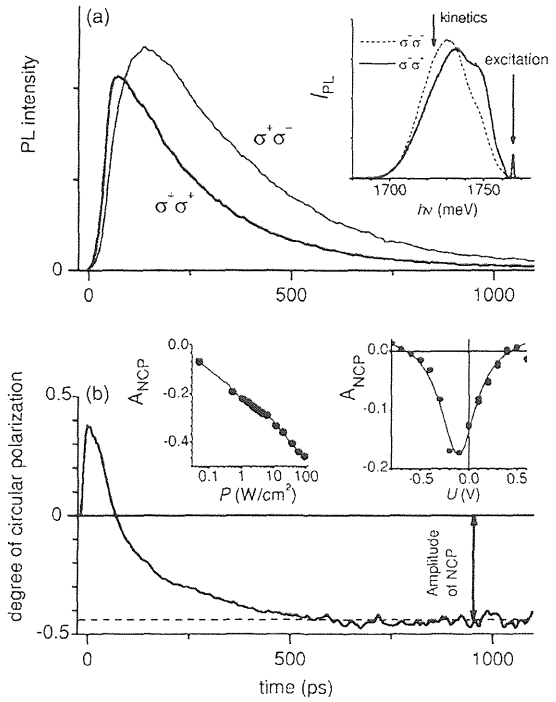


FIG. 1. (a) PL kinetics under strong $\sigma^+$ excitation in copolarization ($\sigma^+\sigma^+$) and cross-polarization ($\sigma^+\sigma^-$). $P_{ex}=90$ W/cm$^2$, $U_{bias}=-0.1$ V, $T=5$ K. The inset shows PL spectra in the copolarization and cross-polarization under excitation at $E_{exc}=1771$ meV. (b) Kinetics of the degree of circular polarization. Left inset shows the dependence of the NCP amplitude on the pump power density. Right inset shows the dependence of the NCP amplitude on the bias voltage at weak excitation $P_{ex}\sim 1$ W/cm$^2$.

the photoexcited electron to the ground state is blocked due to the Pauli principle. However, the combined energy relaxation of the electron and hole with simultaneous flips of their spins (flip-flop process) appears to be allowed in the presence of anisotropic component of the exchange coupling[17] (see middle part of the scheme). As a result, the electron spins become paired while the hole spin orientation appears to be inverted. In this case, the PL polarization determined by the hole spin becomes negative (see right part of the scheme).

In the QDs with initially antiparallel spins of the photoexcited and resident electrons (the $A$-type QDs), the exchange coupling is small, and the flip-flop process is not effective. The polarization of the PL of such QDs coincides with that of the excitation, i.e., the degree of polarization is positive. As a result, the contributions to the PL polarization from the $P$-and $A$-type QDs should partially compensate each other, and the total PL should be almost unpolarized if the resident electron spin has no preferential orientation.

If spins of the resident electrons are polarized by the exciting light,[18] the numbers of the $A$- and $P$-type QDs become unequal and degree of the PL polarization may be changed. We have detected these changes. As the pump power density was increased, we observed a rapid growth of the NCP with a saturation at about $-50\%$ [see left inset in Fig. 1(b)]. An evident reason for this growth is the orientation of the resident electron spins by the exciting beam. Thus, the degree of spin orientation can be found from the measurements of the NCP.

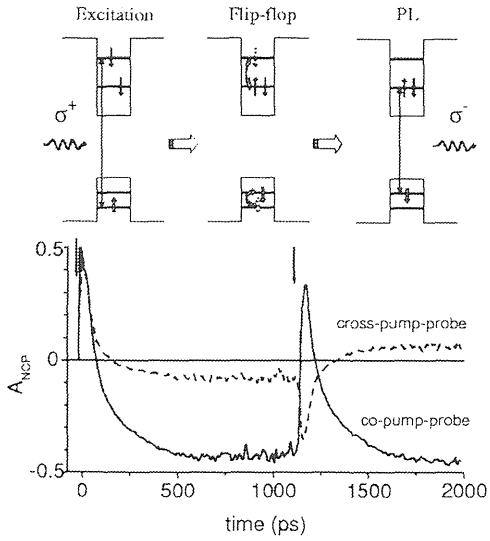


FIG. 2. Kinetics of the degree of circular polarization for the copolarized and cross-polarized pump and probe pulses. Time positions of the pulses are indicated by arrows. The scheme illustrates the model of the NCP formation.

In order to study relaxation of the resident electron spin, we measured kinetics of the PL excited by laser pulses separated in time. For this purpose, the laser beam was split into two beams and one of them was optically delayed (for $\Delta t > 1$ ns) to avoid any overlap in time of the PL excited by each of the pulses. Polarization of each beam could be varied independently. The results of the experiments for the case of equal intensities of the probe and pump beams are shown in Fig. 2. When the QDs are excited by circularly copolarized beams, a large NCP of both PL pulses is observed. However, in the case of excitation by the cross-polarized beams, the PL polarization virtually vanishes.

These results show that the spin orientation created by the pump pulse affects the polarization of the PL excited by the probe one and vice versa. It is evident that, after recombination of the electron-hole pairs ($\tau_{PL}=250$ ps), the information about polarization of the excitation can be stored only in the orientation of the resident electron spin. As it is seen from Fig. 2, the NCP amplitude at co-polarized excitation is approximately the same both after the probe and after the pump pulses, in spite of the fact that the former arrives 11 ns after the latter, while the latter comes 1 ns after the former. This means that the relaxation time of the electron spins substantially exceeds the laser pulse repetition period 12 ns.

To check the conservation of the spin orientation at much longer times, we have radically increased the time delay between the pump and probe excitation pulses. For this purpose, we selected the laser pulses using acousto-optical modulators (AOM) placed into the pump and probe paths. The repetition period of the pump and probe pulse trains, their duration and the delay were controlled by a functional generator connected with the AOMs. To obtain a noticeable

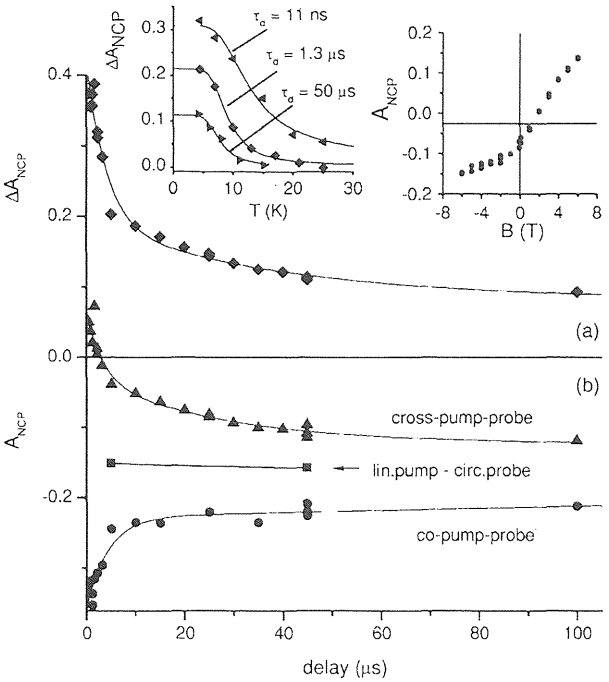


FIG. 3. (a) The time delay dependence of $A_{NCP}$ for circularly polarized probe with copolarized (circles), cross-polarized (triangles), and linearly (squares) polarized pumps. $T=2$ K. (b) The delay dependence of $\Delta A_{NCP}=A_{NCP}(\text{cross})-A_{NCP}(\text{co})$ (diamonds) and multiexponential fit (solid line). Left inset: temperature dependence of $\Delta A_{NCP}$ at different delays $\tau_d$ (symbols); solid curves are the fits by the function $f(T)=f_0(1+a\beta)^{-1}$, where $\beta=\exp(-\Delta E/kT)$. Activation energy $\Delta E=4$ meV for all the curves (Ref. 20). Right inset shows magnetic field dependence of $A_{NCP}$ under cross-polarized excitation for the 11-ns delay.

spin polarization created by the pump beam, the pump power density was chosen to be several W/cm$^2$. The intensity of the probe beam was by a factor of 10–20 lower, because only under these conditions the probe pulse train did not erase the spin polarization created by the pump.

We have measured the dependence of the NCP amplitude of the PL excited by the probe beam on time delay between the pump and probe pulse trains [see Fig. 3(a)]. Under linear polarization of the pump beam, the NCP amplitude slightly exceeds 10% and almost does not depend on the time delay. The circularly polarized pump substantially changes the value of the NCP. These changes are of opposite signs for the copolarized and cross-polarized pumping and are approximately equal in magnitude. Therefore, we attributed the NCP changes to the optical spin orientation rather than to other effects such as, e.g., heating of the structure by the high-power pump. Difference between the NCP amplitudes at the copolarized and cross-polarized pumping can serve as a quantitative characteristics of spin orientation of the resident electrons.

As seen from Fig. 3(b), the spin orientation created by the pump decays in time. Time dependence of the NCP, measured experimentally, cannot be described by a simple exponential function. For the delays of about units of microseconds, one can observe a relatively fast decrease of the orientation and, then, for the time delays exceeding 50 $\mu$s, the orientation comes to a virtually constant level. The reasons for the nonexponential decay of the spin polarization may be related to a spread of the spin relaxation rates in the inhomogeneous ensemble of the QDs caused by the random distribution of uncontrollable paramagnetic defects. The NCP amplitude decreases with temperature and its decay becomes faster. However, even at $T=8$ K, the NCP is observable up to time delay 100 $\mu$s. Temperature dependences of the NCP at different delays is shown in the left inset in Fig. 3.

The main conclusion from these experimental results is that the electron spin orientation can be conserved in the ensemble of InP QDs during 100 $\mu$s and more. As it was mentioned above the reason for this spin memory can be not only slow spin relaxation but also the dynamical nuclear polarization conserving the average orientation of the electron spin. The conservation can be realized by the two opposite ways depending on ratio of the electron-nuclear spin exchange rate to the phonon-mediated electron spin relaxation rate.

Fast electron-nuclear spin exchange would result in creation of the common electron-nuclear spin system. Spin-phonon interaction for nuclei is so small that the only effective channel of spin losses in the system is the phonon-mediated relaxation of the electron spin. This channel serves as a "bottleneck" for the spins accumulated in the nuclear reservoir that gives rise to slowing down spin relaxation in the electron-nuclear system.

In the opposite case, when the phonon-mediated electron spin relaxation is faster than the electron-nuclear spin exchange, the electron and nuclear spins can be considered as the independent, though interacting, systems. The light induced electron spin orientation is partially transferred to the nuclear spins causing the dynamic nuclear polarization. An effective magnetic field created by the nuclear polarization splits the electron spin states. At low temperatures, spin-phonon relaxation results in freezing out of the electron to the lowest Zeeman level.[10] Electron polarization created by this way will hold as far as the nuclear field exists.

Quantitative information about possibility of the electron spin freezing in the nuclear field was obtained by measuring the magnetic-field dependence of the NCP in Faraday configuration. The measurements were performed for the cross-polarized excitation by the probe and pump pulses with equal intensities. Under this excitation, neither the electron spin polarization nor the dynamic nuclear spin polarization may appear, and the only source of orientation is the freezing of the electron spin in the external magnetic field. The experiment reveals nearly linear magnetic field dependence of NCP (see right inset in Fig. 3). We may use this dependence to calibrate the rate of the NCP changes due to the freezing effect: $a_{NCP}\equiv dA_{NCP}/dB_{ext}\approx 0.025$ T$^{-1}$.

In the case of the copolarized pump-probe excitation, the electron spin polarization and, as a result, the dynamic nuclear spin polarization may appear. If we assume that the difference between the NCP amplitudes in small external magnetic field for the cross-polarized and copolarized pumping, $\Delta A_{NCP}=0.35$ (obtained from Fig. 2), is due to establishment of thermal equilibrium in the effective magnetic field of

nuclei, we can estimate the field $B_N=\Delta A_{NCP}/a_{NCP}=14$ T. This value is larger by approximately three order of magnitude than the nuclear field strength obtained experimentally for the InP QDs.[11,19] Therefore the freezing effect cannot be responsible for the long-lived electron spin memory in the QDs under study.

So small nuclear field cannot be also responsible for stabilization of the electronic spin due to its coupling to the nuclear spin system by the mechanism mentioned above. Indeed, the nuclear field $B_N=0.02$ T (Ref. 11) corresponds to orientation of small fraction of the nuclear spins ($<1\%$). If the electron and nuclear spin subsystems are in equilibrium with each other, degree of the electron spin orientation cannot exceed this value.[10] At the same time, the long-lived component of the degree measured experimentally (see Fig. 3) is about 10%. This means that the relaxation rate of the electron spin in the structure under study is really small and quantum information written in such spin system can be conserved for a long time.

In conclusion, our experiments have shown that the quasiresonant excitation of PL of the singly charged InP QDs by a circularly polarized light results in an efficient orientation of the resident electron spins. Decay of the spin orientation is not exponential which is possibly related to the presence of paramagnetic defects in vicinity of the QDs. The long-lived component of the spin orientation is characterized by an effective lifetime exceeding 100 $\mu$s. It is shown that so long-lived spin memory arises from the inherently slow electron spin relaxation in the InP QDs rather than due to the nuclear spin polarization.

The authors thank K. V. Kavokin for fruitful discussions, V. S. Zapaskii for critical reading of the manuscript and W. Maruyama for technical assistance in the experiments. This work was supported by Grant-in-Aid for Scientific Research No. 13852003 and No. 16031203 from the MEXT of Japan, by ISTC (Project No. 2679), by INTAS (Project No. 1B 2167), and by RFBR (Project No. 05-02-19913).

*Electronic address: ivan_gnatiev@mail.ru

[1] D. D. Awschalom, D. Loss, and N. Samarth, *Semiconductor Spintronics and Quantum Computation* (Springer-Verlag, Berlin, 2002).

[2] A. V. Khaetskii and Yu. V. Nazarov, Phys. Rev. B **61**, 12 639 (2000).

[3] J. M. Kikkawa and D. D. Awschalom, Phys. Rev. Lett. **80**, 4313 (1998).

[4] S. Cortez, O. Krebs, S. Laurent, M. Senes, X. Marie, P. Voisin, R. Ferreira, G. Bastard, J-M. Gérard, and T. Amand, Phys. Rev. Lett. **89**, 207401 (2002).

[5] R. Hanson, B. Witkamp, L. M. K. Vandersypen, L. H. Willems van Beveren, J. M. Elzerman, and L. P. Kouwenhoven, Phys. Rev. Lett. **91**, 196802 (2003).

[6] S. Laurent, O. Krebs, S. Cortez, M. Senes, X. Marie, T. Amand, P. Voisin, and J-M. Gérard, Physica E (Amsterdam) **20**, 404 (2004).

[7] M. Kroutvar, Y. Ducommun, D. Heiss, M. Bichler, D. Schuh, G. Abstreiter, and J. J. Finley, Nature (London) **432**, 81 (2004).

[8] S. Yu. Verbin, A. Greilich, D. R. Yakovlev, M. Bayer, V. Stavarache, D. Reuter, and A. Wieck, *Proceedings of 13th International Symposium "Nanostructures: Physics and Technology"*, St Petersburg, Russia, 20–25 June 2005 (Ioffe Institute, St. Petersburg, 2005).

[9] J. S. Colton, T. A. Kennedy, A. S. Bracker, and D. Gammon, Phys. Rev. B **69**, 121307(R) (2004).

[10] *Optical Orientation*, edited by B. Meier and B. P. Zakharchenya (North Holland, Amsterdam, 1984).

[11] R. I. Dzhioev, B. P. Zakharchenya, V. L. Korenev, and M. V. Lazarev, Fiz. Tverd. Tela (Leningrad) **41**, 2193 (1999) [Phys. Solid State **41**, 2014 (1999)].

[12] D. Gammon, Al. L. Efros, T. A. Kennedy, M. Rosen, D. S. Katzer, D. Park, S. W. Brown, V. L. Korenev, and I. A. Merkulov, Phys. Rev. Lett. **86**, 5176 (2001).

[13] A. S. Bracker, E. A. Stinaff, D. Gammon, M. E. Ware, J. G. Tischler, A. Shabaev, Al. L. Efros, D. Park, D. Gershoni, V. L. Korenev, and I. A. Merkulov, Phys. Rev. Lett. **94**, 047402 (2005).

[14] I. E. Kozin, V. G. Davydov, I. V. Ignatiev, A. V. Kavokin, K. V. Kavokin, G. Malpuech, Hong-Wen Ren, M. Sugisaki, S. Sugou, and Y. Masumoto, Phys. Rev. B **65**, 241312(R) (2002).

[15] I. A. Merkulov, Al. L. Efros and M. Rosen, Phys. Rev. B **65**, 205309 (2002).

[16] Similar model was considered in Ref. 4.

[17] K. V. Kavokin, Phys. Status Solidi A **195**, 592 (2003).

[18] The key process for optical orientation of the electron spins is the relaxation of the hole spins. Mechanisms of the optical orientation of spins are extensively discussed in the literature, see, e.g., Refs. 6 and 10.

[19] Our experiments also show that the effective nuclear field in the system under study does not exceed few hundredths of $T$. Results of these experiments will be published elsewhere.

[20] Though discussion of the temperature experiments is outside the scope of this paper, we can mention here that the thermally activated process responsible for the NCP decrease is most probably the hole spin relaxation.

# Spin relaxation mechanism of strain-induced GaAs quantum dots studied by time-resolved Kerr rotation

Atsushi Kanno* and Yasuaki Masumoto
*Institute of Physics, University of Tsukuba, Tsukuba 305-8571, Japan*
(Dated: January 28, 2006)

We observed electron spin precession under magnetic field in single-layer quantum dots (QDs) by highly sensitive time-resolved Kerr rotation measurement. The spin lifetime is longer than that for the quantum well (QW). This is a result of the additional spatial confinement of electrons in QDs. Below 60 K, the spin lifetime is almost constant, and is 7 times shorter than the carrier lifetime. This suggests that the strong electron-hole exchange interaction dominates over the electron spin lifetime in QDs at low temperature.

PACS numbers: 78.47.+p, 78.20.Ls, 42.50.Md, 78.67.Hc

An electron spin in a semiconductor is one of the most hopeful candidates for a quantum bit in the quantum information processing[1]. Especially in a semiconductor quantum dot, an electron spin may have a long spin coherence time due to suppression of spin relaxation by three-dimensional confinement of electrons[2]. Spin relaxation measurements by using various technique have been performed in bulk semiconductors, quantum well and quantum dots. In quantum dots, for example, the spin relaxation measurements by using optical orientation in steady-state and time-resolved photoluminescence have been reported[3-5]. These measurements are made, however, under non- and quasi-resonant excitations because the photoluminescence spectroscopy is difficult to be done under resonant excitation. However, the measurement under resonant excitation is inevitable not only for obtaining direct information on spin relaxation but also for coherent processing of spins. In quantum wells and bulk semiconductors, many time-resolved magneto-optic measurements such as Kerr and Faraday effects have been performed in recent years[6,7]. The methods are suitable to observe electron spin dynamics under resonant excitation. In the single-layer quantum dots, however, such measurements have never been done because of the weak signal[8,9]. In this work, we constructed a new system for highly sensitive time-resolved Kerr rotation measurement (TRKR). The angle resolution of the system was $5\times10^{-6}$ degree, which is highest among those so far reported. As a result, we could observe the carrier spin dynamics in single-layer strain-induced GaAs quantum dots under resonant excitation.

The sample was fabricated by molecular beam epitaxy on a semi-insulating (001) GaAs substrate. An $Al_{0.3}Ga_{0.7}As$ buffer layer was deposited on the substrate. On the buffer layer, a quantum well layer 4 nm thick, an $Al_{0.3}Ga_{0.7}As$ barrier 14 nm thick and a GaAs cap layer 2.3 nm thick were deposited in order. Stranski-Krastanov grown self-assembled InP stressor dots were fabricated on the surface of the cap layer. Since these stressor dots put the local strain into 4 nm quantum well layer, the strain-induced quantum dots were formed in the quantum well layer. The diameter, the hight and the areal density of the InP stressor dots are about 60 nm, 15 nm and $4\times10^{9}$ $cm^{-2}$, respectively. By using the strain-induced quantum dots, we can compare the electron spin relaxation for the quantum dots and the quantum well directly because the quantum dots are formed in the quantum well[10,11]. The optical density of the single-layer quantum dots is about $3\times10^{-3}$, which is estimated by the absorption coefficient for the GaAs quantum well and the coverage ratio of 11 %[12]. The optical density of GaAs quantum dots in our sample is $10^{-2}$ times smaller than that of about 0.5 for the chemically-synthesized CdSe quantum dots studied in Ref. 8, which is a unique report for the quantum dots studied by the time-resolved Faraday rotation measurement.

For the TRKR measurements, the 80 fs pump and probe pulses were generated at a repetition rate of 80 MHz by a mode-locked Ti:sapphire laser. The circularly polarized pump pulse was made by passing through a Glan-laser prism and a quarter waveplate. An optical chopper modulated the pump beam. The probe pulse, temporally delayed with respect to the pump pulse by using an optional delay, was spectrally narrowed by passing through a filter unit made of a grating and a slit. The filter unit was also used to tune the photon energy of the probe beam. Then, the polarization of the probe beam was modulated by a photoelastic modulator. The pump and probe beams were focused by a lens on the sample kept in a superconducting magneto-optic cryostat in the transverse magnetic field geometry. The reflected probe beam from the sample passed through a Wollaston prism serving for an optical bridge and was detected by a balanced photodetector. The detected signal was amplified by a lock-in amplifier at twice the trigger frequency of the photoelastic modulator for the direct detection of the Kerr rotation angle[13]. The output signal of the first lock-in amplifier was amplified again by the second lock-in amplifier at the chopping frequency of the pump beam for the reduction in the noise caused by the scattered light. The excitation densities of the pump and probe beams were about 30 $W/cm^2$ and 3 $W/cm^2$, respectively. The pump pulse generated about one electron-hole pair per quantum dot.

Figure 1 shows the photoluminescence spectrum for the sample. The peaks originated from the GaAs quan-

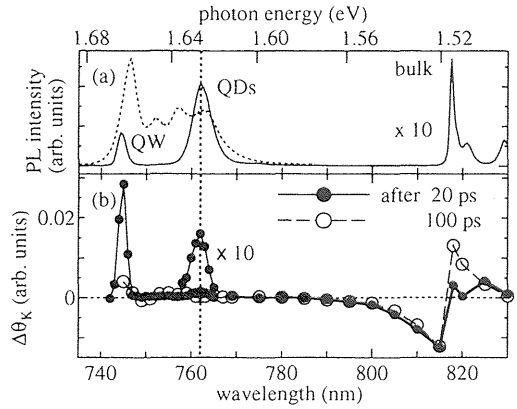


FIG. 1: (a) Photoluminescence spectrum at 10 K for excitation by the frequency-doubled output of a Ti:sapphire laser. The dotted line is under high excitation density. (b) Probe wavelength dependence of the TRKR signal without the transverse magnetic field at 10 K. Closed and open circles indicate the TRKR signals at the delay time of 20 ps and 100 ps, respectively.

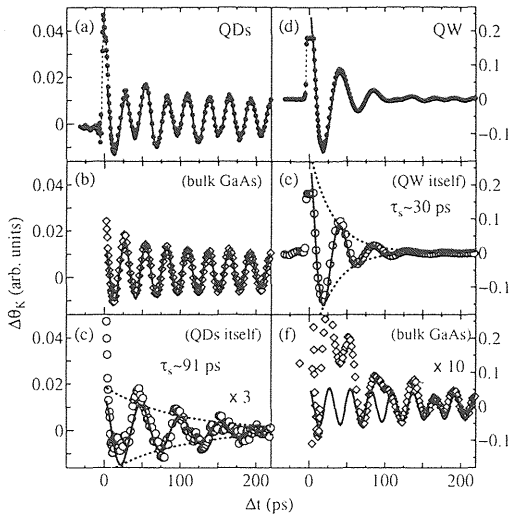


FIG. 2: Component analysis of TRKR signals taken under the magnetic field $B = 6$ T at 10 K. The experimental data (closed circles) for the probe photon energy of 1.622 eV resonant to QDs (a) and those for the probe photon energy of 1.664 eV resonant to QW (d) and calculated signals (solid lines) by sum of two components are shown. The dominant components are shown in the figure (b,e). The minor component in resonance to the QDs is originated from the QDs (c). The dominant component (b) comes from the bulk GaAs substrate. The contribution of the bulk GaAs signal in resonant to the QW is shown in (f).

tum well, the strain-induced quantum dots and the bulk GaAs substrate are clearly observed. The peaks originating from the excited state of the quantum dots are observed under high excitation density. The probe energy dependence of the TRKR signal without the magnetic field are also shown. The peaks of the TRKR signals are in agreement with those in the photoluminescence spectrum. The ratio between the TRKR signal intensity for the quantum well and the quantum dots is about 20:1. As is estimated from the areal density and the diameter of the stressor quantum dots, the coverage ratio 11 % of the InP quantum dots is obtained. It roughly agrees with the intensity ratio between the TRKR signals for the quantum well and the quantum dots.

The TRKR signals under the transverse magnetic field $B = 6$ T at 10 K are shown in Fig. 2. Under the magnetic field, the spin of the photogenerated electrons precesses around the axis of the magnetic field. Thus, the TRKR signal is described by $\Delta\theta_K(\Delta t) \propto \exp(-\Delta t/\tau_s)\cos(\omega\Delta t)$, where $\tau_s$ is the spin lifetime, $\Delta t$ is the temporal separation between the pump and probe pulses and $\omega$ is the Larmor precession frequency. Because of the reflection geometry in the TRKR measurement, the oscillatory component for the bulk GaAs substrate was observed in our experiment as the probe energy is higher than the GaAs band gap energy. The absolute value of the g-factor estimated from the observed oscillation frequency is about 0.43. This is consistent with the electron g-factor of the GaAs. Therefore, we need to divide the experimental data into the individual signals by the formula described by $\Delta\theta_K(\Delta t) \propto \exp(-\Delta t/\tau_s)\cos(\omega\Delta t) + \exp(-\Delta t/\tau_{sGaAs})\cos(\omega_{GaAs}\Delta t)$, where $\tau_{sGaAs}$ ($\omega_{GaAs}$) is the spin lifetime (Larmor precession frequency) of the bulk GaAs. In case of resonance of the quantum well [Fig. 2 (d-f)], the oscillatory signal for the bulk component is seen but is almost negligible because the signal is 10 times weaker than the dominant signal for the quantum well. In Fig. 2 (f), the fitting errors are seen from 0 ps to 100 ps because of the weak signal component. On the other hand, in case of resonance of the quantum dots [Fig. 2 (a)], a modulation in the amplitude of the oscillatory signal is observed due to the large contribution of the bulk component, which is 3 times larger than that for the quantum dots. The observed frequencies for the quantum dots, the quantum well and the bulk substrate are different from each other. In the latter part, we try to state the observed g-factors in detail.

The obtained spin lifetime of about 90 ps for the quantum dots is longer than that of about 30 ps for the quantum well at 10 K [Fig. 2]. The D'yakonov-Perel' (DP) mechanism due to the spin-orbit interaction dominates over electron spin relaxation in the undoped (100) GaAs quantum well and shortens the spin lifetime because the moving electron feels the effective magnetic field due to the lattice[14]. In fact, the spin lifetime reported is below 70 ps at low temperature[15,16]. Our experimental finding suggests that the spin relaxation due to the DP mechanism is suppressed as a result of the additional spatial confinement of electrons in quantum dots.

The spin precession at the frequency $\omega$ is interpreted by the quantum interference between the Zeeman levels separated by $\Delta E = \hbar\omega$ to each other[19]. The magnetic field

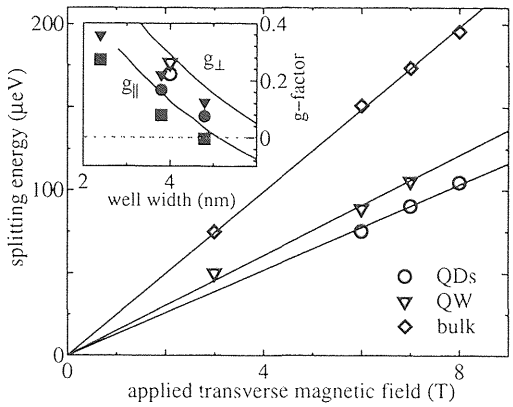


FIG. 3: The magnetic field dependence of the estimated Zeeman splitting energy. Open circles, triangles and diamonds are splittings in the quantum dots, the quantum well and the bulk GaAs substrate, respectively. The straight lines are the least square fittings. Inset: Quantum well width dependence of the electron g-factor. The filled squares, triangles and circles are respectively the g-factor values for the parallel, $g_\parallel$, and perpendicular, $g_\perp$, components for the QW and that for the QDs taken from Ref. 17. Open circle and triangles are our experimental results for the QDs and the QW. The solid lines show the calculated result for the electron g-factors for the single quantum well[18].

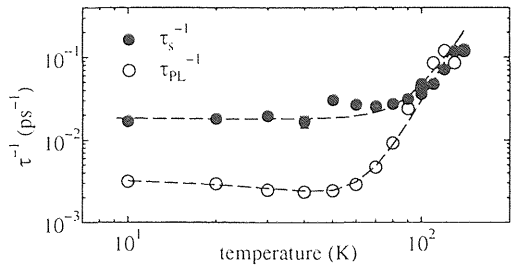


FIG. 4: Temperature dependence of the inverse of spin lifetime and carrier lifetime for the quantum dots under the magnetic field $B = 6$ T. Open and closed circles show the carrier and spin lifetimes, respectively. Dashed lines are guide lines for eyes.

dependence of the observed Zeeman splitting is shown in Fig. 3. These energies show a linear relationship described by $\hbar\omega = g\mu_B B$ with the magnetic field $B$, where g is the g-factor of the electron. Thus, we can estimate the effective g-factors by using the above relation. The observed g-factors for the quantum well and the quantum dots are 0.26 and 0.22, respectively. The effective g-factor is influenced by not only the structure but also the surrounding matrix into which the wavefunction is penetrating. The g-factor for the quantum well is assigned to the perpendicular component $g_\perp$ because the magnetic field applied in perpendicular to the crystal growth axis. The inset of the figure shows the well width dependence of the g-factors. The solid lines show the calculated electron g-factor on the Kane model in an $Al_{0.3}Ga_{0.7}As/GaAs$ single quantum well[18], and the filled marks are the experimental results by the time-resolved photoluminescence quantum beat measurements in the strain-induced GaAs quantum dots[17]. The present report gave slightly larger g-factors than the previous work, because the stressor-induced strain in our sample is weaker than the sample used in Ref. 17. This is because the distance between the surface and the quantum well is longer, and because the diameter of the stressor dots is smaller in the sample used in this work. Thus, the quantum well layer feels smaller strain than that in the sample of the previous work, and approaches the *bare* quantum well. Therefore, the observed g-factor is in good agreement with the calculated result because of the small strain. Because the wavefunction of electron in quantum dot penetrates into the AlGaAs barrier in the similar way as the GaAs quantum well, the effective g-factor for the quantum dots is considered to be close to that for the quantum well. The consistent g-factors shown in the inset of Fig. 3 confirm that we could observe the electron spin precession of the single-layer quantum dots under resonant excitation.

In the strain-induced GaAs quantum dots, the spin lifetime in the dots is lengthened by the suppression of the DP mechanism. Both electron-hole exchange interaction and hyperfine interaction were suggested as the possible electron spin relaxation processes in the quantum dots[2,20,21]. To identify the dominant spin relaxation mechanism for the strain-induced quantum dots, we performed the TRKR measurements at elevated temperatures. Figure 4 shows the temperature dependence of the measured spin lifetime and the carrier lifetime for the quantum dots under $B = 6$ T. The latter was measured by the time-resolved photoluminescence spectroscopy with a streak camera under the quasi-resonant excitation, where the excitation and detection energies were separated by the LO phonon energy of InP (42.5 meV). Above 80 K, the spin and carrier lifetimes showed the similar decrease. This means that the spin lifetime is limited by the carrier lifetime above 80 K. The observed temperature independence of the spin lifetime at lower temperature indicates that the spin relaxation mechanism does not involve phonons. We evaluated the possibility that the g-factor inhomogeneity might shorten the decay of the observed spin precession at lower temperature. However, the inhomogeneous shortening of the observed spin precession lifetime was found negligible. Because the spin lifetime is shorter than the carrier lifetime, some spin relaxation mechanisms are considered to dominate over the electron spin relaxation. In the neutral quantum dots, the electron-hole exchange interaction plays a dominant role in the electron spin relaxation[22,23]. The effective magnetic field due to the exchange interaction is considered to be larger than that due to the hyperfine interaction through the fluctuating nuclear spin orientations, although the spin relaxation due to the hyperfine interaction is important in the quantum dots[21]. It is because the exchange energy reached to an order of 100 $\mu$eV due to the three-dimensional confinement as

is compared with the energy of the fluctuating hyperfine field of an order of 1 $\mu$eV[24,25]. Therefore, it is considered that the electron-hole exchange interaction is the predominant mechanism for the electron spin relaxation in the strain-induced quantum dots, which is referred to as the Bir-Aronov-Pikus mechanism[26]. The exchange interaction is considered to be independent of the temperature and reduce the spin lifetime with increasing electron-hole density because the overlap of the wavefunctions of the carriers increases. We cannot confirm, however, the excitation power dependence of the spin lifetime because of the weak power of the laser. On the other hand, for the quantum well, it is considered that the electron spin is relaxed by the DP mechanism mentioned above. The carrier lifetime limits the spin lifetime above 80 K as is the case for the quantum dots. The spin lifetime is longest at 80 K, but becomes shorter with decreasing temperature. The reason is not clear, but the similar results were observed under the magnetic field for the bulk semiconductors[27,28].

In summary, we could observe the electron spin dynamics for the single-layer quantum dots under resonant excitation. The spin lifetime is longer than that for the quantum well at low temperature as a result of the additional spatial confinement of electrons. This suggests that the DP mechanism, which causes the electron spin relaxation in the quantum well, is suppressed in the quantum dots. The spin lifetime at lower temperature is almost constant, and is shorter than the carrier lifetime. This indicates that the spin relaxation mechanism due to the electron-hole exchange interaction works on the electron spins in the quantum dots.

The authors would like to thank Dr. H. -W. Ren for sample preparation. This work is supported by the Grant-in-Aid for the Scientific Research #13852003 and #16031203 from the MEXT, Japan.

---

* Electronic address: kan@sakura.cc.tsukuba.ac.jp


[1] D. Loss and D. P. DiVincenzo, Phys. Rev. A **57**, 120 (1998).

[2] A. V. Khaetskii and Y. V. Nazarov, Phys. Rev. B **61**, 12639 (2000).

[3] R. J. Epstein, D. T. Fuchs, W. V. Schoenfeld, and P. M. Petroff, Appl. Phys. Lett. **78**, 733 (2001).

[4] V. K. Kalevich, M. Paillard, K. V. Kavokin, X. Marie, A. R. Kovsh, T. Amand, A. E. Zhukov, Y. G. Musikhin, V. M. Ustinov, E. Vanelle, and B. P. Zakharchenya, Phys. Rev. B **64**, 45309 (2001).

[5] I. V. Ignatiev, T. Okuno, S. Y. Verbin, I. A. Yugova, and Y. Masumoto, Physica E **17** 365 (2003).

[6] A. V. Kimel, F. Bentivegna, V. N. Gridnev, V. V. Pavlov, R. V. Pisarev, and Th. Rasing, Phys. Rev. B **63**, 235201 (2001).

[7] D. D. Awschalom, D. Loss, and N. Samarth, eds., *Semiconductor Spintronics and Quantum Computation* (Springer, Berlin, 2002).

[8] J. A. Gupta, D. D. Awschalom, X. Peng, and A. P. Alivisatos, Phys. Rev. B **59**, R10421 (1999); J. A. Gupta, D. D. Awschalom, A. L. Efros and A. V. Rodina, Phys. Rev. B **66**, 125307 (2002).

[9] M. Ouyang and D. D. Awschalom, Science **301**, 1074 (2003).

[10] J. Tulkki and A. Heinämäki, Phys. Rev. B **52**, 8239 (1995).

[11] Little stress effect is expected at the quantum well region separated from stressor dots laterally, because of the high aspect ratio of 150 nm/14 nm (average distance between dots/distance between the quantum well and the surface).

[12] Y. Masumoto, M. Matsuura, S. Tarucha, and H. Okamoto, Phys. Rev. B **32**, R4275 (1985).

[13] K. Sato, Jpn. J. Appl. Phys. **20**, 2403 (1981); K. Sato, H. Hongou, H. Ikekame, Y. Tosaka, M. Watanabe, K. Takanashi, and H. Fujimori, Jpn. J. Appl. Phys. **32**, 989 (1993).

[14] F. Meier and B. P. Zakharchenya, eds., *Optical Orientation* (North-Holland, Amsterdam, 1987).

[15] Y. Ohno, R. Terauchi, T. Adachi, F. Matsukura, and H. Ohno, Phys. Rev. Lett. **83**, 4196 (1999); Y. Ohno, R. Terauchi, T. Adachi, F. Matsukura, and H. Ohno, Physica E **6**, 817 (2000).

[16] Short spin relaxation time in the sample studied may be explained by the shallow depth of the quantum well from the surface. See for examples: C. Obemuller, A. Deisenrieder, G. Abstreiter, K. Karrai, S. Grosse, S. Manus, J. Feldmann, H. Lipsanen, M. Sopanen and J. Ahopelto, Appl. Phys. Lett. **74**, 3200 (1999); C. F. Wang, A. Badolato, I. Wilson-Rae, P. M. Petroff, E. Hu, J. Urayama and A. Imamoglu, Appl. Phys. Lett. **85**, 3423 (2004).

[17] K. Nishibayashi, T. Okuno, Y. Masumoto and H. -W. Ren, Phys. Rev. B **68**, 35333 (2003).

[18] E. L. Ivchenko and A. A. Kiselev, Sov. Phys. Semicond. **26**, 827 (1992).

[19] S. Bar-Ad and I. Bar-Joseph, Phys. Rev. Lett. **66**, 2491 (1991).

[20] S. I. Erlingsson, Yu. V. Nazarov, and V. I. Fal'ko, Phys. Rev. B **64**, 195306 (2001).

[21] I. A. Merkulov, Al. L. Efros, and M. Rosen, Phys. Rev. B **65**, 205309 (2002).

[22] H. Gotoh, H. Ando, H. Kamada, A. Chavez-Pirson, and J. Temmyo, Appl. Phys. Lett. **72**, 1341 (1998).

[23] S. Laurent, O. Krebs, S. Cortez, M. Senes, X. Marie, T. Amand, P. Voisin, and J.-M. Gérard, Physica E **20**, 404 (2004).

[24] M. Bayer, A. Kuther, A. Forchel, A. Gorbunov, V. B. Timofeev, F. Schäfer, J. P. Reithmaier, T. L. Reinecke and S. N. Walck, Phys. Rev. Lett. **82**, 1748 (1999).

[25] D. Gammon, Al. L. Efros, T. A. Kennedy, M. Rosen, D. S. Katzer, D. Park, S. W. Brown, V. L. Korenev, and I. A. Merkulov, Phys. Rev. Lett. **86**, 5176 (2001).

[26] G. L. Bir, A. G. Aronov, and G. E. Pikus, Sov. Phys. JETP **42**, 705 (1976).

[27] J. M. Kikkawa and D. D. Awschalom, Phys. Rev. Lett. **80**, 4313 (1998).

[28] B. Beschoten, E. Johnston-Halperin, D. K. Young, M. Poggio, J. E. Grimaldi, S. Keller, S. P. DenBaars, U. K. Mishra, E. L. Hu and D. D. Awschalom, Phys. Rev. B **63**, 121202(R) (2001).

# Biexciton binding energy in parabolic GaAs quantum dots

Michio Ikezawa,[1] Selvakumar V. Nair,[2] Hong-Wen Ren,[1] Yasuaki Masumoto,[1] and Harry Ruda[2]

[1] *Institute of Physics, University of Tsukuba, Tsukuba 305-8571, Japan*

[2] *Centre for Nanotechnology, University of Toronto, Toronto M5S 3E3, Canada*

(Dated: February 7, 2006)

Biexcitons confined in parabolic quantum dots are investigated both experimentally and theoretically. Biexcitonic beat is observed by using time-resolved four-wave mixing in strain-induced GaAs quantum dots formed in the quantum well. The period of the beat is about 1.5 times shorter than that from the quantum well region in the same well. The shortening of the beat period is a direct evidence of an increase in the biexciton binding energy in the quantum dots due to the lateral confinement induced by the stressors. Magnetic field dependence of the biexciton binding energy is investigated, and is found to be almost independent of the external magnetic field up to 8 T. A theoretical calculation of the biexciton binding energy is presented to explain the observed magnetic field dependence.

PACS numbers: 78.47.+p, 78.67.Hc

## I. INTRODUCTION

Physics of excitons and excitonic complexes such as biexcitons, charged excitons and triexcitons confined in low-dimensional quantum structures has been a subject of intensive study in recent years. In addition to interest of basic physics, these studies are driven by the need for a deep understanding of such confined states for successful application of quantum structures to quantum information technologies. The binding energy of an excitonic complex in nanostructures is expected to be enhanced compared to the bulk material due to the spatial confinement of electrons and holes. Actually, in many kinds of quantum dots (QD) such as Stranski-Krastanov grown dots or dots dispersed in glass matrices, large binding energy of biexcitons has been reported[1]. Large binding energy of the biexciton state is particularly important in light of the recent demonstration of the ability to operate a two-qubit gate using exciton and biexciton states[2].

General considerations point to a strong dependence of the enhancement of the biexction binding energy on dimensionality. It is well known that the biexcitons localized in potential minima originating from well width fluctuations or alloy fluctuations have larger binding energy compared to that of an ideal quantum well (QW)[3–8]. Although these examples demonstrate the enhancement of the biexciton binding energy in reduced dimensionality, the additional lateral confinement potential in these cases is naturally formed and is, therefore, unknown and uncontrollable. For a better understanding of the effect of dimensionality and confinement, it is desirable to study a system with a well-defined confinement potential that could be easily controlled. Strain-induced quantum dots (SIQDs) which are formed in a buried QW by the stress modulation arising from self-assembled islands fabricated on the surface[9] provide such an ideal system. Carriers in SIQDs are confined laterally in the QW by an almost parabolic potential with no defect at the surface, resulting in nearly equally spaced energy levels, which greatly simplifies theoretical treatment. In contrast to other kinds of QDs, the confinement potentials could be finely controlled in SIQDs by changing the QW and spacer widths[9] with mono-layer precision provided by epitaxial growth. Furthermore, as QW and QD coexists inherently in a SIQD sample, we can observe the effect of the additional lateral confinement within the same quantum well. In addition, as the confinement potential is rather deep, QW and SIQD is energetically well separated, which enables us to apply quantum beat technique using ultrafast laser pulses to measure the binding energy in QW and in SIQD separately.

In this paper we report transient four-wave mixing (FWM) in a strain-induced GaAs QD measured by a highly sensitive heterodyne FWM technique. Using this technique, we detected biexcitonic quantum beat that is related to the biexciton binding energy in the SIQD. We also present measurement and theoretical calculation of the magnetic field dependence of the biexciton binding energy.

## II. EXPERIMENTAL DETAILS

The structure of the sample studied is depicted in Fig. 1(a). The SIQDs were formed in a single $GaAs/Al_{0.3}Ga_{0.7}As$ QW of 3.8 nm in width using InP stressors of 90 nm in diameter. The areal density of the stressor was $3 \times 10^9/cm^2$. The width of the $Al_{0.3}Ga_{0.7}As$ barrier on the QW is 9.0 nm. Photoluminescence (PL) spectrum of the sample is shown in the right part of the Figure. The weak peak centered at 1.647 eV is due to PL from the GaAs QW, while the intense peak centered at 1.600 eV originates from the GaAs SIQDs, showing a confinement potential of 47 meV. The energy separation between the lowest state and the first excited state was measured by PL excitation spectroscopy as 16 meV. The detection method employed in this study is based on Refs. 10,11. Recently, a very similar method was successfully utilized to investigate the biexciton binding energy in annealed $In_xGa_{1-x}As$ QDs[12]. We have modified the

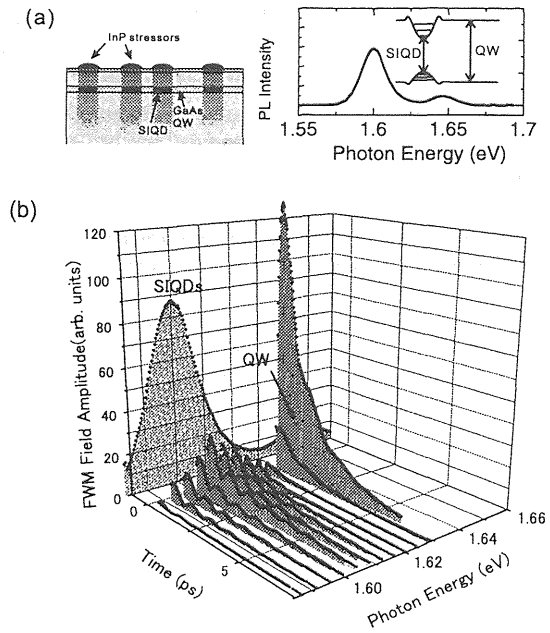


FIG. 1: (a) Structure of the strain-induced GaAs quantum dots and PL spectrum at 2 K. The shades schematically represent strain fields due to InP stressors. (b) FWM signals excited by various photon energies at 20 K. For this measurement, the spectral width of the laser was reduced to 15 meV.

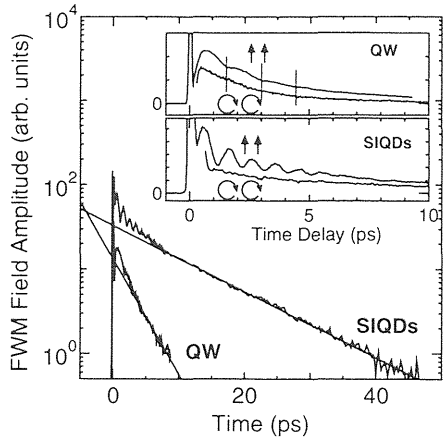


FIG. 2: Logarithmic plot of the FWM signal at SIQDs peak and at QW peak at 2 K. Decay time of the signal at SIQDs (QW) is 12 ps (3.2 ps). Inset: Polarization dependence of the FWM signal of the initial part.

method for reflection geometry. The excitation laser was a mode-locked femtosecond Ti:sapphire oscillator with repetition rate of 80 MHz, and a typical pulse width of 100 fs. The output beam was divided into three beams, and two of them were frequency-shifted by acousto-optic modulators to $\nu$ + 110 MHz and $\nu$ + 111 MHz, respectively, where $\nu$ is the optical frequency. The very weak FWM signal with frequency of $\nu + 220$ MHz induced by the two sequential pulses, the first one ($\nu$) and the second one ($\nu+110$ MHz) delayed by $\tau$, was overlapped with the other strong beam ($\nu+111$ MHz) via a beamsplitter, and detected by balanced PIN-photodiodes. The interference component at $(\nu+220\ \text{MHz})-(\nu+111\ \text{MHz}) = 109$ MHz was extracted by a spectrum analyzer. One of the beams was intensity modulated by an optical chopper, and lock-in detection was utilized. The sensitivity of this system was found to be sufficient to detect the FWM from a single layer of QDs.

## III. RESULTS AND DISCUSSION

In Fig. 1(b), the time-integrated FWM signals measured at 20 K are shown as a function of the center photon energy of the excitation laser. The PL spectrum is plotted in a vertical plane for comparison. When the excitation photon energy is at the center of the PL peak of QW, quite strong FWM signal was observed (not shown). The signal decreases rapidly with decreasing photon energy, and then increases as the energy approaches the SIQDs peak. After the laser photon energy passes through the PL band, the signal fades out. Therefore, it is confirmed that the signal near the SIQDs peak originated from the lowest state in SIQDs. As it appears at first glance, the signals have a pronounced beat structure, which is not clear in the signal from the QW.

The FWM signals measured at the center of QW peak and SIQDs peak at 2 K are shown in Fig. 2. Except for the beat structure, the intensity of the FWM signal decays almost exponentially. The decay time constants for the QW and SIQDs differed from each other, and were independent of the excitation laser power under the present experimental conditions. The dephasing time was determined to be 24 ps for excitons in SIQDs[13]. Polarization dependence was investigated in order to discuss the origin of the beat structures. A clear oscillation with a period of 1 ps was observed for the SIQDs when the two excitation pulses have co-linear polarization, while it disappeared when the pulses were co-circularly polarized as shown in the inset. The polarization dependence of the beat strongly suggests that the biexciton is the origin of the beat, as biexcitons consist of two excitons of opposite spin, and therefore cannot be excited by co-circular polarized pulses[14]. The same is true for the signal from the QW. The difference in the beat periods would therefore represent an enhancement of the biexciton binding energy in SIQDs. In the present sample, the binding energy increases from 2.8 to 4.1 meV, corresponding to an enhancement factor of 1.5. We found that the enhancement factor had a tendency to decrease with decreasing the lateral confinement potential: 1.45 for 44 meV, 1.3 for 36 meV. It seems reasonable to suppose that the biexciton in QW is not localized but free in the present sample, because a theoretical calculation[15] which includes localization of biexciton shows that the localized biexciton in

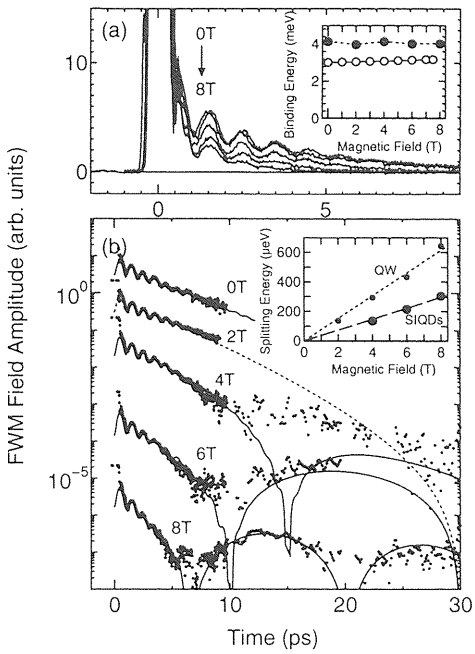


FIG. 3: Magnetic field dependence of the biexcitonic beat (a) and slow beat (b). The biexcitonic beat remains constant up to 8 T. The open circles in the inset represent the result of the theoretical calculation (see text). The slow beat results from the Zeeman splitting of excitons in SIQDs. The g-factor of excitons in SIQDs is deduced as 0.64, while that in QW is 1.3.

3.8 nm QW should have much larger binding energy, and the experimental results cited in the paper also support this assumption.

Next, we measured the magnetic field dependence of the biexciton binding energy in Faraday geometry (Fig. (3)). With increasing the magnetic field, another beat structure emerged and it modified the biexcitonic beat. The frequency of the slow beat depends linearly on the magnetic field (see, Fig. 3(b) inset). This beat is assigned to the quantum beat between the right-circularly polarized exciton and left-circularly polarized exciton separated by the Zeeman splitting. The $g$-factor of excitons in the SIQDs is deduced to be 0.64, and agrees well with that measured by polarized time-resolved luminescence[16]. Turning now to the biexcitonic beat, the beat frequency and corresponding binding energy show practically no change up to a magnetic field of 8 T as shown in Fig. 3(a)[17]. Similar weak dependence on the magnetic field was also reported for the biexciton binding energy in InGaAs QW, but no explanation was given[18]. The weak magnetic field dependence is not caused by the weakness of the magnetic confinement compared to that due to the strain field. It could be understood by theoretical considerations described below.

We calculated the exciton and biexciton states in SIQDs using a configuration interaction approach[19,20].

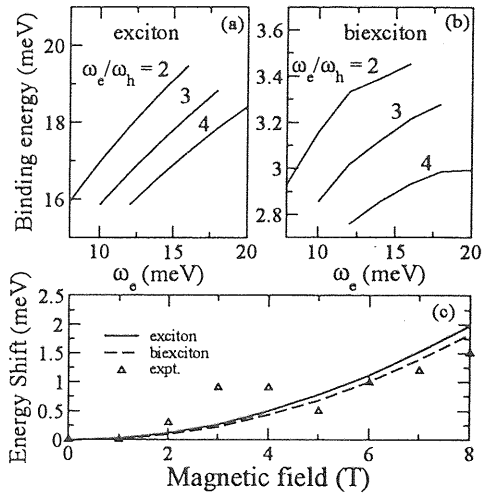


FIG. 4: Calculated binding energies of (a) exciton and (b) biexciton for various values of the confinement parameters $\omega_e$ and $\omega_h$ (see the text for details). The bottom panel (c) shows the magnetic field dependence of the exciton (solid line) and biexciton (dashed line) emission energies for $\omega_e = 12$ meV and $\omega_h = 4$ meV. The points (open triangles) denote experimental data for the exciton.

For single particle electron and hole states, we use a two band effective mass approximation with an isotropic electron band and an anisotropic hole band. Previous theoretical calculations have established that single particle SIQDs could be well described by such a model[21]. Further, we explicitly make use of the cylindrical symmetry of the confining potential in SIQDs. In this approximation, the hole single particle Hamiltonian, $\mathcal{H}_h$, for a given axial angular momentum $l_h$ takes the form,

$$\mathcal{H}_h = E_v + \frac{\hbar^2}{2}\left[\frac{1}{r_h}\frac{\partial}{\partial r_h}\frac{r_h}{m_h^{\perp}}\frac{\partial}{\partial r_h} + \frac{\partial}{\partial z_h}\frac{1}{m_h^{\parallel}}\frac{\partial}{\partial z_h} - \frac{l_h^2}{m_h^{\perp} r_h^2}\right] + V_h(r_h, z_h) \quad (1)$$

where $m_h^{\parallel}$ and $m_h^{\perp}$ denote the hole effective masses along the $z$-direction and in the $x-y$ plane respectively. Both the electron and hole effective masses could be position dependent. The confining potential $V_h(r,z)$ is determined by the band edge discontinuities and the strain distribution induced by the stressor and $E_{c(v)}$ is the conduction (valence) band edge of the barrier material. A similar equation holds for the electron.

Although mixing of heavy-hole(HH) and light-hole(LH) bands is known to affect excitons and biexciton states, the single hole-band model used here is a good approximation. In the quantum well, the HH-LH splitting due to confinement is about 35 meV and, based on early calculations[22], we estimate that the HH-LH mixing would change the exciton binding energy by less than 10% (1meV). In the quantum dot, the band mixing ef-

fects would be even weaker because of increased HH-LH splitting due to the stressor-induced strain. From continuum elasticity calculations we find that, at the location of the quantum well, which is about 11 nm below the stressor, the biaxial strain increases the HH-LH splitting by an additional 15 meV.

We calculated the single particle energies and envelope functions using a finite difference discretization of $\mathcal{H}_e$ and $\mathcal{H}_h$ in the $r-z$ plane. While the confining potentials $V(r,z)$ could be directly related to the structure of the QD, there is considerable uncertainty in the resulting potentials due to inaccuracies in known values of deformation potentials and elastic constants. Here we have opted to use a phenomenological confinement potential given by $V_{e(h)}(r,z) = E_{e(h)}(r,z) \pm m^{\perp}_{e(h)}\omega^2_{e(h)}r^2/2$, where $E_{e(h)}$ describes the band edge discontinuities relative to the conduction (valence) band edges of the barrier and $\omega_e$ and $\omega_h$ are treated as parameters. Once the single particle states are determined, we construct biexciton states within a CI approach[20]. The Coulomb interaction is screened by the bulk dielectric constant of GaAs. We use as high as 50 single particle states leading to more than $10^5$ configurations which is much larger than previous calculations (see Ref. 23).

Finally, in the presence of a magnetic field ($\mathbf{H}$) the single particle Hamiltonian is modified by replacing $-i\nabla$ by $-i\nabla \pm (e/\hbar c)\,A$ where the + sign applies to electrons and − sign to holes and $A = (\mathbf{H}\times\mathbf{r})/2$. All results reported here are for magnetic field along the z-direction.

The calculated binding energies and the magnetic field dependence of exciton and biexciton emission energies is shown in Fig. 4(a–c). The data shown in Fig. 4(c) are for $\omega_e = 12$ meV, $\omega_h = 4$ meV which appears to be most appropriate for our sample[25]. The biexciton binding energy, given by the difference between exciton and biexciton emission energies, is shown in the inset of Fig. 3(a) along with the experimental data. The calculated results are in good agreement with the experiment.

The calculated biexciton binding energy for the above parameters is about 3 meV which is somewhat smaller than the observed value of 4 meV. By a comparison of CI and path-integral-Monte-Carlo methods we have concluded that even the relatively large basis set used by us may not be enough to obtain well-converged biexciton states in these QDs. This point will be addressed in more detail elsewhere[24].

An analysis of the convergence indicates that the calculated weak magnetic field dependence of the biexciton binding energy is not an artifact. In a simple picture one may think that the additional confinement due to the magnetic field will lead to an increase in the binding energy of multi-particle states. In fact, the diamagnetic confinement potential due to a field of 8 T would essentially increase $\omega_e$ from 12 meV to 14.5 meV and $\omega_h$ from 4 meV to 5.6 meV. Considering this effect alone one would expect the exciton binding energy to increase from 16 meV to 18 meV which is indeed in very good agreement with the actual calculated value.

However, the same argument would mean that a field of 8 T should increase the biexciton binding energy from 3 meV to about 3.3 meV in contradiction with the actual extremely weak magnetic field dependence. This behavior is intimately related to the fact that, in QDs smaller than the exciton Bohr radius, the exciton binding energy is predominantly determined by the Hartree term or first order perturbation theory and is insensitive to correlations described by excited state contributions. On the other hand, the biexciton binding is completely determined by correlations and hence by contributions of excited state configurations. The magnetic field causes orbital Zeeman splitting of the excited states and thus reduces the mixing of the ground and excited state configurations. It is this competition between the paramagnetic and diamagnetic terms that lead to a weak dependence of the biexciton binding energy on the magnetic field. Calculations in which the paramagnetic term was artificially switched off confirms this interpretation.

## IV. CONCLUSION

FWM of parabolic GaAs SIQD formed in a GaAs single QW was studied using a highly sensitive heterodyne detection technique. A remarkable enhancement of the biexciton binding energy in SIQD due to the lateral confinement was detected by direct comparison with the QW based on the beating period in the FWM signal. Magnetic field dependence of the binding energy was investigated in Faraday geometry, and was found to be very weak although the exciton emission energy shows a strong shift with magnetic field. A theoretical calculations using the configuration interaction approach supports this observation.

S. V. N and H. R acknowledge support from NSERC and AFOSR.

[1] A. D. Yoffe, Adv. Phys. **50**, 1 (2001) and references therein.
[2] X. Li, Y. Wu, D. Steel, D. Gammon, T. H. Stievater, D. S. Katzer, D. Park, C. Piermarocchi, and L. J. Sham, Science **301**, 809 (2003).
[3] O. Heller, Ph. Lelong, and G. Bastard, Rhys. Rev. B **56**, 4702 (1997).
[4] D. A. Kleinman, Phys. Rev. B **28**, 871 (1983).
[5] K. Brunner, G. Abstreiter, G. Böhm, G. Tränkle, and G. Weimann, Phys. Rev. Lett. **73**, 1138 (1994).
[6] F. Kreller, M. Lowisch, J. Puls, and F. Henneberger, Phys. Rev. Lett. **75**, 2420 (1995); T. Häuptl, H. Nickolaus, F. Henneberger, and A. Schülzgen, Physica Status Solidi B 194, 219 (1996).
[7] U. Woggon, K. Hild, F. Gindele, W. Langbein, M. Het-

terich, M. Grün, and C. Klingshirn, Phys. Rev. B **61**, 12632 (2000).
[8] W. Langbein, and J. M. Hvam, Phys. Rev. B **59**, 15405 (1999).
[9] H. Lipsanen, M. Sopanen, and J. Ahopelto, Phys. Rev. B **51**, R13868 (1995).
[10] M. Hofmann, S. D. Brorson, J. Mørk, and A. Mecozzi, Appl. Phys. Lett. 68, 3236 (1996); A. Mecozzi, J. Mørk, and M. Hofmann, Opt. Lett. **21**, 1017 (1996).
[11] P. Borri, W. Langbein, S. Schneider, U. Woggon, R. L. Sellin, D. Ouyang, and D. Bimberg, Phys. Rev. Lett. **87**, 157401 (2001).
[12] W. Langbein, P. Borri, U. Woggon, V. Stavarache, D. Reuter, and A. D. Wieck, Phys. Rev. B **69**, 161301(R) (2004).
[13] The dephasing time seems rather short for a zero-dimensional system. However, relatively broad homogeneous widths are reported in InGaAs SIQDs by single dot spectroscopy, and "near surface impurity state" is suggested as an additional dephasing mechanism, because the SIQDs are inherently located near the surface. See, for example, C. Obermüller *et al.*, Appl. Phys. Lett. **74**, 3200 (1999).
[14] T. F. Albrecht, K. Bott, T. Meier, A. Schulze, M. Koch, S. T. Cundiff, J. Feldmann, W. Stolz, P. Thomas, S. W. Koch and E. O. Göbel, Phys. Rev. B **54**, 4436 (1996).
[15] A. V. Filinov, C. Riva, F. M. Peeters, Yu. E. Lozovik, and M. Bonitz, Phys. Rev. B **70**, 035323 (2004).
[16] K. Nishibayashi, T. Okuno, Y. Masumoto, and H. W. Ren, Phys. Rev. B **68**, 035333 (2003).
[17] The damping constant of the biexcitonic beat appears to decrease with increasing the magnetic field. This feature arises from the Zeeman splitting of exciton states and it does not mean any other biexciton related phenomena such as inhomogeneous broadening of the biexciton binding energy in magnetic field.
[18] T. Baars, M. Bayer, A. A. Gorbunov, A. Forchel, Phys. Rev. B **63**, 153312 (2001).
[19] L. Bányai and S. W. Koch, *Semiconductor Quantum Dots* (World Scientific, Singapore, 1993).
[20] S. V. Nair, in *Semiconductor Quantum Dots: Physics, Spectroscopy and Applications*, eds., Y. Masumoto and T. Takagahara (Springer, Berlin, 2002).
[21] J. Tulkki and A. Heinamaki, Phys. Rev. B **52**, 8239 (1995).
[22] G. D. Sanders and Y-C. Chang, Phys Rev. B **32**, 5517 (1985); U. Ekenberg and M. Altarelli, Phys. Rev. B **35**, 7585 (1987).
[23] S. Corni, M. Brasken, M. Lindberg, J. Olsen, and D. Sundholm, Phys. Rev. B **67**, 045313 (2003).
[24] M. Wimmer, S. V. Nair, and J. Shumway, Phys. Rev. B (submitted).
[25] The PL spectrum shows an excited state emission 16meV above the ground state. Further, based on strain calculations we estimate the ratio $\omega_e/\omega_h$ to be close to 3.